UNIVERSITÉ DE STRASBOURG

UNIVERSITÉ DE STRASBOURG

Institut Charles SADRON

École Doctorale de Physique et Chimie-Physique

Institut Charles Sadron UPR22

THÈSE présentée par :

Iuliia KONKO

Soutenue le : **09 Décembre 2015**

pour obtenir le grade de : **Docteur de l'Université de Strasbourg**

Discipline/ Spécialité : Physique et Physico-Chimie

SOLUTIONS AQUEUSES DE COMPLEXES FORMES PAR DES POLYELECTROLYTES MODELES DE CHARGE OPPOSEE

THÈSE dirigée par :
  Monsieur Michel RAWISO   Directeur de recherche, ICS, Université de Strasbourg

RAPPORTEURS :
  Monsieur Eric BUHLER   Professeur, Université Paris 7 Diderot
  Monsieur Oleg BORISOV   Directeur de recherche, Université de Pau et des Pays de l'Adour

EXAMINATEURS :
  Monsieur Fabrice COUSIN   Chercheur CEA, Laboratoire Léon Brillouin, Saclay
  Monsieur Albert JOHNER   Directeur de Recherche, Université de Strasbourg
  Mme Regine von KLITZING   Professeur, Université Technique de Berlin

Acknowledgements

First, I would like to express my special appreciation and thanks to my supervisor Dr. Michel Rawiso. I would like to thank you for being a good example of responsibility and honesty in scientific research, for sharing your knowledge with me and for the interesting and challenging idea of the project. I would like to thank you for your support during all beam times at the neutron reactors and the synchrotron and for the work on the thesis manuscript. All our discussions allowed me to grow up as a research scientist. I am a very fortunate to have such a teacher and a mentor like you.

I would also like to express my gratitude to the committee members for their willingness to participate in the defense of my PhD thesis: Prof. Dr. Eric Buhler from Paris Diderot University – Paris 7; Dr. Oleg Borisov from the University of Pau and Pays de l'Adour; Dr. Fabrice Cousin from the Laboratoire Léon Brillouin (CEA); Dr. Albert Johner from the Institute Charles Sadron; Prof. Dr. Regine von Klitzing from the Technical University of Berlin.

Especially I would like to thank our local contacts during beam times at large facilities for their professionally and support during the experiments: Dr. Fabrice Cousin from the Laboratoire Léon Brillouin (LLB); Dr. Isabelle Grillo from Laue-Langevin Institute (ILL); Dr. Javier Perez from SOLEIL. My research would not have been possible without your help.

In the frame of ANR project, I had a great pleasure to participate in fruitful and productive scientific discussions concerning theoretical aspects and simulation studies of polyelectrolyte complexes with Dr. Albert Johner and Dr. Diddo Diddens. Thanks to you for all our meetings.

Of course, I would like to thank Dr. Jean-Marie Catala, Jean-Philippe Lamps and Dr. Philippe Mesini for their help in the synthesis of the high-quality samples for my research and for the time I spent in their laboratories.

Also, I would like to express my gratitude to Romain Reynaud from Soliance for providing sodium hyaluronan materials, that completed the study of the effect of the polyanion stiffness and helped us to realize our scientific ideas.

Great thanks to the members of the Polymer Characterization Platform of the Institute Charles Sadron: Mélanie Legros and Catherine Foussat for the assistance with the SEC analysis; Yves Guilbert and Catherine Saettel for the TGA measurements.

Of course, I would like to thank Dr. André Schroder for the ITC experiments and Dr. Marc Schmutz for Cryo-TEM that bring clarity to the project and completed the results obtained with SAXS and SANS.

My sincere thanks also go to Guillaume Fleith for his "hand of help" and taking care of SAXS instruments. I would like to thank you for your optimism and your good spirit. I am very thankful to Dr. Jérôme Comber for introducing me to IGOR program, which has significantly simplified my work. Thank you also for the long hours you spent with Michel and me during the presentation preparation. Of course, I do appreciate both of you for your teachings in the French culture and language. It would have been a lonely lab without you.

Furthermore, I would like to thank Dr. Philippe Lorchat for his research on the binary aqueous solutions of PDADMAC and PSSNa that made a nice and promising basis for my project.

In addition, I would like to thank all great colleagues from the Institute Charles Sadron and Bureau de Jeunes Chercheurs (BJC) for the great working atmosphere and inspiring coffee breaks.

Great thanks are to my former scientific team from the National Taras Shevchenko University of Kyiv: Dr. Natalia Kutsevol, Dr. Natalia Melnik, Dr. Mykova Bezugliy, Svetlana Filipchenko and many others for enlightening my first steps in the world of research.

In addition, I would like to thank all my friends, who were there for me during this hard working time. First of all, thanks are to my officemates: Natalia, Victoria and Nan for our conversations between work. I am especially grateful to Franck, Ksenia, Marek, Alex and Artem Kovalenko for our shared lunches. Sincere thanks to Stephan and Ali, who accompanied me at the beginning of my life in Strasbourg, and to all others, who I had a pleasure to meet here: Susanne, Valentina, Joe, Patricia, Fabien, Anna, Laurence, Olga, Nina, Cristian, Justin. A lot of thanks to Stéphanie and Hugo for lessons of macaroons cooking. Very special thanks to Goshia, Alex, Jérôme, Guillaume and Greg for climbing; Guido for being an example of dedication to work and effective advice; Pierre for a good mood and his jokes. My acknowledgments would not have been completed without mention the Ukrainian students in Strasbourg: Natalia, Daria, Anna, Artem, Sasha, Sergiy, Ihor, Marianna, Lesya, Valentina, Iryna, Yulia and many others I have certainly forgotten to mention. Finally, I would like to thank to Elzara, Anton, Mykola, Yustina, Pavlo, Viktoriia, Kate and Bovchalyuk's and Boychenyuk's families, who supported me despite the big distance between us. I thank all of you, and if I have undeservedly forgotten anyone, I apologize.

And last but not least, I want to thank my family for supporting and encouraging me throughout my life.

Thank you.

Résumé de thèse

Cette thèse, intitulée « *Solutions aqueuses de complexes formés par des polyélectrolytes modèles de charges opposées* » comprend sept chapitres et une conclusion générale. Elle est structurée de la façon suivante :

-Chapitre 1 *Introduction*

Cette introduction précise les enjeux et objectifs généraux de la thèse et suggère leur importance dans le contexte plus général de la science des polymères et des matériaux associés. Les systèmes modèles étudiés dans la thèse sont également présentés.

-Chapitre 2 *Introduction aux polyélectrolytes et complexes de polyélectrolytes*

Dans ce chapitre sont résumées les principales propriétés des solutions aqueuses de polyélectrolytes et de complexes de polyélectrolytes qui sont pertinentes dans cette thèse.

-Chapitre 3 *Synthèses et caractérisations*

Dans ce chapitre sont présentées les synthèses et les caractérisations des polyélectrolytes modèles utilisés dans cette thèse: PSSNa, PαMSSNa et PDADMAC. Les préparations de leurs solutions aqueuses et de celles des complexes associés sont également décrites en détail suffisant.

-Chapitre 4 *Techniques et analyses des données expérimentales*

Ce chapitre donne un aperçu des différentes techniques expérimentales utilisées et des analyses des données auxquelles elles conduisent. L'accent est mis sur les techniques de diffusion de rayons X et de neutrons aux petites angles.

-Chapitre 5 *Solutions aqueuses de hyaluronate de sodium*

Dans ce chapitre on s'intéresse successivement aux solutions aqueuses diluées en présence de sel ajouté puis aux solutions aqueuses semidiluées et concentrées en absence de sel ajouté du hyaluronate de sodium. L'étude des solutions aqueuses diluées en présence de sel ajouté permet de s'intéresser à la conformation moyenne de l'acide hyaluronique et en particulier à sa rigidité intrinsèque, ou longueur de persistance non-électrostatique.

-Chapitre 6 *Complexes PDADMAC-PSSNa*

Les résultats majeurs de cette thèse sont présentés dans ce Chapitre 6. Ils concernent plus particulièrement la thermodynamique et la structure des solutions aqueuses des complexes formés de Poly(chlorure de diallyldiméthyl ammonium) et de Poly(styrène sulfonate de sodium), PDADMAC-PSSNa. Il s'intéresse également à la thermodynamique des solutions aqueuses des complexes formés de Poly(chlorure de diallyldiméthyl ammonium) et de Poly(α-méthylstyrène sulfonate de sodium), PDADMAC-PαMSSNa, en passant du polyanion PSS au polyanion PαMSS on aborde l'effet d'un faible changement de rigidité intrinsèque du polyanion.

-Chapitre 7 *Complexes PDADMAC-HANa*

Le chapitre 7 s'intéresse à la thermodynamique et la structure des solutions aqueuses des complexes formés de Poly(chlorure de diallylldiméthyl ammonium) et de Hyaluronate de sodium, PDADMAC-HANa. Cette fois, en passant du polyanion PSS au polyanion HA, on étudie plus précisément les conséquences d'un fort changement de rigidité intrinsèque du polyanion.

-Chapitre 8 *Conclusion générale*

Chapitre 1. Introduction

Les complexes de polyélectrolytes (PECs) sont des systèmes multichargés qui, en dépit de leurs nombreuses applications, et des avancées de plusieurs groupes internationaux (Kabanov, Dautzenberg ou Dubin), soulèvent encore de nombreuses questions de recherche fondamentale. Ceux que nous avons étudiés à l'Institut Charles Sadron sont formés de deux polyélectrolytes (PEs) de charges opposées, c'est-à-dire d'un polycation et d'un polyanion avec leurs contreions respectifs.

En ce qui concerne les applications des PECs, on peut citer: la préparation de membranes de pervaporation ou de nanofiltration; le développement de vecteurs pharmaceutiques pour le relargage contrôlé de principes actifs; la thérapie génique; le développement de capteurs et de dispositifs photovoltaïques; les piles à combustible. On peut également préparer des saloplastiques, ou CoPECs, qui sont de nouveaux matériaux (biomatériaux) étirables à souhait et capables de s'auto-réparer lorsqu'ils cassent.

Les complexes de polyélectrolytes résultent d'un processus d'auto-assemblage contrôlé principalement par l'interaction électrostatique et qui bénéficie d'un gain entropique associé au relargage des conterions dans la solution. De nombreux paramètres, comme la nature des polyélectrolytes, leur caractère hydrophile ou hydrophobe, leurs masses molaires moyennes, le pH, pour les polyacides ou les polybases, et la force ionique de la solution jouent un rôle aussi bien dans la thermodynamique et la cinétique du phénomène d'auto-assemblage que dans les structures des complexes auxquelles il aboutit. Toutefois, l'idée directrice de ce travail de thèse était que la rigidité intrinsèque des PEs devait jouer un rôle fondamental. Pour tester cette hypothèse, nous avons étudié les solutions aqueuses de différents complexes formés d'un polycation et d'un polyanion modèles, nous permettant de faire varier la longueur de persistance non-électrostatique du polyanion. De surcroît, nous nous sommes intéressés aux influences de la force ionique et du mode de préparation des PECs qui peuvent également conditionner le processus d'association et son résultat.

Nous avons préparé et étudié trois PECs constitués d'un même polycation, le poly(diallyldiméthyl ammonium), de longueur de persistance non-électrostatique $l_p^0 = 3$ nm, sous forme sel de chlorure (PDADMAC), et de trois polyanions de rigidités intrinsèques distinctes, sous forme de sel de sodium: le poly(styrène sulfonate) (PSSNa, $l_p^0 = 1$ nm), le poly(α-méthyl styrène sulfonate) (PαMSSNa, $l_p^0 = 2.5$ nm) et le hyaluronate, (HANa, $l_p^0 \sim 9$ nm). Ce choix devait nous permettre d'étudier l'effet d'un changement de rigidité intrinsèque du polyanion sur le processus d'association et la structure finale des complexes, en ayant l'avantage de ne considérer que des PEs linéaires modèles, hydrophiles et totalement chargés, dont les structures des solutions aqueuses étaient relativement bien connues.

Chapitre 2. Polyélectrolytes et Complexes de Polyélectrolytes

Les solutions aqueuses de polyélectrolytes (PEs) et de complexes de polyélectrolytes (PECs) sont des fluides complexes dont les structures dépendent de plusieurs paramètres, le plus souvent corrélés. Avant de présenter les techniques expérimentales utilisées dans cette thèse et les résultats obtenus en utilisant ces techniques, nous proposons un rappel des principales propriétés et grandeurs physiques qui caractérisent les solutions de PEs et PECs.

Polyélectrolytes

Dans le cas des solutions aqueuses de polyélectrolytes, on a introduit les paramètres et phénomènes, ou interactions, qui contrôlent la conformation moyenne des chaînes de polyélectrolytes : charge effective, f_{eff}, des macroions et phénomène de condensation des contreions (CIs) de Manning-Oosawa; force ionique des solutions, I, et longueur d'écran de Debye, K_D^{-1}, caractérisant l'interaction électrostatique ; longueur de persistance intrinsèque, ou non-électrostatique, l_p^0, et électrostatique, l_p^e, des macroions, etc. Pour décrire la structure des solutions aqueuses de polyélectrolytes dans le cadre du modèle isotrope, on distingue trois régimes de concentration (dilué, semidilué et concentré), correspondant à deux états de dispersion des macroions distincts (c < c* et c > c*, où c* est la concentration critique de recouvrement des macoions). Nous avons présenté les modèles théoriques et lois d'échelle associés à ces différents régimes. Dans le régime dilué (c < c*), en négligeant certaines hétérogénéités reliées soit à la difficulté d'atteindre l'état fondamental, soit à une tendance à l'auto-association, lorsque l'établissement de liaisons hydrogène est par exemple possible, les macroions sont bien séparés dans la solution. La conformation moyenne des macroions peut alors se décrire en utilisant l'approche de P. J. Flory ou celle de P.-G. de Gennes, qui introduit la notion de blobs électrostatiques pour les PEs faiblement chargés hydrophiles et qui a été adaptée aux PEs hydrophobes par A. R. Khokhlov. Dans les régimes semidilué et concentré (c > c*), les macromolécules s'interpénètrent et forment un réseau temporaire avec une maille de taille moyenne égale à *la longueur de corrélation ξ de la solution*. La structure correspond alors à un empilement compact de blobs de taille ξ (blobs de concentration) et les interactions électrostatiques sont écrantées au-delà de cette longueur ξ. Dans le régime semidilué, la taille du blob électrostatique reste inférieure à ξ (c* < c < c**); dans le régime concentré, la taille du blob électrostatique est supérieure à ξ (c > c**). Dans ce dernier régime du modèle isotrope, la théorie de champ moyen est valide et la statistique des chaînes peut être considérée gaussienne. Au-delà du régime concentré, un ordre d'orientation résultant d'une transition d'Onsager est envisageable, comme le suggèrent les travaux théoriques de I. A. Nyrkova, N. P. Shusharina, A. R. Khokhlov, G. A. Carri et M. Muthukumar. Il a été récemment observé par P. Lorchat et ses collaborateurs en considérant les solutions aqueuses denses d'un polyélectrolyte de rigidité intrinsèque suffisamment grande, comme le PαMSSNa ou le PDADMAC. Mon travail de thèse a confirmé ce travail en considérant les solutions aqueuses de HANa. Sur le plan expérimental, ce sont les techniques de diffusion de rayons X et de neutrons aux petits angles (*SAXS et SANS*)

qui permettent d'étudier la structure des solutions aqueuses de polyélectrolytes. Les intensités diffusées par ces solutions aqueuses en absence de sel ajouté, présentent un maximum large, couramment appelé « pic polyélectrolyte ». Sa position dans l'espace réciproque q*, est reliée à une distance moyenne entre macroions pour les solutions diluées et à un trou de corrélation de taille ξ pour les solutions semidiluées et concentrées. La variation de q* avec la concentration, C, suit une loi d'échelle, $q^* \sim C^{-\alpha}$ et l'exposant α est une signature du régime de concentration. Ainsi, dans le cas des PEs hydrophiles, les exposants $\alpha = 1/3$, 1/2 et 1/4 caractérisent respectivement les régimes dilué, semidilué et concentré. Dans le cas des PEs hydrophobes, le modèle de collier de perles proposé par A. V. Dobrynin, M. Rubinstein et S. P. Obukhov, à la suite des travaux de Y. Kantor et M. Kardar sur les polyampholytes, conduit à des lois d'échelles différentes pour c > c*. Deux régimes successifs caractérisés par les exposants $\alpha = = 1/2$ et 1/3 sont en particulier théoriquement observables.

Pour les solutions denses de PEs hydrophiles, deux comportements sont à considérer suivant la rigidité intrinsèque des macroions. Pour les PEs flexibles, comme le PSSNa, lorsque la distance moyenne entre macroions, ξ, est de l'ordre de la longueur de persistance non-électrostatique des chaînes, l_p^0, l'intensité diffusée présente toujours un maximum mais c'est une loi d'échelle $q^* \sim C^0$ qui prévaut. Cette loi a été observée en premier par K. Nishida, K. Kaji et T. Kanaya et confirmée par P. Lorchat et ses collaborateurs. Le maximum de l'intensité diffusée n'est plus associé à une répulsion électrostatique et sa position ne varie plus avec la concentration. Ce nouveau régime, caractérisé par un exposant α nul, correspond à la formation de clusters de dipôles électrostatiques dont l'existence est due à une forte décroissance de la constante diélectrique du milieu. Les clusters se comportent alors comme des sphères dures et la position du maximum de l'intensité diffusée, q*, donne une information sur leur taille. C'est le régime dit « ionomère ». Pour les PEs semiflexibles, ou semirigides, comme le PαMSSNa, ou le PDADMAC, le comportement est différent. On observe en effet une transition d'Onsager, ou transition isotrope-nématique, lorsqu'on augmente la concentration de telle sorte que ξ devienne de l'ordre ou inférieure à l_p^0. Aux plus fortes concentrations, l'intensité diffusée présente un maximum dont l'origine est purement stérique. Ainsi, contrairement au pic polyélectrolyte, ce maximum ne disparaît pas lorsque la force ionique de la solution augmente et son amplitude augmente avec la concentration. On observe une loi d'échelle $q^* \sim C^{1/2}$ caractéristique d'un ordre local nématique. Lorsqu'on approche du « bulk » (absence de solvant), on ne retrouve le régime « ionomère » qu'avec le PαMSSNa. Aux concentrations intermédiaires, entre les régimes concentré et nématique local, il existe une phase originale,

découverte par P Lorchat, qui est caractérisée par une nouvelle loi d'échelle : $q* \sim C^1$. Ce régime qui précède la transition d'Onsager est caractéristique des PEs semiflexibles. La structure peut alors se décrire comme un empilement compact encombré de cylindres de longueur comparable à l_p^0. L'orientation des cylindres est aléatoire mais résulte d'une compétition entre un effet stérique (Onsager) visant une compacité maximum, soit une orientation parallèles des cylindres les uns par rapport aux autres, et une répulsion électrostatique favorisant, au contraire, une orientation perpendiculaire des cylindres les uns par rapport aux autres. Cette phase est donc une phase métastable frustrée. Nous avons confirmé ces résultats en étudiant la structure des solutions aqueuses denses de HANa par SAXS. Nos résultats sont présentés dans le Chapitre 5 et confirment le rôle primordial que joue la rigidité intrinsèque des PEs sur la structure de leurs solutions aqueuses denses. Il est donc naturel de penser qu'il en est de même pour la structure des solutions aqueuses de PECs.

Complexes de Polyélectrolytes

Les complexes de polyélectrolytes (PECs) auxquels nous nous intéressons sont formés de l'association de deux polyélectrolytes de charges opposées. Ils représentent des systèmes plus compliqués que les PEs et les propriétés de leurs solutions aqueuses dépendent de la nature des polyélectrolytes, de leur rigidité intrinsèque, ainsi que d'autres paramètres comme la force ionique, la température, voire la méthode de préparation des solutions. Les PECs peuvent présenter différentes formes, qui ne sont pas toujours à l'équilibre thermodynamique. Le processus de formation des PECs est contrôlé par deux facteurs: un facteur enthalpique correspondant à l'interaction électrostatique attractive entre les charges positives et négatives des macroions; un facteur entropique associé au relargage des contreions condensés dans la solution. On peut évidemment contrôler la thermodynamique et la cinétique de la réaction de complexation en faisant varier la force ionique de la solution par addition d'un sel. La contribution entropique ΔS est toujours positive mais diminue avec l'accroissement de la force ionique. Au contraire, le terme enthalpique ΔH, ou ΔE, peut être positif ou négatif. Quand la force ionique est faible, le terme enthalpique ΔH est négatif et la complexation est exothermique. Lorsque la force ionique est grande, ΔH devient positif et la complexation est endothermique.

On doit remarquer que la formation des PECs conduit souvent à une séparation de phases macroscopique. Ce phénomène de démixtion est observé dans plusieurs processus naturels et est important d'un point de vue pratique. En fait, nous ne connaissions pas vraiment les

paramètres contrôlant l'étendue des domaines monophasique et biphasique des diagrammes de phases. Nous rappelons dans ce chapitre les principaux travaux théoriques et les principales simulations numériques qui décrivent la thermodynamique de la complexation entre deux polyélectrolytes de charges opposées et les diagrammes de phases des solutions aqueuses de PECs. Cela recouvre les travaux de Overbeek-Voorn; Lee, Popov et Fredrickson; Zhang et Shklovskii; Krotova, Vasileska et Khokhlov; Veis et Aranyi et etc. On peut classer les structures formées par la complexation de deux polyélectrolytes de charges opposées en trois groupes principaux: les complexes solubles, les coacervats et les complexes denses. En fonction de l'aspect visuel et du contenu en eau, la dernier groupe inclut les précipitations solides ou sédimentations et les phases turbides ou gels.

Chapitre 3. Synthèses, Caractérisations et Préparations des solutions de PEs et PECs

Les propriétés des PEs et des PECs dépendent de nombreux paramètres. Nous nous sommes intéressés principalement à l'effet de la rigidité intrinsèque des polyions sur la thermodynamique de la formation des complexes et la structure de leurs solutions aqueuses. Toutefois, nous avons également abordé les influences de la force ionique et de la méthode de préparation des solutions aqueuses de PECs. Corrélativement, nous avons fixé ou laissé de côté d'autres paramètres, comme la température, et d'autres caractéristiques des polyions, comme leurs masses molaires moyennes (M_N, M_W), ou degrés de polymérisation moyens (N_N, N_W), leurs indices de polymolécularité ($I=M_W/M_N$) et leurs fractions de charge chimique (f, fixées à 1). Nous avons réalisé la sulfonation complète de plusieurs chaînes de polystyrène (hydrogéné PS_h ou deutérié PS_d) et de poly(α-méthyl styrène) (PαMS) ainsi que la synthèse de chaînes de poly(chlorure de diallyldiméthyl ammonium) (PDADMAC). Les chaînes de hyaluronate de sodium (HANa) nous ont été fournies gracieusement par la société Soliance (France). Nous avons caractérisé tous ces PEs en utilisant la RMN du proton, la chromatographie d'exclusion stérique multidétection (SEC multidétection), la thermogravimétrie (TGA) et la diffusion de rayons X aux petits angles (SAXS). Les longueurs de persistance non électrostatiques, l_p^0, des polyions sont: 1 nm, pour le PSS; 2.5 nm, pour le PαMSS; 3 nm, pour le PDADMA; 9 nm, pour le HA. Les polyions sont donc flexibles (PSS) ou semi-flexibles (PαMSS, PDADMA and HA). Ils sont aussi fortement chargés (ce qui implique un pH$\approx$7 pour le HA), et parfaitement hydrophiles. En effet, la fraction de charge chimique de tous ces polyions est proche de l'unité (f=1)

Nous avons déterminé les longueurs de persistance non électrostatiques de certaines macromolécules à partir de l'analyse de données de diffusion de lumière statique (DLS), obtenues en solvant Thêta, et de SAXS, obtenues en bon solvant, en tenant compte en particulier de la polymolécularité et en améliorant certaines analyses antérieures réalisées par d'autres chercheurs. Les principales caractéristiques des polyélectrolytes étudiés dans cette thèse, sont données dans un tableau de ce chapitre.

Les solutions aqueuses « mères » de PEs ont été préparées directement par addition d'eau à une poudre de polyélectrolyte dont la teneur en eau était connue au préalable. Leurs concentrations ont été contrôlées, ou déterminées, par pesées. Les solutions aqueuses de PECs ont été préparées en mélangeant deux volumes égaux de solutions mères de PEs de charges opposées. Différentes procédures pour réaliser ces mélanges ont été considérées.

La portée des interactions électrostatiques pendant la formation des complexes a été modifiée en faisant varier la force ionique des solutions « mères » de PEs avant mélange par addition d'un sel monovalent (NaCl). La concentration en sel était fixée à 0.15 mol/l, ce qui correspond aux solutions physiologiques.

Chapitre 4. Techniques expérimentales et analyses des données

Pour étudier les solutions aqueuses de PEs et de PECs, nous avons utilisé plusieurs techniques expérimentales. Tout d'abord, les diagrammes de phases, ou d'états, des solutions de PECs ont été établis par observations visuelles. Ont été distinguées: les zones monophasiques; les zones biphasiques; les gels; les coacervats. Les séparations de phases macroscopiques durant la complexation ont été suivies avec attention. L'analyse du processus de complexation a été faite en solution diluée en utilisant la titration calorimétrique isotherme (ITC), la diffusion dynamique de la lumière (DLS) et des mesures de potentiel zêta. Avec cette approche expérimentale, nous avons pu observer le processus de complexation de PEs de charges opposées, en étudiant les changements thermodynamiques, la taille et la charge des complexe ainsi que leurs rapports de charges [+]/[-], et en déterminant une constante de complexation, K, une enthalpie de complexation, ΔH, la stoechiométrie des complexes, n, les variations d'énergie libre, ΔG, et d'entropie, ΔS, associées à la complexation. La structure des solutions de PECs a été étudiée principalement dans les régimes semidilué et concentré, en combinant les techniques de diffusion de rayons X et de neutrons aux petits angles (*SAXS* et

SANS). Ces deux techniques sont équivalentes du point de vue de la résolution spatiale. Mais, les complexes étant des systèmes hétérogènes, l'utilisation de la technique SANS a permis d'augmenter la résolution chimique (marquage spécifique et variation de contraste). Des images dans l'espace réel des complexes PDADMAC-PSSNa et PDADMAC-HANa ont été obtenues par cryo-microscopie électronique en transmission (cryo-TEM). Toutes les techniques expérimentales sont décrites en rappelant les principales méthodes d'analyse des données auxquelles elles conduisent.

Chapitre 5. Solutions Aqueuses d'Hyaluronate de sodium

Les solutions aqueuses de PSSNa, PDADMAC et PαMSSNa ont été largement étudiées ces dernières années et leur structure est assez bien décrite dans la littérature. Au contraire, la structure des solutions d'hyaluronate de sodium (HANa), ou d'hyaluronane (HA), est moins bien répertoriée dans la littérature, avec des articles souvent contradictoires. Pourtant, ayant d'importantes applications, le HA a fait l'objet de nombreux travaux. Toutefois, ils ne conduisent pas à une description précise et définitive de ses propriétés. L'étude de la conformation moyenne de ce biopolymère en solution est en fait rendue délicate par l'existence de phénomènes d'auto-assemblage, via les liaisons hydrogène, voire la celle de réseaux ou de doubles hélice. La préparation d'une solution de HA réclame donc un soin particulier. Pour examiner la structure des complexes HANa-PDADMAC, la caractérisation des solutions aqueuses de HANa, provenant de surcroît de l'industrie (société Soliance), était donc un préalable nécessaire.

Nous nous sommes d'abord intéressés aux solutions aqueuses diluées de HANa en présence de sel ajouté afin d'étudier la conformation moyenne des polyions HA après écrantage des interactions électrostatiques et mesurer en particulier leur rigidité intrinsèque.

Par diffusion de rayonnement aux petits angles, deux méthodes existent pour déterminer la longueur de persistance, l_p, d'une macromolécule linéaire. Ces deux méthodes correspondent à des explorations de domaines de vecteurs de diffusion, q, distincts. Dans le domaine de Guinier ($qR_g < 1$), on mesure un rayon de giration, R_g, et de sa valeur, ou mieux de sa variation avec la masse moléculaire, M, des macromolécules, on en déduit la longueur de persistance, l_p. Il faut toutefois prendre soin d'éliminer au préalable, ou de pouvoir négliger, les corrélations intermoléculaires afin d'extraire le facteur de forme des macromolécules des mesures

d'intensité diffusée, et respecter certaines conditions relevant des approximations du modèle que l'on utilise pour déterminer l_p. Aux plus grands vecteurs de diffusion q, soit les domaines intermédiaire et asymptotique (respectivement $1/R_g < q < 1/l_p$ et $ql_p > 1$), on peut obtenir la longueur de persistance en analysant le factor de forme des macromolécules en utilisant respectivement le modèle de chaîne gaussienne ou celui de chaîne à longueur de persistance, ou de Porod-Kratky. Après les avoir présenté nous avons utilisé ces modèles, qui décrivent la conformation moyenne des macromolécules linéaires en négligeant les effets de volume exclu, pour analyser successivement les données relatives aux mesures de rayon de giration trouvées dans la littérature et celles résultant de nos propres caractérisations par SEC des chaînes de HANa de la société Soliance et évaluer la longueur de persistance non électrostatique des polyions HA. Pour comprendre, voire réduire, la dispersion des valeurs de l_p de la littérature, nous avons corrigé certaines analyses de données relatives à des mesures de rayon de giration en tenant compte de la polymolécularité. Cela nous a conduit à un ensemble de valeurs dans le domaine $70 < l_p < 110$ Å. Nous avons comparé ces valeurs à celles pouvant être extraites des mesures de viscosité intrinsèque, sans grand succès. Finalement, nous avons montré qu'il était impossible de décrire nos mesures de rayon de giration réalisées par SEC multidétection avec l'éluant H_2O + 0.1M $NaNO_3$ par les modèles de conformation macromoléculaire usuels, et en particulier le modèle de Porod-Kratky. L'élution est en effet incorrecte avec cet éluant, chaque fraction ne correspondant pas à une masse moléculaire unique. Ainsi, pour les expériences de SEC visant à déterminer la longueur de persistance non électrostatique du HA, il semble préférable d'utiliser comme éluant H_2O + 0.1 M NH_4NO_3 plutôt que H_2O + 0.1 M $NaNO_3$.

L'approche alternative par diffusion des rayons X aux petits angles (SAXS) utilise la mesure du facteur de forme des polyions HA en solution aqueuse diluée en présence de sel ajouté (0.3 M NaCl). Nous avons ainsi déterminé la longueur de persistance non électrostatique l_p^0 du HA en appliquant la relation $l_p = 3.5/q^*$, où q* représente le vecteur de diffusion à partir duquel on observe la loi caractéristique en q^{-1} associée au modèle de Porod-Kratky. Un paramètre ajustable est alors la masse par unité de longueur, M_L, des chaînes, ou encore la longueur de contour, a, des monomères. Nous avons obtenu, via la représentation de Holtzer du facteur de forme: $l_p^0 = 87.5$ Å et $a = 11.1$ Å. Aux plus grands vecteurs de diffusion ($q > 0.08$ Å^{-1}), nous avons également mesuré le rayon de giration de la section des chaînes, $R_c = 3.6$ Å. Les mesures, faites à des concentrations supérieures à la concentration critique de recouvrement des chaînes (c > c*) soit dans le régime semi-dilué, ont permis finalement d'établir la loi

d'échelle reliant la longueur de corrélation à la concentration caractéristique du régime semidilué: ξ (Å) = 2.068*[c (mol/l)]$^{-0.77}$.

Les expériences SAXS réalisées à partir de solutions aqueuses denses en absence de sel ajouté, nous ont permis de mettre en évidence l'existence d'un ordre d'orientation (ordre nématique local), soit une transition d'Onsager. Cette transition est particulière aux polyélectrolytes semiflexibles et intervient dans un domaine de vecteurs de diffusion qui succède, non pas directement au régime isotrope concentré comme on pourrait s'y attendre avec la transition d'Onsager, mais à une phase métastable dans laquelle les interactions électrostatiques, même faibles, jouent encore un rôle. Cette phase correspond à un régime que l'on peut qualifier de frustré et son existence confirme les premières expériences réalisées par P. Lorchat et ses collaborateurs à partir des solutions aqueuses de PDADMAC et de PαMSSNa.

Chapitre 6. Complexes Poly(chlorure de diallyldimethylammonium) - Poly(styrène sulfonate) de Sodium

Nous avons étudié les complexes PDADMAC-PSSNa successivement en solutions diluées et semidiluées, voire concentrées. Nous avons pour cela utilisé plusieurs techniques expérimentales.

Chapitre 6.1. Complexes PDADMAC-PSSNa en solutions aqueuses diluées

L'étude du processus de complexation ainsi que la taille et la charge des complexes en régime dilué, en absence et présence de sel monovalent ajouté, a été réalisée en combinant des mesures de titration calorimétrique isotherme (ITC), de diffusion dynamique de la lumière (DLS) et de potentiel zêta.

L'interaction entre polyions PDADMA et PSS en solutions aqueuses dilués (c ≈ 0.01 mol/l) a été étudiée par ITC pour différentes force ioniques (deux cas: 0 et 0.15 M NaCl) sur les domaines de rapports de charge électrostatique $0 < z = [-]/[+]$ ou $z=[+]/[-] < 2$. Ces mesures étaient corrélées à des mesures de potentiel zêta, ζ, et de rayon hydrodynamique, R_H. Elles ont également été faites en titrant le polycation avec le polyanion (mélange directe) et vice-versa, en titrant le polyanion avec le polycation (mélange inverse).

Nous avons proposé pour décrire la complexation entre macroions PSS et PDADMA en solution aqueuse diluée un processus à deux étapes. La première étape ($0 < z < 1$) correspond à la formation de complexes primaires fortement chargés de taille comprise entre 73 et 105 nm. Le signe de la charge effective des complexes est alors: négatif, lorsque la solution de PDADMAC est ajoutée à la solution de PSSNa; positif, lorsque la solution de PSSNa est ajoutée à la solution de PDADMAC. La deuxième étape commence aux alentours de la stoechiométrie de charge, $z = 1$, (dans le domain$1 < z < 2$) ou plus tôt, $z < 1$, voire dès le début du titration (dans l'ensemble du domaine exploré $0 < z < 2$). La taille des agrégats secondaires, qui sont stables dans la solution, est plus grande que 190-200 nm. De surcroît, les plus grands agrégats sédimentent.

Les paramètres thermodynamiques associés à la complexation ont été calculés par ajustements des isothermes à un thermogramme modèle faisant intervenir deux sites indépendants, n'interagissant pas. La formation des complexes est exothermique, indépendamment de la méthode de préparation des solutions de PECs et de leur force ionique. L'enthalpie de la première étape est positive et diminue en présence de sel ajouté car les interactions électrostatiques sont alors écrantées. L'entropie de la seconde étape est positive et l'agrégation des PECs est gouvernée par l'entropie. Ce type d'interactions appartient au phénomène de compensation « entropie–enthalpie ».

L'enthalpie (de -2.9 à -7.4 kJ/mol), le rayon hydrodynamique (de 86 à 105 nm) et la charge effective ou le potentiel ζ (de -30 à -46 mV ou de +45 à +47 mV) ont des valeurs différentes suivant le type de titration (mélange direct ou inverse). Cela montre que les complexes résultant des interaction électrostatiques entre le poly(chlorure de diallyldimethyl ammonium) et le poly(styrène sulfonate de sodium) sont hors-équilibre.

Chapitre 6.2. Complexes PDADMAC-PSSNa en solutions aqueuses semidiluées et concentrées

L'étude de la structure des complexes PDADMAC-PSSNa formés en solutions aqueuses semidiluées et concentrées, en absence et présence de sel monovalent ajouté, a été réalisée principalement en combinant des mesures de diffusion de neutrons et de rayons X aux petits angles (SAXS et SANS).

Diagrammes de Phases ou d'États

Afin d'étudier les solutions aqueuses des complexes formés entre le polycation PDADMA et les polyanions PSS et PαMSS sur un large domaine de concentrations, nous avons tout d'abord établi des diagrammes de phases par observation visuelle. Comme les complexes PDADMAC-PSSNa et PDADMAC-PαMSSNa ne sont pas forcément à l'équilibre thermodynamique, nous préférons parler de diagrammes d'états plutôt que de diagrammes de phases. On y distingue les régions biphasiques des régions monophasiques et les phases liquides transparentes des phases liquides turbides (colloïdes ou coacervats). Ces diagrammes d'états se réduisent à deux dimensions, avec deux axes associés aux concentrations du polycation (les ordonnées) et du polyanion (les abscisses). Les concentrations étant exprimées en mol/L et les monomères des deux polyélectrolytes étant tous ionisés, la ligne de stoechiométrie de charge ($z = [+]/[-] = 1$) correspond alors à la première bissectrice des diagrammes d'états. De façon générale, les états n'évoluent plus au bout d'environ deux semaines après la préparation des solutions de PECs. L'allure de ces diagrammes pour les complexes PDADMAC-PSSNa et PDADMAC-PαMSSNa (polyanions encore assez flexibles) est en accord avec ce que prévoient les théories de champ moyen et les simulations numériques pour les PECs formés de deux PEs flexibles. En particulier, une augmentation de la force ionique réduit l'étendue des régions biphasiques. Aux plus fortes concentrations ($c > 0.05$ mol/L), on observe une séparation de phases « liquide - liquide » avec une phase turbide riche en polymère, qui contient des « flocs» (agrégats gélifiés ou gel) et une phase transparente pauvre en polymère, qui reste néanmoins visqueuse. Lorsque la concentration diminue, la phase riche en polymère évolue vers une phase de coacervats et on observe un phénomène de sédimentation, voire de précipitation (les coacervats sont plus denses que les flocs). Dans ce cas, la séparation de phases devient de type « solide – liquide ». On n'observe les régions monophasiques qu'aux faibles concentrations ($c < 0.05$ mol/L) ou lorsque les rapports de charge, z, s'écartent franchement de l'unité, c'est-à-dire loin de la ligne de stoechiométrie de charge dans les diagrammes d'états. Ce sont les macroions libres qui s'opposent alors à la séparation de phases macroscopique. Les états des régions biphasiques, qui résultent de séparations de phases macroscopiques, dépendent légèrement de la méthode de préparation des solutions de PECs. La comparaison des diagrammes relatifs aux complexes PDADMAC-PSSNa et PDADMAC-PαMSSNa suggère une influence de la rigidité intrinsèque du polyanion. Le diagramme d'états des complexes PDADMAC-PαMSSNa est ainsi moins symétrique, par rapport à la ligne de stoechiométrie de charge, que celui des complexes PDADMAC-PSSNa.

Complexation entre polyélectrolytes de charges opposées: analogie avec un processus de gélification

Aux plus fortes concentrations (régimes semidilué et concentré), on peut décrire la complexation entre deux polyélectrolytes de charges opposées comme un processus de gélification. On rappelle que dans le régime semidilué ou concentré, la structure d'une solution aqueuse de polyélectrolyte se décrit comme un réseau temporaire (avec une maille de taille ξ) constitué par l'interpénétration des polyions. C'est le modèle isotrope proposé par P.-G. de Gennes et ses collaborateurs. À la résolution spatiale ξ, la conformation des polyions correspond à une marche par hasard sur réseau. Ce réseau peut également être considéré comme le bain de réaction pour la complexation avec un polyélectrolyte de charge opposée. Le processus de complexation devient alors analogue à un processus de gélification dans lequel les ponts interchaînes, ou jonctions, résultent des interactions électrostatiques attractives entre monomères des polyanions et polycations. De surcroît, les interactions électrostatiques sont suffisamment fortes pour assurer des durées de vie aux jonctions suffisamment longues. De cette manière, le polyion du polyélectrolyte de charge opposée à celui constituant le bain de réaction joue un rôle d'agent gélifiant qui, en formant des ponts électrostatiques interchaînes, contribuent à l'élasticité. Les polyions du polyélectrolyte de charge opposée peuvent être décrits comme des marches au hasard supplémentaires liées à celles associées aux polyions du bain de réaction par de simples points d'attache, ou « Tie-points » (cas A). Toutefois, les jonctions ou ponts interchaînes peuvent également impliquer de plus longues séquences chimiques des deux polyélectrolytes de charges opposées (cas B). Les deux cas, A et B, sont évidemment reliés à la rigidité intrinsèque des polyions: le cas A valant pour les polyions flexibles; le B, pour les polyions semi-rigides ou rigides. À ce stade, nous pouvons noter que si les concentrations des solutions de PEs initiales sont égales, un mélange équivolumique de ces solutions conduira à une solution de PECs de concentration équivalente et donc à une taille ξ de maille qui peut être proche de celles associées aux solutions de PEs initiales, mais qui sera différente suivant que l'on considère le cas A ou le cas B. Avec le cas B, on s'attend aussi à ce que les charges électrostatiques portées par les polyions soient davantage neutralisées que pour le cas A.

Comme pour tout gel, les jonctions, provenant de la complexation entre polyions de charges opposées, vont avoir tendance en pratique à former des hétérogénéités de grande taille. Celles-ci vont se superposer à la structure en réseau décrite précédemment. De tels hétérogénéités peuvent correspondre à l'existence de larges régions de l'espace où la densité de noeuds électrostatiques est plus grande que dans d'autres (fluctuations de concentrations

additionnelles). Elles sont alors de nature statistique (structures fractales ou ramifiées). Mais, elles peuvent également correspondre à des clusters provenant du caractère mauvais solvant de l'eau pour les jonctions, ou nœuds électrostatiques (résultant des interactions électrostatiques attractives entre monomères de charges opposées). Ces clusters peuvent avoir une géométrie bien définie, avec une interface. Mais ils peuvent aussi être ténus et s'interpénétrer partiellement. Dans les deux cas, ils peuvent être polydisperses en forme ou en taille et, suivant leur compacité, conduire à une turbidité du gel.

Lorsque les clusters tendent à précipiter, il y a une compétition entre gélification et précipitation qui conduit à une séparation de phases macroscopique entre phases sol et gel. Ce processus est également observé dans les solutions aqueuses semidiluées de PECs.

Nous avons utilisé cette analogie pour comprendre et comparer les structures des complexes: PDADMAC-PSSNa et PDADMAC-HANa, via l'analyse des diagrammes SAXS et SANS de leurs solutions aqueuses. Les différences entre les deux PECs sont principalement reliées à la différence de rigidité intrinsèque des deux polyanions PSS et HA. Cette analogie entre la complexation de PEs de charges opposées en régimes semidilué et concentré et la gélification est essentielle pour comprendre les résultats de SAXS et SANS.

En se basant sur cette analogie, on peut facilement prévoir que l'intensité diffusée par les PECs est différente de l'intensité diffusée par une solution semidiluée, ou concentrée, de polymères ou de polyélectrolytes. La fonction de corrélation, ou de structure, d'une solution semidiluée de polymère neutre présente principalement deux régimes. Dans le domaine de vecteurs de diffusion $q\xi < 1$, $S(q)$ est, en représentation log-log, une courbe presque plate (empilement compact de blobs de taille ξ). Dans le domaine de vecteurs de diffusion $q\xi > 1$, $S(q)$ se réduit au facteur de forme $g_1(q)$ qui, pour une macromolécule neutre et au delà du domaine de Guinier ($qR_g > 1$), est proportionnel à $q^{-1/\nu}$ (ν est alors l'exposant de volume exclu) si l'on néglige la conformation locale.

Pour les solutions de polyélectrolytes, en régime semidilué et en absence de sel ajouté, la répulsion électrostatique à longue portée entre monomères conduit à un trou de corrélation dans le cadre du modèle isotrope qui a comme conséquence l'existence d'un maximum pour la fonction de corrélation, $S(q)$, à un vecteur de diffusion $q^* = 2\pi/\xi$. ξ est toujours la longueur de corrélation dans l'espace direct, ou la taille de la maille du réseau temporaire formé par l'interpénétration des polyions. Au-delà de ce maximum, $S(q)$ tend vers le facteur de forme des

polyions, lequel se décrit soit avec une statistique de Gauss, soit avec le modèle de chaîne à longueur de persistance, ou modèle de Porod-Kratky avec éventuellement un terme d'épaisseur, ou de section, si l'on tient compte de la rigidité locale des polyions.

Aux faibles vecteurs de diffusion (dans la limite thermodynamique $q \to 0$), $S(q)$ est relié à la compressibilité osmotique $X_T = \frac{1}{c}\frac{\partial c}{\partial \Pi}$ de la solution. Toutefois, pour un gel associé à un PEC, la présence d'hétérogénéités (clusters ou fluctuations de concentration de grande amplitude) conduit à une remontée de l'intensité diffusée aux plus petits angles (un « upturn »).

En principe, l'intensité diffusée par le réseau primaire, ou la solution semidiluée constitutive, doit également être considérée. Cependant, dans ce domaine de vecteurs de diffusion q, le signal du réseau est beaucoup plus faible que celui associé aux hétérogénéités, sauf dans la région de crossover $q \approx \frac{1}{\xi}$, où une Lorentzienne est toujours observable pour les solutions de polymères neutres ou celles de polyélectrolytes en présence de sel ajouté. Pour les solutions de polyélectrolytes en absence sel, c'est le pic polyélectrolyte qui devrait être observé. Finalement, dans le domaine $q > \frac{1}{\xi}$, c'est la conformation moyenne des macroions à l'intérieur les blobs de concentration du réseau primaire, ou de la solution semidiluée constitutive, qui est explorée. On retrouve alors la diffusion précédemment décrite pour les solutions semidiluées.

Pour présenter l'influence des hétérogénéités sur les fonctions de diffusion, ou de corrélation, des solutions semidiluées ou concentrées, nous avons utilisé un modèle dans lequel les hétérogénéités sont décrites comme des étoiles Gaussiennes monodisperses. La compacité, ou densité interne, peut alors être modifiée facilement en changeant la fonctionnalité des étoiles. La solution semidiluée, ou concentrée, de polyélectrolytes est, elle, décrite en utilisant le champ moyen (RPA). En négligeant les corrélations intermoléculaires, la fonction de diffusion des clusters, $S_{cluster}(q)$, se réduit au facteur de forme d'une étoile Gaussienne.

Avec ces deux fonctions de corrélation, nous pouvons proposer un modèle approximatif pour la fonction de structure d'un gel résultant de la complexation de deux polyélectrolytes de charges opposées, en solution semidiluée ou concentrée. Le terme croisé étant négligé, on peut en effet utiliser une équation simple:

$$\frac{S_{Gel}(q)}{c} = g(q,c) = \Phi \frac{S_{cluster}(q)}{c_{cluster}} + (1-\Phi)\frac{S(q,c)}{c}$$

où Φ et $(1-\Phi)$ sont les fractions volumique des deux milieux (clusters et réseau constitutif).

Nous avons présenté des exemples de fonctions de corrélation, $S_{Gel}(q)$, relatives à des gels ayant 5% d'hétérogénéités de compacités distinctes, en variant la fonctionnalité de l'étoile Gaussienne les représentant (f = 5 ou f = 100), et en considérant l'absence ou la présence d'un sel monovalent ajouté (n = 0 ou 0.15 mol/L). En règle générale, au-delà de q = 0.001 Å^{-1}, deux régimes sont observés: un premier, qui correspond au domaine de vecteurs de diffusion q intermédiaire du facteur de forme des clusters; un second, qui correspond au domaine de vecteurs de diffusion q asymptotique, lequel est associé au facteur de forme des polyions. En absence de sel ajouté, entre ces deux régimes, on retrouve le pic polyélectrolyte caractéristique d'une solution semidiluée ($q*$ proche de $2\pi/\xi$). Lorsque les hétérogénéités sont de plus faible taille, leur domaine de Guinier se déplace vers les plus grands vecteurs de diffusion (0.01 au lieu de 0.001 Å^{-1}) et masque leur domaine intermédiaire.

Résultats des expériences SAXS et SANS

Les résultats expérimentaux obtenus par SAXS et SANS ont confirmé ce modèle de structure pour les complexes PDADMAC-PSSNa, soit un réseau constitutif de polyélectrolytes interpénétrés et des hétérogénéités immergées dans ce réseau. Nous nous sommes concentrés sur les complexes situés sur les lignes de stoechiométrie de charge des diagrammes d'états, de manière à pouvoir négliger a priori l'existence de chaînes libres. Nous avons ainsi étudié séparément la structure de cinq « gels » et de cinq « liquides transparents » issus de solutions de PECs se situant sur les lignes de stoechométrie de charge. Les intensités diffusées par SAXS et SANS ont certaines caractéristiques similaires et d'autres différentes. Dans les deux cas, un maximum, ou « pic polyélectrolyte », est observé à un vecteur de diffusion $q*$ aussi bien pour les « gels » que pour les « liquides transparents » issus de solutions de PECs formés en absence de sel ajouté. Ce maximum disparaît ou diminue très fortement en présence de sel ajouté. Au-delà de ce pic (q > 0.25 Å^{-1}), l'intensité diffusée par SAXS décroît en q^{-4}. Cette décroissance en q^{-4} est associée au facteur de forme des contreions condensés sur les deux polyions (et plus particulièrement les contreions Na$^+$ condensés sur les polyions PSS$^-$). La même loi de puissance avait été observée par P. Lorchat, en étudiant les solutions aqueuses denses de PSSNa. Par SANS, on observe une loi de puissance en q^{-2} à la place de cette loi en q^{-4}. Cela n'est pas surprenant puisque le signal est alors dominé par les polyions, la contribution des contreions étant négligeable pour les expériences de SANS. Ces décroissances en q^{-4} (SAXS) et q^{-2} (SANS) sont indépendantes de la force ionique (présence ou l'absence de sel ajouté) et de la phase considérée (« gel » ou « liquide transparent »). Elles sont également indépendantes de la concentration des solutions de PECs initiales. De surcroît, les intensités

diffusées normées à la concentration se superposent parfaitement. Cela indique que la conformation moyenne des chaînes de polyélectrolytes, reste identique pour tous les complexes, quelle que soit la concentration de la solution semidiluée, ou concentrée, initiale.

Les positions des maxima, ou pics polyélectrolytes, relatifs aux deux phases (« gel » et « liquide transparent » sont identiques et ne dépendent que de la concentration, c, des solutions de PECs initiales. Cette observation montre que la structure des réseaux constitutifs des deux phases « gel » et « liquide transparent » est similaire, avec une maille de taille ξ ne dépendant que de c. Le fait que les conterions condensés ne contribuent pas au signal SANS a comme conséquence que la position q^* du pic polyélectrolyte mesurée par SANS est légèrement différente de celle déterminée par SAXS. Dans le domaine de concentrations étudié, q^* augmente avec c suivant une loi d'échelle caractéristique des solutions de polyélectrolytes en régime semidilué, $q^* \sim c^{1/2}$.

En présence de sel ajouté (NaCl), le maximum disparaît complètement et, dans le domaine $0.025 < q < 0.25$ Å^{-1}, l'intensité diffusée correspond au signal caractéristique d'une solution semidiluée de polymère neutre (décroissance Lorentzienne, ou d'Ornstein-Zernike).

Aux plus petits angles, c'est évidemment le signal des clusters, ou hétérogénéités des gels qui dominent. Ainsi, le expériences SAXS et SANS dans le domaine $0.013 < q < 0.025$ Å^{-1}, conduisent à une décroissance de l'intensité diffusée en $q^{-\alpha}$ avec α de -1.7 à 4. Ces hétérogénéités de grande dimension (> 300 nm) sont introduites dans le réseau de polyélectrolytes interpénétrés via la complexation entre monomères de charges opposées qui constituent des nœuds physiques, encore dénommés ponts ou jonctions électrostatiques, des gels et leurs associations. En absence de sel ajouté, l'intensité diffusée des gels décroît suivant une loi de puissance d'exposant $\alpha = 4$. Pour l'intensité diffusée des « liquides transparents », qui sont moins visqueux et moins denses macroscopiquement que les flocs, l'exposant de la loi de puissance est légèrement plus faible: $\alpha = 3.4$ au lieu de 4. En présence de sel ajouté, l'exposant se réduit à 1.7. Le domaine de vecteurs de diffusion $q < 0.013$ Å^{-1} n'a été exploré qu'avec la technique SANS. Dans ce domaine, l'intensité diffusée des gels décroît suivant la loi de puissance $q^{-2.5}$. Cela correspond à une loi précédemment observée pour des hétérogénéités fractales. Finalement, le domaine de Guinier de ces hétérogénéités était inaccessible avec les diffractomètres de nos expériences SAXS et SANS.

En conséquence, pour les complexes PDADMAC-PSSNa en régimes semidilué et concentré, deux échelles spatiales sont à considérer: la première correspond au réseau des deux

polyélectrolytes interpénétrés, $q > 0.02$ Å^{-1}; la seconde, aux clusters ou hétérogénéités, $q < 0.02$ Å^{-1}. Ces observations sont en parfait accord avec l'analogie que nous avons proposée entre processus de complexation et de gélification. Cette architecture à deux niveaux rappelle le processus en deux étapes proposé dans le régime dilué pour l'analyse de nos mesures de titration calorimétrique isotherme (ITC), diffusion dynamique de la lumière (DLS) et potentiel zêta. Dans le régime dilué, l'interaction entre polyions poly(diallyldiméthyl ammonium) et poly(styrène sulfonate) conduit à la formation de complexes primaires qui, dans une seconde étape, s'agrègent. Dans les régimes semidilué et concentré, on peut considérer que la formation de jonctions, nœuds physiques ou complexes électrostatiques entre monomères de charges opposées, constitue une première étape, qui est suivie du seconde étape correspondant à la formation de clusters principalement dus à l'agrégation des jonctions.

Par SANS, nous avons également mesuré les fonctions de structure, ou de corrélation, partielles des deux macroions PSS et PDADMA. Pour cela, nous avons considéré des complexes PSS$_d$Na-PDADMAC, formés de chaînes de PSSNa deutéré et de chaînes de PDADMAC hydrogéné, et utilisé différents mélanges H$_2$O-D$_2$O comme solvants (méthode d'effacement du contraste). Les mesures faites sur des solutions de PSS$_d$Na-PDADMAC dans 100% de D$_2$O ont permis de déterminer la fonction de structure partielle du polycation PDADMA et donné une information sur la structure des chaînes de PDADMA dans les complexes. Les mesures faites sur les solutions de PSS$_d$Na-PDADMAC dans un mélange H$_2$O-D$_2$O de fraction volumique de D$_2$O de 3% ont, à l'inverse, permis d'évaluer la fonction de structure partielle du polyanion PSS et donné une information sur la structure des chaînes de PSS dans les complexes. Avec le même complexe PSS$_d$Na-PDADMAC dans un mélange H$_2$O-D$_2$O de fraction volumique en D$_2$O de 55%, c'est une combinaison linéaire des trois fonctions de structure partielles (terme croisé inclus) qui est mesurée. La contribution des contreions condensés est négligeable dans les trois situations de contraste.

Les fonctions de corrélation partielles du PDADMA et du PSS présente une décroissance en q^{-2} identique dans le domaine $q > 0.15$ Å^{-1}. La même loi de puissance est observée pour l'ensemble du complexe et attribuée au signal d'un brin de polyélectrolyte du réseau constitutif. Les conformations locales du PSS et du PDADMA observées aux plus grands vecteurs de diffusion, sont semblables. Cela indique que les deux polyions participent au réseau constitutif. Celui-ci est donc bien formé des deux polyélectrolytes interpénétrés. Le modèle de structure en échelle des complexes, dans lequel les polyions de charges opposées sont parallèles et en forte interaction, est donc improbable, ou irréaliste. Nos résultats montrent que la structure des

complexes PDADMAC-PSSNa est plutôt proche du modèle de structure en « œufs brouillés » proposé par la théorie et les simulations. Corrélativement, dans les gels et en absence de sel, les fonctions de structure partielles des deux polyions présentent un pic polyélectrolyte aux vecteurs de diffusion intermédiaires. Cela nous indique en particulier qu'un grand nombre de monomères restent chargés, ou qu'ils ne sont pas neutralisés, lors de la complexation entre polyions de charges opposées. La position du pic, qui résulte de la répulsion entre polyions, est relié à la longueur de corrélation, ξ, ou la taille de la maille du réseau constitutif. Dans le domaine des faibles vecteurs de diffusion (q < 0.02 Å^{-1}), les fonctions de corrélation du PDADMA présentent deux décroissances successives en q$^{-2.5}$ et q^{-4}, qui sont reliées aux hétérogénéités et à leur structure. Les polyions PDADMA sont donc présents dans les hétérogénéités des gels. Dans le même domaine de vecteurs de diffusion, les fonctions de corrélation du PSS n'ont qu'une décroissance en q$^{-2.5}$. Aussi bien dans la phase « liquide transparent » que dans la phase « gel », les fonctions de corrélation du PSS présente toujours un pic polyélectrolyte. Pour le PDADMA, ce maximum est absent et remplacé par un quasi-plateau s'étendant dans le domaine 0.02 < q < 0.09 Å^{-1}. Cette observation pourrait résulter d'une contribution plus importante des hétérogénéités à la fonction de corrélation partielle du PDADMA, mais également d'un écrantage plus fort de l'interaction électrostatique entre polycations, voire d'une neutralisation plus importante des monomères du PDADMA. La comparaison des amplitudes des fonctions de structure partielles montre que le PDADMA n'est pas distribué de manière uniforme entre les deux phases. Il y a davantage de PDADMA dans le « flocs » quelle que soit la force ionique des solutions de PECs initiales. Par contre, les chaînes de PSS sont distribuées de façon quasi-équivalente entre les deux phases et la position q* du pic polyélectrolyte de la fonction de corrélation du PSS est la même dans les deux phases.

Rôle de la méthode de préparation des PECs

La complexation entre polyions PSS et PDADMA en solution aqueuse semidiluée ou concentrée peut se décrire comme un processus de gélification. Ainsi, la structure des solutions de ces complexes ressemble à celle d'un gel ou d'un prégel. Comme la structure d'un gel dépend le plus souvent de la méthode de préparation, nous avons étudié l'effet de la méthode de préparation des PECs sur leur structure. Les solutions des complexes PDADMAC-PSSNa ont ainsi été préparées de trois manières distinctes: ou bien la solution de PDADMAC était ajoutée à celle de PSSNa; ou bien, au contraire, la solution de PSSNa était ajoutée à celle de PDADMAC; ou bien finalement les deux solutions de PSSNa et de PDADMAC étaient mélangées simultanément.

Cinq concentrations (0.10 M, 0.15 M, 0.20 M, 0.25 M, 0.30 M) ont été considérées pour des solutions de PECs, en absence et en présence de sel ajouté, situées sur la ligne de stoechiométrie de charge des diagrammes d'états. Ces solutions ont été étudiées par SAXS et SANS. La méthode de préparation de ces solutions ne joue un rôle que dans le domaine de vecteurs de diffusion q < 0.02 Å^{-1} et n'influence donc que la structure des hétérogénéités. La conformation locale des polyions ainsi que les caractéristiques du réseau interpénétré qu'ils forment restent identiques quelle que soit la méthode utilisée pour préparer les solutions de complexes PDADMAC-PSSNa.

Cryo-TEM

La phase « gel » d'une solution aqueuse 0.3 M, en absence de sel ajouté, de complexes PDADMAC-PSSNa a été observée par cryo-microscopie électronjque. Les images de TEM après la cryofracture montre des objets de taille finie. Ces objets, qui correspondent à des taches blanches et noires sur fond gris, représentent les clusters, ou hétérogénéités, du gel. Les clusters sont denses et localisés au hasard dans l'image de cryo-TEM. Ils sont également polydisperses en taille et en forme. Des tailles comprises entre 30 et 60 nm ont été mesurées. Ce résultat de cryo-TEM est cohérent avec les conclusions de nos expériences SAXS et SANS.

Chapitre 7. Complexes Poly(chlorure de diallyldiméthyl ammonium) – Hyaluronate de Sodium

Nous avons étudié les complexes PDADMAC-HANa successivement en solutions diluées et semidiluées, voire concentrées, comme les complexes PDADMAC-PSSNa. Nous avons pour cela, de la même manière, utilisé plusieurs techniques expérimentales.

Chapitre 7.1. Complexes PDADMAC-HANa en solutions aqueuses diluées

Pour étudier la thermodynamique du processus de complexation et corrélativement la taille et la charge effective des complexes en régime dilué, nous combiné des mesures de titration calorimétrique isotherme (ITC), diffusion dynamique de la lumière (DLS) et potentiel zêta. Ces mesures ont été réalisées pour deux forces ioniques distinctes (en absence ou en présence de 0.15 M sel NaCl ajouté) sur les domaines de rapports de charge électrostatique 0 < < z = [-]/[+] ou z =[+]/[-] < 2.

Nous suggérons que la complexation entre polyions PDADMA et HA est un processus à une étape. Les complexes PDADMAC-HANa formés en absence de sel, sont fortement chargés et d'une taille de 100-120 nm. Le signe de leur charge effective est définie par le polyélectrolyte qui est titré. En présence de sel ajouté, les complexes sont de grands agrégats, chargés négativement. La complexation entre les deux polyélectrolytes conduit à une enthalpie de formation positive, indépendamment de la force ionique et de la méthode de préparation des solutions de PECs. La nature endothermique de la complexation, provient probablement de la destruction de liaisons hydrogène qui existent dans la structure du hyaluronane. Toutefois, cette conjecture reste à démontrer, en utilisant en particulier la spectroscopie infrarouge.

Chapitre 7.2. Complexes PDADMAC-HANa en solutions aqueuses semidiluées et concentrées

Diagrammes de Phases ou d'États

Nous avons établi les diagrammes d'états des solutions aqueuses, en absence et présence de sel ajouté, des complexes PDADMAC-HANa, par observation visuel. De façon générale, les états n'évoluent plus au bout de deux jours après la préparation des solutions de PECs, quelle que soit la force ionique. En absence de sel ajouté, on distingue quatre régions. Aux concentrations de HA dans le domaine $0.025 < C < 0.15$ mol/L, il y a une séparation macroscopique en deux phases liquides (région (I)): phase jaune très visqueuse, riche en complexes hydrophobes, ou coacervats; phase transparente, qui est du solvant pur ou une solution extrêmement diluée de complexes. La phase jaune correspond au modèle théorique d'une « goutte seule ». La nature hydrophobe des complexes est due à la neutralisation importante des charges pendant la formation des complexes. Aux plus fortes concentrations de HA (0.20 - 0.25 mol/L) et des rapports de concentrations molaires [PDADMAC]/[HANa] < 1, un état gel (région (II)), monophasique, est observé. Une troisième région est associée à une solution turbide (« dispersion » (III)) correspondant à un système de gouttes denses et riches en polymère. Finalement, une région (IV), qualifiée de « colloïde », est en fait proche de la région (III). Elle est toutefois formée de gouttes de plus petites tailles.

En présence de sel ajouté (0.15 M NaCl), nous n'avons préparé que des complexes situés sur la ligne de stoechiométrie de charge. On a néanmoins observé quatre régions: une région monophasique, « gel transparent clair»; une région biphasique, avec une phase correspondant à un « gel turbide » et une autre qui est un « surnageant transparent »; un liquide turbide correspondant à un « état colloïdal »; une dispersion de gouttes ou « dispersion turbide jaune ».

Une augmentation de la force ionique gêne, ou empêche, évidemment la séparation de phases macroscopique.

Résultats des expériences SAXS

L'étude de la structure des complexes PDADMAC-HANa a été abordée par SAXS. Les profils d'intensité diffusée SAXS suggèrent l'existence de complexes primaires de forme cylindrique ayant une section de 8.3 Å et disposés sur le réseau des deux polyélectrolytes interpénétrés. La complexation peut toujours être décrite comme une gélification, où le polyanion HA joue le rôle d'agent gélifiant. La rigidité intrinsèque du polyanion HA est alors responsable de la forme allongée des complexes. Par ailleurs, elle est indirectement responsable de la nature hydrophobe des complexes, car elle conduit à une forte neutralisation des charges électrostatiques le long des séquences chimiques des PEs pendant le processus de complexation. Cette diminution du nombre de charges effectives le long des séquences chimiques des PEs, et a fortiori des complexes, conduit, en particulier, à une absence de pic électrostatique dans les diagrammes SAXS. Les complexes primaires cylindriques se rassemblent pour former des agrégats plus grands: des cylindres (de longueur 12.6 nm et de section de diamètre 6 nm) et des disques (de section 36 nm et d'épaisseur 5.6 nm). Le caractère hydrophobe des complexes, associé à une forte neutralisation des charges électrostatiques le long des séquences chimiques des polyions, elle-même due à leurs rigidités intrinsèques, joue un rôle important. La contribution des interactions électrostatiques devient négligeable. En fait, on devine la variété des structures à l'échelle macroscopique en suivant les changements d'états visuellement. Des clusters denses de taille 30-40 nm ont été observés sur des images de cryo-TEM. Cette taille correspond aux complexes en forme de disque.

Nos résultats montrent que la structure des complexes PDADMAC-HANa est plutôt en accord avec le modèle de structure en échelle (« ladder») proposé par la théorie et les simulations pour les polyélectrolytes rigides. Corrélativement, en absence de sel ajouté, les fonctions de structure ne présentent aucun pic polyélectrolyte aux vecteurs de diffusion intermédiaires. Cela indique qu'un grand nombre de monomères sont neutralisés lors de la complexation entre polyions de charges opposées.

Chapitre 8. Conclusion générale

Dans cette thèse, la thermodynamique, le comportement macroscopique et la structure des solutions aqueuses de complexes formés entre un même polycation, le poly(diallyldiméthyl ammonium) de longueur de persistance non-électrostatique $l_p^0 = 3$ nm, et trois polyanions de rigidités intrinsèques distinctes (le polystyrène sulfoné, $l_p^0 = 1$ nm ; le poly(α-méthyl styrène) sulfoné, $l_p^0 = 2.5$ nm ; le hyaluronate, $l_p^0 = 9$ nm) ont été abordés. L'idée directrice était d'étudier l'influence de la rigidité intrinsèque des polyions sur la structure des complexes de polyélectrolytes de charges opposées (PECs).

Tous les polyélectrolytes ont été préparés et utilisés sous forme sel: de chlorure, pour le polycation; de sodium, pour les polyanions. Nous avons ainsi réalisé la sulfonation de plusieurs chaînes de polystyrène hydrogéné ou deutérié et de poly(α-méthyl styrène) hydrogéné, conduisant aux polyélectrolytes PSSNa et PαMSSNa, ainsi que la synthèse de chaînes de chlorure de poly(diallyldiméthyl ammonium) hydrogéné, ou PDADMAC, de différentes masses molaires. Les échantillons de hyaluronate de sodium, HANa, nous ont été fournis gracieusement par la société Soliance. Nous avons caractérisé tous ces polyélectrolytes en utilisant la RMN du proton, la chromatographie d'exclusion stérique multidétection (SEC), la thermogravimétrie et la diffusion de rayons X aux petits angles (SAXS).

Les solutions aqueuses des complexes des polyélectrolytes ont été préparées en absence ou en présence d'un sel monovalent ajouté (150 mM NaCl), suivant différentes méthodes dans une large gamme de concentrations. Elles ont été étudiées en utilisant différentes techniques selon la gamme de concentrations considérée. Dans le régime dilué, la formation des PECs a été examinée par titration calorimétrique isotherme (ITC) et des mesures de potentiel zêta et de rayon hydrodynamique. Dans les régimes semidilué et concentré, la structure des PECs a été étudiée en utilisant les techniques de diffusion de rayons X ou de neutrons aux petits angles (SAXS et SANS) et, plus occasionnellement, la cryo-microscopie électronique.

L'analyse des résultats obtenus conduit aux conclusions suivantes:

Pour les complexes PSS-PDADMA:

- La stoechiométrie des complexes PSS-PDADMA est égale à 1 et indépendante de la concentration, la force ionique et leur méthode de préparation. L'interaction entre les

deux polyélectrolytes est de nature exothermique et bénéficie d'un gain entropique associé au relargage de leurs contreions dans la solution.

- On peut décrire la complexation entre les deux polyélectrolytes de manière différente suivant le domaine de concentrations que l'on explore. En solution diluée, la complexation se fait en deux étapes: la première étape conduit à la formation de complexes primaires; la seconde correspond à l'agrégation de ces complexes primaires. En solution semidiluée ou concentrée, elle est analogue à un phénomène de gélification. Le réseau temporaire constitué par un des deux polyélectrolytes peut ainsi être considéré comme un bain de réaction et le polyélectrolyte de charge opposée devient l'agent gélifiant. La structure des complexes PSS-PDADMA correspond alors à un réseau formé de l'interpénétration des deux polyions et de points de jonctions associés aux interactions électrostatiques entre monomères de charges opposées qui forment en s'associant (l'eau est un mauvais solvant de ces paires d'ions quasi neutres) des hétérogénéités, ou clusters, de plus grande taille. Ces deux mécanismes de formation des PECs peuvent en fait être suggérés par les observations visuelles de différents phénomènes de séparation de phases.

- Dans les régimes semidilué et concentré, la structure des solutions de PECs dépend de la méthode de préparation de ces solutions et de leur force ionique. Plus précisément, l'ordre prévalant au mélange des solutions de polyélectrolytes initiales et parentes ainsi que leur force ionique jouent un rôle sur la structure des hétérogénéités. Toutefois, la maille du réseau dans lequel elles sont immergées conserve la même taille.

- Une augmentation de la force ionique empêche la séparation de phases et la région monophasique des diagrammes d'états, ou de phases, s'étend vers les plus fortes concentrations en présence de sel (NaCl) ajouté. Elle rééquilibre également la distribution du PDADMAC entre phases séparées macroscopiquement.

- La ligne de transition entre les domaines colloïdal et biphasique est reliée au crossover entre régimes semidilué et concentré des solutions aqueuses de PDADMAC.

Pour les complexes PαMSS-PDADMA:

- La force ionique et la concentration des solutions de polyélectrolytes initiales, ou parentes, jouent des rôles équivalents dans la complexation entre le PαMSS et le

PDADMA et celle entre le PSS et le PDADMA. L'augmentation de la rigidité intrinsèque du polyanion en passant du PSS au PαMSS conduit à un changement de la stoechiométrie des complexes et à une extension de la région monophasique dans les diagrammes d'états ou de phases.

Pour les complexes HA-PDADMA:

- L'augmentation supplémentaire de la rigidité intrinsèque du polyanion en passant du PSS au HA change le processus de complexation avec le PDADMA en régime dilué. Cela devient un processus à une étape de nature endothermique. De surcroît, la stoechiométrie des complexes HA-PDAMA n'est plus égale à 1.

- En régime semidilué ou concentré, la complexation entre le HA et le PDADMA peut toujours se décrire comme un phénomène de gélification dans lequel le polyion hyaluronate joue le rôle d'agent gélifiant. Toutefois, les jonctions entre polyions de charges opposées ne peuvent plus être considérées comme ponctuelles. Elles impliquent ainsi des séquences chimiques plutôt que des unités monomères isolés le long des polyions.

- Corrélativement la structure des complexes HA-PDADMA ne correspond plus au modèle en « œufs brouillés » prévalant pour les complexes PSS-PDADMA). Elle correspond davantage au modèle de structure en « échelle ». En particulier, l'organisation spatiale des solutions aqueuses des complexes HA-PDADMA peut devenir anisotrope lorsque ces solutions sont cisaillées.

- La complexation entre le HA et le PDADMA conduit à une neutralisation des polyanions HA et donc à une réduction du rôle des interactions électrostatiques dans la formation des structures secondaires. Les interactions hydrophobes jouent alors un rôle plus important.

- Les transitions entre principaux domaines des diagrammes d'états ou de phases sont reliées aux crossovers entre régimes semidilué et concentré d'une part ainsi que régimes concentré et encombré d'autre part, des solutions aqueuses du HA.

Content

Chapter 1

Introduction

Polyelectrolyte complexes (PECs) are formed between oppositely charged macroions and constitute a large family of multicomponent polymeric materials with rich functionalities. Prepared by different methods, PEC membranes have already been utilized in pervaporation, nanofiltration and fuel cells to control material selection. Dense macroscopic "saloplastic" tubes, films and fibers with specific mechanical properties and thermal stability are possible to be prepared using the laboratory extruder based on PECs. Applications of polyelectrolyte complexes have been strongly influenced by the opportunities presented by multi-layered polyelectrolyte assemblies that provides a simple and affordable route in creating new systems for drug delivery, gene therapy, sensors, photovoltaic devices and surface coatings. Protein-polyelectrolyte complexes are the particular case of PECs deserved to be mentioned due to their importance for biology and medicine.

The formation of the polyelectrolyte complexes is close to the self-assembly process that proceeds due to the electrostatic interactions between opposite charges and the counterion release. The properties of PECs are strongly related to their structure, which depends on numerous parameters: characteristics of the components (average molecular weight, polydispersity index, intrinsic stiffness, chemical nature of ionic groups, chemical charge fraction and charge distribution along the chemical sequence, hydrophilic-hydrophobic character of macroions and chemical nature as well as valence of counterions), pH, ionic strength etc. Despite the decades of the important research in the field of polyelectrolyte complexes, the full understanding of the PEC formation process and architecture is far from complete.

In this fundamental study, we focus on the particular and most frequent kind of complexes that are formed between model linear polyanions and polycations. We also mainly consider their aqueous solutions, more often prepared by mixing two initial solutions of polyanions and polycations, respectively. The polycation, poly(diallyldimethylammonium chloride) (PDADMAC) (intrinsic or non-electrostatic persistence length $l_p^0 = 3$ nm), and three polyanions, poly(sodium styrene sulfonate) (PSSNa) ($l_p^0 = 1$ nm), poly(sodium α-methyl styrene sulfonate) (PαMSSNa) ($l_p^0 = 2.5$ nm) and sodium hyaluronate (HANa) ($l_p^0 \sim 9$ nm) were considered to form PECs. This selection was motivated by

several factors. First, it results from the main objective of this thesis, which was to understand the role of the intrinsic persistence length l_p of the polyanion on the polyelectrolyte complex formation and structure. The properties of the aqueous solutions of these hydrophilic strongly charged flexible and semiflexible (pH $\approx$ 7 for HANa) polyelectrolytes were relatively well-known. We were interested as well in the effect of the ionic strength and the way of preparing the polyelectrolyte complex aqueous solutions that could equally affect the self-assembly process between polyelectrolytes of opposite charge and its result. We focused toward the correlation between the morphology of the polyelectrolyte complexes with that of the initial binary polyelectrolyte solutions. Finally, we wished to study the possible differences between the complexation processes in dilute and semidilute or concentrated polyelectrolyte regimes.

Chapter 2

Basics in polyelectrolytes and polyelectrolyte complexes

Polyelectrolytes (PEs) and multicharged systems as polyelectrolyte complexes (PECs) are known to be interesting objects of specific properties allowing developing distinct applications in drug delivery, gene therapy, sensors, photovoltaic devices and surface coatings. This study is focused mainly on the structure investigation of PECs in solution. Their morphology has a strong correlation with that of initial polyelectrolyte in solution. In this chapter, the basic properties of both sorts of material will be reviewed in order to give better apprehension and explanation for the results presented in the following experimental parts.

2.1. Polyelectrolytes

Polyelectrolytes (PEs) are polymers containing ionizable groups, which dissociate into macroions, and mobile counterions (CIs) when dispersed in a polar solvent as water. Depending on the sign of the charges tied to the macroions, we distinguish polycations and polyanions, or macrocations and macroions. Sometimes the term *polysalts* is used to name polyelectrolytes with counterions different from H^+ or OH^-. Polyampholytes are macromolecules that bear both cationic and anionic repeat groups. According to the number and the nature of dissociated groups along the chemical sequence, polyelectrolytes are strong or weak, as well as acids or bases. The number of charged monomer units is characterized by the *chemical charge fraction, f*. For quenched polyelectrolytes, the distribution of charges on the macroions is static. Then f is determined by the chemical synthesis and does not depend on pH. On the contrary, for annealed polyelectrolytes, f depends on pH and the charge distribution is dynamic. Weak polyelectrolytes (as for example, poly(acrylic acid), poly(methacrylic acid), poly(2-vinyl pyridine or polysaccharides) are commonly annealed as their number of dissociated groups is determined by the pH of the solution[1]. They are mostly partially charged.

After dissociation counterions are either dispersed in the solution or condensed onto the macroions. The free counterions lead to an entropy gain and make a large contribution in the solubilization of polyelectrolytes. The dissociation and the existence of the charges on PE backbone lead to properties more complex, than those of neutral polymers mainly because the electrostatic interactions are long-ranged and possibly screened by additional salts. In a poor solvent, the complexity results from the competition between electrostatic repulsions and short-range attractions associated with the poor solubility. In both cases, other degrees of freedom are brought by counterions that also play a crucial role. For example, the presence of free counterions results in exceeding the osmotic pressure of polyelectrolyte solutions comparing to neutral macromolecule ones. The osmotic coefficient is then proportional to the number of free counterions[2]. Also, the semidilute regime of PEs is reached at a lower concentration, indicating an extended average conformation of macroions. The reduced viscosity of dilute PE solutions decreases as concentration increases (Strauss-Fuoss' law[3]) while that of uncharged polymer solutions is proportional to the concentration.

In the following, we will discuss in details the parameters that control the average conformation as well as the dispersion state of PEs and will present the most important models that describe the structure of their solutions. Specifically, the dispersion states of PEs will be associated with different regimes characterized by distinct scaling laws.

2.1.1. Counterion condensation and effective charge of macroions

After dissociation, the macroions have an overall charge density, or *chemical charge fraction f* varying from 0 to 1. However, for highly charged PEs, a counterion condensation process leads to a renormalization of the charge density through the *effective charge fraction f_{eff}*. That is the Manning-Oosawa phenomenon[4–7]. The Bjerrum length l_B plays a central role in the limiting law of the CI condensation process. It is the average distance at which the electrostatic interaction between two unscreened elementary charges is comparable to the thermal energy k_BT. It is defined as:

$$l_B = \frac{e_0^2}{4\pi\varepsilon_0\varepsilon_r k_B T},$$
(1)

where e_0 is the elementary charge; ε_0 and ε_r, the dielectric constant of vacuum and the relative dielectric constant of the solvent, respectively; k_B, the Boltzmann constant; T, the absolute temperature in Kelvin. For water at room temperature $l_B = 7.14$ Å.

If the distance between two charges on the macroion is larger than the Bjerrum length, there is none counterion condensation. The concentration of free counterions in the solution is equal to the concentration of charged monomer units. When the distance between two neighbouring ionized groups are closer than l_B, some counterions condense on the macroion and thus reduce its charge density. The Manning-Oosawa approach is a two-state model as it divides all counterions into two states: free (scattered in the solvent) and condensed (close to the macroions but still mobile and forming a sheath around them with a cylindrical symmetry). The counterion localization onto the macroions results in a loss of translational entropy. For monovalent CIs the effective charge of macroions, f_{eff}, is:

$$f_{eff} = \frac{b}{l_B},$$

(2)

where b is the size, or contour length, of a monomer unit.

PEs with mixed valence counterions are described elsewhere including ion binding and ion localization approaches[8].

The counterion condensation process is significant as it introduces equilibrium between free and condensed counterions that determines the effective charge fraction of the macroions. The average conformation and the dispersion state of polyelectrolytes in solution are indeed controlled by the effective charge fraction, f_{eff}, instead of the chemical one, f.

2.1.2. Ionic strength and Debye screening length

The electrostatic interaction between charged groups is long-range but can be screened by increasing the ionic strength I of the medium through the presence of an additional electrolyte, as for example a low molecular weight salt. The ionic strength of a solution can be defined as:

$$I = \sum_i z_i^2 C_i$$

(3)

where C_i is the concentration (mol/l) of the ith electrolyte of valence z_i. The electrostatic interaction then persists on distances lower than the Debye screening length:

$$k_D^{-1} = (4\pi l_B I)^{-1/2}$$

(4)

Taking into account the already mentioned counterion condensation process, the ionic strength for a salt-free polyelectrolyte solution of concentration C should include the effective charge fraction f_{eff}:

$$I = z^2 f_{eff} C \tag{5}$$

$$k_D^{-1} = (4\pi l_B z^2 f_{eff} C)^{-1/2} \tag{6}$$

z is the counterion valence. If an additional monovalent salt is present in the solution at concentration C_s:

$$I = z^2 f_{eff} C + 2 C_s \tag{7}$$

$$k_D^{-1} = \left(4\pi l_B \left(z^2 f_{eff} C + 2 C_s\right)\right)^{-1/2}. \tag{8}$$

The presence of an added salt has an influence on the polyelectrolyte conformation if the Debye screening length exceeds its average size[2]. When the Debye screening length is smaller than the electrostatic blob size, polyelectrolytes have the same conformation than the related neutral macromolecules in a good solvent[2]. At the intermediate length scale lying between the macroion and electrostatic blob sizes, electrostatic repulsions between monomer units play a role at distances smaller than the k_D^{-1}.

2.1.3. Average conformation of polyelectrolytes in solution

Two competitive factors determine the average conformation of polyelectrolyte in an athermal or good solvent. The repulsion between charged monomers causes a swelling of polyelectrolytes. However, this conformational change leads to an entropy loss, which is opposed to the swelling. The average PE conformation results from an equilibrium between these two trends. The Flory theory gives first estimations of both contributions to the free energy. It was introduced for a Gaussian coil of mean end-to-end distance R_0 ($R_0^2 = Nb^2$), $R_0^2 = Nb^2$ with N units of length b for infinite dilution at zero salt concentration[9]. A first term, corresponds to the free energy for an isolated macromolecule. It is the free energy of the neutral Gaussian chain that would be obtained by neglecting the electrostatic repulsion between charges:

$$F_{conf}(R) \approx k_B T \frac{R^2}{b^2 N}. \tag{9}$$

If f is the fraction of charged monomers, the chain carries the total electrical charge fNe. The electrostatic interactions tend to stretch the chain to the size $R > R_0$, and contributes to the free energy by the term:

$$F_{electr}(R) \approx k_B T \frac{(Nf)^2 l_B}{R^2}.$$ (10)

The total free energy of the polyelectrolyte is then:

$$F(R) = F_{conf}(R) + F_{electr}(R) \approx k_B T \left(\frac{R^2}{b^2 N} + \frac{(Nf)^2 l_B}{R} \right).$$ (11)

The minimization of equation (11) with respect to R by setting $\frac{dF}{dR} = 0$ gives an equilibrium size of the chain R:

$$R \approx Nf^{\frac{2}{3}}(l_B b)^{\frac{1}{3}},$$ (12)

R is proportional to N and scales as $f^{2/3}$. So the electrostatic interactions tend to swell the chain.

The Flory approach is not realistic as it presents a weakly charged, flexible polymer chain as a Gaussian one. Moreover, it assumes that charge monomers are uniformly distributed within the volume R^3. It neglects the correlation between monomers and overestimates their repulsion energy. Nevertheless, the Flory theory is simple and provides an easy way to introduce important concepts that help to understand the average polyelectrolyte conformation. In the presence of an added salt, the average conformation is expected to tend to that of a neutral chain, with the scaling law:

$$R \sim N^\nu.$$ (13)

A more realistic theory describing the polyelectrolyte conformation is based on the concept of electrostatic blobs. It was introduced by de Gennes et al[10–15]. The chain is then described as a linear set of electrostatic blobs, of size ξ_e. Within a blob, electrostatic interactions are negligible and the chain conformation is either Gaussian (theta solvent) or of the excluded volume type (good solvent). The electrostatic interactions for distance larger than the blob size, lead to a strong elongation of the polyelectrolyte chain into an array of blobs. Then the chain size is expressed as $(\frac{N}{g})\xi$. The conformation of the polymer inside the blob is not perturbated by the electrostatic interactions and depends on the quality of solvent. In good or θ-solvent the energy of the electrostatic interactions between all charged monomers inside a blob is on the order of the thermal energy $k_B T$:

$$\left(\frac{g}{a}\right)^2 e^2/(\varepsilon\xi) \approx k_B T, \tag{14}$$

where a is the average number of monomers between charges; g/a, the number of charges per blob; e, the elementary electrostatic charge; ε, the dielectric constant of the solvent.

In a poor solvent, the problem was first tackled by Khokhlov[14]. The electrostatic blob size is the result of a balance between the electrostatic energy of a blob and the polymer/solvent interfacial energy. If the electrostatic interactions were absent, the polymer would be completely collapsed into a globular state. In the presence of electrostatic interactions, the conformation becomes an array of globular blobs. The size of a globular blob should be enough to overcome the interfacial energy that must be paid when monomers are exposed to the solvent. Writing the interfacial tension as $\gamma \approx \tau^2 kT/b^2$ and the reduced temperature as $\tau = (\theta - T)/T$, then:

$$\frac{\left(\frac{g}{a}\right)^2 e^2}{\varepsilon\xi} \approx \gamma\xi^2. \tag{15}$$

So, the blob size ξ and the number of monomers in each blob g have the following relations with different swelling exponents depending on the solvent quality:

$$\xi \sim b g^{3/5}, \qquad T > 0 \tag{16}$$

$$\xi \sim b g^{1/2}, \qquad T = 0 \tag{17}$$

$$\xi \sim b\left(g/\tau\right)^{1/3}, \qquad T < 0 . \tag{18}$$

Including the charge fraction f, we get:

$$T < 0 \quad \xi \sim b \, (f^2 l_B/b)^{-1/3} \tag{19}$$

$$g \sim \tau(f^2 l_B/b)^{-1} \tag{20}$$

$$T = 0 \quad \xi \sim b \, (f^2 l_B/b)^{-1/3} \tag{21}$$

$$g \sim (f^2 l_B/b)^{-2/3} \tag{22}$$

$$T > 0 \quad \xi \sim b \, (f^2 l_B/b)^{-3/7} \tag{23}$$

$$g \sim (f^2 l_B/b)^{-2/3} \tag{24}$$

According to this approach of Khokhlov, the solvent quality only changes the conformation inside the electrostatic blob. On distances larger than the blob size, the electrostatic blobs repel each other due to the electrostatic interactions. The solvent quality does not have any effect on the average conformation of the polyelectrolyte chain, which is an extended assembly of electrostatic blobs. At this stage, must, however, emphasize that this model of polyelectrolyte in a poor solvent has been challenged some years after by the more realistic pearl-necklace model[16].

2.1.4. Dispersion states of hydrophilic polyelectrolytes

Previous models were introduced for isolated polyelectrolytes, i.e. PEs in solution at infinite dilution. The Debye screening length is then larger than the average distance between macroions. At limiting values of concentration, chains do not overlap each other, but the electrostatic interactions between macroions are of the same order of magnitude or bigger than the thermal energy. It was suggested by de Gennes[10] that the centres of mass of the macroions could be organized either in a three-dimensional periodic lattice or with a liquid-like local order. Then, the average distance between them scales as $C^{-1/3}$, C being the PE concentration. On the other hand, the scattering, or correlation functions of polyelectrolyte solutions, measured through various scattering techniques, display a maximum, referred as polyelectrolyte peak, which is a signature of electrostatic interactions[11]. Its position in the reciprocal space is characterized by a scattering vector q*. In the dilute regime, q* scales as $C^{1/3}$, showing a direct correlation with the average distance between the mass centers[17]. The PE peak, therefore, results from a position order in this regime, that is characterized by the scaling law[17]:

$$q^* \sim (C/N)^{1/3}. \tag{25}$$

With an increase of the concentration the chains overlap each other. The Debye screening length becomes of the order of the distance between chains and the critical overlap concentration C^* scales as N^{-2} with the degree of polymerization, in agreement with an extended conformation for the macroions[11,15]:

$$C^* \sim N^{-2} \tag{26}$$

Above C*, the structure of a PE solution is mainly described through the isotropic model[10]. The macroions are entangled and form a temporary network as in semidilute or concentrated solutions of

neutral polymers. The mesh size of this network, or the so-called correlation length ξ, is then the main parameter. It is independent of N and its variation with concentration is described by a scaling law with a specific exponent, characterizing the structure, or the regime, of the PE solution. In the semidilute regime, ξ scales as $C^{-1/2}$ and we have:

$$q^* \approx \frac{2\pi}{\xi} \sim C^{1/2}. \tag{27}$$

This law has been confirmed by numerous small angle radiation (light, X-ray, and neutron) scattering[10,18,19]. Moreover, it was also shown that other characteristic lengths, as the macroion persistence length, were locked to the correlation length[20,21].

This scaling approach of de Gennes for the semidilute regime was extended by Dobrynin et al[12]. The polyelectrolyte chain conformation is proposed to be a random walk of correlation blobs of size ξ (Figure 2.1).

Each of these blobs contains an extended sequence of electrostatic blobs of size ξ_e and the concentration blob ξ is given by the relationship[8]:

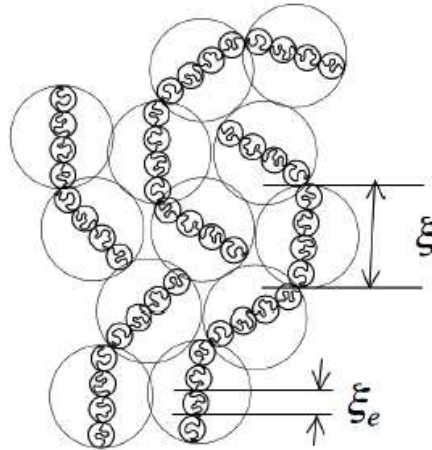$$\xi = f_{eff}^{-2/7} \left(\frac{l_B}{b}\right)^{-1/7} (bC)^{-1/2} \tag{28}$$

Figure 2.1. Schematic representation of a semidilute polyelectrolyte solution according to the scaling approach associated with the isotropic model[2]

This scaling law was proved experimentally through the position of the PE peak $q = \frac{2\pi}{\xi}$ [8,17,18,22]. The next regime of polyelectrolyte solutions, i.e. the concentrated one, has been less investigated and

appears at concentration $C > C^{**}$ (C^{**} is the semidilute-to-concentrated crossover concentration)[23–25].

$$C^{**} \approx b^{-3} f^{2/3} \left(\frac{l_B}{b}\right)^{1/3} . \qquad (29)$$

This crossover from the semidilute regime to the concentrated one goes with a change in the exponent of the scaling law Eq. (27). It becomes:

$$q^{*} \approx \frac{2\pi}{\xi} \sim C^{1/4}. \qquad (30)$$

The concentration fluctuation is indeed negligible comparing to the ones in dilute and semidilute regimes[26]. Moreover, macroions contribute into the electrostatic screening[12]. The electrostatic blobs ξ_e are now close-packed and the mesh size of the temporary network describing the structure of the solution, ξ, is the same or less than ξ_e. The polyelectrolyte conformation is then assumed to be Gaussian on a length scale larger than ξ[23]. Then, the correlation, or scattering, functions can be computed using the Random Phase Approximation (RPA)[24,27]. Thus, the macroion correlation function is:

$$\frac{C}{S(q)} = \frac{1}{g_0} + cv + w^2 c^2 + \frac{4 l_B f}{k_D^2 + q^2} \qquad (31)$$

where $g_0(q)$ is the form factor of a Gaussian chain (Debye function):

$$g_0(q) = N[x - 1 + \exp(-x)] \qquad (32)$$

that can be reduced to $g_0(q)^{-1} = (N)^{-1}[1 + g(Nq^2 b^2/6)]$. v is the excluded volume; w^2, the third virial coefficient; κ_D^{-1}, the Debye screening length defined by Eq. (8)[23].

The scattering function (31) has a peak at a scattering vector q^{*} given by the relation:

$$(q^{*2} + k^2)^2 = \frac{24\pi l_B f^2 C}{b^2/3} \qquad (33)$$

leading to the characteristic scaling law mentioned above ($q \approx \frac{2\pi}{\xi} \sim C^{1/4}$). It is in good agreement with distinct radiation scattering experimetns[2,17,28,29].

A further increase in concentration can lead to an isotropic swollen, or bulk, state that is no longer a real solution, provided the polyelectrolyte is flexible. The scattering function of such a swollen state always displays a maximum[17], but it has a different nature, or origin, that the PE peak. Specifically, for salt-free aqueous solutions of sodium poly(styrene sulfonate), its position, q*, does

not depend on the concentration anymore. Actually, there is a rather strong decrease in the dielectric constant of the medium resulting from the high PE volume fraction. Therefore, polyelectrolytes would involve electrical dipoles rather than electrical charges, due to a strong decrease in the dielectric constant. Such dipoles tend to form clusters, and the maximum in the scattering function is related to the hard core or steric repulsion between these clusters. This is the 'ionomeric" regime of flexible polyelectrolytes at extreme concentrations, for which: $q^* \sim C^0$ or constant, allowing to evaluate the cluster size[30].

The question was raised if an orientation order could also take place in a polyelectrolyte solution at high concentration. Indeed, an Onsager transition to a nematic phase[17] was expected for polyelectrolytes of higher intrinsic stiffness than one of polystyrene sulfonate[31,32] and observed for rigid natural polyelectrolytes such as collagen[33], DNA[34] or viruses[35,36]. Small-angle X-ray and neutron scattering experiments on solutions of highly charged semi-flexible polyelectrolytes allowed replying to this issue. They led to a new sequence of scaling laws beyond the dilute regime [$q^* \sim c^{1/2}$; $c^{1/4}$; c^1; $c^{1/2}$], revealing the existence of a nematic local order at high concentration ($q^* \sim c^{1/2}$) preceded by a new regime ($q^* \sim c^1$). The new regime appears in dense polyelectrolyte solutions, above the concentrated regime, only for polyelectrolytes with intermediate intrinsic stiffness (non-electrostatic persistence length larger than 25 Å), provided the ionic strength is sufficiently low. It is quite original and absent for solutions of short rigid macromolecules that only display an Onsager (first order) transition. Moreover, it disappears at the benefit of the nematic local order as the concentration of added salt is increased[30]. This regime corresponds to a jammed random close packing of equivalent solid rods of length comparable to the intrinsic persistence length. It results from a competition between the excluded volume interaction, contributing to an alignment of the macroions at the length scale close to ξ, and the electrostatic repulsion in favour of their perpendicular orientation (Figure 2.2) as well as the thermal fluctuations introducing disorder.
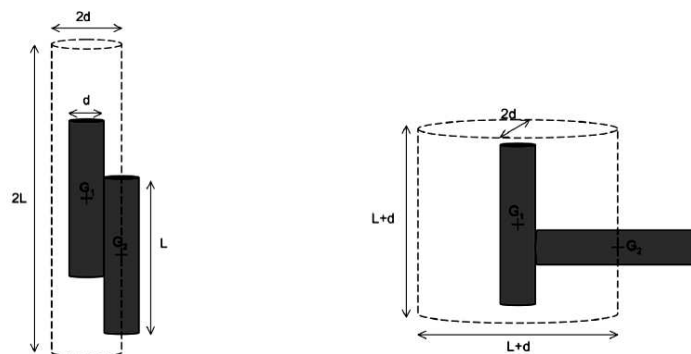

Figure 2.2. Excluded volume between two cylinders in parallel (a) and perpendicular orientation (b)

Let us consider a simple model to describe the phenomenon and evaluate the excluded volume in both orientation cases (Figure 2.2). Two hard cylinders of length L and diameter d are considered. Their volume is $V_i = \pi \frac{d^2}{4} L$. For the parallel configuration the excluded volume, or the correlation hole around each cylinder is $V_{II} = \pi d^2 * 2L$, that is proportional to the square diameter. For the perpendicular configuration, it has an ellipsoidal shape with axes $L + d$ and $2d$ that reduces to a volume $V_\perp = \pi d L^2 / 2$, as L>>d. It is proportional to the diameter. The electrostatic interaction promotes this perpendicular orientation and correlatively an isotropic local state. On the contrary, the excluded volume interaction promotes the parallel orientation and therefore the nematic local order. The critical concentration for the appearance of such a nematic local order depends on the ionic strength of the solution[32].

Actually, d represents the closest distance of the approach between two cylinders (analogy with the correlation hole in the model of hard spheres). This distance is therefore related to the position q* of the maximum of the scattering function (q* ~ 1/d). For a jammed system, the compactness argument can be summarized by assuming that the whole volume is the sum of all the excluded volumes associated with the molecules. A solution of volume V and concentration C consists of CV monomers and CV/L monodisperse hard cylinders or rods. The compactness argument then leads to:

$$\frac{CV}{L} * V_{ex} = V. \tag{34}$$

And the minimal distance d and the position q* of the maximum of the scattering function have the following concentration dependences:

for the parallel orientation $(V_{ex} \approx Ld^2)$: $q^* \sim d^{-2} \sim C^{1/2}$ $\qquad q^* \sim c^{-1/2}$ $\qquad$ (35)

for the perpendicular orientation $((V_{ex} \approx L^2 d))$: $q^* \sim d^{-1} \sim C$ $\qquad q^* \sim 1/_{Lc} \sim c^{-1}$ (36)

The nematic local order corresponds to the first scaling law; the new regime, to the second one $q^* \sim c^{-1}$.

2.1.5. Intrinsic and electrostatic persistence lengths

Another important structural parameter determining the local conformation of a polymer chain is the persistence length, l_p. It characterizes the chain local stiffness, which is due to the rotational isomerism, or sometimes some hydrogen bonding, for neutral macromolecules. In the case of polyelectrolytes, the electrostatic repulsions between monomer units cause an additional stiffness.

The total persistent length of a polyelectrolyte thus consists of two parts: the intrinsic or bare persistent length, l_p^0, and the electrostatic persistent length, l_p^e:

$$l_p = l_p^0 + l_p^e. \tag{37}$$

The intrinsic persistent length, l_p^0, comes from the rigidity of the equivalent uncharged polymer chain. It is also called non-electrostatic persistent length. The electrostatic persistence length, l_p^e, results from the electrostatic short-range interactions between charges along the chemical sequence of the macroion. Various approaches were proposed to calculate the electrostatic persistence length.

The first one is that of Odijk[37], Skolnick and Fixman[38] (OSF). The electrostatic interaction is then considered as a perturbation of the elastic free energy. For a highly charged polyelectrolyte, taking into account the Manning-Oosawa approach for the counterion condensation, the electrostatic persistence length l_e is reduced to $\frac{1}{4k_D^2 l_B}$, where k_D^{-1} is the Debye screening length and l_B is the Bjerrum length. The total persistence length is therefore:

$$l_p = l_p^0 + \frac{1}{4k_D^2 l_B}. \tag{38}$$

The important result is that the electrostatic persistence length scales as k_D^{-2}. The main limitation of the OSF approach is that the electrostatic interaction is considered as a perturbation. Therefore, the total persistence length is mainly the intrinsic contribution ($l_e \ll l_o$) and the theory mainly concerns semi-flexible or rigid polyelectrolytes. Other results have been obtained numerically[39,40]. A scaling theory for weakly charged flexible macromolecules also leads to $l_p = \frac{1}{4k_D^2 \xi_e}$ [13].

When the electrostatic contribution dominates ($l_p^e \gg l_p^o$), Barrat and Joanny[41] suggested an alternative theory taking into account the thermal fluctuations and the chain behaviour at very short scale. It leads to an electrostatic persistence length depending on the length scale considered. At short scale, electrostatic interactions are irrelevant and the persistence length is l_0. At large length scales, the persistence length is that the OSF theory. If a local persistence length is included in the blob description, the condition for the chain to remain flexible is that the blob size is larger than the persistence length. In this case, the persistence length was shown to have a linear dependence on the Debye-Huckel screening length:

$$l_p^{BJ} \sim k_D^{-1}. \tag{39}$$

2.2. Polyelectrolyte complexes

Polyelectrolyte complexes (PECs) are formed between oppositely charged macroions. The variety of PEC categories is wide as the possible domain of their applications. In this study, we focus on the particular and most frequent kind of interpolyelectrolyte complexes that are formed between linear polyanions and polycations. We also mainly consider their aqueous solutions, most often prepared by mixing two aqueous solutions of polyanions and polycations.

2.2.1. Thermodynamics of the complex formation

The formation of complexes from two oppositely charged macroions is mainly controlled by two factors: the electrostatic attractive interaction between positive and negative charges, borne by the monomer units, and the entropy gain, related to the release of counterions. The association can be described by the following chemical equation[42]:

$$(>A^- c^+)_n + (>C^+ a^-)_m \rightarrow (>A^- C^+<)_x + (>A^- c^+)_{n-x} + (>C^+ a^-)_{m-x} + xa^- + xc^+, \qquad (40)$$
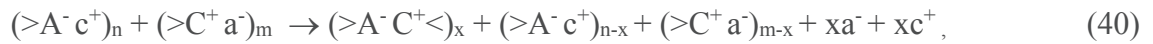
where A^- and C^+ are the charged monomer units of the polyanion and the polycation, respectively; a^- and c^+, their counterions; n and m, the initial numbers of anionic and cationic groups; x, the number of ionic bonds between polyanions and polycations. Such an association between positively and negatively charged monomer units often has a spontaneous character. This is specifically the case for the complexation between highly charged polyelectrolytes of opposite charge at low, or moderate, ionic strength (strong coupling limit). The links between the oppositely charged macroions are strong and cannot dissociate easily once they are formed. The related complexes are not at thermodynamic equilibrium and their structure depends on the way of preparing them.

In the complexation process, the double layers surrounding both macroions are destroyed to a certain extent and counterions are released in the solution. This implies changes in both the energy and entropy of the system, which mainly depend on the ionic strength.

The entropy change ΔS is mainly due to the release of counterions initially confined in the double layers. This entropy gain, thus positive contribution, becomes smaller as the ionic strength is increased. However, the negative contribution corresponding to the loss of configurational and

translational entropy of macroions is less important, provided the chains are long enough. As a result, ΔS is positive and the complexation is usually favoured entropically.

On the contrary, the enthalpy term ΔH, or ΔE, can be negative or positive. At low ionic strength, the complexation leads to a strong decrease in the total electrostatic energy, since the complexes are rather dense. The enthalpy term is, therefore, negative and the complexation is exothermic. At high ionic strength, it becomes endothermic and ΔH is positive. That has been confirmed by calorimetric investigations[43]. The salt concentration of the crossover from exothermic to endothermic complexation depends on the nature of the polyelectrolytes. Obviously, the complexation energy also varies with the chemical charge fraction of polyelectrolytes[44]. Thus, it is endothermic for highly charged polyelectrolytes and exothermic for weakly charged ones. Figure 2.3 presents the effect of an added salt on the total free energy of complexation ($\Delta F = \Delta H - T\Delta S$). The complexation can be exothermic or endothermic according to the salt concentration (Figure 2.3).

Except for the long-range ionic bounding, other interactions such as Van der Waals forces[45–47], hydrophobic interaction[48–50], hydration force or formation of H-bonds[46] may play an important role in polyelectrolyte complex formation. However, any clear understanding of the influence of all these additional interactions has not been obtained so far.
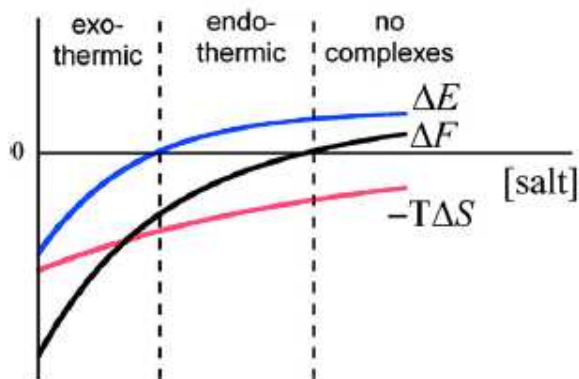

Figure 2.3. The effect of salt on the total free energy of complexation (ΔF), and on the counterion release entropy ($-T\Delta S$) as well as the Coulomb energy (ΔE). Depending on the added salt concentration, the complexation can be exothermic or endothermic

2.2.2. Theory and simulations of phase separation in polyelectrolyte mixture solution

At large enough concentration, the electrostatic interactions between oppositely charged polyelectrolytes often lead to a macroscopic phase separation. This phenomenon has been observed in various natural processes and is of significant practical interest. Yet, it is not clear what controls the width of the regions in the phase diagrams where soluble complexes exist. A general rule is that if all the macroion charges are not neutralized by complexation, complexes may remain soluble. Correlatively, near charge neutrality, complexes typically aggregates to form dense phases[51]. According to this rule, complexes corresponding to the line of stoichiometric charge compositions in the phase diagrams tend to be denser. Nevertheless, the neutralization of the charges remains determined by the possibilities of steric arrangement and other factors.

The first theory concerning the complexation between two flexible polyelectrolytes of opposite charges was proposed by Overbeek and Voorn (OV theory)[69]. The total free energy is estimated as a sum of a mixing entropy term and an electrostatic contribution that is just the Debye-Hückel expression for a simple electrolyte solution. The former favors homogeneous mixing, i.e. a dilute phase; the latter, the formation of a dense complex phase. This OV approach is a mean field theory that neglects: the counterion condensation onto the macroions; the connectivity of the charges on the macroions. Thus, it does not account for the entropy gain of the released counterions in a proper way (the driving force of the complexation is underestimated). Despite such severe approximations, it allows analysing experimental data of numerous systems and predicting general trends of the phase diagrams.

Figure 7 shows a phase diagram calculated using the OV theory for a solution of polycations (P) and polyanions (Q), each having 100 charged segments, in the presence of a monovalent salt. We note that:

- The biphasic region, which corresponds to a phase separation between a dilute polymer solution and a dense complex phase, is centered on the line representing the stoichiometric charge composition. The tie-lines are somewhat parallel to this line;

- The width of the biphasic region is reduced, when the salt concentration increases. Above a certain critical ionic strength, the complexation is suppressed;
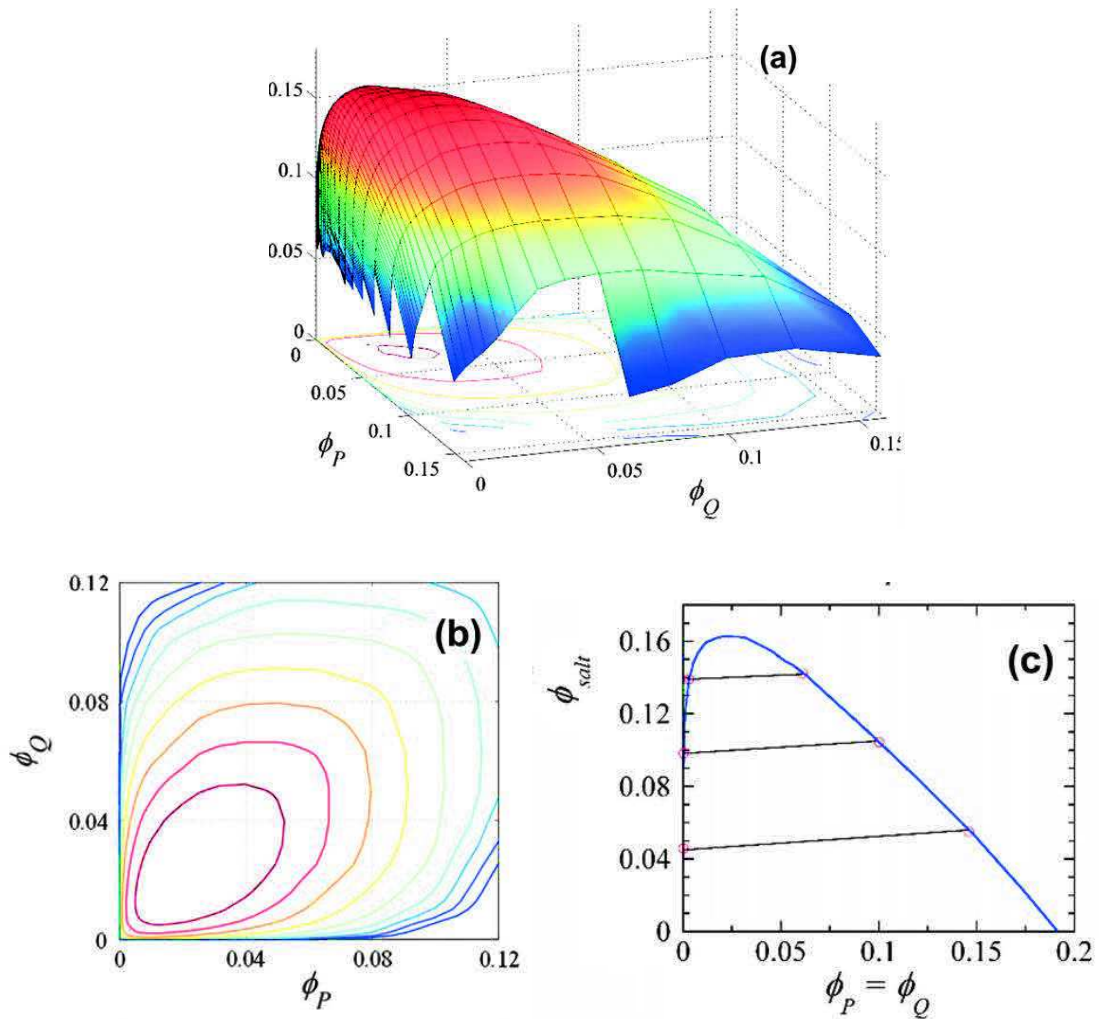
Figure 2.4. Phase diagram for polyelectrolyte complexation calculated using the Overbeek and Voorn theory[52]: (a) three-dimensional representation of the phase diagram (Φ_P, volume fraction of polycation; Φ_Q, volume fraction of polyanion, Φ_{salt}, volume fraction of salt; $N_P=N_Q=100$). Compositions corresponding to points below the draw surface are unstable. (b) Two-dimensional representation of the same phase diagram; bimodal lines for different salt concebtrations are shown, as well as three tie-lines connecting co-existing phases. (c) Binodal line and several tie-lines for a stoichiometric mixture of polyelectrolytes.

- The width of the biphasic region also depends on the length of the macroions. Actually, the critical ionic strength increases with the chain length;

- The tie-lines in Figure 2.4 (b) indicate that there is a slight accumulation of salt in the concentrated complex phase;

- The monophasic region corresponds to non-stoichiometric charge compositions (large ratios). The excess polyelectrolyte behaves like an added electrolyte[70].

- For salt-free solution, both polyelectrolytes accumulate in the concentrated phase. However, as the ionic strength increases, the distribution of the polyelectrolytes in the two phases becomes more and more equivalent.

As mentioned, the OV theory neglects the connectivity of charges along the chemical sequences of the polyelectrolyte chains. Within the weak coupling approach, this was corrected by using the RPA. That corresponds to the theories of Borue and Erukhimovich[27], Castelnovo and Joanny[53,54] as well as Kudlay and de la Cruz[47]. Theoretical phase diagrams and stability limits were thus precised. Loop expansions that go beyond the RPA were also used. Phase boundaries were then obtained by determining the onset of instability from the correlation function for weakly charged flexible polyelectrolytes[53].

The OV theory also neglects the counterion condensation and/or the formation of a double layer of counterions and co-ions around each macroion. This phenomenon plays an important role in the electrostatic potential of the complexes. This is corrected by the model of Biesheuvel and Cohen Stuart[55,56] that applies to more strongly charge correlations (strong coupling approach). Cylindrical cells are considered around each polyelectrolyte chain and the distribution of salt ions around the macroions is determined by solving the Poisson-Boltzmann equation. However, this approach is no longer valid for very dense complex phases. Several simulations[57] were carried out for the strongly correlated phases, but they did not provide phase diagrams.

For a salt-free solution of symmetric and flexible polycation-polyanion mixture, a phase diagram has been proposed by Lee, Popov and Fredrickson, resulting from field theoretic simulations[58]. A demixing phase transition to form a "complex coacervate" is observed in strongly charged systems. It results in one phase of nearly pure solvent and another phase of the 'coacervates' that contains the majority of polymers.

Zhang and Shklovskii[59,60] have discussed the phase diagram of a solution of strongly charged long flexible polyanion (PA) and short flexible polycation (PC) (asymmetric mixture) (Figure 2.5). Different ratios of total charges of PA and PC as well as distinct ionic strengths of the solution were considered (Figure 2.6). In this strong coupling approach, the Coulomb interaction is the most significant driving force. All other interactions are neglected. Moreover, the translational entropy of polyelectrolytes is neglected to compare with the electrostatic energy, but that is probably not always justified.
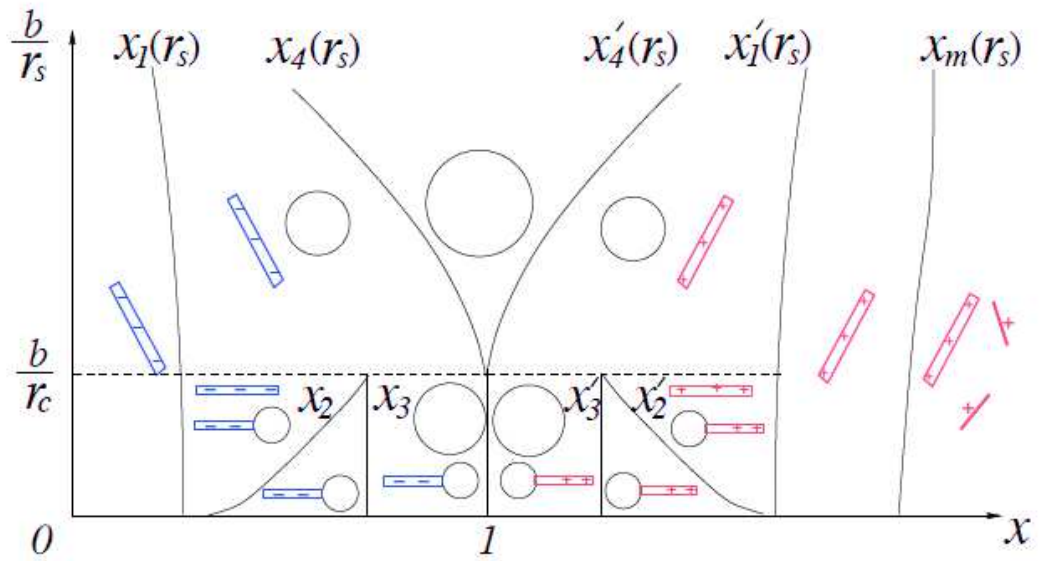
Figure 2.5. Phase diagram of a solution obtained by mixing long polyanions PA and short polycations PC. X is the ratio of total charges of PC and PA in the solution; b/r_s, the ratio of the length of monomer unit of the PA molecule; r_s, the Debye screening length
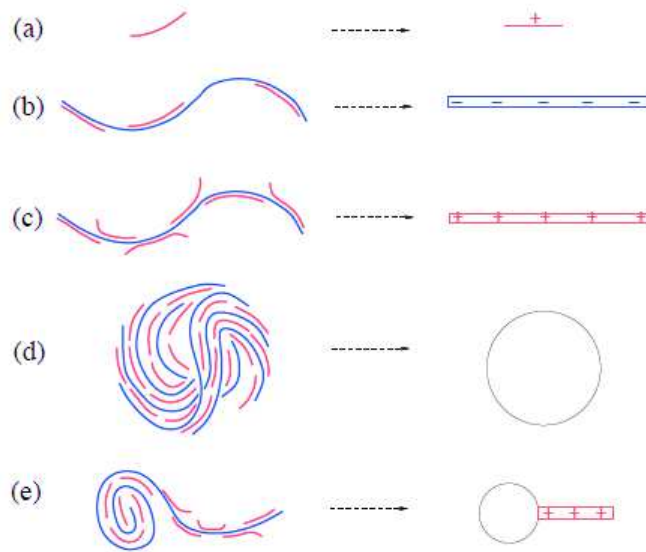

Figure 2.6. Objects appearing in a solution of long polyanions PA and short polycations PC and the related symbols used in Figure 2.5. A single macromolecule of PA (a); negative PA-PCs complex (b); positive PA-PCs complex (c); condensate of almost neutral complex (d); tadpole formed by PA-PCs complex (e)

In this strong coupling approach, in the absence of added salt, the strongly charged polyanions and polycations form a single macroscopic drop of neutral dense liquid that separates in a distinct phase from the solvent. It corresponds to x = 1 in the phase diagram. Inside the macroscopic drop, the positive and negative charges have some well-ordered arrangement to minimize the short-range correlation energy. The fact that the monomer units on the surface of the liquid drop do not have this

energy gain leads to the existence of two types of disproportion at the non-stoichiometric ratios between the negatively and positively charged monomer units. Intercomplex disproportion or partial condensation takes place when PCs locate in the complex to neutralize it. This part of the complexes forms a single drop and coexists with the rest of the formed complexes that remains highly charged and free in the solution. Intracomplex disproportion occurs for a disproportion of PCs inside the complex that results in the "tadpole" phase (see Figure 2.6). This model is called Shklovskii's condensate model.

In the presence of added monovalent salt, the regions of the condensate phases are wider. As the salt concentration is increased, the range of the Coulomb interaction becomes smaller, contrary to the unaffected short-range interactions. The ionic strength of the solution increases along the axis b/r_s in Figure 2.5. At a certain salt concentration, the short-range interactions are also screened and the macroscopic liquid drop is dissolved. Inter and intra disproportions are affected by a lower Coulomb energy and a higher surface energy than in salt-free solutions. Thus, the "tadpole" phases are not preferred.

The capability of a low-molecular weight electrolyte to block the complexation at a certain critical concentration has been shown for oppositely charged and partially hydrophobic polyelectrolytes by Krotova, Vasilevska, and Khokhlov[50].

Another aspect that was not considered in the approaches mentioned above is the influence of smaller soluble complexes on the phase diagram. To account for this, Veis and Aranyi have proposed for the complex formation, or coacervation, a two-step process[61]. First, neutral Symmetrical Aggregates (SA) are spontaneously formed by electrostatic interactions. Then, through a secondary aggregation due to hydrophobic interactions, these primary complexes rearrange to form a macroscopic concentrated coacervate phase.

Among all the models presented for the complexation between polyelectrolytes of opposite charges, just the Shklovskii's condensate model accounts for the redistribution of counterions as part of the complex organisation.

2.2.3. Main average structures of polyelectrolyte complexes

Due to some kinetics of the complex formation, the structure of the complexes can strongly depends on the conditions of their preparation. According to the characteristics of the polyelectrolytes

(weak or strong, charge fraction and distribution along the chemical sequence[6,113–115], molecular weight[65] and composition of the mixture), the conditions of preparation (solvent quality, pH[45,48,66–6869], ionic strength[48,65–67,69–73] and temperature[74]), the mixing procedure (polyelectrolyte titration[75,76], jet mixing[75], order of mixing[77,787670], time of mixing[75]), a large spectrum of PEC morphologies can be obtained. Three main categories of PEC structures can be defined: water-soluble, colloidal and dense.

The possibility to obtain water-soluble polyelectrolyte complexes was shown first by Kabanov[79–82] and Tsuchida[83,84]. In this case, the association takes place between weak polyelectrolytes of distinct molecular weights for a certain ionic strength. These complexes can be formed at extremely non-stoichiometric charge ratios when the polyelectrolytes are able to interact cooperatively and usually have a ladder structure[79–82]. As a result, the polyelectrolyte complex consists of hydrophilic single-stranded units and hydrophobic double-stranded units[85].
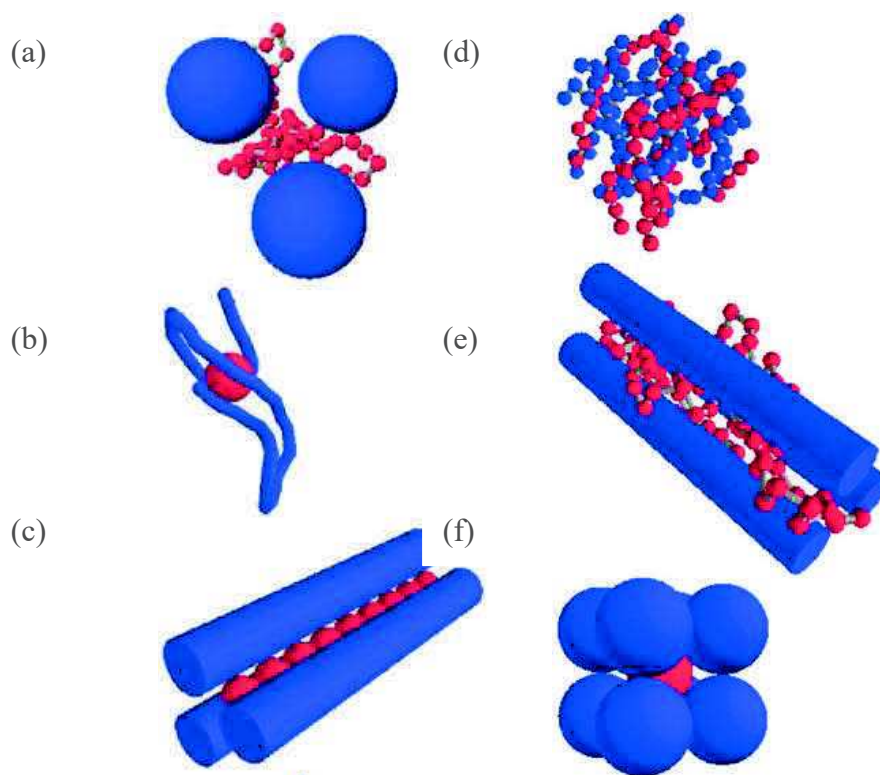

Figure 2.7. Structures of PECs formed by macroions of different intrinsic stiffnesses: flexible linear + globular (a); semiflexible linear + globular (b); rodlike linear + globular (c); flexible linear + flexible linear (d); rodlike linear + flexible linear (e); globular + globular (f)[51,89]

Colloidal complexes can be formed based on polyelectrolytes of close molecular weights if they are stabilized by a charge excess[42,86,87].

Dense complexes include coacervates, precipitates or cloudy phases depending on the water content and their visual appearance[65,69,88]. Having large water content, coacervates remind viscous liquids. On the contrary, precipitates have small amounts of solvent and have solid-like structures (glass polymer). Cloudy phases are intermediate states between precipitates and coacervates. Precipitates and cloudy phases could be non-equilibrium structure while coacervates are formed through a phase separation. To describe the structure of dense PECs the 'scrambled egg model' was proposed. They are formed by non-cooperative binding of numerous overlapping polyelectrolytes[42]. Later theoretical and simulation studies proposed more detailed illustrations. For instance, Figure 2.7 presents different models of PECs formed with polyelectrolytes of distinct intrinsic stiffness[51,89]. Useful tools such as small-angle X-ray and neutron scattering techniques give experimental possibilities to describe the details of the polyelectrolyte complexes with the different architecture: rod-like[90–93]; core-shell[94,95]; randomly branched[91]; close to a neutral polymer[96] or to the interpenetrated overlapping polymer solution[97].

Chapter 3

Syntheses, characterizations and sample preparations

The structure of polyelectrolyte complexes depends on numerous parameters. The most significant parameters are the characteristics of their components such as their average molecular weight, their polydispersity index, even their molecular weight distribution, their intrinsic stiffness, the chemical nature of their ionic groups including the one of counterions, their charge fraction and their distribution along the chemical sequence, their tacticity, their hydrophilic or hydrophobic character.

This study aims at investigating first the influence of the intrinsic stiffness of polyelectrolytes on the structure of the aqueous solutions of polyelectrolyte complexes. It also tackles the influences of the polyelectrolyte concentration, the presence of a low molecular weight added salt as well as the way of preparing the aqueous solutions. We fixed, as much as possible, other parameters. Thus, all polyelectrolytes are linear and hydrophilic. The polymerization degrees of the oppositely charged macroions were close or identical. We used just salt forms with sodium and chloride counterions for polyanions and polycations, respectively. Sodium chloride then corresponds to the added salt that is used to control the ionic strength of the aqueous solutions, in particular during the complex formation. The presence of just one couple of low molecular weight cations and anions simplifies the investigation of the polyelectrolyte complexes solutions.

This chapter describes the polyelectrolytes that were employed for preparing and studying the PEC aqueous solutions (Figure 3.1.). We have synthesized some of them in our laboratory, at Institute Charles Sadron (ICS). The related procedures are given in this chapter. Soliance, France, kindly provided fractions of polysaccharide hyaluronan, which was used as polyanion. A section of this chapter summarizes all the characteristics of these polyelectrolytes. Another one describes the ways used to prepare all the binary (polyelectrolyte-solvent) and ternary (polyanion-polycation-solvent) systems used in our study.
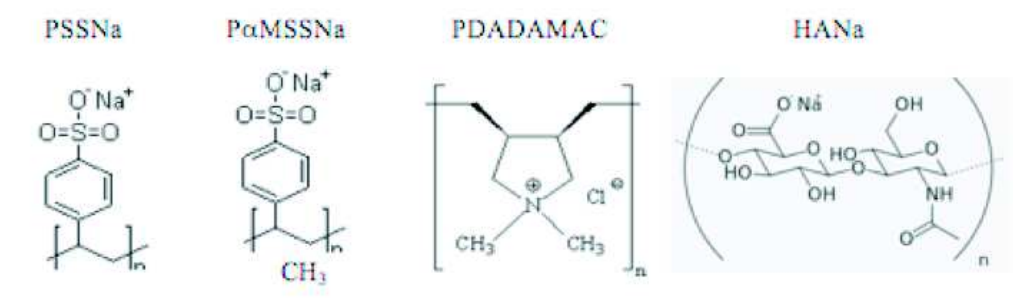
Figure 3.1. The four polyelectrolytes used in this study

3.1. Polyelectrolytes

3.1.1. Syntheses

3.1.1.1. Poly(sodium styrene sulfonate)

The polyanion, poly(sodium styrene sulfonate) (PSSNa), is a highly charged flexible polyelectrolyte, as it corresponds to a fully sulfonated polystyrene (PS), which is often employed as a model compound. We used hydrogenated (PSS$_h$Na) and completely deuterated (PSS$_d$Na) forms in order to carry out some contrast variation in neutrons scattering experiments. Both, PSS$_h$Na and PSS$_d$Na, were obtained by sulfonation of atactic hydrogenated or deuterated PS previously synthesized by anionic polymerization.

There are several ways to sulfonate PS. The methods introduced by Turbac allows controlling cross-linking during sulfonation[98,99]. The sulphuric agent, sulphur trioxide triethyl phosphate, gives reproducible water-soluble products. But this complex system is corrosive and therefore not really suitable. Carrol and Eisenberg[100] have proposed another sulfonation procedure involving 100% sulfuric acid in the presence of Ag$_2$SO$_4$. This way requires several preparation steps. In the method of Vink, the sulfonation is carried out in concentrated sulfuric acid in the presence of Ag$_2$SO$_4$ or phosphorus pentoxide[101]. We used this sulfonation method with more simplified procedure proposed by Makowski et al[102,103]. This method allows obtaining either partially or fully sulfonated PS macromolecules. In our case, only 100% sulfonated hydrophilic polystyrene chains were prepared.

The synthesis was done in our laboratory under the guidance of J.-M. Catala and J.-P. Lamps. The procedure was performed by adding a double excess of sulfuric acid in the presence of acetic anhydride. Preliminary, poly(styrene) was dissolved in 1,2-dichlorethane. The reaction mixture was kept at 50°C for 30 min and then 70 °C for 4 h.
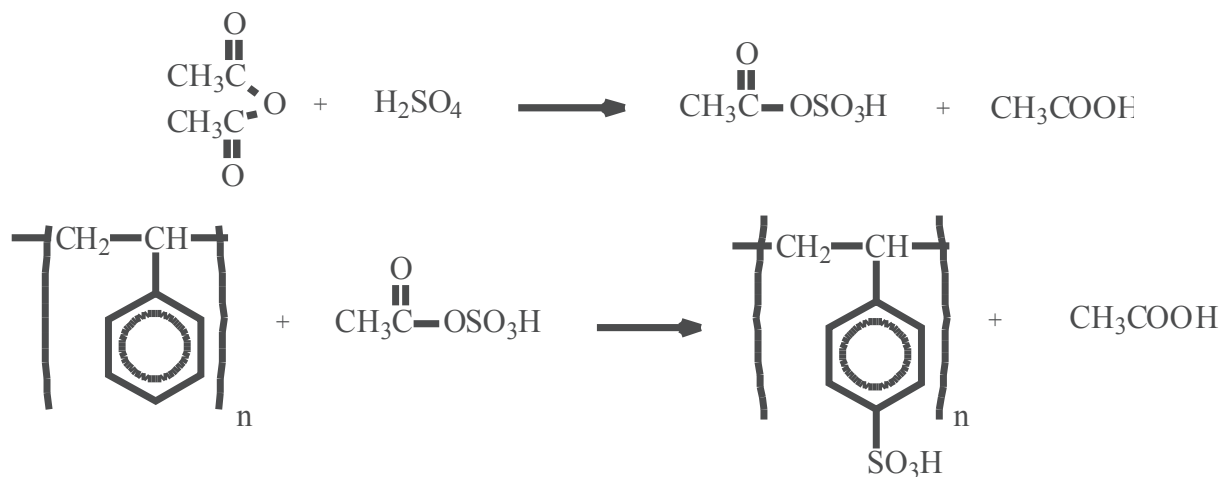
Figure 3.2. Sulfonation of poly(styrene)

After the end of the reaction, the mixture contained two immiscible phases. We decanted the liquid part and added deionized water to the rest of the polymerization solution. Afterwards, an addition of sodium hydroxide until pH 12 neutralized the colourless viscous liquid. Alkaline pH is needed to avoid the existence of sulfonic bridges. The PSSNa aqueous solutions were then purified by extended dialysis against pure water. Membranes CelluSep with cut-off 3500Da were prepared in deionized water by heating at 70°C. The end of the dialysis was controlled by conductivity measurements of the order of 1 μS. The content of the membrane was finally concentrated before freeze-drying.

The degree of sulfonation is defined as the ratio of sulfonated monomers to the total number of monomers. This value is quite important, as it determines the hydrophilic or hydrophobic character of PSSNa. In our case, just hydrophilic samples with sulfonation degrees larger than 90% were wished. For the acid, PSSH, the degree of sulfonation was evaluated by ^{1}H NMR of the test solution taken directly from the reactor. The ratio of the integrated intensity of aromatic hydrogens to aliphatic ones is 4:3 for the fully sulfonated PS, and 5:3 for PS. ^{1}H NMR spectrum of the taken test in the reaction mixture corresponded to 100% sulfonated PS. The degree of sulfonation for deuterated PSSNa was determined by elemental analysis after freeze-drying and was 100% as well[30].

The PS and PSSNa macromolecules were characterized by multi-detector size exclusion chromatography (SEC) using THF and a mixture 80% H_2O-20% ACN (acetonitrile) with 0.1M $NaNO_3$ as eluents, respectively. The main characteristics of PSS_hNa and PSS_dNa are listed in Table 3.2.

3.1.1.2. Poly(sodium α-methyl styrene sulfonate)

Polyanion, poly(sodium α-methyl styrene sulfonate) (PαMSSNa), has a methyl group in α position that specifically results in a higher intrinsic stiffness comparing to PSSNa[104].

This polyelectrolyte was obtained following the same sulfonation and purification procedures as for poly(styrene sulfonate). Parent poly(α-methyl styrene) was first prepared by J.-M. Catala. The synthesis method is described in patents[105,106]. We note that the sulfonation of PαMS is more delicate than the one of PS because of the equilibrium between polymer, monomer, and carbanion.

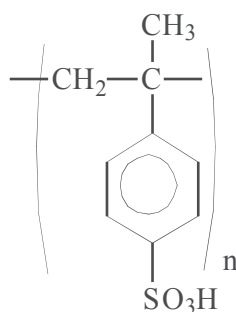PαMS and PαMSSNa macromolecules were characterized as PS and PSSNa ones, respectively.

Figure 3.3. Chemical structure of poly(α-methyl styrene sulfonate)

3.1.1.3. Poly(diallyldimethylammonium chloride)

Poly(diallyldimethylammonium chloride) (PDADMAC) is a cationic semiflexible polyelectrolyte that is extensively used in different areas of polyelectrolyte research[107–109]. Its unique pyrrolidinium structure and simple way of synthesis make PDADMAC an attractive polyelectrolyte. The article of Wandrey[110] reviews: the kinetics and mechanistic of the diallyldimethyl ammonium homo- and copolymerizations; the chemical structures; the polyelectrolyte behaviour in solution; the molecular characterization; the interactions in solution and at interface.

The free radical polymerization of diallyldimethylammonium chloride in aqueous solution proceeds as a cyclopolymerization[111]. The resulting polymer contains configurational isomers of pyrrolidimium rings with a cis-trans ratio 6:1 linked by ethylene groups as monomer units. The ratio

between cis and trans configurations does not change with the solvent nature (water, acetone, 1-methyl-2-pyrrolidone, tetramethylurea, dimethylformamide), the initiator and the reaction temperature[110]. Additionally, the polymer contains less than 2 % of pendent double bonds resulting from either chain propagation without cyclization or a transfer to monomer (Figure .4). To study PECs, based on PDADMAC, linear macromolecules were considered.
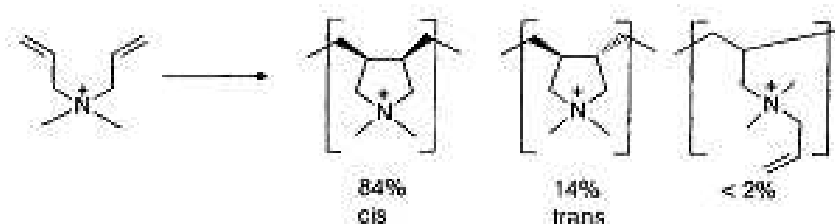

Figure 3.4. Chemical structure of PDADMAC at low conversion

The homopolymerization of diallyldimethylammonium chloride is possible using various water-soluble initiators. There are ammonium persulfate[112], ammonium persulfate/triethanolamine[113], ammonium persulfate/allyldimethylamine[114] and azoinitiators[113]. According to such initiators different overall polymerization rates were obtained. But, in any case, the initiation is going together with several side reactions such as the formation of chlorine atoms, which both initiate the polymerization and terminate the growing chain. To avoid chain branching by the pendent allylic double bonds, the reaction has to be stopped at low conversion (less than 10%)[111].

We chose an azoinitiator, 2,2'-azobis(2-methylpropionamidine) dihydrochloride (V-50) (Figure 3.5), to prevent chemical side reactions[115]. The decay time of the initiator has to be larger than the time of the polymerization. That is the criterion of the permanent radical concentration for the quasi-stationary polymerization process. For V-50, the decay time is 10 hours that is sufficient for the used polymerization conditions.
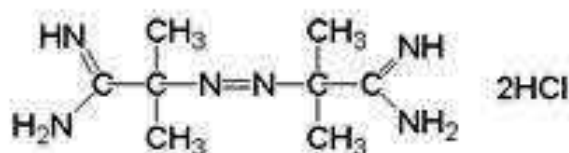

Figure 3.5. Chemical structure of 2,2'-azobis(2-methylpropionamidine) dihydrochloride

The polymerization of diallyldimethylammonium chloride is different from the ideal polymerization and has numerous derivations from other cationic monomers[114,116–118]. The DADMAC also plays a role of low molecular electrolyte that increases the ionic strength of the solution. It suppresses the electrostatic repulsion between the growing polymer cationic radical and the monomer cation, which increases the polymerization rate. The monomer exponent becomes larger with the monomer concentration and reaches a maximum at [M] = 0.15 mol/l.

As a result, the polymerization rate for the water-soluble azoinitiator can be described by the following equation[119]:

$$V_p = (\frac{2fk_ik_p^2}{k_t})^{0.5}[I][M]^2,$$ (41)

where V_p is the overall polymerization rate; f, the initiator efficiency; k_i, the constant rate of decomposition; k_p, the constant rate of propagation; k_t, the constant rate of termination; [I], the initiator concentration; [M], the monomer concentration.

The polymers were prepared by radical polymerization of the commercially available monomer and initiator purchased from Aldrich and Waka, respectively. Both were used without further purification. The experimental conditions for obtaining linear PDADMAC chains with a narrow molecular weight distribution and with average molecular weights close to those of the PSSNa chains were chosen after several calibration syntheses based on the kinetic model proposed by Jaeger[113,119].

First, the syntheses were performed for small quantities. The reaction mixtures were obtained by combining the monomer and initiator stock aqueous solutions (Table 3.1.). The concentration of monomer was varied in the range between 0.9 mol/l < c < 3 mol/l; that of initiator, in the range 0.0025 mol/l < c < 0.04 mol/l. Fifteen different samples were prepared. Polymerizations run between 30 and 400 min. The constant rate of decomposition k_i for V-50 is larger at a higher temperature than at room temperature. Thus, after degassing, the polymerization mixture was thermostated at 50°C. Polymerization was stopped by cooling. The monomer conversion was determined by ^{1}H-NMR characterizations of samples taken directly from the polymerization mixtures. Typically, a ^{1}H-NMR spectrum of a polymerization mixture is a linear combination of monomer and polymer signals (Figure 3.6 and Figure 3.7, respectively). Both polymer and monomer have 16 protons. The peaks with the chemical shift values of 5.7-5.8 ppm and 6.1 ppm are assigned to allyl [1]H. Taking part in the pyrrolidimium ring formation these protons change the signal position to 3.9-4.0 ppm because of the opening of double bonds. The peaks at 3.0-3.3 ppm correspond to the aliphatic hydrogens of the methyl groups. The four protons of N^+-$(CH_2)_2$ are at the chemical shift values of 4.0 ppm. The

polymerization rate or monomer conversion degree is calculated as the ratio between the integrated intensity signals corresponding to the polymer and the sum of the integrated intensity signals of the whole mixture. Its reaction time dependence is presented in Figure 3.8.
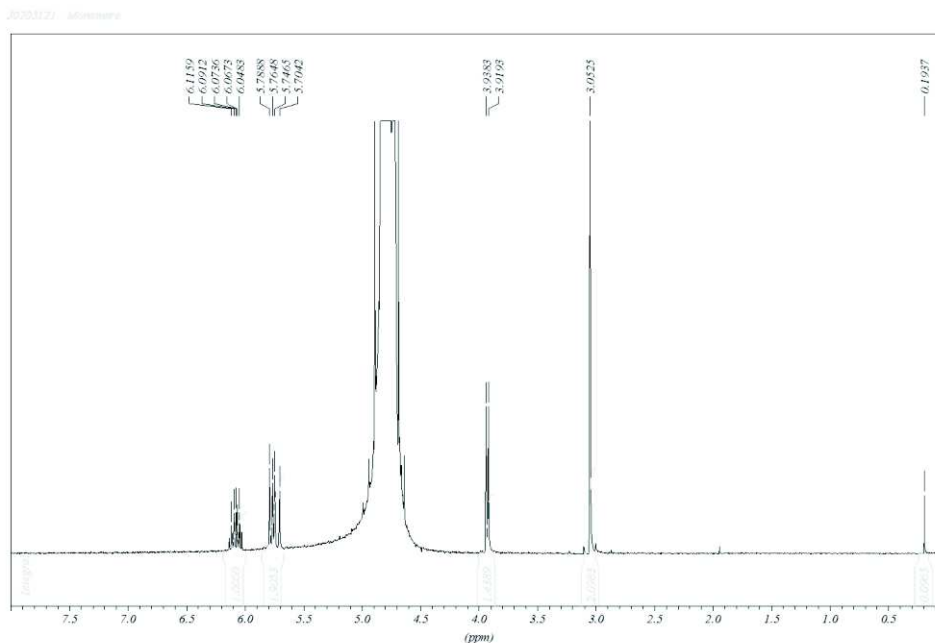

Figure 3.6. ^{1}H-NMR spectrum of diallyldimethylammonium chloride monomer
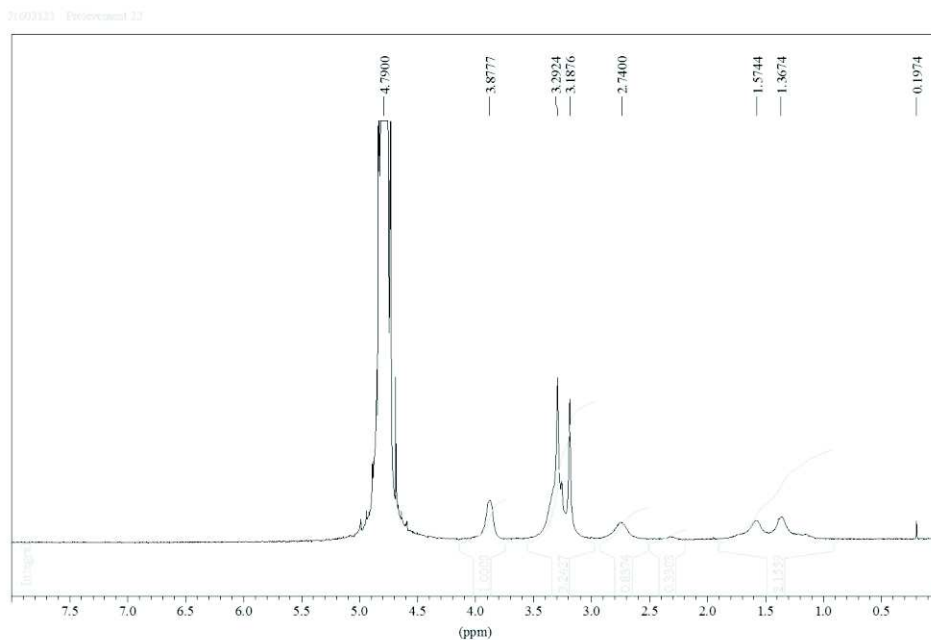

Figure 3.7. ^{1}H-NMR spectrum of poly(diallyldimethylammonium) chloride

The PDADMAC aqueous solutions were purified by dialysis against pure water MilliQ by using membranes Cellu Sep T1/Nominall (MWCO: 3500 Daltons). The membranes were prepared by heating at 70 ºC. The end of the dialysis was controlled by the conductivity measurements (≤ 1 µS). Afterwards, PDADMAC macromolecules were obtained by freeze-drying. Their molecular weight distributions were determined by multi-detector size-exclusion chromatography (SEC). A series of PDADMAC samples, in enough quantity for preparing polyelectrolyte complexes with other polyelectrolytes of opposite charge, were thus prepared. The experimental conditions for these five further syntheses have been derived from the obtained kinetics data of the polymerization process described above, as well as from the molecular weights and polydispersity indexes of the resulting PDADMAC samples. The low conversion condition (conversion less than 10 %) was taken into account as well (Table 3.1).
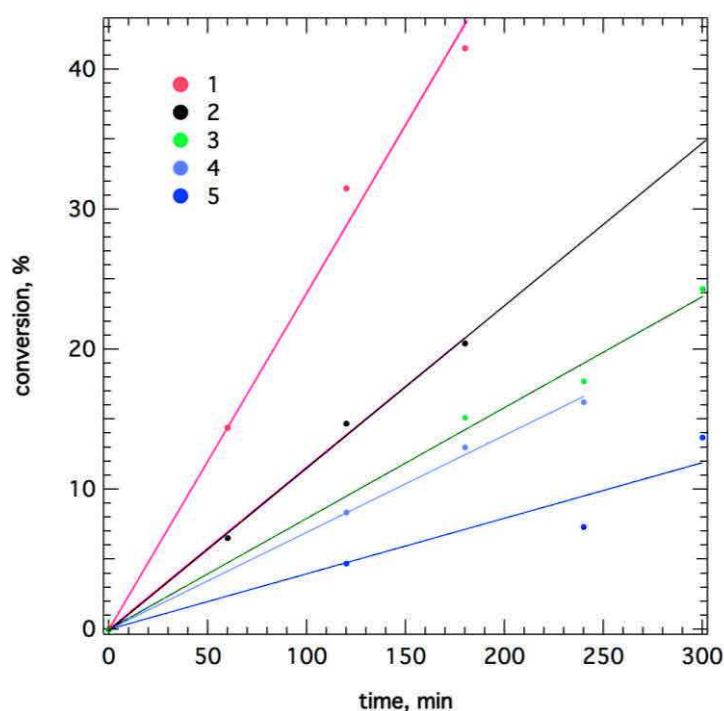

Figure 3.8. The dependence of monomer conversion as a function of time

Table 3.1. Experimental conditions for the various PDADMAC synthesises. [M] and [I] are the initial monomer and initiator concentrations, respectively, in a polymerization mixture

Composition	[M], mol/l	[I], mol/l	Polymerization time, min
Composition 1	1.5	0.04	45
Composition 2	1.5	0.01	85
Composition 3	0.9	0.01	150
Composition 4	1.5	0.005	135
Composition 5	1.5	0.0025	300

3.1.2. Hyaluronan

Hyaluronan (hyaluronic acid HA, in its acid form; sodium hyaluronate HANa, in its salt form) is a linear semi-flexible anionic polysaccharide. The monomer unit of the HANa is sodium-β-D-glucuronate-[1-3]-β-N-acetyl-D-glucosamine-[1-4] (Figure 3.9). The molecular weight of this biomacromolecule can reach millions.
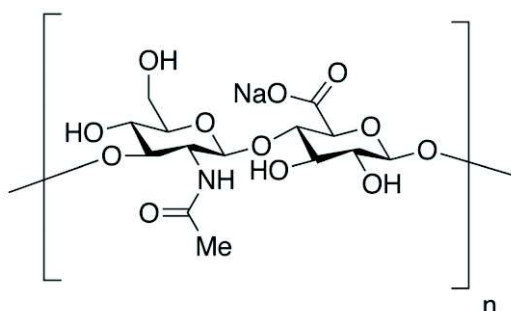

Figure 3.9. Chemical structure of the sodium hyaluronate

First time HA was discovered in the vitreous humor of bovine eye by Karl Meyer in 1934[120]. The salt form, hyaluronate, of this polysaccharide presents in the human body (around 15 g), mainly in connective, epithelial and neutral tissues[121]. Naturally the biomolecules are synthesized by a class of integral membrane proteins[121]. Industrial hyaluronan has a number of sources but the most important are: animal, based on extraction from natural material, and bacterial, production using

Streptococcus bacterium[122]. The HA degradation can be carried out by different types of enzymes with the production of oligosaccharides or low molecular weight biomacromolecules. It is used in industry to create short hydrosoluble polymer chains. Also, under the strong alkaline condition, the formation of oligosaccharides is possible[123].

Because of its biocompatibility, non-toxicity, and anti-inflammatory properties, hyaluronan is widely used in neurosurgery, skin regeneration and cosmetic practice[122,124,125]. HA polymers are also significant materials in the preparation of gels in drug delivery systems for eyes and treatment of dry eyes syndrome[126]. Numerous anti-cancer drug delivery systems are constructed based on hyaluronan because of its affinity to special receptors[127,128]. HA is fully soluble in water, producing a gel[129]. Due to its high viscosity, the hyaluronan applications include treatment of joint and pulmonary pathologies[122,124,130,131]. Water soluble and water insoluble materials in the form of films and cryogels are possible to be prepared[132,133].

Hyaluronic acid is a weak acid with pK_a equal to 3.2. Rheology measurements show a relatively weak influence of pH on the behaviour of HA solutions in the range $1.6 < pH < 12.6$[134]. In acidic conditions ($pH < 1.6$), the net charge is reduced and the acetamido groups can be protonated. The H-bond network takes place and the cooperative intermolecular interaction results in a gel-like behaviour of HA solutions. An alkaline medium ($pH > 12.6$) destroys the H-bond network. The salt form of HA in pure water can be considered as a completely charged polyelectrolytes (chemical charge fraction equals to 1) with negative COO^- groups[135].

We used commercial HANa samples kindly provided by Soliance (France). Their purity, as well as their average molecular weights, was specifically determined by multi-detector size-exclusion chromatography.

3.2. Characterizations

All synthesized, modified or industrial polymers were characterized by ^{1}H-NMR spectroscopy with a Bruker Avance 400 spectrometer at T=25.0 ± 0.1 °C, specifically to control the polymerization conversion in the PDADMAC synthesises or the sulfonation degrees of PSSNa and PαMSSNa macroions. The polymer solutions were prepared in D_2O.

Size exclusion chromatography (SEC), coupled with a multi-angle light scattering diffractometer (LS), a refractometer (RE) and an UV-visible absorption spectrometer (UV) as detectors, was used to control and determine the unimodal molecular weight distribution of each polymer. In principle, it allows to measure M_w, the weight-average molecular weight; M_n, the number-average molecular weight; $I = M_w/M_n$, the polydispersity index; $<R_G^2>_z$, the z-average of the square radius of gyration; R_H, the hydrodynamic radius. The SEC characterizations of poly(styrene) and poly(α-methylstyrene) were done using THF as an eluent and PS chains as standards as well as the direct LS detection. The eluents for the SEC characterizations of the different polyelectrolyte were: H_2O-TFAc mixture, with 10% of TFAc and 0.1M NaCl + NaN_3 (bacteriostatic agent), for PDADMAC; H_2O-ACN mixture, with 40% of ACN and 0.1M $NaNO_3$ + NaN_3, for PSS_hNa, PSS_dNa and $P\alpha MSSNa$; H_2O and 0.1 M $NaNO_3$ + NaN_3, for HANa.. The measurements were carried out at 25 °C. The flow rate was kept at 0.5 ml/min.

The polymer characteristics determined by SEC, with their non-electrostatic persistence length l_p^0 and their effective charge fraction f_{eff} that account for the Manning-Oosawa counterion condensation process, are summarized in Table 3.2. The effective charge fraction, f_{eff}, is calculated as $f_{eff} = b/l_B$, where b is the monomer unit length and l_B is the Bjerrum length (l_B = 7.14 Å for water at room temperature). The effective charge fraction of the PDADMAC, f_{eff} = 0.66, has been measured by capillary electrophoresis[136]. We must consider an average molar mass of the monomer units, taking into account the Manning-Oosawa counterion condensation process. Using the value f_{eff} = 0.66, we obtain an average molar mass $<m>$ = 138.27 g.mol^{-1} and a mass per unit contour length $M_L = <m>/b$ = 29.42 g*mol^{-1}*Å^{-1}[30]. With this M_L value, an analysis of the specific experimental results of Dautzenberg et al[119] through the wormlike chain model by taking into account the limit $M/(M_L l_p) <$ 300 to neglect the excluded volume interactions and the polydispersity of the samples, led to a reliable estimation of the intrinsic persistence length of the PDADMAC, $<l_p>$ = 30.1 Å[30].

The persistence length of polystyrene chains of mass per unit length M_L = 41.2 g*mol^{-1}*Å^{-1} could be determined from an analysis of the experimental scaling law of the chain radius of gyration measured in a theta solvent according to the molecular weight. The value obtained taking into account the polydispersity is l_p = 10 Å[137]. The effective charge fraction of the PSS macroions is $f_{eff} = b/l_B$ = 0.36 since the monomer unit length b = 2.53 Å. For PαMSS, the same analysis of the radius of gyration measurements in a theta solvent has suggested a helical wormlike chain local structure with l_p = 24 Å at room temperature[104].

Concerning HA, there is a wide dispersion of values obtained for its non-electrostatic persistence length, in the literature. The discrepancies between all the values proposed by different authors reflect the contribution of polydispersity, which is rarely taken into account, and the differing degrees of correction for the excluded volume effects. From this point of view, the measurements of the form factor of the HA chains in aqueous solutions with added salt using SAXS or SANS is probably the best way to obtain a reliable persistence length via the comparison with the form factor of the wormlike chain model. Indeed, there is none effect of the polydispersity as well as the excluded volume interactions on the local average conformation of chains investigated at high scattering vectors q. This approach will be described in Chapter 5 using SAXS. It leads to l_p = 87.5 Å in the agreement with the similar approach previously carried out by SANS[138]. The effective charge of the HA macroions is equal to the chemical charge f = 1, because b is quite close to l_B = 7.14 Å. Thus, there is none condensed counterion onto the macroions.

The crossover concentrations C* between dilute and semidilute regimes were calculated for the used samples using the following ways:

- For PSSNa in salt-free aqueous solutions[139]:

$$C^*(mol/l) = 1620 * N^{-2}, \text{ where N is the degree of polymerization.} \qquad (42)$$

- For PDADMAC in salt-free aqueous solutions, we deduce the relationship from Eq. (42) taking into account the difference in the scattering laws between PSS and PDADMA macroions[30]:

$$C^*(mol/l) = 151 * N^{-2} \qquad (43)$$

- For HA in salt-free aqueous solutions from the SAXS measurements results of J. Combet:

$$C^*(mol/l) = 225 * M_w^{-2} \qquad (44)$$

The values of the crossover concentration C** between the semidilute and concentrated regimes were measured experimentally for PDADMA, PSS and PαMSS by P. Lorchat[30] and for HA in Chapter 5 of this thesis.

The water contents in the dry polymers (powders) were determined by thermogravimetric analysis (TGA) before any sample preparation and after sufficient exposures of the powders to air at atmospheric pressure. The mass fraction of H_2O slightly varied with the polyelectrolytes: 16-21.7 % for PDADMAC; 14-17 % for PSSNa and PSSH; 10-15 % for HA.

Table 3.2. Main characteristics of the polyelectrolytes used in this study: M_w, the weight average molecular mass, N_w, the weight average degree of polymerization; f, the chemical charge fraction; f_{eff}, the effective charge fraction obtained from f using the Manning-Oosawa approach; l_p^0, the non-electrostatic persistence length; C^* is the crossover concentration between dilute and semidilute regimes; C^{**} is the crossover concentration between semidilute and concentrated regimes.

Sample	M_w (g/mol), 10^5	$I= M_w/M_n$	N_w	f	f_{eff}	l_p^0 (nm)	C^* $(10^{-3}$ mol/l)	C^{**} (mol/l)
PDADMAC22	0.87	1.91	540	1	0.66	3	0.5	0.12
PDADMAC23	0.61	1.72	383	1	0.66	3	1	0.12
PDADMAC24	1.34	1.57	830	1	0.66	3	0.2	0.12
PDADMAC26	1.20	1.69	740	1	0.66	3	0.3	0.12
PDADMAC J150412	1.1	1.70	680	1	0.66	3	0.3	0.12
PDADMAC J240412	0.31	1.64	190	1	0.66	3	4	0.12
PSSNa$_h$ J301012	2.20	1.06	1078	1	0.26	1	1.4	1.3
PSSNa$_h$ IK290914	2.10	1.61	1019	1	0.26	1	1.6	1.3
PSSNa$_d$ J311012	2.11	1.08	990	1	0.26	1	1.7	1.3
PαMSSNa	2.48	1.06	1127	1	0.36	2.4	1.3	0.5
HA1 PRYMALHYAL 50 (12271A)	0.53	1.60	140	1	1	4-5[140]; 7-10[140]	5	0.1
HA2 PRYMALHYAL 300 (12314F)	3.95	2.06	986	1	1	4-5[140]; 7-10[140]	2	0.1
HA3 PRYMALHYAL 50 (14150A)	0.41	1.59	108	1	1	4-5[140]; 7-10[140]	6	0.1
HA4 CRYSTALHYAL (14151A)	7.29	1.82	1929	1	1	4-5[140]; 7-10[140]	1.5	0.1

3.3. Sample Preparations

3.3.1. Polyelectrolyte aqueous solutions

The behaviours of poly(diallyldimethyl ammonium) chloride, sodium poly(styrene sulfonate) and poly(α-methyl styrene sulfonate) in water were the subjects of numerous studies. Nevertheless, binary PDADMAC/H_2O and PSSNa/H_2O mixtures were investigated by small-angle X-ray scattering to have references and to compare the scattered intensities from these PE solutions with those of the related PEC ones, as necessary. HANa/H_2O salt-free aqueous solutions were also prepared in a wide concentration range (0.01 mol/l < c < 2.10 mol/l) to complete the study of the salt-free aqueous solutions of semiflexible polyelectrolytes started with PDADMAC and PαMSSNa by P. Lorchat[30].

The binary systems PDADMAC/H_2O, PSSNa/H_2O and PαMSSNa/H_2O were prepared by dissolving dry polymers in ultrapure water Milli-Q or a solution 0.15 M NaCl in water Milli-Q. The presence of the added salt changes the ionic strength of the aqueous solution. The concentration of the monovalent salt, 0.15 M, was chosen for several reasons. First, it corresponds to the classical studies on polyelectrolyte multilayers performed by our colleagues at ICS. PE multilayers are particular cases of polyelectrolyte complexes at interfaces. This gives an opportunity to compare the results obtained from PEC solutions with those of PE multilayers. Second, the concentration 0.15 M is below the critical concentration for which electrostatic interactions between polyelectrolytes are screened[78]. Third, the chosen concentration is that of the physiological medium.

To avoid self-association and to reach thermodynamic equilibrium, all PDADMAC, PSSNa and PαMSSNa solutions were heated at 45 ºC for one hour and then let to stay at least three days before measurements or complex preparation. The final polymer solutions were kept at room temperature.

To avoid any degradation at high temperature, the HANa/H_2O solutions were not heated. To obtain homogeneous solutions, we waited five days for concentrations less than 0.01 M and seven days for higher concentrations than 0.01 M. The stock HANa solutions for complex formation with PDADMAC were prepared in water Milli-Q or 0.15 M NaCl in water Milli-Q. But, we also increased the salt concentration till 0.3 M for the solutions that were investigated by SAXS to determine the persistence length of hyaluronan as well as the correlation length in the related semidilute regime. Such a salt concentration was used to screen completely the electrostatic interactions between COO$^-$ groups. In 0.3 M NaCl water solutions, the Debye screening length is of the order of 7 Å.

3.3.2. Polyelectrolyte complex solutions

Polyelectrolyte complexes (PECs) were formed in vials by mixing polycation and polyanion solutions of equal volumes (0.5 ml for SAXS and 1.0 ml for SANS studies). The polyelectrolyte solutions were prepared separately in the wide range of concentrations from 0.002 mol/l to 0.6 mol/l.

In the first part of this study the phase behaviour of polyelectrolyte complexes systems was examined by visual observation. In order to review and summarize the phase behaviours, the visual investigation of PEC solutions are presented through two dimensions phase or state diagrams. Obviously, the concentrations on the diagram axes are equal to those of PE solutions before mixing divided by two since PE solutions of equal volume are mixed to obtain PEC solutions. The state diagrams presented in the next chapters correspond to PDADMAC solutions added to polyanion ones. However, we will also consider other ways of preparing PEC solutions

The significant changes in the PEC solutions were observed during the first two weeks. After, the solutions were stable for months. To study the structure of the PEC solutions by small-angle X-ray and neutron sattering techniques, PECs were left for 3 days after mixing for equilibration.

Chapter 4

Experimental techniques and data analyses

This section reminds the basic principles and general description of the experimental techniques that we used to investigate polyelectrolyte complexes. These methods were selected to obtain macroscopic and microscopic pictures of PECs and to reply to the main issues of our study.

4.1. Small-angle X-ray and neutron scattering techniques

4.1.1. General principle of a small-angle scattering experiment

Small-angle X-ray and neutron scattering techniques (SAXS and SANS) aims at studying the structure of large particle systems[141,142]. These systems involve colloidal dispersions, polymer or surfactant solutions, emulsions, biological systems and materials, nanocomposites, supramolecular or self-assembly systems, pharmaceutical objects, foods etc.

Actually, SAXS and SANS give information about the average structure of the systems, i.e. the average size and shape of the particles as well as their dispersion state in the solvent or the matrix of the systems. This is the static approximation.

In a typical scattering experiment (Figure 4.1), an incident beam of wavelength λ, or wave vector $\vec{k_0}$, passes through a sample and is scattered in distinct directions defined by scattered wave vectors $\vec{k}$. As concerns isotropic scattering, the scattered wave vector $\vec{k}$ is only depending on the scattering angle θ. With the static approximation, any energy exchange between radiation and matter is neglected ($|\vec{k}| \approx |\vec{k_0}|$) and the scattered intensity is only measured according to the scattering angle θ. The transmitted beam is usually stopped by a beam stop, but can also be used for measuring the transmission factor or absorption term.

Using the momentum conservation law for the particle collision process associated with scattering, we define the scattering vector $\vec{q}$:

$$\hbar\vec{k}_0 = \hbar\vec{k} + \hbar\vec{q} \Rightarrow \vec{q} = \vec{k}_0 - \vec{k} \tag{45}$$

And as $|\vec{k}| \approx |\vec{k_0}|$ the modulus of the scattering vector $\vec{q}$ is:

$$q = \frac{4\pi}{\lambda}\sin\left(\theta/2\right) \tag{46}$$

That is the Bragg law used in crystallography (the refractive index of the matter is equal to 1 for SAXS and SANS)[143]; and q, which is the most significant parameter of the scattering experiment, is the inverse of a distance.
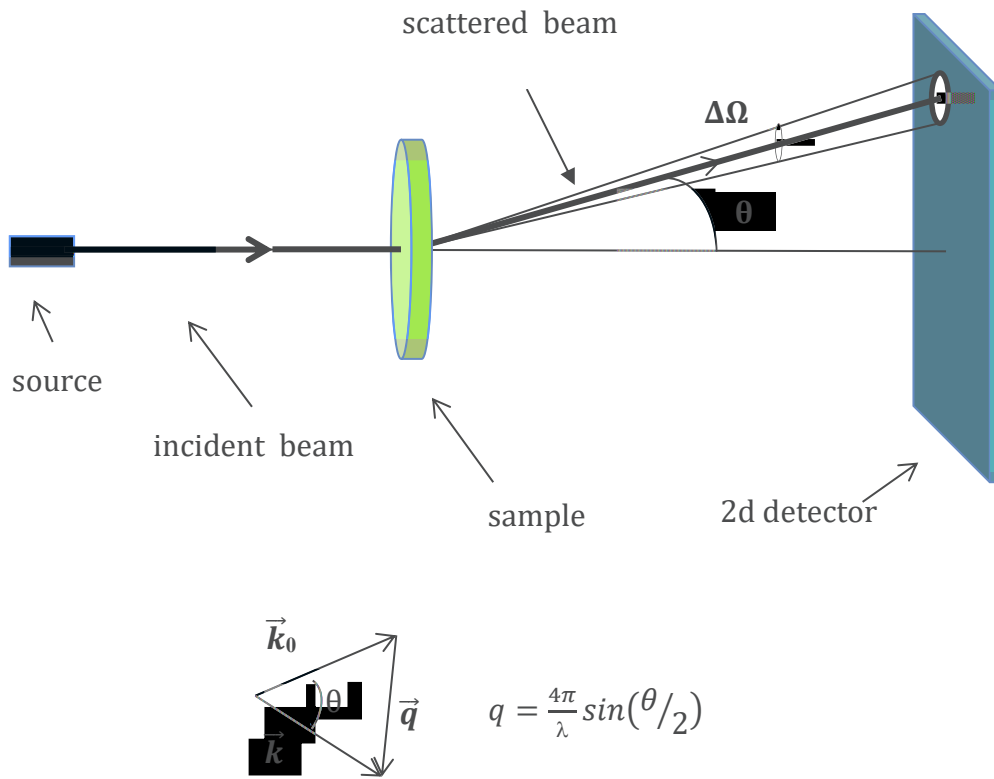

Figure 4.1. Geometry of a scattering experiment and definition of the scattering vector q

The scattered intensity is, therefore, depending on this distance in the reciprocal space, q. The scattered pattern registered by the detector results basically from the interferences between all the scattered waves by the elementary scatterers of the sample. It is proportional to the number of particles (photons or neutrons) $\frac{d\delta}{d\Omega}$, scattered at the scattering vector q, or the scattered angle θ, in the solid angle ΔΩ and normalized to the counting time and to the volume of the sample[143]:

$$I(q) = \Phi(\lambda)\frac{d\delta}{d\Omega}\Delta\Omega, \tag{47}$$

$\Phi(\lambda)$ is the flux of the incident beam and the scattered intensity I(q) has the unit of a surface over volume (cm^{-1}).

According to the linear response theory, the scattered intensity per unit volume can be written as:

$$I(\vec{q}) = \sum_{\alpha,\beta} a_\alpha a_\beta S_{\alpha\beta}(\vec{q}) = \frac{1}{V}\sum_{\alpha,\beta} a_\alpha a_\beta <\delta n_\alpha(\vec{q})\delta n_\beta(-\vec{q})> \qquad (48)$$

or

$$I(\vec{q}) = \sum_{\alpha,\beta} a_\alpha a_\beta S_{\alpha\beta}(\vec{q}) = \frac{1}{V}\sum_{\alpha,\beta} a_\alpha a_\beta <\delta n_\alpha(\vec{q})\delta n_\beta(-\vec{q})> \text{ for } q \neq 0 \qquad (49)$$

with $\qquad n_\alpha(\vec{q}) = \int d^3r \exp(-\vec{q}.\vec{r}) n_\alpha(\vec{r})$ $\qquad\qquad\qquad\qquad\qquad$ (50)

and $\qquad n_\alpha(\vec{r}) = \sum_k \delta(\vec{r} - \vec{r}_k^\alpha).$ $\qquad\qquad\qquad\qquad\qquad\qquad$ (51)

Where a_α and a_β are the scattering lengths (cm) of the elementary scatterers associated with the sample components α and β, respectively; $S_{\alpha\beta}(\vec{q})$, the scattering functions per unit volume (cm^{-3}) characterizing the structure of the sample; $n_\alpha(\vec{q})$ and $\delta n_\alpha(\vec{q})$, the Fourier transforms of the density operator $n_\alpha(\vec{r})$ related to the component α and its fluctuation $\delta n_\alpha(\vec{r})$, respectively; $n_\alpha(\overline{-q})$ and $\delta n_\alpha(\overline{-q})$, their conjugated complexes.

Obviously, the scattering lengths represent the interactions between radiation and elementary scatterers while the scattering functions characterize the structure of the sample independently of the radiation.

This formalism contains the Born approximation for the scattering process and neglects any multiple scattering.

The small-angle scattering domain corresponds to the q-range $q < 0.6$ Å^{-1} (Figure 4.2), and thus explores the average distances larger than 10 Å in the real space and practically distances lying between 10 and 1000 Å. On this spatial scale, the solvent molecules, as H_2O, and most of the monomer units can be considered as elementary scatters. They lead to a constant scattering, which does not depend on q. More generally, any set of atoms having a size less than the spatial resolution of the experiment can be considered as an elementary scattered. The spatial resolution is defined as $R = 2\pi/q_{max}$, where q_{max} is the highest q value explored in the scattering experiment.
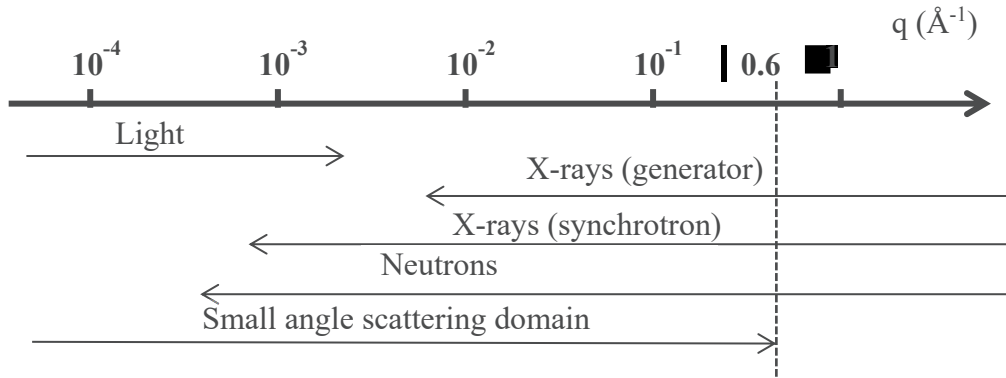
Figure 4.2. Spatial resolution: q-ranges explored by the different SAS techniques

For q < 0.6 Å^{-1}, or average distances less than 10 Å in the real space, density fluctuations can be neglected. Only concentration fluctuations then provide a signal, i.e. a scattering depending on q. This is the incompressibility hypothesis. It leads to simplifying the formalism and replacing the relations (48) and (49) by:

$$I(\vec{q}) = \sum_{\alpha,\beta} K_\alpha K_\beta S_{\alpha\beta}(\vec{q}) = \frac{1}{V} \sum_{\alpha,\beta} K_\alpha K_\beta < n_\alpha(\vec{q}) n_\beta(-\vec{q}) > \tag{52}$$

$$I(\vec{q}) = \sum_{\alpha,\beta} K_\alpha K_\beta S_{\alpha\beta}(\vec{q}) = \frac{1}{V} \sum_{\alpha,\beta} K_\alpha K_\beta < \delta n_\alpha(\vec{q}) \delta n_\beta(-\vec{q}) > \qquad \text{for } q \neq 0 \tag{53}$$

The scattered intensity per unit volume becomes a linear combination of the partial scattering functions only associated with the components of the solute. Indeed, as the density fluctuations are negligible, the solvent or the matrix of the system, i.e. one component of the system, can be eliminated. K_α and K_β are now the contrast lengths with respect to the solvent, or the matrix, of the components α and β of the solute, respectively. For a system containing p components, there will be $\frac{p(p+1)}{2}$ partial scattering functions ($S_{\alpha\beta}(\vec{q}) = S_{\beta\alpha}(\vec{q})$). Obviously, the first aim of a small angle scattering experiment is to separate out all these partial scattering functions. With SANS, this can be carried out by the use of the contrast variation method and the labelling of some parts of the system with deuterium atoms[144]. In a second step, each scattering function could be compared with a scattering function calculated from a structural model based on the densities as well as their fluctuations in the real space. Indeed, it is often illusive to try extracting reliable information by using an inverse Fourier transformation of the scattering function. The scattering functions are most of the

time only measured in a finite q-range. Finally, we should still demonstrate the uniqueness of the used structural model.

4.1.2. Scattering length density and contrast length

The strength of the interaction between the radiation and an elementary scatterer is represented by a scattering length a (cm). It depends on both the radiation and the elementary scatterer that are considered. It is, actually, defined as the sum of the scattering lengths of all the atoms, or nuclei α, which form the elementary scatterer: $a = \sum_{\alpha} a_{\alpha}$.

X-rays are scattered by electrons. The coherent X-ray scattering length of an atom or an ion is thus proportional to its number of electrons and is positive:

$$a \text{ (cm)} = 0.282 \ 10^{-12} \ Z \tag{54}$$

Where Z is the number of electrons of the elementary scatterers containing the atoms or the ions α.

In this study, we are mainly concerned with the nuclear interaction of neutrons with matter. The coherent scattering lengths of the nuclei are tabulated because they have an experimental origin[145]. They can be quite different according to their isotopic states. That is specifically the case with the hydrogen atom since for ^{1}H, $a_H = -3.739 \ 10^{-13}$ cm, while for deuterium ^{2}H, $a_D = 6.671 \ 10^{-13}$ cm. These coherent scattering lengths have not the same sign. Such a difference is quite remarkable and makes the neutron scattering technique essential for studying the soft matter. It allows improving the chemical resolution through the use of the deuterium labelling and the contrast variation methods.

To compare the amplitudes, scattered by distinct elementary scatterers, we need, however, to introduce the coherent scattering length density, which is defined as:

$$\rho = \frac{a}{v} N_A \tag{55}$$

where N_A (mol^{-1}) is the Avogadro's number; v (cm^3*mol^{-1}), the molar volume of the elementary scatterer; a (cm), its coherent scattering length. The ρ unit is cm^{-2}.

The neutron scattering has both coherent and incoherent parts. Only the coherent scattering contains structural information, provided the static scattering is only considered. The incoherent scattering is caused by the isotopic disorder of the nuclei as well as the interaction between the spins of the neutrons and nuclei. However, it only leads to a flat background that must be subtracted correctly from the measured scattering intensity in order to obtain its coherent part.

Finally, the contrast lengths introduced in Eq. (52) and (53), are defined as:

$$K = \frac{v}{N_A} \Delta\rho = \frac{v}{N_A}(\rho - \rho_s)$$

(56)

K (cm) is the contrast length of the elementary scatterers of molar volume v (cm^{3}mole^{-1}); ρ (cm^{-2}), its scattering length density; ρ_s, that of the solvent or the matrix; N_A, the Avogadro's number. K^2 (cm^2) is the contrast of the elementary scatterers with respect to the solvent, or the matrix.

All the characteristics of the elementary scatterers involved in the aqueous solutions investigated by SAXS and SANS in this study are listed in Table 4.1. In this Table 4.1, condensed or free counterions, as well as free co-ions, are not bonded[146]. As the ions are bound, their volumes can be calculated using their ionic radii (0.97 Å and 1.80 Å for Na$^+$ and Cl$^-$, respectively)[147]. In the case of condensed and free hydrophilic counterions or ions (Na$^+$ or Cl$^-$), the elementary scatterer is the solvated ion with a certain number of solvent molecules. The molar volume of H$_2$O or D$_2$O in the solvation shell is smaller than in the solvent (at 25 ºC, 16 cm^{3}mol^{-1} instead of 18.07 cm^{3}mol^{-1}) due to the hydrophilic character of some counterions or co-ions. The scattering length densities for the free ions are determined by taking into account the number of their shell of solvated water molecules: 5 and 2 for sodium and chloride, respectively[148,149].

In an aqueous solution of a highly charged polyelectrolyte, due to the dissociation and condensation processes, the solute has two components: the monomer units of the macroions and the counterions. The scattered intensity can then be written as a linear combination of three partial scattering functions:

$$I(\vec{q}) = K_m^2 S_{mm}(\vec{q}) + K_c^2 S_{cc}(\vec{q}) + 2K_m K_{mc} S_{mc}(\vec{q}),$$

(57)

K_m and K_c are the contrast lengths of the monomer units of macroions and the counterions, respectively. The three partial scattering functions are that for the macroions $S_{mm}(q)$, the one for the counterions $S_{cc}(q)$ and the cross term $S_{mc}(q)$. From Table 4.1, as the neutron contrast lengths, K_c, of Na$^+$ and Cl$^-$ are rather small, their contribution to the scattered intensity could be considered as negligible for the SANS experiments. That is no longer the case for the SAXS experiments.

Table 4.1 Characteristics of the various elementary scatterers (E.S.) involved in this study. Z is their number of electrons; V_m, their molar volume; V_0, the volume of one related molecule; a_x, their X-ray scattering length; ρ_x, their X-ray scattering length density; a_N, their neutron scattering length; ρ_N, their neutron scattering length density; σ^{inc}, their neutron incoherent scattering cross section.

E.S.	Z	V_m, cm³mol⁻¹	V_0, Å³	SAXS		SANS		
				a_x, 10^{-13}cm	ρ_x, 10^{10} cm⁻²	a_N, 10^{-13} cm	ρ_N, 10^{10} cm⁻²	σ^{inc}, 10^{-24} cm²
H_2O	10	18.07	30.00	28.20	9.40	-1.68	-0.56	159.80
D_2O						19.15	6.38	4.08
PSS_h^- ($C_8H_7SO_3^-$)	96	113.2	188.00	270.72	14.40	47.25	2.51	561.91
PSS_d^- ($C_8D_7SO_3^-$)						120.12	6.39	14.37
$P\alpha MSS_h^-$ ($C_9H_{10}SO_3^-$)	104	130.7	217.04	293.28	13.51	42.68	1.97	802.72
$PDADMA^+$ ($C_8H_{16}N^+$)	70	103.6	172.04	197.40	11.47	2.70	0.16	1284.83
HA^- ($C_{14}H_{20}NO_{11}^-$)	200	224	372.00	564.00	15.16	91.46	2.46	1605.91
Na^+(bounded)	10	2.3	3.82	28.20	73.83	3.63	9.50	1.62
Na^+ (free) Na^+, $5H_2O$	60	73.4	121.9	169.20	13.88	-4.75	-0.39	800.62
Na^+, $5D_2O$						99.36	8.15	22.02
Cl^- (bounded)	18	14.7	24.40	50.76	20.79	9.58	3.92	5.30
Cl^- (free), Cl^-, $2H_2O$	38	55.2	91.66	107.16	11.69	6.23	0.68	324.90
Cl^-, $2D_2O$						47.87	5.22	13.46
(NaCl)	28	16.6	27.57	78.96	28.44	13.21	4.79	6.92

4.1.3. Form factor and intermolecular scattering function

By considering a polymer solution or a solution of homogeneous particles, the scattered intensity measured by SAXS or SANS allows determining a single scattering function. This scattering function, which is associated with the polymers or the particles, however, involves two terms: an intramolecular one, which gives information about the average size and/or shape of the polymers or the particles, and an intermolecular term, related to the dispersion state of the polymers or particles. We have:

$$I(q) = K^2 S(q) \tag{58}$$

$$S(q) = c[g_1(q) + cg_2(q)] = c[NP(q) + cg_2(q)] \tag{59}$$

K^2 (cm^2) is the contrast factor of the monomer units, or elementary scatterers of the particles, with respect to the solvent; c (mol.cm^{-3}), the concentration of the solution; $g_1(q)=NP(q)$, the form factor of the polymers or particles (unitless), with P(q) normalized in such a way that P(q=0) = 1; N, the degree of polymerization of the polymers or particles; cg$_2$(q), the intermolecular term (unitless).

When the interactions between polymers or particles are repulsive, $cg_2(\vec{q})$ is negative, at least at small q value.

The same approach can be used with the partial scattering functions associated with macroions and counterions for a solution of highly charged polyelectrolytes.

We can also note that for SANS, using a mixture of hydrogenated and deuterated particles, the intra- and intermolecular terms can be separated out in the absence of any model for the intermolecular term. Specifically, the Zero Average Contrast (ZAC) Method allows measuring directly the form factor. Such approaches, which are more or less related to the contrast variation method, are tackled in the following.

4.1.4. Contrast variation and deuterium labelling

Any particle component can be made invisible by cancelling its contrast length. Using a solvent having the same scattering length density than the one of the component can do that. Such a contrast cancellation is usually achieved by using a mixture of deuterated and hydrogenated solvent molecules with a suitable composition. Indeed, for instance for water as solvent, the scattering length density of a mixture of D$_2$O and H$_2$O molecules with a volume fraction of D$_2$O, $\Phi_V^{D_2O}$, is:

$$\bar{\rho} = \Phi_V^{D_2O} \rho_{D_2O} + (1 - \Phi_V^{D_2O})\rho_{H_2O} \,, \tag{60}$$

where ρ_{D_2O} and ρ_{H_2O} are the scattering length densities of D$_2$O and H$_2$O, respectively (see Table 4.1). It is, therefore, enough to adapt the D$_2$O volume fraction to have an average scattering length density equal to that of the considered component. However, this method is reliable only if the considered component has a scattering length density sufficiently distinct from those of the other ones. Thus, most of the time, the particle has first to be made enough inhomogeneous from the contrast point of

view. For SANS, the labeling of the considered component or the other ones is made through the hydrogen-deuterium exchange. By varying continuously the scattering length density of the solvent, via the Eq. (60), it is also possible to separate out the partial scattering functions of a ternary system (a solute with two components, so three partial scattering functions). As the number of components is increased, this contrast variation method must be coupled with some specific labeling in order to obtain more than three partial scattering functions. Obviously, the hydrogen-deuterium exchange is assumed not to modify the structure of the system. Most of the time, this assumption is correct. However, transitions between phases can be slightly shifted.

In this work, mixtures of two polymers with distinct labeling, one hydrogenated (PDADMAC) and the other deuterated (PSSNa), have been considered in order to obtain the partial scattering functions of the PSS-PDADMA PECs using the contrast variation method in SANS experiments. Indeed, for SANS, the contribution of counterions to the scattered intensities is negligible. So, we have:

$$I(q,C) = K_{PSS}^2 S_{PSS}(q,C) + K_{PDADMA}^2 S_{PDADMA}(q,C) + 2K_{PSS}K_{PDADMA}S_{PSS-PDADMA}(q,C) \qquad (61)$$

Where K_{PSS} and K_{PDADMA} are the contrast length in the considered solvent of deuterated PSS$_d$ macroions and hydrogenated PDADMA$_h$ ones, respectively; $S_{PSS}(q,C)$ and $S_{PDADMA}(q,C)$, the partial scattering functions of PSS and PDADMA macroions, respectively; $S_{PSS-PDADMA}(q,C)$, the cross term. C is the concentration of the solution. Obviously, Eq. (61) assumes that all the macroions are involved in the PECs and that there is none free chain. In the dilute regime, such experiments would be restricted to the charge stoichiometry line in the state diagrams a priori. According to the scattering length densities listed in Table 4.1, the partial scattering function of PDADMA is determined by using D$_2$O as solvent (its scattering length density matches that of PSS); the one of PSS requires the use of a D$_2$O-H$_2$O mixture with a D$_2$O volume fraction close to 3%; finally, a D$_2$O-H$_2$O mixture with a D$_2$O volume fraction equal to 54% allows to determine a linear combination of all the partial scattering functions from which the cross term can be inferred.

From these partial scattering functions, the density structure function, $S_{nn}(q,C) = \langle n(\vec{q})n(-\vec{q}) \rangle$ with $n(\vec{r}) = n_{PSS}(\vec{r}) + n_{PDADMA}(\vec{r})$ is the total density, as well as the charge structure function, $S_{nn}(q,C) = \langle z(\vec{q})z(-\vec{q}) \rangle$ with $z(\vec{r}) = -n_{PSS}(\vec{r}) + n_{PDADMA}(\vec{r})$ is the total charge of PECs can be inferred:

$$S_{nn}(q,C) = S_{PSS}(q,C) + S_{PDADMA}(q,C) + 2S_{PSS-PDADMA}(q,C) \qquad (62)$$

$$S_{ZZ}(q,C) = S_{PSS}(q,C) + S_{PDADMA}(q,C) - 2S_{PSS-PDADMA}(q,C) \qquad (63)$$

Such a contrast variation method could not be used in SAXS. All the more, the scattering from the counterions is no longer negligible. From this point of view, the comparison in between SAXS and SANS results is always useful. The difference in between the X and neutron contrast lengths of counterion allows getting some information about the localization of counterions in a system from a simple comparison of SAXS and SANS results.

Moreover, we have also considered mixtures of two PSSNa polymers of the identical degree of polymerization, one hydrogenated (PSS$_h$Na) and the other deuterated (PSS$_d$Na), with a hydrogenated PDADMAC to determine the form factor of the PSS macroions in the PSS-PDADMA PECs. A solvent of scattering length density equal to that of PDADMA was then considered. As counterions can be neglected for SANS, only the partial scattering functions associated with both PSS$_h^-$ and PSS$_d^-$, i.e. S$_{HH}$(q,C), S$_{DD}$(q,C) and S$_{HD}$(q,C), therefore, contributed to the scattered intensities from these PEC solutions. Some basic equations can be given for this case. Only the coherent scattering length K_H and K_D of both PSS macroions are different. Even the volumes of their scattering units are identical. We will denote x, the fraction of deuterated PSS in the mixture PSS$_d$-PSS$_h$. So, the average contrast length of the mixture is:

$$\overline{K} = xK_D + (1-x)K_H \qquad (64)$$

And the scattered intensity, as well as the partial scattering, functions are[144]:

$$I(\vec{q}, C) = K_H^2 S_{HH}(\vec{q}, C) + K_D^2 S_{DD}(\vec{q}, C) + 2K_H K_D S_{DH}(\vec{q}, C); \qquad (65)$$

$$S_{HH}(\vec{q}, C) = (1-x)C g_1(\vec{q}, C) + ((1-x)C)^2 g_2(\vec{q}, C); \qquad (66)$$

$$S_{DD}(\vec{q}, C) = xC g_1(\vec{q}, C) + x^2 C^2 g_2(\vec{q}, C); \qquad (67)$$

$$S_{HD}(\vec{q}, C) = x(1-x)C^2 g_2(\vec{q}, C); \qquad (68)$$

$$I(\vec{q}, C) = [xK_H^2 + (1-x)K_D^2]C g_1(\vec{q}, C) + [xK_H + (1-x)K_D]^2 C g_2(\vec{q}, C). \qquad (69)$$

As the average contrast length is non-null ($\overline{K} \neq 0$), to separate out $g_1(\vec{q}, C)$ and $g_2(\vec{q}, C)$, two measurements with different x values at the same concentration C should be enough. In practice, three or four hydrogenated-deuterated PSS mixtures are used. The form factor, $g_1(\vec{q}, C)$, is then obtained by a simple extrapolation to x = 0.

As the average contrast length is null ($\overline{K} = 0$), this is the Zero Average Contrast (ZAC) method, which allows obtaining the form factor $g_1(\vec{q}, C)$ from just one measurement[150]. The second part of the right side of Eq. (70) is indeed disappearing:

$$K = xK_H + (1 - x)K_D = 0 \tag{70}$$

$$I(\vec{q}, C) = [xK_H^2 + (1 - x)K_D^2]Cg_1(\vec{q}, C) \tag{71}$$

$$K_H = -K_D = K \tag{72}$$

$$I(\vec{q}, C) = K^2 Cg_1(\vec{q}, C) \tag{73}$$

4.1.5. Data reduction

For SAXS, all data were treated according to standard procedures for isotropic small angle X-ray scattering. After radial averaging, the spectra were corrected from the electronic noise of the detector, empty cell, absorption and sample thickness. A ^{55}Fe source was used for the corrections of geometrical factors and detector cells efficiency as well as a Silver Behenate sample, for the q-calibration. The normalization to the unit incident flux was then obtained using water or Lupolen as standard samples. After all these data treatments, the scattered intensities were corrected from the scattering of the solvent, added salt as well as released counterions included. Because all SAXS experiments were performed in a large q-range extending until q $\geq$ 1 Å^{-1}, this correction was carried out by using the "far-away point" method. This method assumes that the density fluctuations are almost identical for the background and the solution. The background can therefore be obtained from the scattered intensity of the solvent, which is modified by a constant factor (simple multiplication or addition) in order to be superimposed to the scattered intensity of the solution at high q values (q > 0.6-0.8 Å^{-1}), i.e. in a q-range where the concentration fluctuations are negligible. Such an approach is particularly useful when the concentration of salt and free counterions in the solution is rather unknown. However, it was also controlled through SAXS measurements of various aqueous solutions in the presence of NaCl salt at different concentrations. According to such a procedure, the scattered intensity I(q) containing all the structural information is obtained for each solution.

For SANS, similar basic data treatments were carried out. However, the background corresponds to the sum of the scattering from the solvent and the incoherent scattering of the solute.

The incoherent scattering of the solute was calculated from the incoherent cross sections listed in Table 4.1 and the concentrations of the component of the solute.

4.2. Isothermal titration calorimetry

The thermodynamic characteristics of the polyelectrolyte complexation process in solution can be investigated by isothermal titration calorimetry (ITC). The heat released or absorbed during the interaction between the components of PECs, which is determined by this technique, is used to extract thermodynamic parameters: the binding constant K, the binding enthalpy ΔH and the stoichiometry of the complexation n. Based on these quantities other fundamental parameters, the changes in free energy ΔG and in entropy ΔS, can be determined[151–153]:

$$\Delta G = -RTlnK; \tag{74}$$

$$\Delta S = (\Delta H - \Delta G)/T. \tag{75}$$

PEC components were mixed by incremental titration. Degassed polyelectrolyte solutions were used for the syringe and the measuring cell. The concentrations were 10 mM in the syringe and 0.5 mM in the measuring cell. The titration consisted in following 20 injections of 5.03 µL with a time interval of 15 min. Measurements were performed at 25 ºC and repeated 3 times.

ITC experiments were accompanied by zeta potential and dynamic light scattering measurements in order to follow the changes in charge and size for different polycation/polyanion ratios.

4.3. Zeta potentiometry

The zeta potential is a significant parameter characterizing the electrokinetic properties of a system. It is linked to the degree of electrostatic repulsion between colloidal particles that is responsible for their stabilization. Moreover, the zeta potential can give us the information about the stoichiometry of the complexation and the distribution of ions surrounding polyelectrolyte complexes.

The separated phases for the biphasic region and the prepared samples of the colloidal domain were investigated by using a Zetasizer Nano ZS (Malvern Instrument, Germany). The samples were held in clear disposable zeta cells. The values of three measurements cycles each containing 12 single measurements were averaged.

A typical zeta cell has two electrodes at both ends to which a potential is applied. Particles move towards the electrode and their velocity is measured.

4.4. Dynamic light scattering

Dynamic light scattering (DLS) is a scattering analytical technique. As another scattering measurement, the principle is based on the study of the scattered radiation due to density fluctuations in a tested sample. The contrast in DLS is defined by the square of the reflectivity index increment of the solute with respect to the solvent.

The dynamic behaviour of particles is described by an autocorrelation function of the registered scattered intensity:

$$g^2(q;\tau) = \frac{\langle I(t)I(t+\tau)\rangle}{\langle I(t)\rangle^2}, \tag{76}$$

where $g^2(q;\tau)$ is the autocorrelation function; τ, the delay time, I, the registered intensity.

DLS is used to determine the particle size, based on its Brownian motion, and gives the hydrodynamic diameter D_h. This hydrodynamic diameter has to be measured in the hydrodynamic limit that corresponds to $qR_H < 1$ or $qD_h < 2$.

4.5. Cryo-transmission electron microscopy

As it was already mentioned, small-angle scattering techniques are based on the measurements of the mean square density fluctuations of a system in the reciprocal space. Microscopy gives us a structural information through the picture in the real space of the sample density and in the moment of the observation. Using microscopy a part of the sample is investigated, on the contrary to scattering,

where we get an average result over all the sample. In SAXS or SANS, the phases of the density fluctuations are lost, that makes difficult, even impossible, to obtain a 2D or 3D representation of the studied objects as we can do with microscopy. Due to the averaging principle of scattering, some local structure details are difficult to extract. Therefore, small angle scattering and microscopy should be used together to describe the full structure of a sample as they give complementary results.

To observe the structure of polyelectrolyte complexes in the direct space, we chose a cryo-electron microscopy (cryo-TEM). An unknown sample is freeze at cryogenic temperature and then cut into two parts (cryo-fracture cut). In such a case, the observation of fixed structure of a solution in the native environment is possible. For cryo-TEM, we used exactly the same samples that were prepared for small-angle X-ray and neutron scattering.

Chapter 5

Aqueous solutions of sodium hyaluronate

Hyaluronan is a biopolymer with a broad range of medical and industrial applications. The extended domain of its practical use causes this polysaccharide to be widely described in the literature. However, there are still a lot of gaps in the understanding of the behaviour of this biopolymer. Different experimental conditions and preparation methods can lead to a large variety of structures. Experimental results could even be contradictory depending on the preparation methods. The most significant reviews, which have summarized the numerous aspects of the hyaluronan structure, were presented by Lapcik[154], Hargittaie[155], Cowman[140] and Necas[121]. Depending on the experimental conditions, the structure of hyaluronan could be[156]:

- molecular chain dispersed in a dilute solution;

- double helix;

- two antiparallel helices without coiling around each other;

- single helices in a tighter arrangement;

- six chains in an ordered arrangement;

- chains in a compact arrangement;

- fully extended individual chains.

The structure of hyaluronan aqueous solutions is complicated by different phenomena such as self-association[135,138,157], network formation[158,159], double helix[156,160,161] etc. Chains molecularly dispersed in aqueous solutions however exist and their average conformation can be described through the wormlike chain model[162,163]. In the presence of an added salt (at high ionic strength), the chain local stiffness, or the persistence length, is the intrinsic one of the polysaccharide backbone. It is also defined as the non-electrostatic persistence length. The basic concepts presented in the literature and that concern all possible average conformations of the hyaluronan reported values for

the non-electrostatic persistence length, l_p, in the large range between 3-4.5 nm[160,164–167] and 7-10 nm[138,159,168].

To investigate correctly the interactions between the hyaluronan and the oppositely charged poly(diallyldimethylammonium chloride) during the interpolyelectrolyte complex formation, the used industrial (Soliance) sodium hyaluronate samples should be well-characterized. Such a characterization was carried out in our laboratory, using multi-detector Size Exclusion Chromatography (SEC) as well as small-angle X-ray scattering (SAXS). It was done from dilute, or low concentrated, aqueous solutions of HA (c << 0.15 mol/l) in the presence of an added monovalent salt (0.1 M NaNO$_3$ or 0.3 M NaCl) with the aim of determining the form factor of the HA macroions, dispersed in a brine aqueous solution. Several hyaluronan samples were then considered: HA1, with an average molecular weight M_W=53300 g.mol^{-1} and a polydispersity index I=M_W/M_N=1.6; HA2, with M_W=395500 g.mol^{-1} and I=M_W/M_N=2.06; HA3, with M_W=41400 g.mol^{-1} and I=M_W/M_N=1.59; HA4 with M_W=729200 g.mol^{-1} and I=M_W/M_N=1.82.

Salt-free aqueous solutions of hyaluronans of different molecular weights were also studied by SAXS in a larger concentration range. The tested HA samples were HA1 and HA2. The explored concentration range was 0.01 < c < 2.09 mol/l and corresponds to the well-known semidilute and concentrated regimes for both HA (Table 3.2). Dissolved in water, hyaluronan formed a gel or a solution with high viscosity even at low concentration. The largest investigated polysaccharide concentrations were 2.09 mol/l and 1.61 mol/l for HA1 and HA2, respectively. A further increase in concentration made the sample preparation impossible. The heating of the concentrated solutions led to the formation of a glass-like state.

5.1. Average conformation of sodium hyaluronate in brine aqueous solutions

In this part, we study the average conformation of hyaluronan in brine aqueous solutions. The aim is to evaluate its intrinsic, or non-electrostatic, persistence length, l_p. First, we recall the main models describing the average conformation of linear macromolecules. Second, we describe the main characterization methods that allow determining l_p^0. The analyses of the results, previously obtained by distinct authors, as well as those resulting from our own experiments are presented. Obviously, we are mainly concerned with HANa dilute aqueous solutions in the presence of an added salt, which

allows screening the electrostatic interaction. However, the small-angle X-ray scattering (SAXS) experiments, performed in the semidilute regime, also provide a scaling law for the concentration dependence of the correlation length ξ.

5.1.1. Models for the average conformation of linear macromolecules

Information about the average conformation, and specifically about the persistence length, l_p, of a linear macromolecule can be obtained from radiation scattering experiments using two distinct approaches, according to the explored scattering vector q-range. In the Guinier range ($qR_g < 1$; R_g being the chain radius of gyration), this information is extracted from the molecular weight M dependence of the radius of gyration R_g. At higher q values ($qR_g > 1$), i.e. in the intermediate or asymptotic q-range, it is got through the analysis of the chain form factor. In this q-range, we have direct information about the chain statistics from only one sample, i.e. one molecular weight. Moreover, polydispersity has no longer influence.

5.1.1.1. Ideal or Gaussian chain

The chain is ideal because there is none interaction between monomers and a chain conformation then corresponds to a random walk. In practice, this model applies to macromolecules in a theta solvent or in a melt of identical macromolecules.

The chain radius of gyration is defined by[11,169]:

$$R_g^2 = \frac{lp}{3M_L}M,$$
(77)

where M is the molecular weight; l_p, the persistence length; M_L, the mass per unit contour length ($M_L = M/L$, where L is the total contour length of the macromolecule).

From Eq. (77), we are therefore able to determine l_p, since M_L can be evaluated independently from a molecular model.

In fact, due to some polydispersity, we measure the z-average of the square radius of gyration $< R_g^2 >_Z$ and the weight average molecular weight M_W. Then, the Eq. (77) becomes:

$$< R_g^2 >_W = \frac{lp}{3M_L}M_W,$$
(78)

And by introducing polydispersity via the Schulz-Zimm molecular weight distribution, we have:

$$< R_g^2 >_W = \left[\frac{(1+U)}{(1+2U)}\right] < R_g^2 >_Z, \tag{79}$$

where M_W/M_N is the polydispersity index, M_N being the number average molecular weight of the macromolecules, and $U = (M_W/M_N - 1)$.

The form factor of an ideal chain was calculated by Debye[170]:

$$g_1(q) = NP_D(q) = N\left\{\frac{2}{x^2}[x - 1 + \exp(-x)]\right\} \tag{80}$$

with $x = (qR_g).^2$

Also, N is the polymerization degree, or the number of monomer units, of the macromolecule.

For $qR_g > 1$, the form factor $g_1(q)$ does no longer depend on the degree of polymerization N, or molecular weight M. We have:

$$g_1(q) = \frac{6M_L}{mlp}\frac{1}{q^2}, \tag{81}$$

where M_L is the mass per unit contour length; m, the molar mass of the monomer unit; l_p, the persistence length. We find again the scattering behaviour of a fractal having a fractal dimension D = 2.

5.1.1.2. Chain with excluded volume interaction

A chain conformation then corresponds to a self-avoiding random walk and the model applies to macromolecules in a good solvent[11]. The chain is swollen by the excluded volume interactions between monomers and the radius of gyration scales as[169]:

$$R_g^2 = B\,M^{2\nu} \tag{82}$$

ν is the excluded volume exponent ($\nu = 0.588 \approx \frac{3}{5}$); B, a prefactor that involves the chain local stiffness as well as the excluded volume parameter $v(T)$. It is therefore no longer possible to extract the persistence length from the variation of the radius of gyration with the molecular weight.

The form factor becomes for $qR_g > 1$:

$$g_1(q) = \frac{g_\infty}{q^{1/\nu}} \tag{83}$$

This scattering behaviour is that of a fractal with a fractal dimension $D = 1/\nu$. Again, the prefactor of this scaling law, g_∞, does no longer allow determining the persistence length, l_p.

5.1.1.3. Wormlike chain

This model for the chain statistics accounts for the local stiffness of macromolecules, via the persistence length, l_p, but neglects the excluded volume interaction. Thus, the chain is ideal beyond curvilinear distances such as $s >> lp$ along the chemical sequence. The radius of gyration of a wormlike chain was calculated by Benoît and Doty[171]:

$$R_g^2 = 4lp^2 \left[\frac{y}{6} - \frac{1}{4} + \frac{1}{4y} - \frac{1}{8y^2} \{1 - \exp(-2y)\}\right] \tag{84}$$

with $y = \dfrac{L}{2lp} = \dfrac{M}{M_L}\dfrac{1}{2lp}$

where L is the chain contour length; l_p, its persistence length; M, its molecular weight; M_L, its mass per unit contour length.

Basically, the Eq. (84) allows determining the persistence length from a radius of gyration measurement carried out in the Guinier range ($qR_g < 1$). However, it assumes quite negligible polydispersity as well as none excluded volume interaction. The latter is associated with the validity domain that is, with the same notation[169]:

$$\frac{L}{lp} < 30 \ \text{ or } \ \ \frac{M/M_L}{lp} < 300 \tag{85}$$

Concerning polydispersity, in the Guinier range, we actually measure the z-average of the square radius of gyration $< R_g^2 >_Z$ and the weight average molecular weight M_W. So, a useful relationship should account for polydispersity. By introducing polydispersity via the Schulz-Zimm molecular weight distribution, we have[172]:

$$< R_g^2 >_Z = \frac{(1+2U)}{(1+U)}\frac{M_W}{M_L}\frac{lp}{3} \left\{1 - \frac{(1+U)}{(1+2U)}\frac{M_L}{M_W} 3lp \left(1 - \frac{M_L}{M_W} 2lp\right) - \frac{(1+U)^2}{(1+U)}\left(\frac{M_L}{M_W}\right)^3 6lp^3 \left[1 - \right.\right.$$

$$\left.\left.\left(1 + \frac{U}{1+U}\frac{M_W}{M_L} 2lp\right)^{-\frac{1}{U}}\right]\right\} \tag{86}$$

with always the same notation and $U = (M_W/M_N - 1)$.

Therefore, polydispersity has to be taken into account for determining l_p from a single radius of gyration, even though the molecular weight of the macromolecule is enough low. Neglecting polydispersity via the use of Eq. (84), with the validity condition (85), can lead to significant errors.

The asymptotic behaviour of the form factor of an infinite wormlike chain has been obtained by des Cloizeaux[173]:

$$g_1(q) = \frac{\pi M_L}{m} \frac{1}{q} + \frac{2M_L}{3mlp} \frac{1}{q^2} \tag{87}$$

m is the molar mass of the monomer unit; M_L, the mass per unit contour length of the macromolecule; $\frac{M_L}{m} = \frac{1}{a}$, the inverse of the monomer contour length.

The characteristic q^{-1} scattering behaviour of a rod-like molecule is also found for the wormlike chain. Only the second term is different. Actually, the characteristic q^{-1} scattering behaviour is observed as soon as $ql_p > 3.5$, provided the chain cross-section does not still play a role in this q-range. This condition $ql_p > 3.5$ can then be used for determining the persistence l_p[169]. The Holtzer plot $qg_1(q)$ versus q is then the suitable representation to evaluate l_p as the q^{-1} scattering behaviour becomes a plateau. Moreover, the height of this plateau allows measuring M_L, or a, and that is an additional control for the analysis through the wormlike chain model.

However, the q^{-1} scattering behaviour can also be masked by a chain cross-section effect. That is the case for flexible macromolecules. In the Guinier range of the cross section ($qR_c < 1$; R_c being the radius of gyration of the chain cross section), the form factor can then be written as:

$$g_1(q) = \frac{\pi M_L}{m} \frac{1}{q} \ exp\left(-\frac{q^2 R_c^2}{2}\right) \tag{88}$$

Thus, by considering the plot $LN[qg_1(q)]$ versus q^2, the square of the chain cross-section radius of gyration can also be measured.

The persistence length of a macromolecule can also be determined from the analysis of the molecular weight dependence of its intrinsic viscosity, as demonstrated by Yamakawa-Fujii-Yoshizaki[174–176], which is based on the relationship:

$$\left(\frac{M^2}{[\eta]_0}\right)^{\frac{1}{3}} = A_\eta + B_\eta \tag{89}$$

with $\qquad A_\eta = A_0 M_L \phi_{0,\infty}^{-\frac{1}{3}} \tag{90}$

and $\qquad B_\eta = B_0 \phi_{0,\infty}^{-\frac{1}{3}} \left(\frac{M_L}{2lp}\right)^{-\frac{1}{2}} \tag{91}$

M is the molecular weight of the macromolecule; $[\eta]_0$, its intrinsic viscosity (none excluded volume effect); M_L, its mass per unit contour length; l_p, its persistence length; $\phi_{0,\infty}$, the limit of the viscosity function ($\phi_{0,\infty} = 2.86 \ 10^{23}$ leading to $\phi_{0,\infty}^{-\frac{1}{3}} = 1.5178 \ 10^{-8}$). The average conformation is always assumed to be unperturbated by the excluded volume interactions. A_0 and B_0 correspond to:

$$A_0 = 0.46 - 0.53 \ log\left(\frac{d}{2lp}\right) \tag{92}$$

$$B_0 = 1.00 - 0.0367 \ log\left(\frac{d}{2lp}\right) \tag{93}$$

where d is the effective hydrodynamic diameter of the macromolecule. The validity domains of these equations A_0 and B_0 are $\frac{d}{2lp} < 0.1$ and $\frac{d}{2lp} < 1$, respectively.

By considering an average value for B_0 ($B_0 = 1.05$), the persistence length, l_p, is obtained directly from the slope B_η of the plot $\left(\frac{M^2}{[\eta]_0}\right)^{\frac{1}{3}}$ versus $M^{\frac{1}{2}}$. Indeed, the mass per unit contour length M_L is independently evaluated from a molecular model. However, in the general case, both the intercept A_η and the slope B_η of this plot are required for determining l_p, using Eqs. (91) and (93).

5.1.2. Determinations of the hyaluronan non-electrostatic persistence length

Here, we describe the main characterization methods that allow determining l_p, using either data reported in the literature or data obtained from our own SEC and SAXS measurements.

5.1.2.1. Radius of gyration and molecular weight measurements reported in the literature

These measurements were basically carried out using the static light scattering technique. To neglect the excluded volume interactions, we only considered the results associated with HA of low molecular mass, i.e. satisfying the condition (85): $\frac{L}{lp} < 300$ or $\frac{M/M_L}{lp} < 300$. Moreover, the sample polydispersity was taken into account Eq. (86).

From multidetection SEC measurements using $H_2O + 0.1$ M NH_4NO_3 as eluent[177]:

The previous condition leads to consider 5 values of M_W in the range $130000 < M_W < 810000$ g.mol^{-1}, with a rather strange common polydispersity index $M_W/M_N = 1.3$. As $M_L = m(HA)/a = 378.31/10.2 = 37.089$ g.mol^{-1}Å^{-1}, we obtain $l_p = 110.3$ Å (11.03 nm).

-From the work of Esquenet and Buhler[135] using the same approach, only two values of M_W could be considered, in the range $85000 < M_W < 610000$ g.mol-1. We obtain $l_p = 69.2$ Å (6.92 nm).

-From the work of Buhler and Boué[138] using the same approach and considering two values of M_W in the range $85000 < M_W < 160000$ g.mol-1, we obtain $lp = 78.4$ Å (7.84 nm).

5.1.2.2. Intrinsic viscosity measurements reported in the literature

We have estimated l_p for the hyaluronan by analyzing the intrinsic viscosity measurements of distinct authors through the method described in Chapter 5.1.1.3[174–176]. The polydispersity of the HA samples was however neglected.

-According to Cleland[178], from viscosity measurements of HA solutions in H_2O + 0.2 M NaCl, the intrinsic viscosity is found, for $M_W < 22000$ g.mol^{-1}, to scale as:

$$[\eta]\ (\text{mL.g}^{-1}) = 0.004165*[M_W\,(\text{g.mol}^{-1})]^{0.959}$$

and l_p is found close to 37 Å (3.7 nm). Such a l_p-value is rather low and seems to be unrealistic for HA.

-According to the study[177] from viscosity measurements of HA solutions in H_2O + 0.3 M NaCl (Figure 5.1), the intrinsic viscosity is found for $130000 < M_W < 1860000$ g.mol^{-1} to scale as:

$$[\eta]\ (\text{mL.g}^{-1}) = 0.0264*[M_W\,(\text{g.mol}^{-1})]^{0.781}$$

The related plot $\left(\frac{M_W^2}{[\eta]}\right)^{\frac{1}{3}}$ versus $M_W^{\frac{1}{2}}$ is reported in Figure 5.1. and l_p is then found close to 129 Å (12.9 nm).
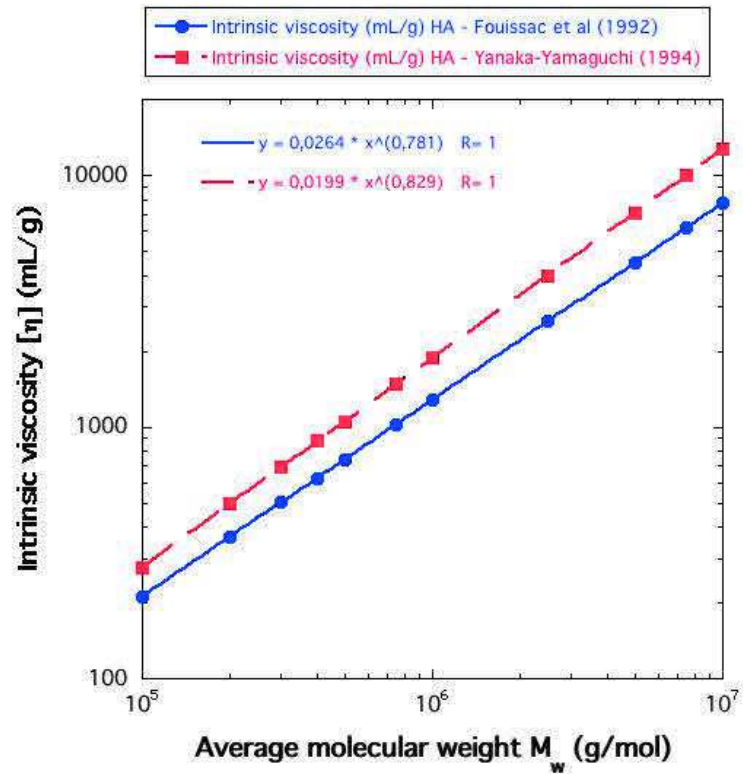
Figure 5.1: Intrinsic viscosity $[\eta]$ versus average molecular weight M_W for HA in brine aqueous solutions[135,177]

-According to Yanaka and Yamaguchi[179] from viscosity measurements of HA solutions in H_2O + 0.2 M NaCl, the intrinsic viscosity is found for $M_W > 400000$ g.mol^{-1} to scale as:

$[\eta]$ (mL.g^{-1}) = 0.0199*[M_W (g.mol^{-1})]$^{0.829}$

The related plot $\left(\frac{M_W{}^2}{[\eta]}\right)^{\frac{1}{3}}$ versus $M_W{}^{\frac{1}{2}}$ is reported in Figure 5.2.

l_p is then found close to 186 Å (18.6 nm). This value seems to be also unrealistic.
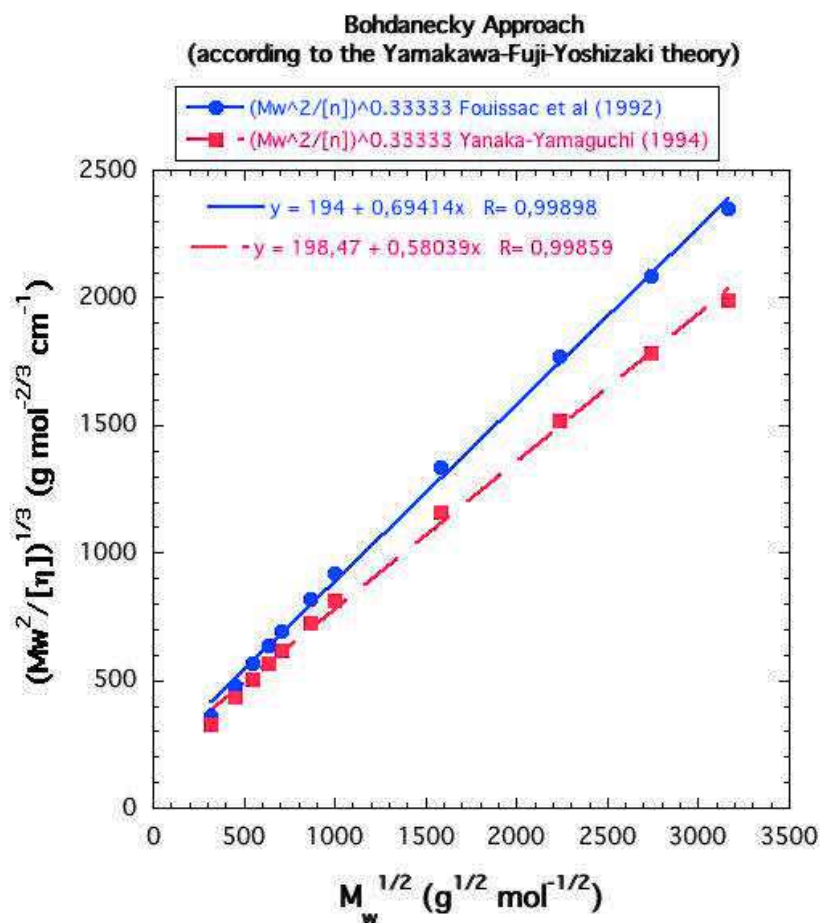
Figure 5.2. $\left(\frac{M_W{}^2}{[\eta]}\right)^{\frac{1}{3}}$ versus $M_W{}^{\frac{1}{2}}$ for HA in brine aqueous solutions[135,177]

5.1.2.3. Multidetection SEC measurements using H_2O + 0.1 M $NaNO_3$ as eluent

The characterization by multidetection SEC can allow obtaining information about the average conformation of macromolecules, since the light scattering detector provides the molar mass of each fraction as well as their related radius of gyration. We have therefore access to the variation of the radius of gyration with the molecular weight and, since each fraction could be considered as monodisperse, the corresponding law does not need to be corrected for any polydispersity effect. That is a significant advantage.

Several hyaluronan samples were characterized, leading to the following average molecular weights:

HA-1 M_W = 53330 g.mol^{-1}, M_W/M_N = 1.60

HA-2 M_W = 395470 g.mol^{-1}, M_W/M_N = 2.06

HA-3 M_W = 41370 g.mol^{-1}, M_W/M_N = 1.58

HA-4 M_W = 29200 g.mol^{-1}, M_W/M_N = 1.82

For each HA, we selected the fractions that were correctly eluted. The results obtained at the exclusion limit and those corresponding to some small dubious parts of the chromatograms were thus eliminated. By this way, we obtained a single curve linking the radius of gyration, R_g, to the molecular weigh, M, in a large range of molecular weight (Figure 5.3). All the studied HA samples focus on the same curve, indicating the reliability of our measurements.
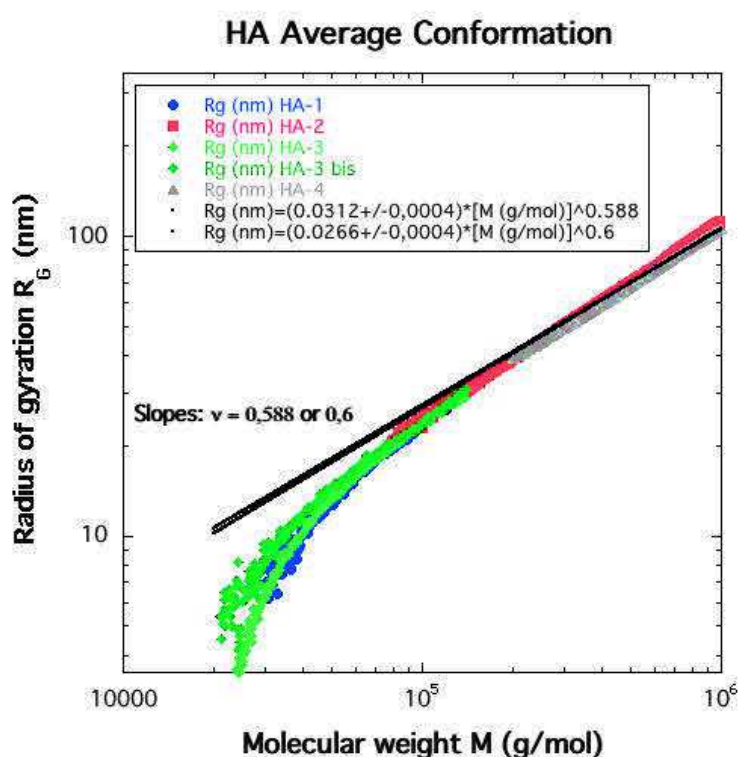
Figure 5.3. The radius of gyration R_g versus molecular weight M for the various HA samples characterized by multidetection SEC using H_2O + 0.1 M $NaNO_3$ as eluent. The best fit of the data corresponding to $M > 10^5$ g.mol^{-1}, with the scaling law $R_g \sim M^\nu$, is also shown.

First, we tried to fit this single curve with the model of a chain with excluded volume interactions (Figure 5.3). Such a fit was not reliable. That is not surprising since considering for HA a mass per unit contour length M_L = 37.089 g.mol^{-1}.nm^{-1} and an intrinsic persistence length l_p = 9 nm, the excluded volume effect should only be effective, and therefore observable, provided $M > 300*l_p*M_L$, i.e. $M > 10^6$ g.mol^{-1}. Moreover, the ratio between the hydrodynamic radius and the radius

of gyration R_h/R_g that was determined for HA-2 (0.528) or HA-3 (0.453) was quite distinct from that of the chain with excluded volume effect (0.71). Second, we tried to fit this single curve with the wormlike chain model, using the Benoît-Doty relationship[171], fixing the mass per unit contour length to M_L= 37.089 g.mol^{-1}.nm^{-1}. Distinct molecular weight ranges were then considered:

*For $M < 10^6$ g.mol^{-1}, we obtain l_p = 10.77 nm. However the fit is not suitable (see Figure 5.4a)

*For 30000 < M < 140000 (low molecular weights are only considered), we obtain l_p = 6.44 nm. But, the fit still remains quite unrealistic (see Figure 5.4 (b)).

(a)   (b)
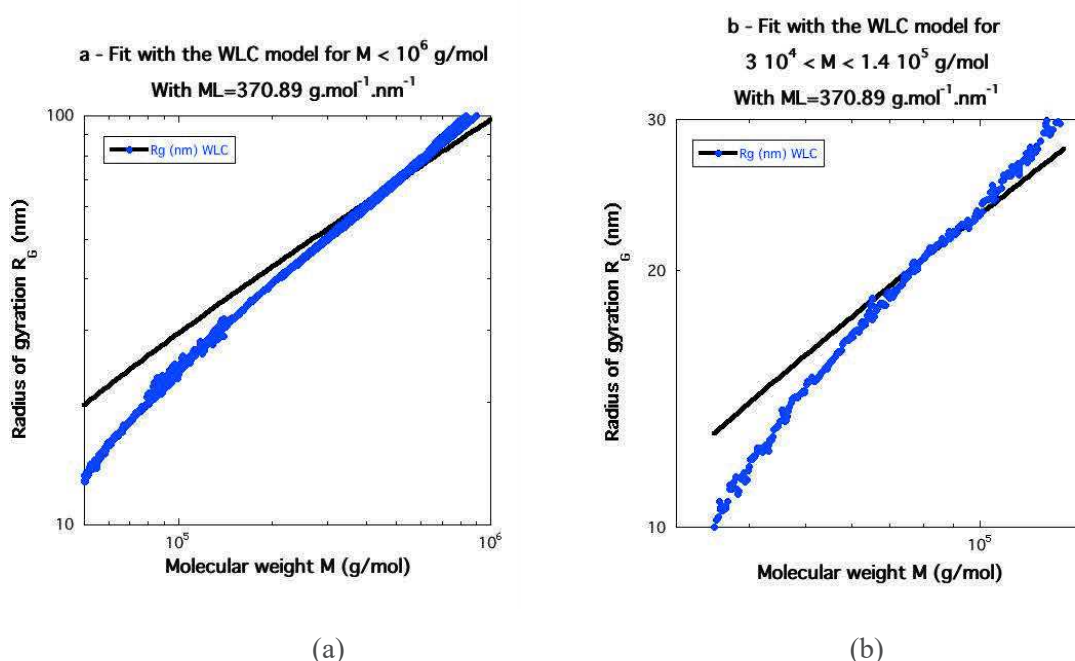
Figure 5.4. Radius of gyration R_g versus molecular weight M for the various HA samples characterized by multidetection SEC using H_2O + 0.1 M $NaNO_3$ as eluent. The best fits of the data with the wormlike chain and M_L = 370.89 g.mol^{-1}.nm^{-1}. Figure (a) represents the range $M < 10^6$ g.mol^{-1} and Figure (b) the range $3 \; 10^4 < M < 1.4 \; 10^5$ g.mol^{-1}

Alternatively, M_L could also be considered as an adjustable parameter. The fits can then be superimposed to the data and reasonable l_p values are obtained (close to 9 nm). However, in these cases, the obtained M_L values are no longer realistic.

The conclusion of this analysis is that the fractionation of the various HA macroions is not really correct in the eluent H_2O + 0.1 M $NaNO_3$, even though the chromatograms seems quite reasonable in a first approximation. There would be some additional retention phenomena that could lead to some mixing (each fraction would no longer be monodisperse). Our best proposal would be

to perform additional multidetection SEC experiments, by replacing the eluent $H_2O + 0.1$ M $NaNO_3$ by $H_2O + 0.1$ M NH_4NO_3, according to some authors[180].

5.1.2.4. SAXS measurements using $H_2O + 0.3$ M NaCl as solvent

SAXS experiments were carried out on HA solutions in $H_2O + 0.3$ M NaCl. Two HA samples and three concentrations for each were considered:

HA-3 $Mw = 41370$ g.mol^{-1} $Mw/M_N = 1.58$ $c = 0.0201$; 0.0482; 0.0941 mol/l

HA-4 $Mw = 729200$ g.mol^{-1} $Mw/M_N = 1.82$ $c = 0.0241$; 0.0530; 0.1423 mol/l

The intrinsic viscosity measurements reported in Chapter 5.1.2.2 allow estimation the critical overlap concentration c^*, defining the crossover between the dilute and semidilute regimes, for each HA sample. We used the relationship $c^* = 1/[\eta]$, via:

$$c^*(\text{mol/l}) = c^*(\text{g/dL})*(10^3/[m(HA)(\text{g/mol})]) = (1/([\eta]\ (\text{mL/g}))*(10^3/[m(HA)(\text{g/mol})])$$

That leads to:

For HA-3 $c^* \approx 0.022$ mol/l

For HA-4 $c^* \approx 0.0022$ mol/l

Obviously, there was only one concentration for HA-3 corresponding to the dilute regime. Other concentrations for HA-3 and HA-4 are associated with the semidilute regime.

The following Figure 5.5 shows the SAXS profiles for all these concentrations and both HA macroions. We consider the scattered intensities, $I(q,c)$ (cm^{-1}), normalized to the contrast factor, K^2 (cm^2), and the concentration, c (mol/cm^3), i.e. the unitless scattering function $g(q,c)$ defined as:

$$g(q,c) = I(q,c)/(K^2cN_a) = g_1(q) + cg_2(q) \tag{94}$$

N_a is the Avogadro's number ($6.022\ 10^{23}$ mol^{-1}); $g_1(q)$, the form factor ($g_1(q) = NP(q)$, N being the degree of polymerization of the macromolecules and $P(q)$, the form factor such as $P(0)=1$); $g_2(q)$, the intermolecular term. The contrast is calculated from the characteristics listed in Table 4.1 (Chapter 4) and by taking into account the presence of all the counterions (Na^+) as well as the added salt (NaCl) in the solvent. The counterions and the added salt slightly change the scattering length density of the solvent. However, this change could also be considered negligible in a first approximation.
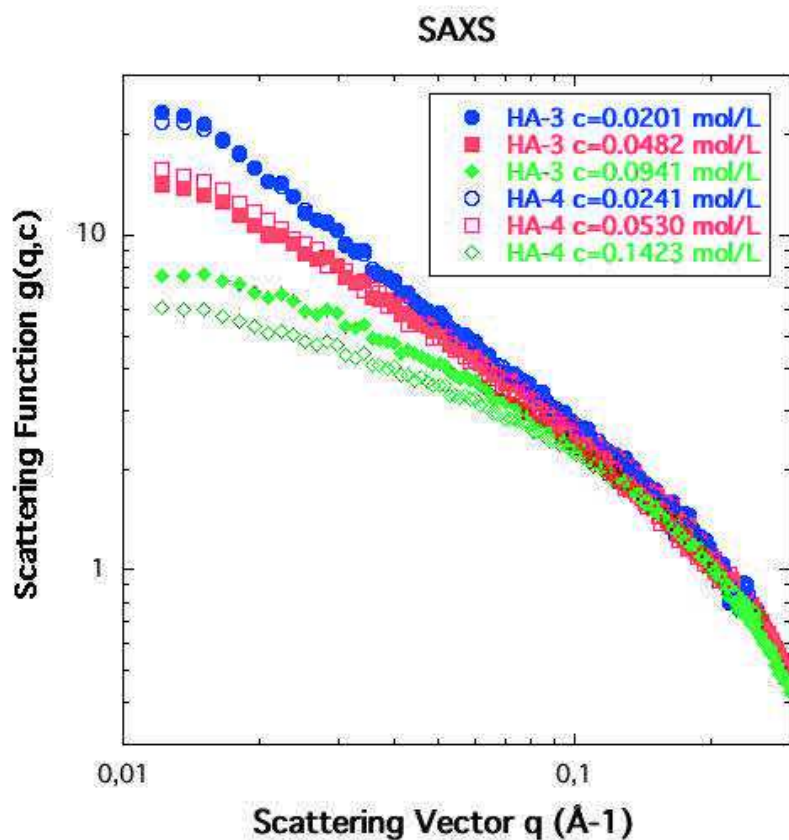
Figure 5.5. $g(q,c)$ for HA-3 and HA-4 in H2O + 0.3 M NaCl, at different concentrations

Obviously, only the asymptotic q-range is really explored in these experiments. The Guinier range for both HA macromolecules would involve measurements at smaller q-values ($q < 0.01$ Å^{-1}). Nevertheless, since for the lowest concentrations ($c \approx 0.02$ mol/l) both HA samples lead to the same scattering function $g(q,c)$, it is reasonable to neglect the intermolecular correlations for the lowest concentrations in the investigated q-range ($q > 0.01$ Å^{-1}). $g(q,c)$ is then equal to $g_I(q)$. The HA form factor is thus presented in the following figure, using both Holtzer as well as Kratky representations ($q*g_I(q)$ and $q^2*g_I(q)$ versus q, respectively).

(a)

(b)
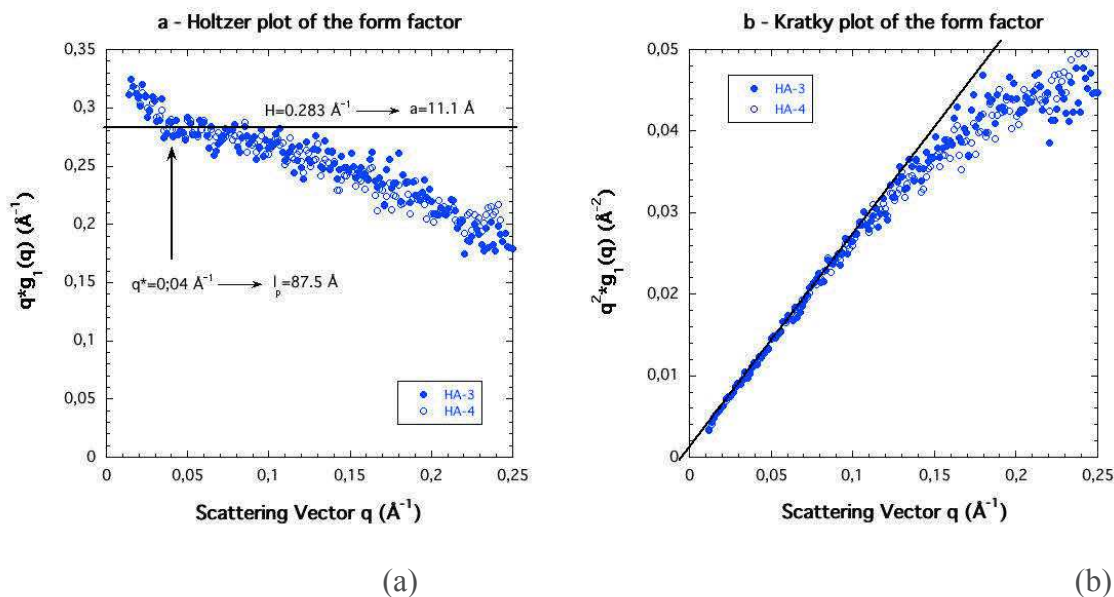
Figure 5.6. Form factor of the HA macroions in brine aqueous solution (solvent H_2O + 0.3 M NaCl): Holtzer (a) and Kratky (b) representations

Remarkably, the characteristic q^{-1} scattering behaviour of a wormlike chain is observed in a small q-range just above $q^* = 0.04$ Å^{-1}. That allows determining the intrinsic persistence length according to the criterion $l_p = 3.5/q$. We obtain $l_p = 87.5$ Å (8.75 nm), which is in agreement with the non-electrostatic persistence length previously measured from SANS experiments, by using a similar approach[138,181]. Correlatively, the height of the related plateau in the Holtzer representation, $H = 0.283$ Å^{-1}, leads to a monomer contour length, a, quite close to that determined by different authors. Thus, the relationship $H = \pi*M_L/m(HA)] = \pi/a$ leads to $a = 11.1$ Å (1.11 nm). This value for the monomer contour length is close to that, reported by different authors[135], a = 10.2 Å, and does not induce any counterion condensation.

At high q-values ($q > 0.08$ Å^{-1}), the cross section of the HA macroions is no longer negligible. In the Holtzer representation, the curve thus moves away from the plateau. The square of the radius of gyration of the chain cross section can then be determined using a plot $LN[q*g_1(q)]$ versus q^2, provided $qR_c < 1$. We obtain: $R_c^2 = 13.0$ Å^2 and $R_c = 3.6$ Å.

-For $c > 0.02$ mol/l, we are concerned with the semidilute regime for both HA-3 and HA-4. It is then reasonable to fit the scattering functions $g(q,c)$ by the Lorentzian form proposed by Edwards[182,183]:

$$g(q,c) = g(0,c)/(1+q^2\xi^2) \qquad \text{with } q\xi < 1 \tag{95}$$

ξ is the correlation length or the blob size of the temporary network formed by the interpenetrating polymer chains. It can be determined using a Zimm representation of the scattering function $g(q,c)$, i.e. the plot $g(0,c)/g(q,c)$ versus q^2. Data are on a straight line, which crosses the x-axis (q^2 axis) on a point that allows measuring ξ^2. Figure 5.7 shows the variation of the correlation length, ξ, measured by this way, with the concentration, c. A scaling law can describe it $\xi(\text{Å}) = 2.068*[c \text{ (mol/l)}]^{-0.77}$. The exponent corresponds to the one predicted by the scaling approach, i.e. $\nu/(1-3\nu)$ with $\nu = 0.588$[10].
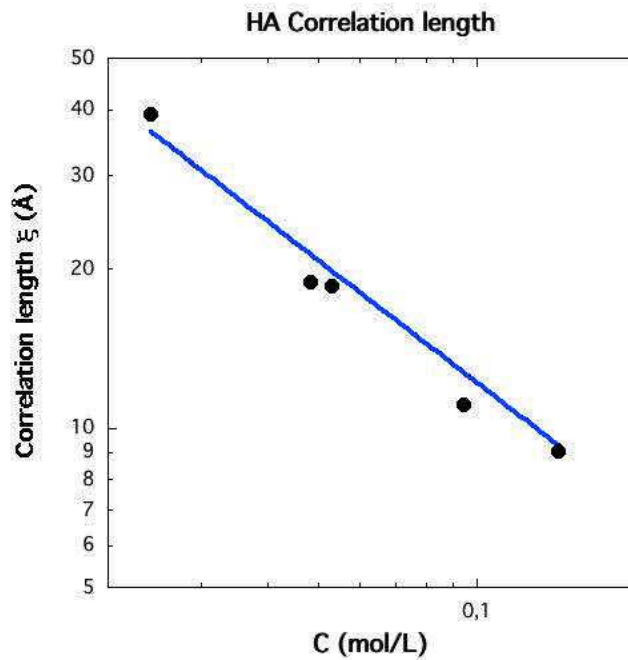
Figure 5.7. Concentration dependence of the correlation length in semidilute brine aqueous solutions of HA (solvent H_2O + 0.3 M NaCl)

5.2. Salt-free aqueous solutions of sodium hyaluronate

In the absence of an additional low-molecular weight electrolyte, or salt, the ionic strength is just related to the concentration of free counterions. With HA, all Na^+ counterions are free (the HA effective charge fraction is f_{eff}=1). Indeed, the curvilinear distance between two negative carboxylate groups along the polysaccharide chemical sequence (the monomer length a is of the order of 10.2 Å[138]) exceeds the Bjerrum length (l_B = 7.14 Å). So, the Manning-Ossawa condensation phenomenon does not proceed in such conditions, provided counterions are monovalent. The comparison between SAXS and SANS could give the experimental proof that all counterions are free. But, this is out of the present work and is left for future perspectives. Since the Na^+ counterions are not condensed onto polyions, the SAXS scattered intensity is only related to the signal of HA macroion scattering function $S_{mm}(q,c)$:

$$I(q,c) = K_m^2 \, S_{mm}(q,c), \tag{96}$$

$I(q,c)$ is the measured scattered intensity of the HA aqueous solution at concentration c; $S_{mm}(q,c)$, the macroion scattering function; K_m, the contrast length of the macroion monomer unit with respect to H_2O with the free counterions.

Hyaluronan has a low electron density and therefore a low contrast length with respect to H_2O, K_m = 21.425 10^{-12} cm. The scattered intensities from its aqueous solutions were, therefore, low and that had a great importance especially for the lowest concentrations. The running time for one sample was varied in the range between 15 and 72 hours.

5.2.1. Concentration dependence of the scattering curves

The SAXS profiles of the HA salt-free aqueous solutions will be presented after normalizing the scattered intensities to the concentrations of the related solutions. On the other hand, two distinct scattering behaviours were observed in the largely explored concentration range. Thus, they are shown separately in both Figures 5.8 and 5.9, focusing on two different scattering vector q-ranges.

At low q (Figures 5.8), a strong increase in the scattered intensity is observed. In the usual case, it is attributed to the existence of large heterogeneities that also lead to the existence of a slow mode in quasielastic light scattering experiments. The origin of such heterogeneities was debatable. For common neutral macromolecules in a good solvent, they are mainly observed in the semidilute regime

and can be due to an incomplete dissolution at a molecular scale (well-known Picot-Benoît effect[184,185]; a rather long time is necessary to reach the ground state). They can also be observed in the dilute regime for few neutral macromolecules. Then, they result from the existence of self-associations (via Hydrogen bonding for example)[186]. With polyelectrolyte solutions, such heterogeneities are observed in dilute as well as semidilute solutions, whatever the existence of any self-association process. The slow mode in dynamic light scattering is then related to the fluctuations of large domains as polyelectrolyte concentration is increased[187,188]. But, the issue of these upturns, or heterogeneities, is still quite speculative as neither of the reasons can be confirmed or disproved completely[189–191]. Remarkably, in this study, the upturns do not have any dependence on the hyaluronan concentration. Taking into account the high viscosity of the hyaluronan aqueous solutions, we assume that they correspond to static aggregates. Correlatively, for HA of higher molecular weight, the upturns are a bit increased, as it is more difficult to separate at the molecular scale the self-assembled longer polysaccharide chains. These upturns were not disturbing for the determination of the position, q*, of the polyelectrolyte peak appearing at higher q-values.

The lowest concentrations, presented in Figure 5.8 (a, b), correspond to the semidilute solutions. For both hyaluronan samples, HA1 and HA2, a well-documented and typical polyelectrolyte peak is observed. This correlation maximum yields from the electrostatic repulsion between the charged macroions, or specifically carboxylic groups belonging to two distinct macroions. Unlike the synthetic polyelectrolytes or other polysaccharides (as for example, xanthan[192]), for hyaluronan the peak is hardly observed experimentally[193]. For the first time, Villetti and co-workers have reported it to the HA semidilute solutions, applying shear to make the peak visible[192]. Without any supplementary manipulation, the peak was observed in the very dilute regime by Alber and co-workes[194]. In the semidilute regime, through the isotropic model of P.-G. de Gennes[10], the position of the maximum q* is related to the correlation length ξ of the temporary network representing the average structure of the polyelectrolyte solution. The presented peak positions are in agreement with the mentioned SAXS measurements from hyaluronan solutions. As the concentration increases, the position of the PE peak $q*$ is shifted towards higher q-values and a decrease in the scattered intensity is observed. Both means that the correlation length ξ and the strength of the electrostatic interactions, decrease with concentration.
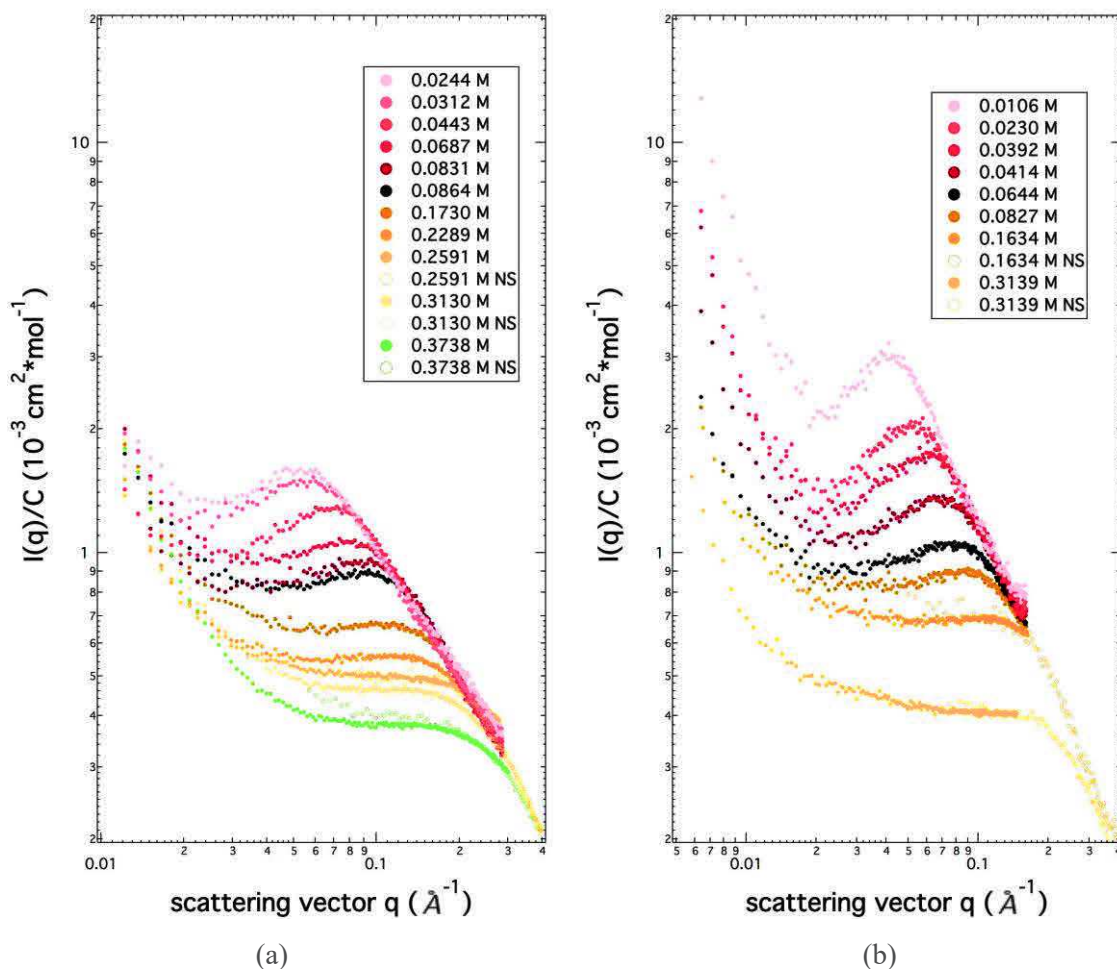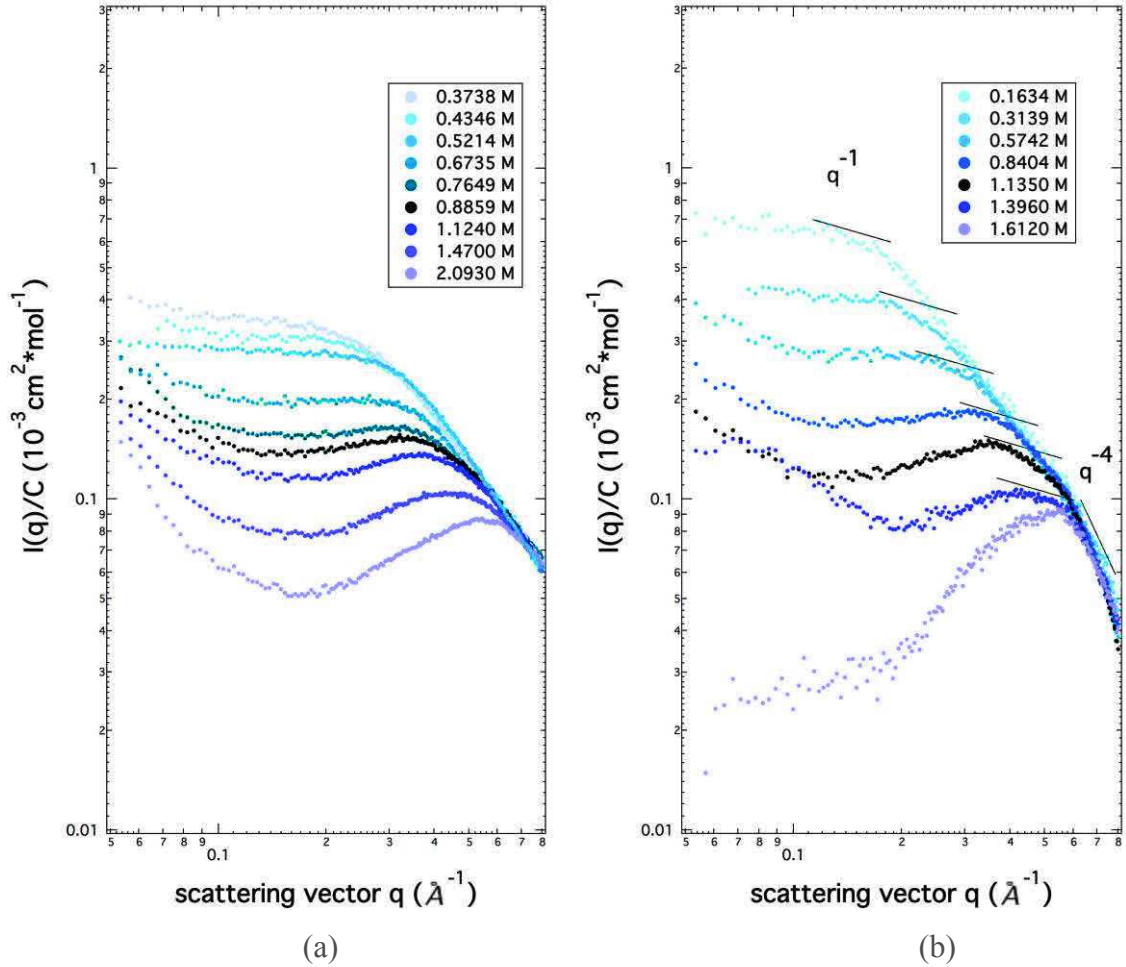
(a)   (b)

Figure 5.8: SAXS profiles of salt-free aqueous solutions for two HA of distinct average molecular weight: M_w = 53 300 g.mol^{-1} (HA1) (a); M_w = 395 500 g.mol^{-1} (HA2) (b) – Explored concentration range: $0.01 < c < 0.38$ mol/l (semidilute and concentrated regimes)

In the concentrated regime, above the crossover concentration $C^{**} \approx 0.10$ mol/l (Figures 5.8 (a) and 5.8 (b)), the scattered intensity continues going down due to a further screening of the electrostatic interaction. The PE peak is broader and more asymmetrical comparing to the one observed in the semidilute regime. It remains a shoulder. The peak progressively disappears in the concentration range between 0.4 and 0.5 mol/l. Then the scattering curves are almost monotonous.

(a) (b)

Figure 5.9. SAXS profiles of salt-free aqueous solutions for two HA of distinct average molecular weights: M_w = 53 300 g.mol^{-1} (HA1) (a), M_W = 395 500 g.mol^{-1} (HA2) (b) – Explored concentration range: 0.15 < c < 2.10 mol/l (beyond the concentrated regime)

As concentration is further increased, for both average molecular weights (HA1 and HA2), a new maximum, always broad but nevertheless of distinct origin, or nature, reappears at the critical concentration $C^{***} = C_{cylinder} \approx 0.41$ mol/l with a position q^* around 0.14 Å^{-1}. This new maximum actually corresponds to a new regime in dense polyelectrolyte solutions, located just above the concentrated one, provided the polyelectrolyte intrinsic stiffness is large enough. As previously shown by P. Lorchat using PDADMAC and PαMSSNa, the non-electrostatic persistence length has to be larger than 2.5 nm[30]. Of course, that is the case with hyaluronan for which l_p = 9 nm. This new regime can be ascribed to a jammed random close packing of equivalent solid rods of length, comparable to the intrinsic persistence length. Their orientation results from a competition between the excluded volume interaction, or steric effect, contributing to an alignment of the macroions at the length scale close to ξ, and the electrostatic repulsion in favor of their perpendicular orientation as

74

well as the thermal fluctuations introducing disorder. The scattering maximum position can be assigned to the minimal distance between hard cylinders. Above $C_{cylinder}$, the orientation of the hard cylinders is maintained perpendicular to each other. At first, the intensity of the maximum is very low and the maximum is broad. The peak intensity increases and its width decreases as the concentration is increased. The distribution of the average intermolecular distance becomes thinner and the system, close to a local orientation order state. At the critical concentration $C_{nematic} \approx 1.2$ mol/l, $q* = 0.40$ Å^{-1}, the system displays a nematic local order and the hard cylinders have parallel orientation inside small domains.

5.2.2. Concentration dependence of the peak position and crossover concentrations

The variation of the peak position, $q*$, with concentration, c, for HA1 and HA2 and the comparison with another macroion, PDADMA[30], is summarized in Figure 5.10. Four regimes are clearly seen for both HA macroions. The first one is the semidilute regime with the experimentally obtained exponent 0.45, close to the expected one ½ within the isotropic model of de Gennes[10] ($q* \sim c^{1/2}$). This concentration range exceeds up to the semidilute-to-concentrated crossover concentration $C** \approx 0.1$ mol/l. The PE peak position $q*$ scales as $C^{0.26}$, with an exponent close to the expected one (1/4) for the concentrated regime ($q* \sim c^{1/4}$). Above the concentrated-to-jammed state crossover concentration $C*** \approx 0.41$ mol/l, $q*$ becomes proportional to C^1 ($q* \sim c^1$) until the next critical concentration $C**** \approx 1.2$ mol/l from which $q* \sim C^{0.49}$ ($q* \sim c^{1/2}$), scaling law associated with a nematic local order. As expected, these scaling laws are independent of the hyaluronan molecular weight.

Three crossover concentrations, $C**$, $C***$ ($C_{cylinder}$) and $C****$ ($C_{nematic}$) have been found experimentally. The crossover between dilute and semidilute solutions $C*$ was not observed only because the average molecular masses of the studied HA macroions were too high. The discussed concentration dependence of the peak position and the change in the peak intensity with concentration are in agreement with the recent measurements conducted in our laboratory by P. Lorchat with PDADMA and PαMSS[28]. The transition between concentrated and isotropic new regimes occurs at $q*$ related to the value of the persistence length l_p and ratio q*(HA)/q*(PDADMA) is close to the ratio of the related intrinsic persistence lengths l_p^0(HA)/l_p^0(PDADMA) = 3[31]. The critical crossover concentrations $C***$ and $C****$ are observed earlier for hyaluronan than for PDADMA due to a

higher intrinsic stiffness: 0.41 mol/l instead of 0.90 mol/l and 1.2 mol/l instead of 2.0 mol/l (Figure 5.10). The comparison between the small-angle scattering investigations of HA (through SAXS) and PDADMAC (through SANS) was done more precisely in the study[28]. The variation of the peak position with the concentration is universal from the semidiute regime until the nematic local order. The existence of an orientation order in dense aqueous solutions of semiflexible polyelectrolytes is in agreement with theory. However, only experiments were able to show the existence of the new regime for which q^* is proportional to C.
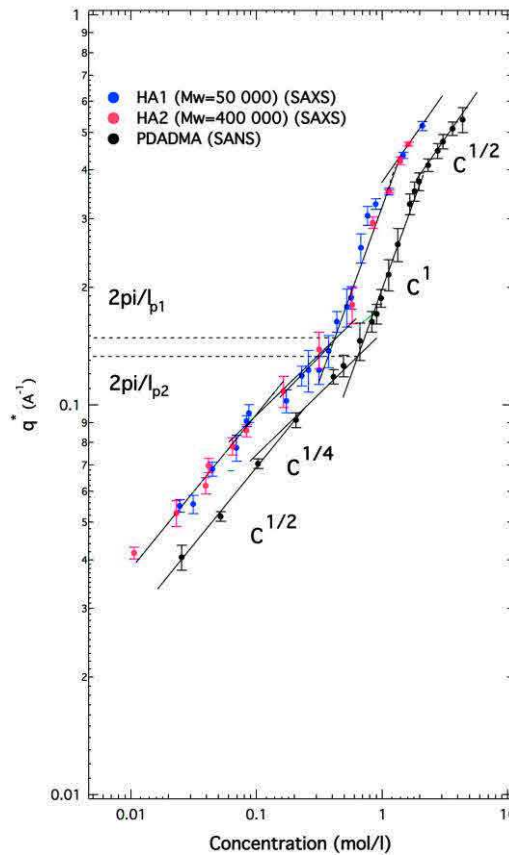
Figure 5.10. Concentration dependence of the peak position q^* for hyaluronan macroions of distinct molecular weight (red for HA2; blue for HA1) and PDADMA (black). The data about the variation of PDADMA peak position q* is kindly given by P. Lorchat[30]

The value (≈ 0.1 mol/l) obtained for C^{**} was compared with the ones proposed by the theory. Assuming that the correlation lengths for the two regimes should agree with each other at a crossover concentration though theoretically the crossover occurs gradually, the theoretical crossover concentration C^{**}_{MU} due to the Muthukumar[25] is obtained as:

$$C^{**}_{MU} = 0.79 \left(\frac{w_l}{l_p}\right)^{1/3}/l_p^3 \tag{97}$$

Where w_l is the strength of the electrostatic potential:

$$w_c = \left. \frac{4\pi Z_p^2 e^2 \alpha^2}{\varepsilon \varepsilon_0 k_B T} \right. \tag{98}$$

Z_p is the number of charges per segment; e, the elementary charge; α, the ionization degree per chain or the effective charge fraction; ε, the relative dielectric constant of the medium; ε_0, the absolute dielectric constant of the vacuum; k_B, the Boltzmann constant; T, the absolute temperature. In the case of PSS[17], taking $Z_p = 1$, $\alpha = 0.35$, $K_r = 78.4$ for water at 25°C and T = 298 K, resulting in $w_c = 138.3$ Å. When the persistence length of non-ionized NaPSS, b_0, is taken to be 12 Å, we obtain $l = 24$ Å and then $C^{**}_{MU} = 0.17$ mol/l. This value is one order of magnitude lower than the observed one of 1.2 mol/l. As is expected from Eq. (97), C^{**}_{MU} is strongly dependent on the value of l. The estimation of l causes a great change in C^{**}_{MU}; the difference by a factor in l is amplified to that by one order of magnitude in C^{**}_{MU}. Therefore, we reconsidered the value of the persistence length of NaPSS. Using our original data[195], the observed value of persistence length b_t, were extrapolated to $C^{-1/2} = 0$ to obtain $b_0 = 9 \pm 2$ Å or $l = 18 \pm 4$ Å. The value of $l = 18$ Å gives $C^{**}_{MU} = 0.44$ mol/l. The agreement with the observed C^{**} has been greatly improved. If we employ $b_0 = 7$ Å or $l = 14$ Å as the lower limit, we obtain $C^{**}_{MU} = 1.03$ mol/l, which is very close to the observed C^{**}, but there is no reason for doing so. Barrat and Joanny[23] also gave the theoretical crossover concentration based on the electrostatic blob concept that the electrostatic blob size ξ_b is nearly equal to the mesh size ξ of the isotropic structure in the semidilute regime. However, their crossover concentration seems considerably high in more than two orders of magnitude compared with observed value. One reason for this discrepancy may be due to the used theory for the concentration dependence of persistence length[37].

Obviously, in the calculation of Kaji et al[196], l is the Kuhn statistical length, i.e. the double of the non-electrostatic persistence length of the macroions $2l_p°$; α is the effective charge fraction of the macroions, i.e. $\alpha = f_{eff}$; Z_p is the number of charges per segment. As Z_p is considered equal to 1 for PSS, we can assume that "segment" means "monomer" for the authors.

Finally, to obtain C^{**}_{MU} in mol/l, instead of Eq. (79) we must use the following equation:

$$C^{**}_{MU}(mol/l) = \{[0.79 \ (w_c/l)^{1/3}/l^3]/6.022\} 10^4 \tag{99}$$

in which w_c and l are expressed in Å.

We note that w_c scales as Z_p^2 and α^2, or f_{eff}^2. $f_{eff} = b/l_B$, b being the monomer contour length this time and l_B the Bjerrum length (7.13 Å at 25°C). The persistence length dependence of C^{**}_{MU} is quite significant, as emphasized by Kaji et al. These two dependences can be summarized through the relationship:

$$C^{**}_{MU} = 0.79 \ K \ Z_p^{2/3} \ f_{eff}^{2/3}(2l_p^\circ)^{-(3+1/3)} \tag{100}$$

with

$$K = 4\pi e^2/K_r \varepsilon \varepsilon_0 \ k_B T \tag{101}$$

and where l has been replaced by $2l_p^\circ$.

From these relations and by considering one charge per monomer ($Z_p = 1$), we are able to obtain the following values for C^{**}_{MU} for PSS, PDADMA, PαMSS and HA, using experimental data from different literature sources and personal discussions:

Macroion	$l = 2l_p^\circ$ (Å)	$\alpha = f_{eff}$	w_c (Å)	C^{**}_{MU} (mol/l)	C^{**}_{exp} (mol/l)
PSS (Kaji et al)	24	0.35	138.3	0.17	1.2
PSS (P. Lorchat)	20	0.36	146.3	0.32	1.2
PαMSS (P. Lorchat)	48	0.36	146.3	0.017	0.4
PDADMA (P. Lorchat)	60	0.66	491.8	0.012	0.2
HA (I. Konko)	180	1	1129.0	0.0004	0.08
HA (J. Combet)	180	1	1129.0	0.0004	0.034

On the other hand, by considering one charge per Kuhn statistical length $l = 2*$non electrostatic persistence length ($Z_p = 2l_p^\circ/b$), we are able to obtain the following values for C^{**}_{MU}:

Macroion	Z_p	$\alpha = f_{eff}$	w_c (Å)	C^{**}_{MU} (mol/l)	C^{**}_{exp} (mol/l)
PSS (P. Lorchat)	$20/2.5 = 8$	0.36	9363	0.16	1.2
PαMSS (P. Lorchat)	$48/2.5 \approx 19$	0.36	53932	0.12	0.4
PDADMA (P. Lorchat)	$60/4.7 \approx 13$	0.66	80149	0.005	0.2
HA (I. Konko)	$180/10.2 \approx 18$	1	351709	0.0002	0.08
HA (J. Combet)	$180/10.2 \approx 18$	1	351709	0.0002	0.034

At this stage, we should rather compute $l_p°$ or $2l_p°$ from the experimental value of C^{**} (inverse process) or replace $l = 2l_p°$ by $\xi = 2\pi/q^*$ (from q^* value at C^{**}).

By replacing l by $2\pi/q^*$ with q^* measured at $c = C^{**}$, we obtain:

Macroion	$l_p°$ (Å)	C^{**}_{exp} (mol/l)	$q^*(C^{**})$ (Å^{-1})	$\xi = 2\pi/q^*$ (Å)	$\alpha = f_{eff}$	w_c (Å)	C^{**}_{MU} (mol/l)
PSS (Kaji)	12	1.2	0.19	33.1	0.35	138.3	0.058
PSS (P.Lorcha)	10	1.2	0.18	34.9	0.36	146.3	0.05
PαMSS (P.Lorcha)	24	0.4	0.12	52.4	0.36	146.3	0.013
PDADMA (P.Lorcha)	30	0.2	0.08	78.5	0.66	491.8	0.005
HA (I. Konko)	90	0.08	0.09	69.8	1	1129.0	0.094
HA (J. Combet)	90	0.034	0.068	92.4	1	1129.0	0.037

All the previous approaches seem to be not satisfying, since the differences in between c^{**}_{MU} (in red) and C^{**}_{exp} (in blue) are rather significant.

Finally, we can derive l from the measured C^{**} value (C^{**}_{exp}) and compared it to $2l_p°$. For that, we inverse the Eq. (100). We obtain:

$$l = [(0.79(w_c)^{1/3}60220)/C^{**}_{exp}]^{1/(3+1/3)} \tag{102}$$

in which w_c and l are expressed in Å and C^{**}_{exp}, in mol/l. That leads to the following table:

Macroion	l_p° (Å)	C^{**}_{exp} (mol/l)	$\alpha = f_{eff}$	w_c (Å)	l (Å)	$l/2l_p^\circ$	$\xi = 2\pi/q^*$ (Å)
PSS (Kaji)	12	1.2	0.35	138.3	39.22	1.63	33.1
PSS (P. Lorchat)	10	1.2	0.36	146.3	39.44	1.97	34.9
PαMSS (P. Lorchat)	24	0.4	0.36	146.3	54.84	1.14	52.4
PDADMA (P. Lorchat)	30	0.2	0.66	491.8	76.22	1.27	78.5
HA (I. Konko)	90	0.08	1	1129.0	109.03	0.61	69.8
HA (J. Combet)	90	0.034	1	1129.0	140.94	0.78	92.4

Also we have noted that despite the same c-dependence of q^*, HA1 and HA2 have distinct scattering behaviours at high q-values, above the concentrated regime. The superposition of the scattering curves for the short HA1 and the long HA2 displays a $q^{-1.5}$ decreasing, or scattering behaviour, in distinct q-ranges: between 0.3 and 0.8 Å^{-1}, for HA1; between 0.2 and 0.6 Å^{-1}, for HA2 (Figure 5.9). The $q^{-1.5}$ scattering behaviour does not depend on concentration. It is, therefore, a characteristic of the form factor of the HA macroions. The long HA2 also shows, at $q > 0.12$ Å^{-1} and in a limited q-range, the q^{-1} scattering behaviour. We would propose that the increase in the molecular weight could improve the local orientation order of the macroions.

In high concentrated solutions, or films with nanodrops, of high-molecular weight HA, the possibility of the highly ordered stable superstructure was shown by infrared spectroscopy[197–200], ^{13}C-NMR, X-ray fiber diffraction[201] and electron microscopy[158]. According to Scott, the molecular model of HA is described as a highly cooperative system of overlapping antiparallel hyaluronan chains stabilized by H-bonds and hydrophobic interactions[201]. Such ordered arrangements could be explained by the increase in the possible cross-links of the HA network with longer polysaccharides

and they are not stable with low molecular weight polysaccharides[197]. The formation of such structures is also a peculiarity hyaluronan of animal origin. That plays an important role in biological phenomena and explains the presence of HA in the soft tissue and extracellular matrix.

At $q > 0.58$ Å^{-1}, the scattering curves of the high-molecular weight HA display a q^{-4} decay that could suggest the existence of interfaces and could be attributed to some microphase separation leading to clusters that involve highly ordered arrangements. The possibility of HA to be organized in highly oriented structures or to crystallize in the presence of sodium, potassium and calcium cations has been reported by several authors[155,192,202–204].

5.3. Conclusions

We have first studied the average conformation of HA macroions in dilute brine aqueous solutions. Specifically, we have measured the form factor of the HA macroions and determined their non-electrostatic persistence length (l_p close to 90 Å), by using the SAXS technique.

Our SAXS study of the salt-free aqueous solutions of hyaluronan, from the semidilute regime until the glassy state, has revealed the typical polymorphism of the salt-free aqueous solutions of semiflexible polyelectrolytes. The intermediate intrinsic chain stiffness makes possible the transition from an isotropic state to a nematic local order. However, this transition is not totally similar to the classical Onsager transition since it occurs through the existence of a new phase ($q^* \sim c^l$) associated with a frustration and characteristic of polyelectrolytes. The critical concentration and the peak position of the transition are related to the intrinsic persistence length of the macroions.

Chapter 6

Poly(sodium Styrene Sulfonate) – Poly(diallyldimethyl ammonium Chloride) Complexes

6.1. Complexes formed in the dilute regime

6.1.1. Combined ITC, DLS and zeta potential measurements

We investigated the interaction between PDADMAC and PSSNa in dilute aqueous solution at distinct ionic strengths, using different mixing procedures or sample preparations. The free energy of the interaction between oppositely charged polyelectrolytes results from the enthalpy of bonding formation and the entropy of counterions release. The electrostatic interaction belongs to the non-specific interactions as it differs from the covalent ones[151]. The PDADMAC aqueous solution was added drop-by-drop into the PSSNa one (direct mixing) and *vice-versa* (reverse mixing).

As it has been already mentioned in the experimental description (Chapter 4), we used a combination of three techniques: isothermal titration calorimetry (ITC), dynamic light scattering (DLS) and zeta potential analysis. It allows us to follow correlation between thermodynamics, size and charge changes. Thus, ITC, DLS and zeta potential measurements were performed under the same conditions. We remind that poly(sodium styrene sulfonate) is negatively charged and poly(diallyldimethylammonium chloride) has positive zeta potential. The same approach was used by Berret and co-workers for studying the poly(diallyldimethylammonium chloride)-poly(sodium acrylate) complexation[77].

Figures 6.1-6.4 present the thermograms and the binding isotherms obtained for poly(diallyldimethylammonium chloride)-poly(sodium styrene sulfonate) complexation process in the dilute regime. The thermograms show the time dependence of the heat exchange during the titration procedure. The responses of the calorimeter are shown starting at 4000 s, after stabilization

of the system and measurement of a baseline. The presented heat exchange, or the apparent binding enthalpy, is the summation of the reaction enthalpy, or the real/intrinsic binding enthalpy, and the heat of dilution of the polyelectrolyte in buffer (blank). The dilution heat of polyelectrolytes is endothermic as expected from the counterion condensation phenomenon. The normalized heats were corrected subtracting this dilution contribution. The first peak in thermogram is typically smaller than the following peaks due to a smaller amount of reagent injected at the first interval. It comes from an air bubble staying in the syringe, which acts as a physical barrier to prevent contact between the reagents in the cell and the syringe barrel. All titration curves have a sigmoidal shape or close to it. The time dependences of the enthalpy for direct mixing (PDADMAC in PSSNa) display the change from an exothermic to an endothermic process with the increase in the mole ratio (Figure 6.1 and Figure 6.3). In the absence of salt, the further addition of PDADMAC results in the rapid decrease in the heat exchange ΔH when the critical mole ratio is close to 1 (or reaches 1). In the presence of an added salt, such a decrease up to zero takes place beyond $Z = 1.5$ and indicates the absence of any interaction upon further polycation titration. The enthalpy of complexation through reverse mixing (PSSNa solution into PDADMAC one) always stays exothermic independently of the ionic strength.

After the careful analysis of the thermograms and binding isotherms, we propose that the PSS-PDADMA complexation is a two-step process. The primary process is initiated at low charge ratio, following the first injection of added polyelectrolyte solution. It is related to the sigmoidal shape of the binding isotherms. The divergence from the sigmoidal titration trajectory comes from the existence of a second step. The fact that the secondary process follows the primary one is well illustrated by the presence of a shoulder after each peak in the response of the calorimeter. This is well observed in Figure 6.1 (PDADMAC into PSSNa in the absence of salt) at the injections number 8 ($Z = 0.8$) and 9 ($Z = 0.9$). Thus, every peak in the response of calorimeter can be divided into two parts with different response times. The primary step has a characteristic response time of 120 seconds. The kinetics of the secondary step is lower, with a relaxation time up to 15 min. The existence of the second step complicates the integration of peaks and the analysis of the ITC data.
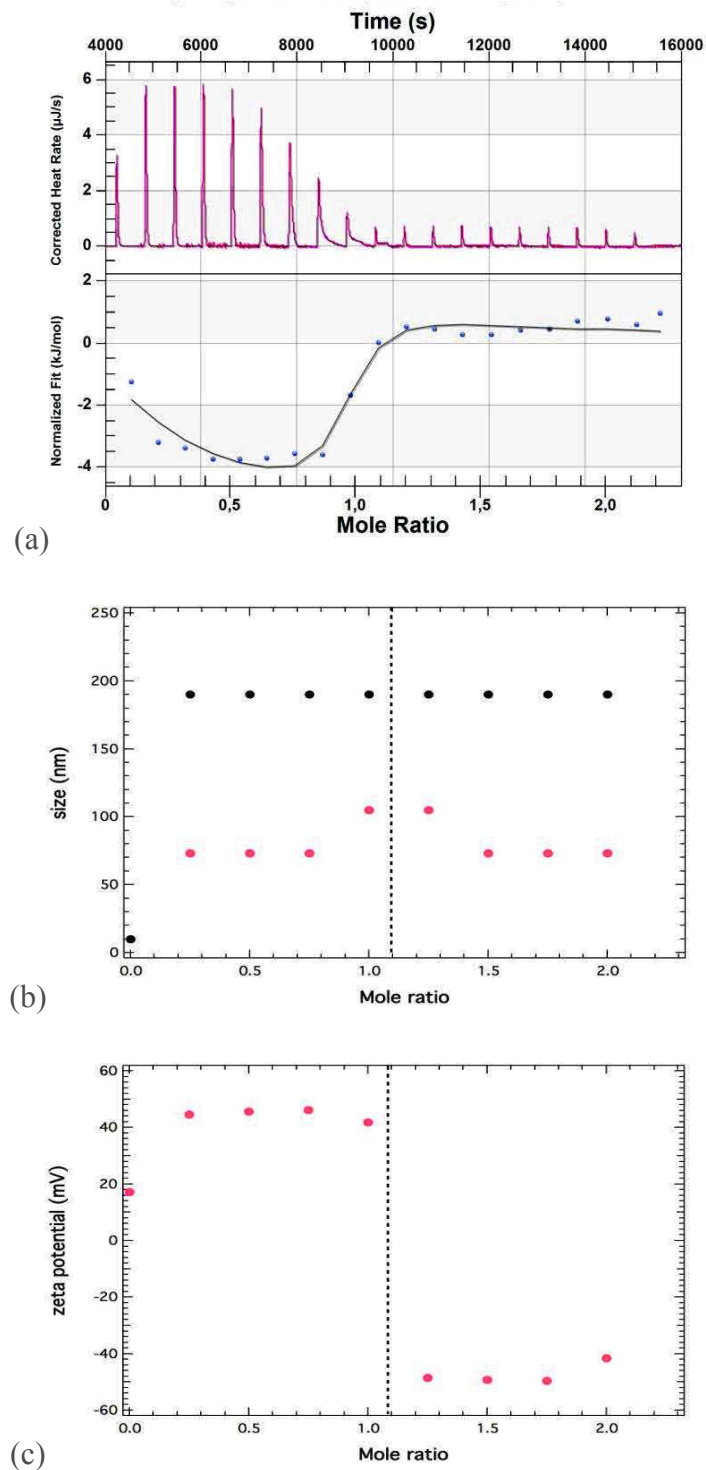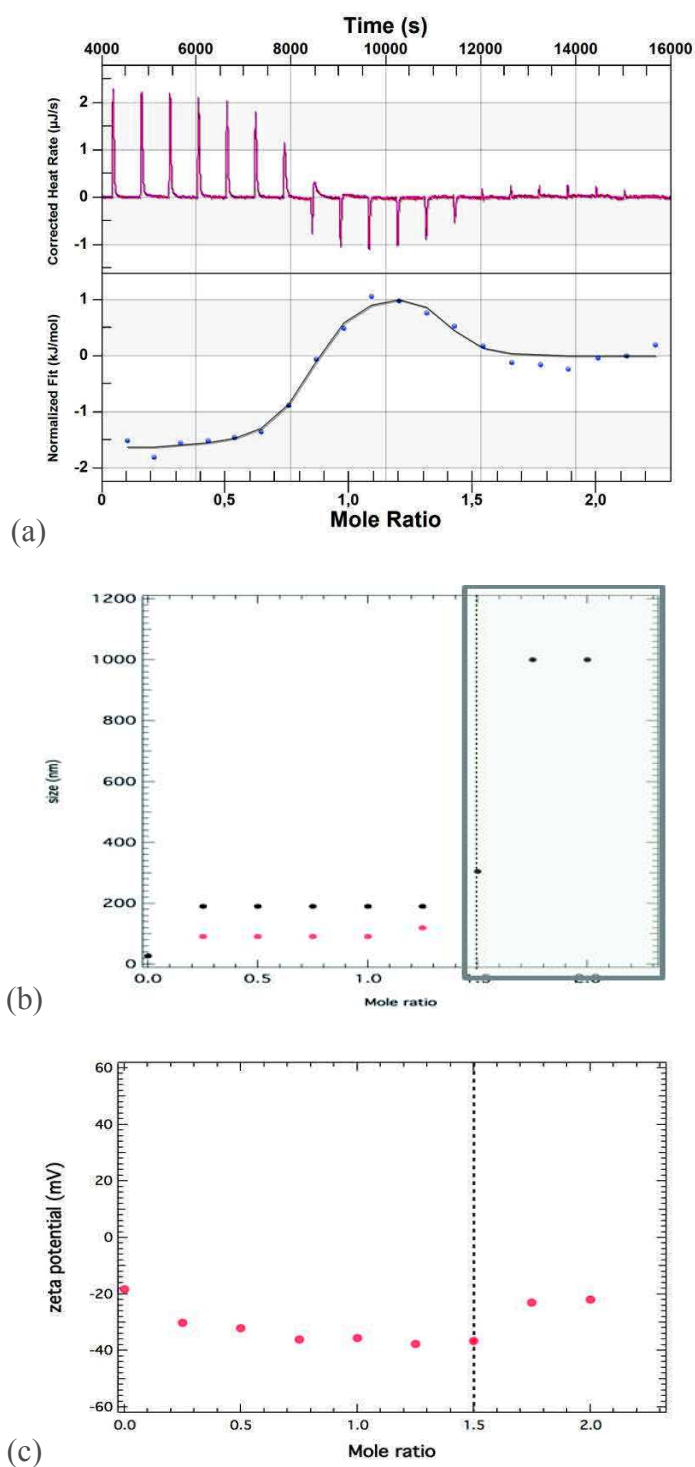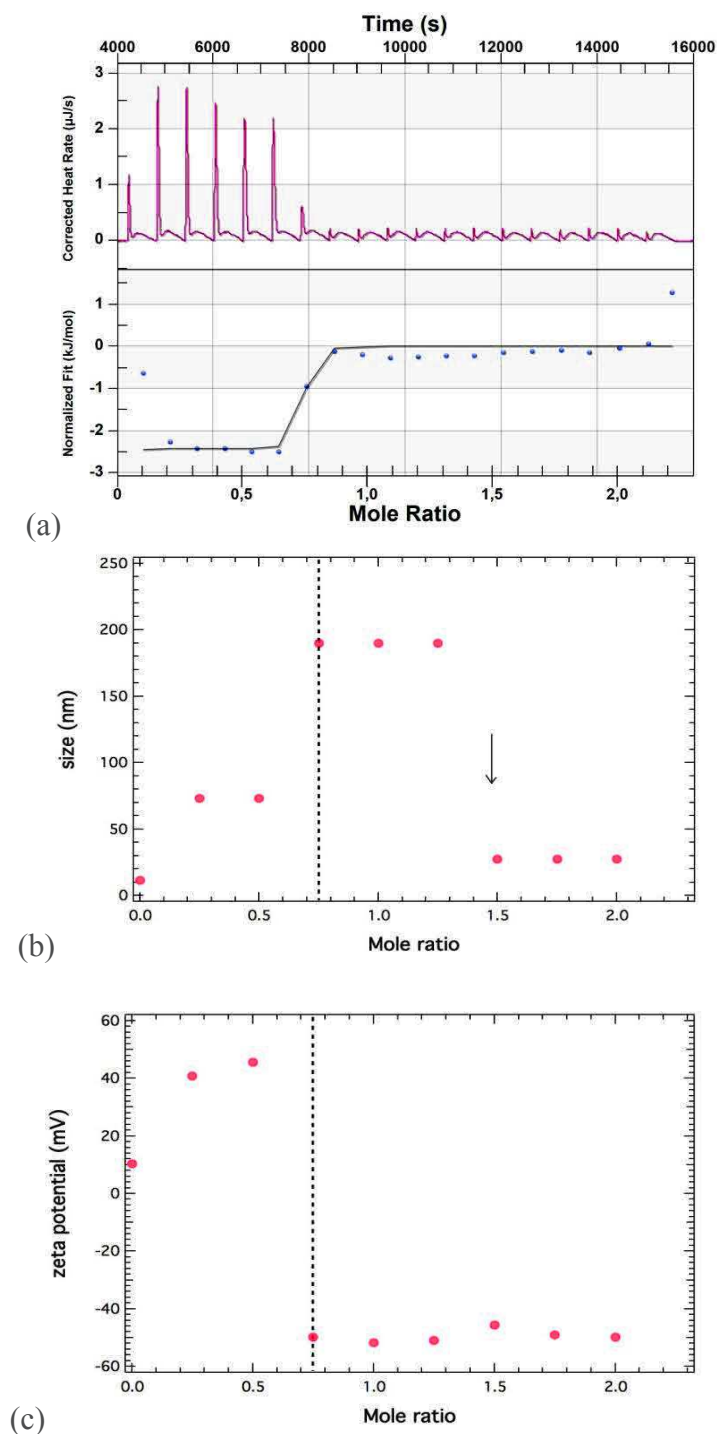
(a)

(b)

(c)
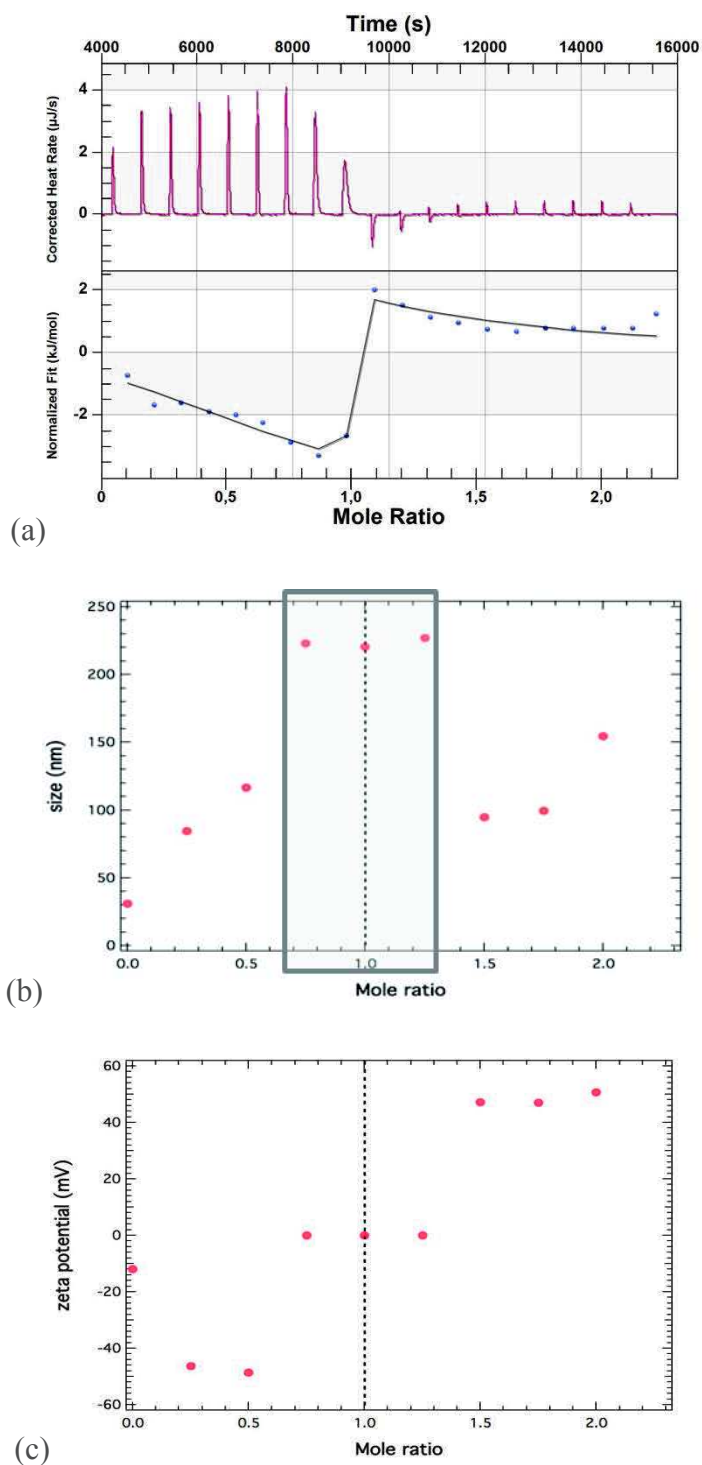
Figure 6.1. Thermogram (top) and binding isotherm (bottom) (a), hydrodynamic diameter (b) and zeta potential (c) observed for polyelectrolyte complexes formed through adding the PDADMAC solution into the PSSNa one. The normalized heats were corrected by subtracting the dilution contribution. Grey rectangle shows cases, where the measured size of complexes was out of the equipment limitation (hydrodynamic domain $qR_h<1$). Mole ratio corresponds to charge ratio [+]/[-]

(a)

(b)

(c)

Figure 6.2. Thermogram (top) and binding isotherm (bottom) (a), hydrodynamic diameter (b) and zeta potential (c) observed for polyelectrolyte complexes formed through adding the PSSNa solution into the PDADMAC one. The normalized heat was corrected by subtracting the dilution contribution. Dark and red points represent two different modes, which were observed with the DLS experiments and associated with two distinct particle sizes. Mole ratio corresponds to charge ratio [+]/[-]

(a)

(b)

(c)

Figure 6.3. Thermogram (top) and binding isotherm (bottom) (a), hydrodynamic diameter (b) and zeta potential (c) observed for polyelectrolyte complexes formed through adding the PDADMAC solution into the PSSNa one, both solutions being in the presence of 0.15 M NaCl. The normalized heats were corrected subtracting the dilution contribution. Grey rectangle shows cases, where the measured size of complexes was out of the equipment limitation (hydrodynamic domain $qR_h < 1$).

(a)

(b)

(c)

Figure 6.4. Thermogram (top) and binding isotherm (bottom) (a), hydrodynamic diameter (b) and zeta potential (c) observed for polyelectrolyte complexes formed through adding the PSSNa solution into the PDADMAC one, both solutions being in the presence of 0.15 M NaCl. The normalized heats were corrected by subtracting the dilution contribution

Few interesting observations were made, comparing the isothermal titration calorimetry data with the corresponding size and charge changes. Figure 6.1 displays the relationship between the enthalpy of binding, the hydrodynamic diameter and the ζ potential for direct mixing of the free-salt solutions. The addition of polycations initiates the complexation with the formation of the negatively

charged (-46 mV) particles of average size 86 nm. Up to the critical mole or charge ratio of 0.75, the addition of PDADMAC causes an increase in the complex size without any significant change in its effective charge. In the mole ratio range between 0.75 and 1.25, the measured values of hydrodynamic diameter were out of the hydrodynamic domain $qR_h < 1$. Formed at these conditions complexes are rather neutral. Beyond $Z = 1.25$ the zeta potential increases rapidly reaching high positive value (+47 mV) and the particle size decreases to 90-105 nm. In parallel, a similar decrease is observed for the intensity of scattered light, when passing the critical point $Z = 1.25$. We attribute this to the sedimentation of the associations formed by the primary complexes. Thus, at $Z = 1.25$ the DLS signal is proportional to the number of complexes that did not participate in the secondary process at that moment. The zeta potential values stay continuously highly positive till the end of the titration. The change in the particle size demonstrates the existence of an additional aggregation process, subsequent to the complexation, in the system. Based on these observations, the size of the primary complexes is suggested to be in the range of 86 to 105 nm. The largest PEC aggregates found in the solution, which have not precipitated, are larger than 200 nm.

The reverse mixing order does not change the zeta potential ζ scenario since there is always a charge inversion at $Z = 1$ (Figure 6.2). Indeed, starting from the plateau at +45 mV, ζ shows an abrupt transition to -50 mV at critical charge ratio $Z = 1$ and keeps this value till the end of the titration. The charges of PECs at low and high total charge ratio Z in the direct and reverse ways of mixing are perfectly opposite. The change in the titration order introduces a difference in the size evolution. The addition of PSSNa to PDADMAC results in the formation of two particle populations having distinct sizes (73 nm and 190 nm). For all systems under study, the light scattering intensity is the sum of two contributions related to both populations. The contribution of the fraction with larger particle size increases with the mole or charge ratio. Consequently, the secondary aggregation starts at low Z and becomes more important with the addition of polyanion. The size of primary complexes and aggregates, formed by adding PSSNa to PDADMAC, are suggested to be 73 and 190 nm, respectively. The D_H of primary complexes slightly increases from 73 nm to 105 nm close to the transition point at the charge stoichiometry. Thus, the way of titration plays a major role.

In the direct mixing of the brine solutions of PDADMAC to that of PSSNa, the similar bimodality in the particle size is observed. Both 78-105 nm and 190 nm particles are present in the system up to the critical value of $Z = 1.5$. The next injection of polycation results in a quick increase in the particle size due to the aggregation. However, at $Z = 1.5$ and beyond, light scattering is no longer appropriate to determinate the sizes of the formed structures. D_H was set at 1000 nm only to display the abrupt increase in size. The DLS measurements are further complicated by sedimentation

process in the system. With the addition of polycation the zeta potential ζ decreases from -30 mV at Z = 0.25 to -37 mV at Z = 0.75. Beyond Z = 0.75, ζ has a plateau till Z=1.5. At mole ratio larger than 1.5, the zeta potential measurement gives -22.5 mV, which is close to the charge obtained from 0.15 M NaCl aqueous solution of PSSNa (Z = 0). This titration procedure (PDADMAC into PSSNa in the presence of added salt) is the unique case, for which the transition in ζ potential was not observed. Probably, at Z=1.5-2.0, there is no interaction between PDADMA and PSS as the heat exchange is close to zero. We consider Z=1.5 as the critical charge ratio.

In the reverse titration way, always in the presence of an added salt (Figure 6.4), the transition of the zeta potential from +45 mV to -50 mV takes place at Z = 0.75. At the first injection of PSSNa, the hydrodynamic diameter D_H of the formed complexes is 73 nm. The D_H increases to 190 nm with the polyanion concentration due to some association. The aggregation starts at low charge ratio and is in agreement with the indication of a slow process on the thermogram. At Z = 1.25, the addition of PSSNa results in the formation of large aggregates that sediment. This precipitation is accompanied by a decrease in the D_H value and in the scattered intensity. At Z = 1.5-2.0, the measured size is 27.4 nm that corresponds to the average size of PSS macroions in 0.15 M NaCl (Z = 0 in Figure 6.4 (c)). The changes in the average size and effective charge are summarized in Table 6.1.

Table 6.1. Characteristics of PSS/PDADMA complexes formed under different conditions

System	D_H (nm)	ζ (mV) at low Z	ζ (mV) at high Z	Z of transition
PDADMAC into PSSNa	86	-46	+47	0.75 - 1.25
PSSNa into PDADMAC	73; 190	+47	-50	1.1
PDADMAC into PSSNa in 0.15 M NaCl	78-105; 190	-30	-37	1.5
PSSNa into PDADMAC in 0.15 M NaCl	73	+45	-50	0.75

6.1.2. Analysis of the ITC data using the two-step process model

Based on the described observations, the interaction between oppositely charged poly(sodium styrene sulfonate) and poly(diallyldimethylammonium chloride) is suggested to be a two-step process. Consequently, the measured heat exchange is the sum of two contributions: ΔH^1, for the PEC

formation, and ΔH^2, for the aggregation. Both complexation and association processes are sequential and should be correlated, but the relationship between these two contributions is difficult to describe according to a mathematical equation. Thus, we assumed that PEC complexation and association are independent processes. Fitting the raw data with a model that represents the set of two independent non-interacting sites did the analysis of the ITC results. According to this model, a macromolecule has several 'binding sites', to which ligands can be bound. The binding probability is independent of the occupation rate of the other sites.

The interaction process is presented as:

$$A + B \overset{K}{\leftrightarrow} AB \tag{103}$$

And the equilibrium binding constant is:

$$K_b = \frac{[AB]}{[A][B]}. \tag{104}$$

In a typical ITC experiment, the heat exchange is measured by addition of a small amount of the component B. As a result, the measured quantity represents the derivative of the heat with respect to the [B] molar concentration. Introducing the charge ratio Z, the enthalpy obtained from thermograms will be:

$$\Delta H\,(Z,n,r) = \frac{1}{2}\Delta H_b(1 + \frac{n-Z-r}{\sqrt{(n+Z+r)^2-4Zn}}), \tag{105}$$

Where r = 1/(K[A]); [A] is the molar concentration of the polymer in the measuring cell; K, the binding constant; n, the number of non-interacting binding sites available on each polymer. The equation is equivalent to that provided in the ITC software NanoAnalysis. Both functions ΔH^1 and ΔH^2 were then described with the Eq. (105).

The result of the fitting procedure is displayed together with the raw data in Figure 6.5 for all PDADMAC-PSSNa systems. The separated contributions of ΔH^1 and ΔH^2 are indicated as black and blue lines, respectively. The thermodynamic parameters resulting from the fits are summarized in Table 6.2.

(a)

(b)

(c)

(d)
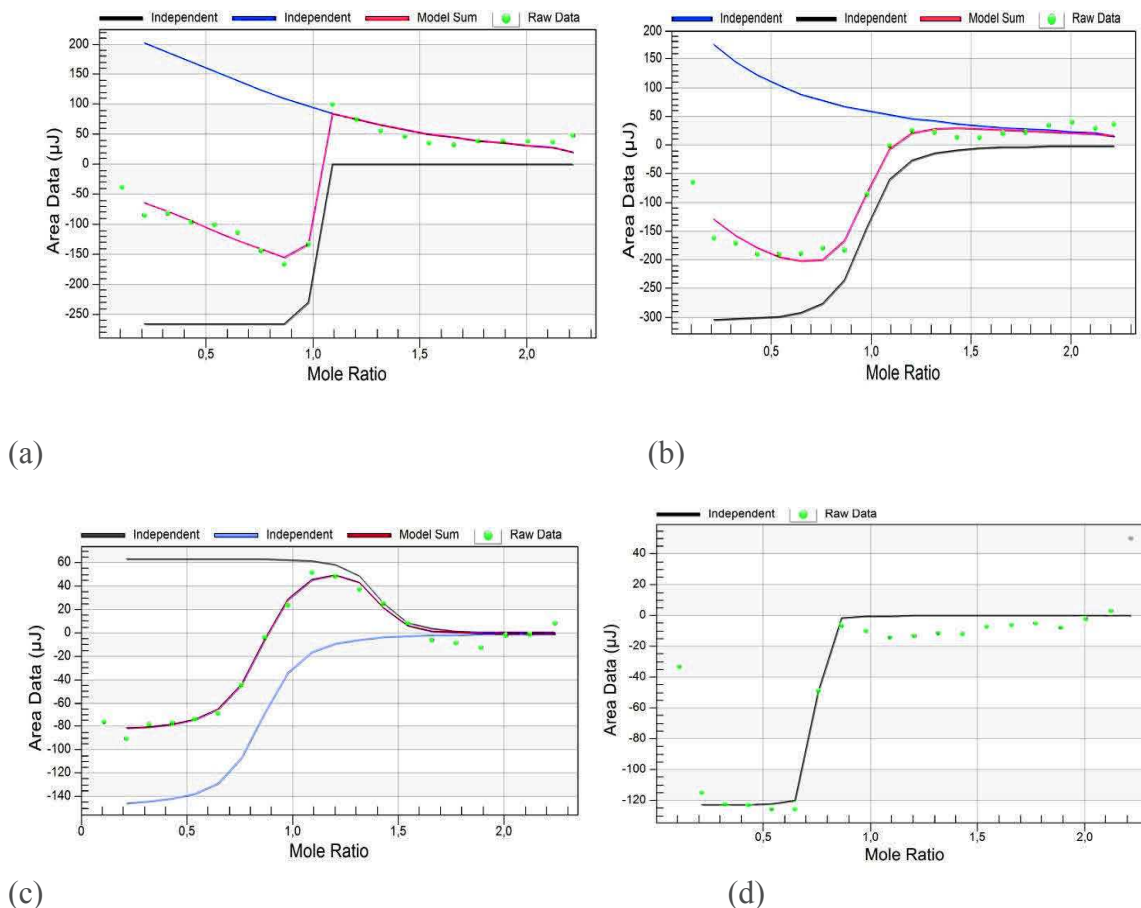
Figure 6.5.Binding isotherms for PSSNa-PDADMAC systems obtained through different preparation procedures (titration ways) and varying ionic strengths (a) PDADMAC solution into PSSNa solution, without added salt; (b) PSSNa solution into PDADMAC solution, without added salt; (c) PDADMAC solution in PSSNa solution, with 0.15 M NaCl; (d) PSSNa solution in PDADMAC solution, with 0.15 M NaCl. Black thin line corresponds to the fit according to the model of independent sites, proposed for the primary complexation process. Blue thin line shows the results coming from the fit according to the independent model for the secondary association process. Red line is the sum of both steps and green points are the raw ITC data points

Table 6.2. Thermodynamic parameters obtained from the fits according to the set of two independent processes. Both primary (complexation; index 1) and secondary (association; index 2) processes are characterized by a binding constant K, a stoichiometry n, an entropy ΔH, a free energy ΔG and an enthalpy change ΔS

Primary process (complexation)	K^1 (M^{-1})	n^1	ΔH^1 (kJ*mol^{-1})	ΔG^1 (kJ*mol^{-1})	ΔS^1 (kJ*mol^{-1}*K^{-1})
PDADMAC into PSSNa	10^9	0.99	-5.13	-51.4	+155.1
PSSNa into PDADMAC	$2.1*10^5$	0.92	-7.4	-30.0	+75.7
PDADMAC into PSSNa in 0.15 M NaCl	$2.0*10^5$	0.81	-2.9	-30.2	+91.5
PSSNa into PDADMAC in 0.15 M NaCl	$5.6*10^5$	0.70	-3.84	-34.0	+101.0
Secondary process (association)	K^2 (M^{-1})	n^2	ΔH^2 (kJ*mol^{-1})	ΔG^2 (kJ*mol^{-1})	ΔS^2 (kJ*mol^{-1}*K^{-1})
PDADMAC into PSSNa	$3.9*10^3$	0.79	+7.51	-20.4	+93.5
PSSNa into PDADMAC	$2.9*10^3$	0.1	+56.62	-19.7	+256.4
PDADMAC into PSSNa in 0.15 M NaCl	$6.9*10^5$	1.27	+1.27	-33.3	+116.1
PSSNa into PDADMAC in 0.15 M NaCl	not calculated				

The ITC data obtained for the PSSNa solution added to the PDADMAC solution, in the presence of an added salt, was an exception among this set of experiments. The raw data of this titration way could be fitted just with the model related to one type of independent sites. In this system, we observed the strong sedimentation of the secondary formed aggregates. This complicates the separation in two processes and subsequently doesn't obey the mathematical expression foreseen for two independent processes. We suggest that the aggregation starts at the mole ratio 0.75. The secondary process contributes to the value of the binding enthalpy at mole ratio larger than 0.75 and causes the difference between the fitted curve and the raw data. Therefore, the correct equation for calculating the thermodynamic parameters of the secondary process could not be provided.

The polyelectrolyte complex formation is exothermic for all mixing modes and ionic strength conditions. The absolute value of the enthalpy of the primary process decreases in the presence of an added salt due to the screening of the electrostatic interaction. These conclusions correlate with a change in the growth regime of layer-by-layer polyelectrolyte multilayer films[73] as well as the results of previous simulation studies for interpolyelectrolyte complexes[44,52]. The entropies of the secondary

association processes are positive and the PEC aggregations are entropy-driven. The enthalpy gains of the reactions are of the order of k_BT and the entropy costs of the reaction correspond to $10*k_BT$.

The stoichiometric coefficient n_1 is close to 1 in salt-free aqueous solution. The presence of an added salt slightly decreases the [+]/[-] and [-]/[+] charge ratios. That is related to the more compact average conformation of the polyelectrolytes in the presence of an added salt and correlatively to the lower access to the binding groups. The stoichiometry of primary interaction is in a good agreement with the transitions observed in DLS and zeta potential analyses. The secondary process starts either around the charge stoichiometry (PDADMAC into PSSNa titrations) or at the beginning of the titration, according to the comparison of ITC and DLS. The initiation of the process around charge stoichiometry [+]/[-]=1 is caused by the high binding constant and, respectively, the high binding affinity of PDADMAC to PSSNa. In the rest of cases, when K^1 is lower, the aggregation process could no longer be negligible comparing to the primary complexation. Below n_1 the absolute value of the enthalpy of the primary PEC formation is larger than that of the secondary process. The aggregation becomes more important beyond n_1.

The mixing procedure influences the binding constant and the enthalpy. The reverse mixing of polyelectrolyte solutions slightly shifts the stoichiometry of the primary process n_1 to lower Z values, comparing to the stoichiometry observed in the direct protocol. These differences are related to the conformational changes of the polyelectrolytes at different concentrations.

Our analysis of the ITC data was based on the set of two independent processes. However, it could be improved by applying the concept of sequential processes and by taking into account the conformational changes of the polyelectrolytes during the titration.

6.1.3. Summary

Based on the combination of ITC, DLS and zeta potential analysis, the complexation between oppositely charged PSS and PDADMA macroions in dilute solutions is proposed to be a two-step process. The first step corresponds to the formation of highly charged complexes with a size of the order of 73-105 nm. The sign of their effective charge is defined by the polyelectrolyte in the measuring cell. It is negative in the case associated with the PDADMAC solution added to the PSSNa one, and positive in the reverse case. The second step starts either around the charge stoichiometry (PDADMAC solution into PSSNa solution), or straightforwardly at the beginning of the titration. The

size of the secondary aggregates, which are stable in solution, is larger than 190-200 nm. The larger formed aggregates precipitate.

The thermodynamic parameters were calculated by fitting the raw data (binding isotherms) to a mathematic model representing a set of two independent non-interacting sites. The polyelectrolyte complex formation is exothermic independently of the mixing order or the ionic strength. The absolute value of the enthalpy of the primary process decreases with the presence of an added salt due to the screening of the electrostatic interaction. The entropy of the secondary association is positive and the PEC aggregation is enthalpy-driven. This type of interactions belongs to the entropy-enthalpy compensation phenomena[151].

The values for the binding enthalpy, the hydrodynamic size and the effective charge (ζ potential) differ for the complexations carried out through distinct mixing protocols. This pathway dependence shows that the complexes formed as a result of electrostatic interactions between poly(diallyldimethylammonium chloride) and poly(sodium styrene sulfonate) are far from the thermodynamic equilibrium.

The next interesting question in the PSSNa-PDADMAC PEC aqueous solutions is if and how the two-step process proceeds in the semidilute and concentrated regimes.

6.2. Complexes formed in the semidilute and concentrated regimes

6.2.1. Macroscopic phase or state diagrams

The electrostatic interaction between oppositely charged polyelectrolytes often leads to macroscopic phase separation that is important for practical use of PECs. The study, done by Sukhishvili and co-workers[205], presents a good example of relationship between the phase behaviour of polyelectrolyte complexes in solution and polyelectrolyte multilayer (PEM) growth on a surface. Phase diagram summarizes visual observations and is a prerequisite for understanding the behaviour of polyelectrolyte complexes. The PDADMA/PSS polyelectrolyte pair is often chosen for PEM construction. We hope that phase or state diagrams reported here would help to predict and control PEM design. The phase diagrams for the ternary system PDADMAC/PSSNa/water has been already investigated and reported through the classical triangle representation by Plantenberg and Kotz[206]. The authors of the article suggested the formation of a liquid crystalline structure. In this work, the employed PSSNa had a smaller molecular weight than the ones we used (M_w=82 200 g/mol, M_n=16 900 g/mol; I=4.86). The partial ternary phase diagram in weight fraction was established for limited fractions for PSS/PDADMA/H_2O with KBr as a released salt.[207]

One of the biggest difficulties in PECs study is the spontaneous character of the interaction process and its reproducibility. Previous studies[42,208] and our ITC measurements showed the interaction of oppositely charged polyelectrolytes yielded to systems that are far from thermodynamic equilibrium. Terminologically 'a phase' is a uniform distinct space of matter containing one or several substances in an equilibrium stable state. Thus, we propose to call the diagrams examined in this work as state diagrams. They correspond to the PE complex systems, or aqueous solutions, formed by adding PDADMAC solution into PSSNa solution.

6.2.1.1. Influence of ionic strength

Presented Figures 6.6 - 6.9 are state diagrams, plotted in the coordinates of both PE concentrations in the final mixture. The state diagrams are shown in unusual log-log representation in order to give a view on all tested systems, especially in the low concentration range. Depending on the composition and ionic strength of solutions, different regions associated with distinct phase behaviours can be distinguished for PDADMAC/PSSNa complexes. First, each domain with a specific macroscopic phase behaviour will be discussed in details, starting with the systems formed

in the absence of added salt just after their preparation. However, the salt-free PDADMAC/PSSNa systems show a slow evolution in time during two weeks of observation after their preparation. This time evolution will then be presented after a general description of the different domains.

State diagram of salt-free PSSNa-PDADMAC aqueous solutions

At C > 0.1 mol/l ('biphasic region' (I)), just after mixing the stock PE solutions, large jellified aggregates, 'flocs', in solution coexist with a 'transparent viscous' liquid, separated by a well-defined meniscus. Macroscopically, the 'flocs' are more tenuous with the decrease in the initial PE concentration. The time of the dense 'flocs' formation in the free-salt solutions lies between several seconds and a few hours. There are two types of macrophase separation that are common in polymer solutions: segregative and associative. The first one takes place when the mixing entropy could not favour overall mixing of both polymer solutions. The mixture separates into two phases, each of them being rich in one component. Associative phase separation occurs in case of the presence of a strong attractive interaction between components. Consequently, both components stay in the same phase ('rich in material' phase), while another phase is pure solvent or dilute solution of complexes ('poor in material' phase). The phase separations observed in this work belong to the associative type and confirm the attractive interaction between polymers. The large 'flocs' belong to 'polymer-rich' phase and the transparent liquid part of the mixture is the dilute phase. The phase separation is characterized as 'liquid-liquid'.

At C < 0.1 mol/l (colloid (III)) in salt-free PEC solutions, white turbid suspensions are obtained, presenting a time evolution. The formed complexes are colloidal particles that scatter light. Phenomologically, the intensity of the scattered light is proportional to the polyelectrolyte complex number and size of the colloidal particles. PECs sediment slowly during two weeks after preparation and concentrate into a white powder precipitate, forming phase 'colloid (IV)'. The phase separation line is daubed and not clear. The colloidal particles exist at stoichiometric concentration ratio 1:1 as well as at non-stoichiometric concentration ratio.

In the concentration range 0.05 < C < 0.25 mol/l, a white bulk precipitate coexists with a viscous transparent liquid (biphasic region (II)). The phase separation is then characterized as 'solid-liquid'. This region is proposed to be an intermediate state between biphasic region (I) with well-defined macroscopic separation and colloid region (III, IV).

The interacting polyelectrolytes are strong and that leads to the formation of 'flocs' and 'precipitates', but not to a 'liquid coacervate' phase[209]. The latter rather results from interaction between weak PEs.
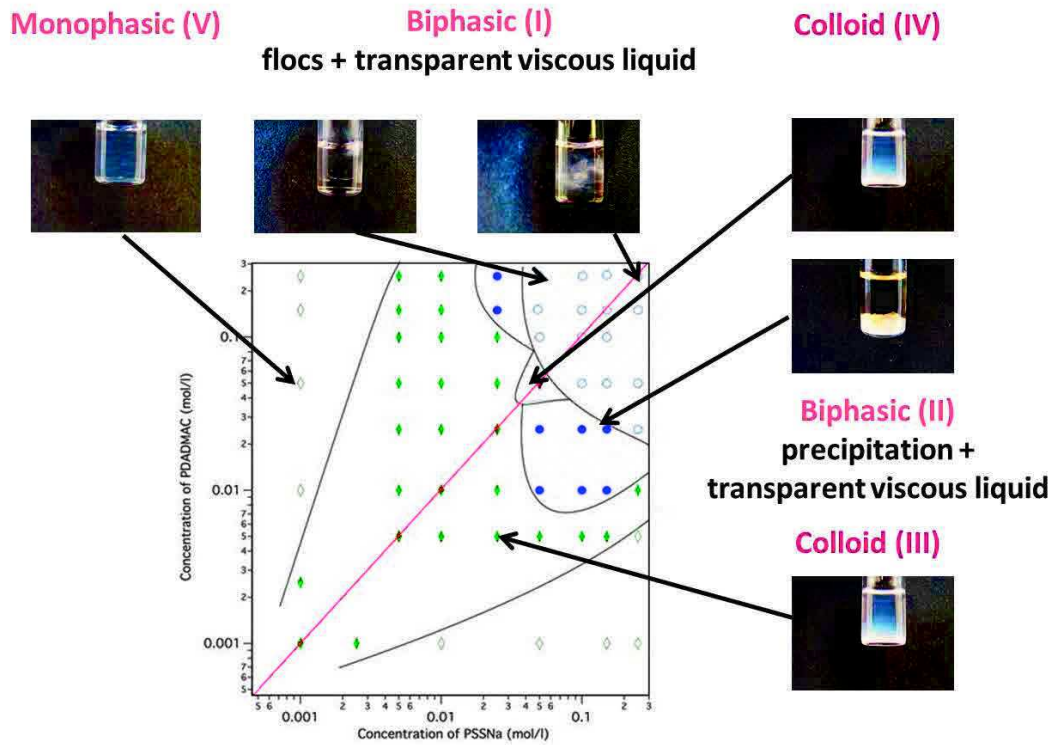
Figure 6.6. State diagram of salt-free PSSNa-PDADMAC aqueous solutions just after preparation:

○ Biphasic region (I): transparent viscous liquid / fluid flocs; ● Biphasic region (II), transparent viscous liquid / white precipitate; ◆ Homogeneous colloid (III); ◆ Colloid (IV) with unclear separation line or transparent / white precipitate; ◇ Monophasic region. Red line corresponds to the stoichiometric component ratio as well as the stoichiometric electrical charge ratio ([+]/[-]=1). The degrees of polymerization of the used polyelectrolytes are: N(PSSNa J301012) =1078 and N(PDADMAC 24)=830

(a)　　　　　　　　　　　　　　　　　(b)

(c)　　　　　　　　　　　　　　　　　(d)
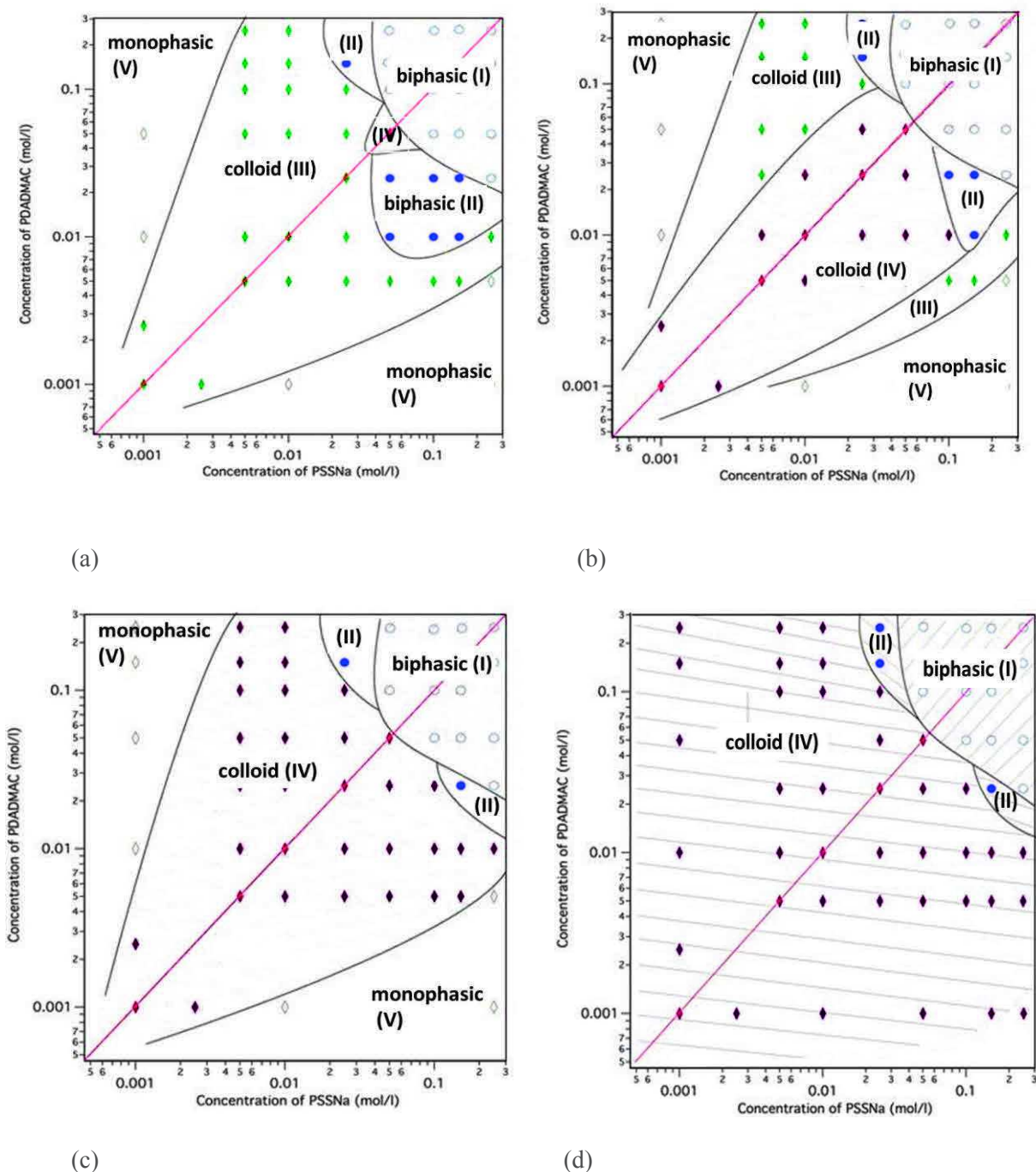
Figure 6.7. Time evolution of the state diagram for the salt-free PSSNa-PDADMAC aqueous solutions: (a) immediately after mixing (Figure 6.6); (b) two days after preparation; (c) three days after preparation; (d) two weeks after preparation. The degrees of polymerization of the used polyelectrolytes are: N(PSSNa J301012) =1100 and N(PDADMAC 24)=830

Time evolution of salt-free PSSNa-PDADMAC aqueous solutions

The time evolution of the state diagram for the salt-free PDADMAC-PSSNa PEC aqueous solutions is shown in Figure 6.7. Polyelectrolyte complexes remain to be stable for months with two exceptions. The first is the PEC sedimentation in the colloid domain (III→IV). The second is the transformation of the biphasic region (II), 'transparent viscous liquid' / 'white precipitate', into the colloid region (IV) mainly due to the condensation of the precipitate. We suppose that, at this concentration, the interaction between polyelectrolytes leads first to the formation of contacts between polymers and then to a further structure rearrangement, or a packing of the complexes. Further changes in the systems were not noticed. We assume that, in this experimental time scale of two weeks after the mixing of the stock PE solutions, the PEC systems reached their background states.

State diagram of PSSNa-PDADMAC 0.15 M NaCl aqueous solutions

The state diagrams, obtained for the complexes formed in the presence of an added salt (0.15 M NaCl), show few similar regions with respect to the salt-free case (Figure 6.8).

These regions are:

- The biphasic region (I) with macroscopic phase separation into 'flocs' (gel) and 'liquid' (viscous solution) parts;

- The biphasic region (II) with separation into solid 'precipitate' and 'liquid';

The colloid region (III) with slow sedimentation process. The time evolution is presented in Figure 6.9.
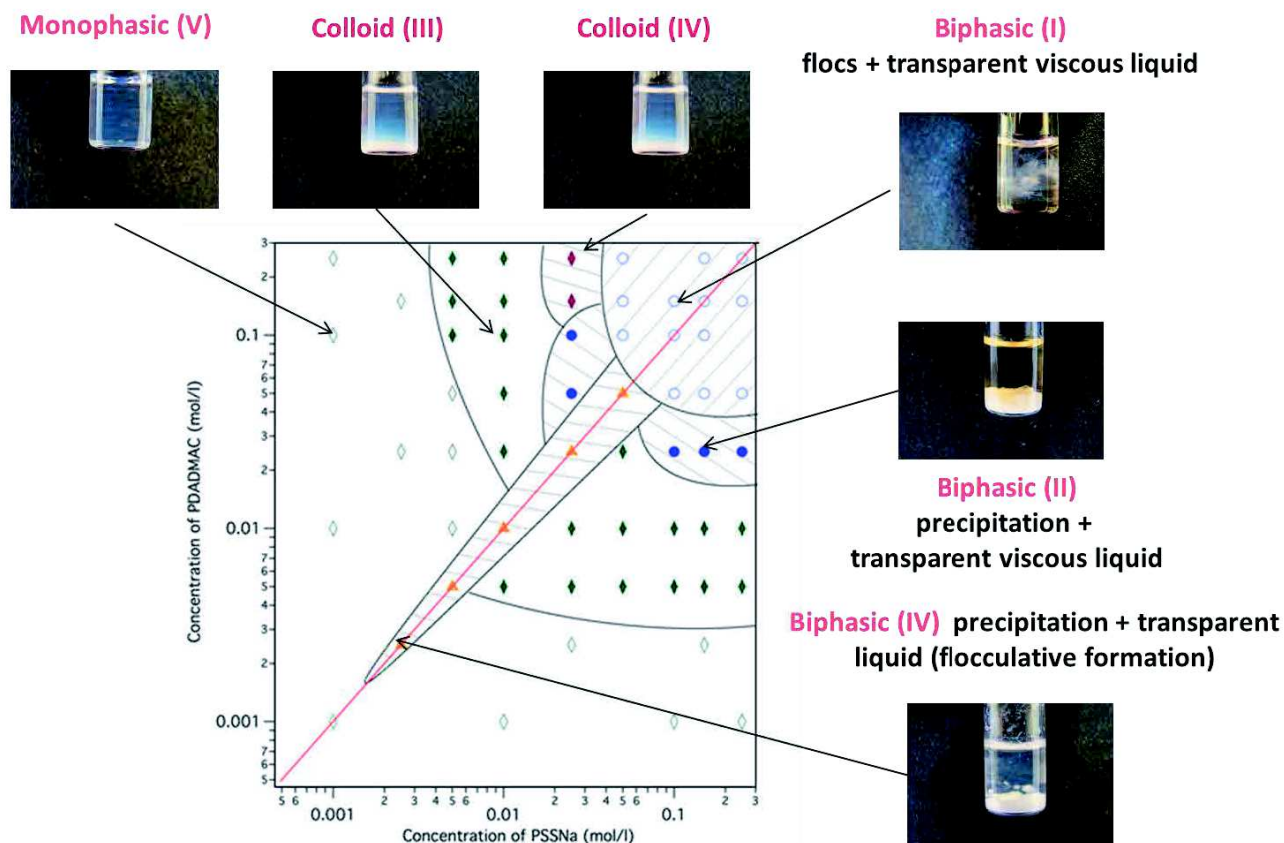
Figure 6.8. State diagram of the PSSNa-PDADMAC PEC aqueous solutions formed in the presence of 0.15 mol/l NaCl, just after their preparation: ○ Biphasic region (I): transparent viscous liquid / flocs; ● Biphasic region (II), transparent viscous liquid / white precipitation; ▲ Biphasic region with 'flocculative' phase separation, transparent liquid / white precipitate; ◆ Homogeneous colloid (III); ◆ Colloid (IV) with unclear separation line or transparent liquid/ white precipitate; ◇ Monophasic region. Red line corresponds to the stoichiometric component ratio, as well as the stoichiometric electrical charge ratio ([+]/[-]=1). The degrees of polymerization of the used polyelectrolytes are: N(PSSNa J301012) = 1078 and N(PDADMAC 26) = 740

Comparing to salt-free systems, the presence of an added salt yields to a decrease in PEC internal density for the domain of large aggregates ('flocs'/'transparent liquid') according to macroscopic observation. The presence of added salt changes the kinetics of the complex formation process as we can judge based on visual observations. for the region (I) in the absence of added salt, the phase separation occurs immediately. In the presence of added salt the large aggregates appear just the next day after the complex preparation.

Two new domains are also observed. At C < 0.005 mol/l, a stable monophasic region ('monophasic' (V)) of transparent liquid appears. This region of the polyelectrolyte phase diagram was only observed in salt environment at rather low concentration and by deviating from the charge stoichiometry line. The same effect has been already observed in the experimental study of PEC phase behaviour in solution[210].

Flocculative formation of complexes (domain VI) is observed exceptionally in the presence of added salt on the stoichiometric line in the concentration range 0.0025 < C < 0.5 mol/l. Large white aggregates are formed and sediment during the first three-four minutes after the mixing of the stock PE solutions. A supernatant stays transparent and clear. Normally, the stabilization of the particles in a solution results from the combination of ionic and steric contributions. The difference in the macromolecule lengths of used polyelectrolytes is slight. That should reduce or completely remove the steric part. The salt thus screens the repulsive interaction between ionic stabilization shells around PECs and induces the fast aggregation.

The formation of complexes between PDADMA and PSS was characterized as a two-step process based on the thermodynamic study. We suggest that the observed colloidal particles, scattering light, and having a high level of heterogeneity, are the result of the secondary process in the complexation between PSS and PDADMA macroions.
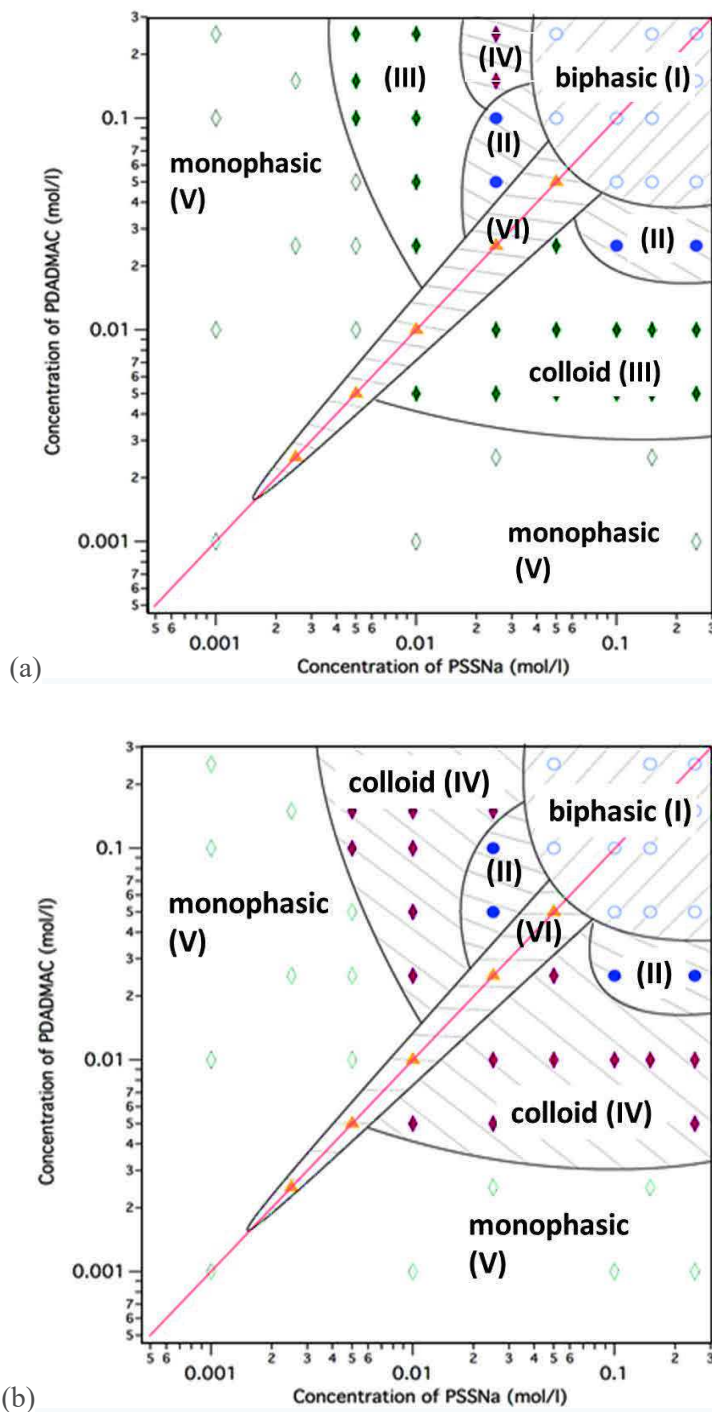
Figure 6.9. Time evolution of the state diagram for the PSSNa-PDADMAC PEC aqueous solutions formed in the presence of 0.15 mol/l NaCl : immediately after mixing (a) (Figure 6.8.); two weeks after preparation (b). The degrees of polymerization of the used polyelectrolytes are: N(PSSNa J301012) = 1078 and N(PDADMAC 26) = 740
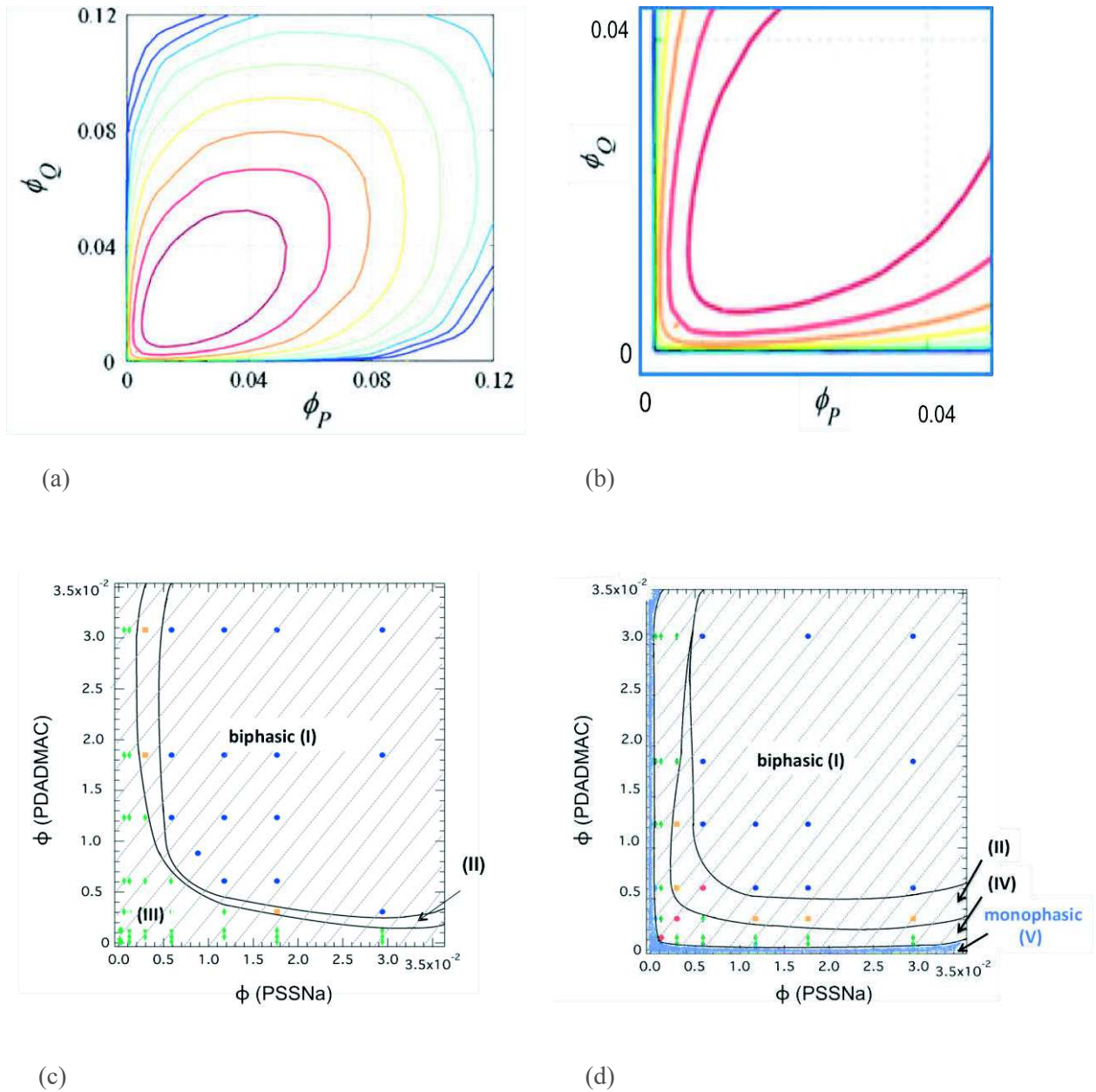
Comparison with the mean field theory

(a)

(b)

(c)

(d)

Figure 6.10. Comparison of the experimental state diagrams with the predicted phase diagrams obtained by simulation: (a) binodal transition lines for different salt concentrations in two-dimensional volume fraction representation based on the Overbeek and Voorn theory[52]; (b) zoomed region of the phase diagrams (a) in the volume fraction ranges that correspond to the experimental conditions; (c) experimental state diagram for the salt-free PDADMAC-PSSNa PEC aqueous solutions, in volume fraction scale; (d) experimental state diagram for the PDAMAC-PSSNa PEC aqueous solutions in the presence of 0.15 M NaCl, in volume fraction scale

The biphasic regions in the experimental diagrams are focused around, and symmetrical with respect to, the 1:1 concentration or volume fraction line. It is in a good agreement with the stoichiometric symmetry predicted by the simulation study based on mean field theory (Figure 6.10)[52]. The symmetry of the state diagrams in semidilute and concentrated regimes is also coherent with the value of the thermodynamic parameter n close to 1, obtained in the thermodynamic study of the complexes formed in the dilute regime (Chapter 6.1.2).

The focusing of the state diagrams around the concentration stoichiometry line, which is also the chemical charge stoichiometry line, suggests that the condensed counterions have been released completely. Otherwise, if the condensed CIs stay condensed, because of the Manning-Oosawa condensation phenomenon, it would be:

$[+]/[-] = f_{eff}^{PDADMA} * [PDADMAC]/f_{eff}^{PSS} * [PSSNa] =$

$= 0.66 * [PDADMAC]/0.36 * [PSSNa] = 1.8 * ([PDADMAC]/[PSSNa])$ (106),

and the charge stoichiometric line would deviate from the bisector for the factor 1.8 in the concentration representation (green line in Figure 6.11).
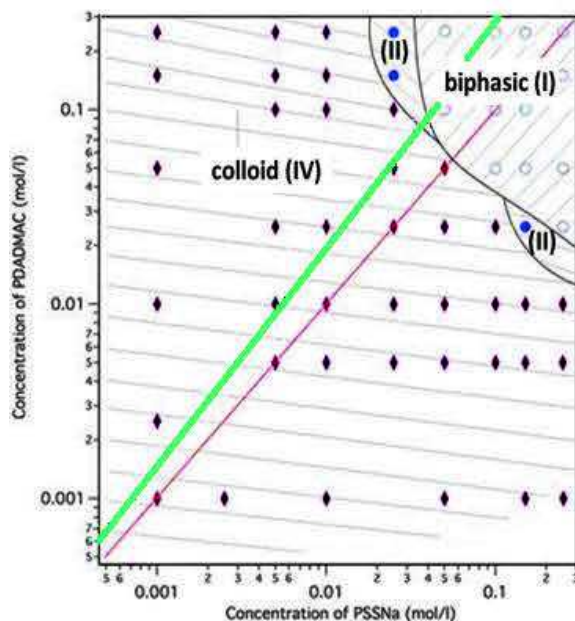
Figure 6.11. State diagram of the salt-free PSSNa-PDADMAC PEC aqueous solutions with the effective charge stoichiometric line estimated by accounting for the condensation of counterions

The slight difference in the symmetry of the state diagrams corresponding to the stoichiometric line could be explained by the difference in the intrinsic stiffness of the polyelectrolytes. The width

of biphasic domains depends on the presence of added salt, or ionic strength. That is in a good agreement with the theory[52,56,211].

The change in the ionic strength more affects the semidilute solution structure of PSSNa. Probably, the morphology variety of the formed polyelectrolyte complexes results from different polyanion average conformations. That is one of the questions that should be clarified by small-angle scattering analysis in the next chapter.

The complexation between PDADMA and PSS in the dilute regime (Chapter 6.1) was shown to be mainly driven by the entropy gain associated with the condensed counterions release and is therefore less affected by the presence of added salt. In the regions of the state diagrams corresponding to a high aggregation level, the electrostatic interaction is highly screened in the polycation solution. As in the dilute regime, the entropy gain associated with the counterions release is suggested to be favorable in the PEC formation process.

6.2.1.2. Increase in the polyanion intrinsic stiffness via the replacement of PSSNa by PαMSSNa

To tackle the problem of the intrinsic persistence length effect on the phase behaviour of the polyelectrolyte complexes, we replaced PSS polyanions by the PαMSS ones of close polymerization degree (N(PSSNa) =1100 and N(PαMSSNa)=1130). According to this replacement, we slightly increase the intrinsic stiffness (from 10 to 25 Å) of polyanions without changing its interactions with polycations.

The state diagrams of PαMSSNa-PDADMAC PEC aqueous solutions will be presented in the same order than for state diagrams of PSSNa-PDADMAC PEC aqueous solutions in Chapter 6.2.1.1. First, we will report and discuss the state diagram of PE mixtures achieved in the absence of added salt and its evolution in time. Second, the effect of the presence of an added salt will be shown. All state diagrams (Figure 6.12. - 6.15) are plotted in the coordinates of component concentrations. When the mixture of PαMSSNa-PDADMAC is prepared, the next type of systems can be distinguished following the visual examination.

State diagram of salt-free PαMSSNa-PDADMAC aqueous solutions
At the right top corner and C > 0.05 mol/l (biphasic region (I)), PαMSSNa-PDADMAC systems show associative phase separations similarly to PSSNa-PDADMAC systems. Large jellified aggregates 'flocs' ('rich in polymer material' phase) in solution coexist with a transparent viscous liquid ('poor in polymer material' phase). The well-defined meniscus separates both mixture parts.

Reducing the concentration range along the stoichiometric line till C between 0.005 mol/l and 0.05 mol/l colloid region (III) is obtained, which strongly scatters light. At the left bottom corner at C lower than 0.005 mol/l, the interaction between oppositely charged polyelectrolyte brings the system to a monophasic region (monophasic (V)). In the narrow range of non-stoichiometric ratios with a concentration of each component close to 0.05 mol/l and 0.15 mol/l, the biphasic region (II) with solid 'precipitate' and viscous 'transparent liquid' is observed. This region (II) is supposed to be intermediate between the biphasic (I) with well-defined macroscopic phase separation and turbid coacervate colloid systems ((III) and (IV)).

The state diagram of PEC solutions evolving over 2 weeks after preparation is shown in Figure 6.13 (a) – (c). The 'biphasic' (I) region stayed stable during all the observation time. The strongly scattering light white 'suspensions' (III) turn into two regions depending on concentration: 'biphasic' (II) and 'colloid' (IV). The more concentrated systems transit to white solid 'precipitate' that coexists with viscous supernatant ('biphasic' (II)). The less concentrated mixtures turn progressively in white powder sediment and clear or almost clear fluid supernatant ('colloid' (IV)).

The state diagrams of PαMSSNa-PDADMAC lost their symmetry with respect to the line of charge stoichiometry (Figure 6.13 (c)) that was in the case of PSSNa-PDADMAC (Figure 6.13 (d)). Specifically, a monophasic region is observed by considering poly(sodium α-methyl styrene sulfonate) as polyanions even in the salt-free case, which was not noticed for PSS-PDADMA. The concentration range of PαMSSNa, in which the macroscopic phase separation takes place, is narrowly comparing to poly(sodium styrene sulfonate). The monophasic region can be the signature of two cases: either the interaction between polyelectrolytes is prevented, either the formed complexes are soluble. Both situations can result from the same reason. The increase in the polyanion intrinsic stiffness and the presence of the side methyl groups on the polyanion backbone decrease the internal degrees of freedom of PαMSSNa. and reduce its interaction with the oppositely charged poly(diallyldimethylammonium) chloride. Even though the complexes are formed, the structural complication lowers the number of interacting units of the oppositely charged polyelectrolytes and lowers the compactness of the complexes. That could stabilize PECs electrostatically and sterically.
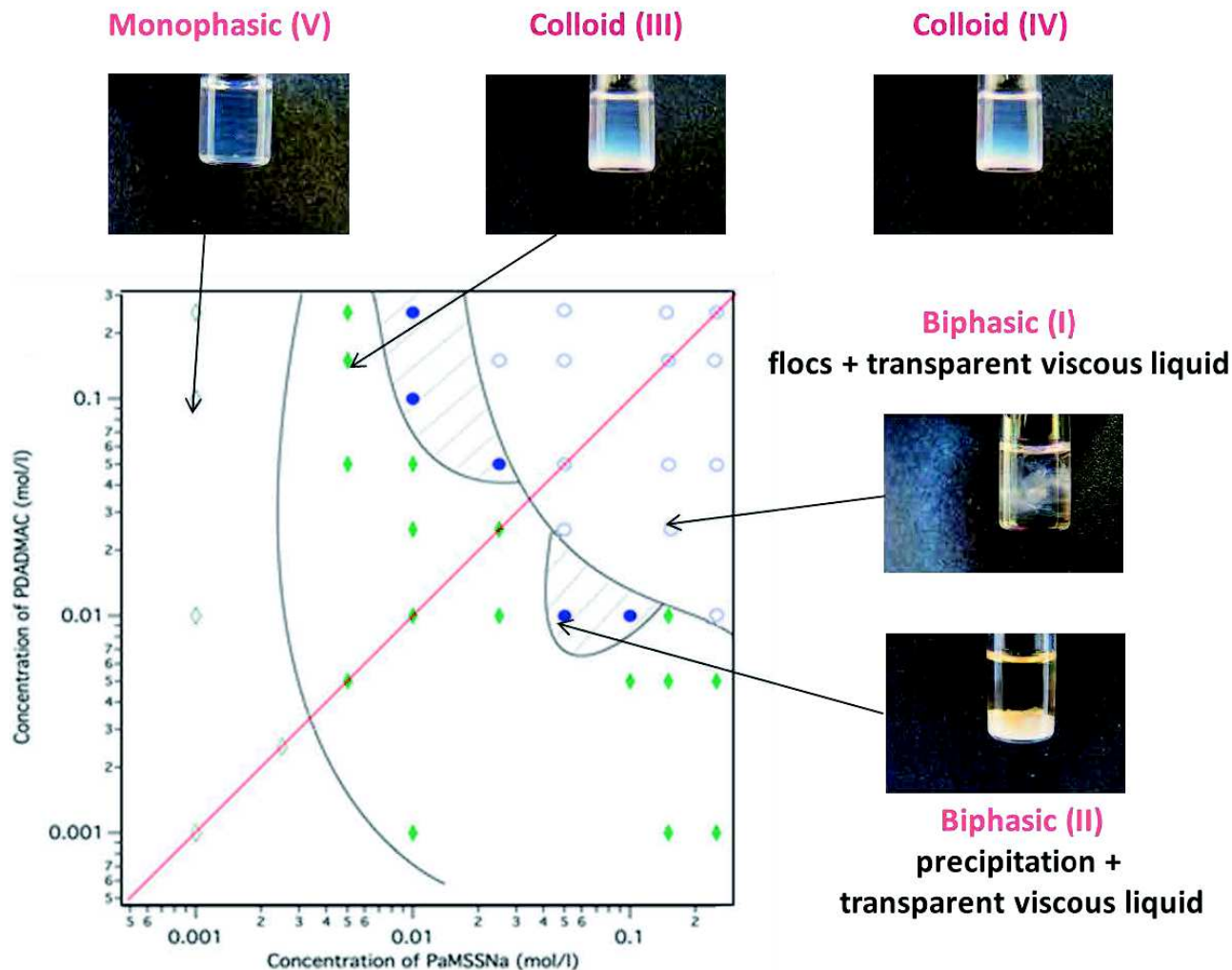
Figure 6.12. State diagram of the salt-free PαMSSNa-PDADMAC PEC aqueous solutions at the day of preparation: ○ Biphasic region (I): transparent viscous liquid / flocs; ● Biphasic region (II), transparent viscous liquid / white precipitate; ◆ Homogeneous colloid (III); ◆ Colloid (IV) with unclear separation line or transparent / white precipitate; ◇ Monophasic region. The red line corresponds to the stoichiometric component ratio as well as the stoichiometric electrical charge ratio ([+]/[-]=1). The degrees of polymerization of the used polyelectrolytes are: N(PαMSSNa J301012) = 1130 and N(PDADMAC 22) = 540

(a)

(b)

(c)

(d)
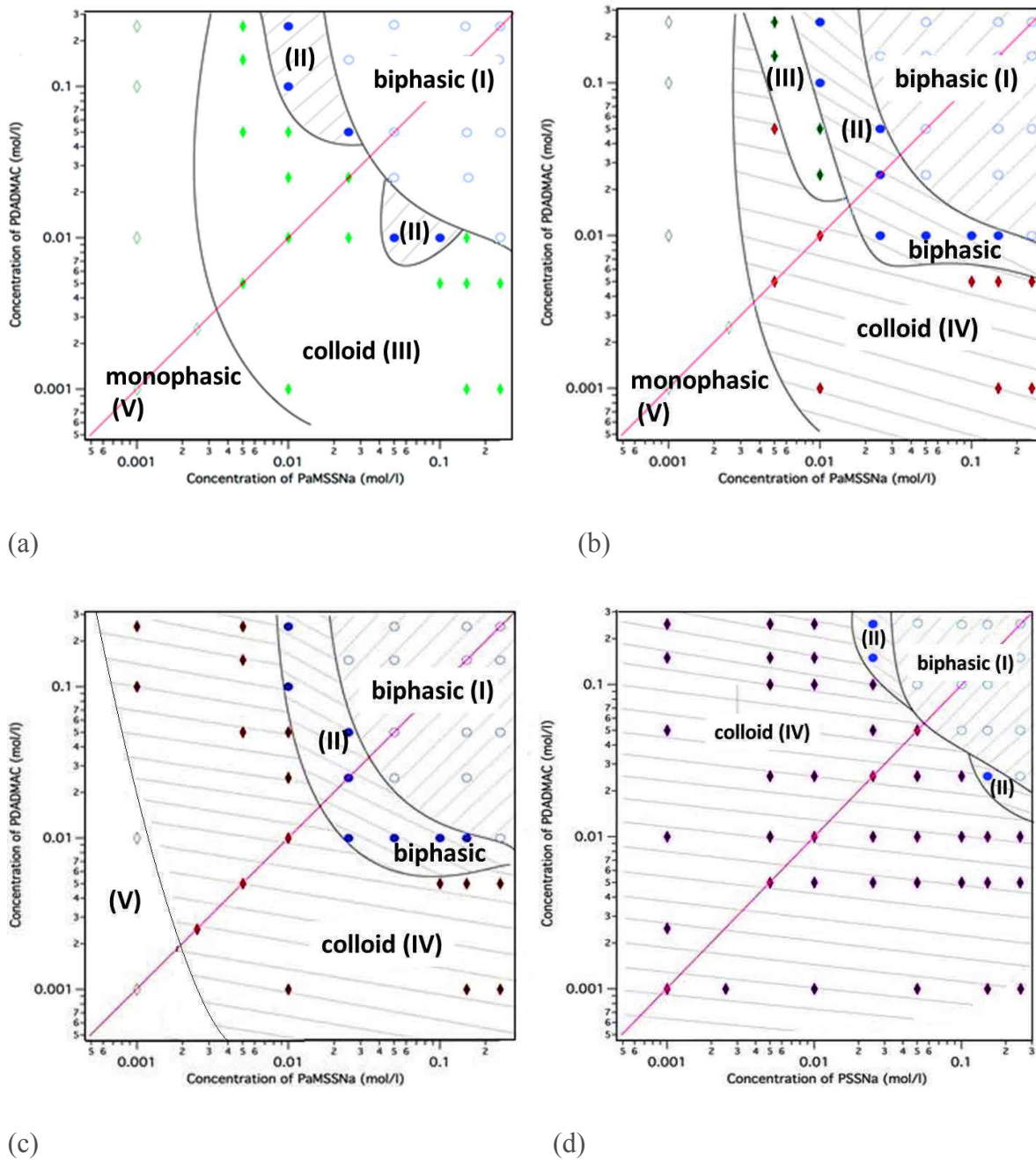
Figure 6.13. Time evolution in time of the state diagram for the salt-free PαMSS-PDADMAC PEC aqueous solutions: (a) immediately after mixing; (b) two days after preparation; (c) two weeks after preparation. For comparison, the state diagram of PSSNa-PDADMAC systems two weeks after preparation is also shown (d)

State diagram of PαMSSNa-PDADMAC 0.15 M NaCl aqueous solutions

The presence of an added salt during the PαMSS-PDADMA PEC formation reduces the biphasic region comparing to salt-free systems. That is in a good agreement with the theory and correlates with the conclusion drawn from the PSSNa-PDADMAC systems. The state diagrams of the PαMSS-PDADMA mixtures at the day of preparation are shown in Figure 6.14. The formed complexes have slow evolution in time that is described in Figure 6.15.

The increase in the ionic strength does not play a role in the symmetry of the state diagrams. The focusing of the state diagram along the stoichiometric line only depends on the used polyelectrolyte properties. The flocculation formation of the polyelectrolyte complexes observed in the PSSNa-PDADMAC systems, resulting from the matching the polyanion chains, is no longer observed with PαMSS (Figure 6.15 (b) and Figure 6.15 (c)).

As a concluding remark, we can highlight that the increase in the polyanion intrinsic stiffness leads to two main effects: the lost of the symmetry with respect to the charge stoichiometry line of the state diagram and the disappearance of the 'flocculative' domain. Both results from the reduction of the matching between polycation and polyanion monomer units.
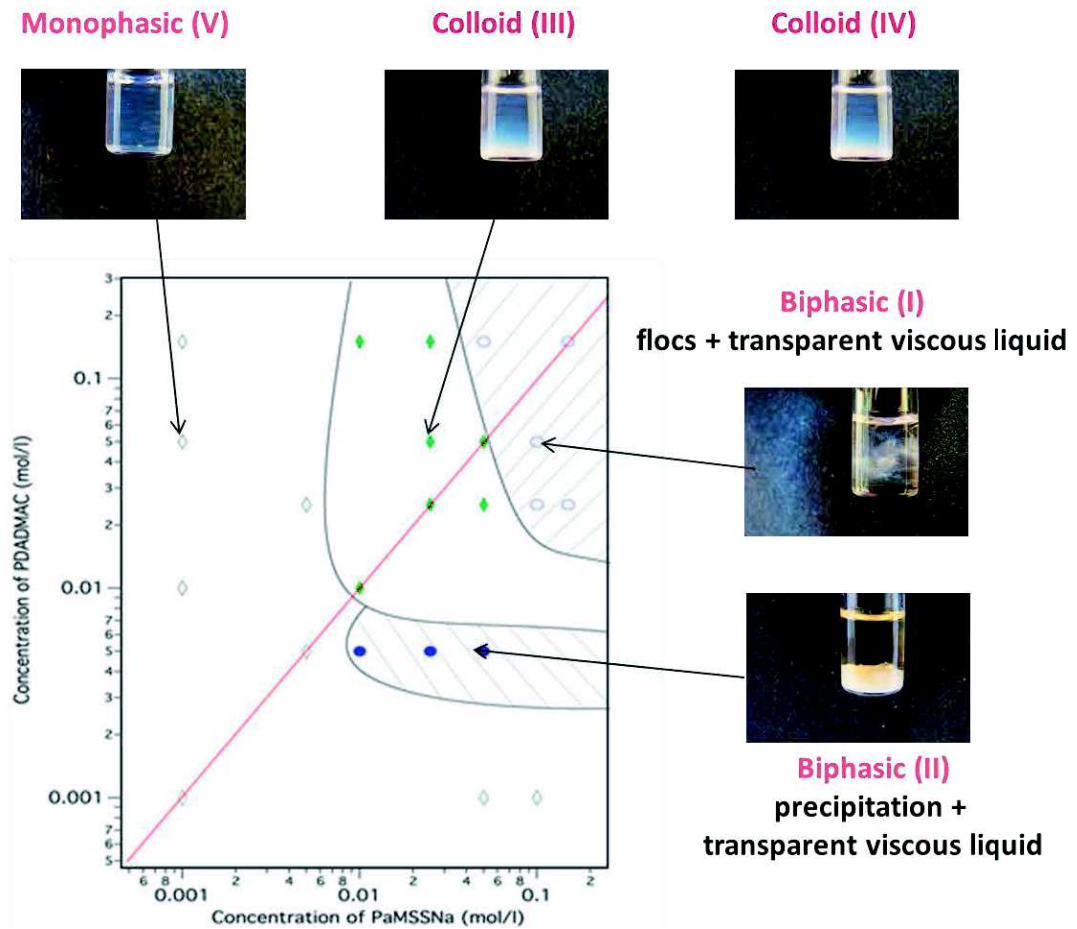
Figure 6.14. State diagram of PαMSS-PDADMAC PEC solutions formed in the presence of 0.15 mol/l NaCl immediately after mixing: ○ Biphasic region (I): transparent viscous liquid / flocs;

● Biphasic region (II), transparent viscous liquid / white precipitate; ◆ Homogeneous colloid (III); ◆ Colloid (IV) with unclear separation line or transparent / white precipitate; ◇ Monophasic region. The red line corresponds to the stoichiometric component ratio as well as stoichiometric charge ratio ([+]/[-]=1). The degrees of polymerization of the used polyelectrolytes are: N(PαMSSNa J301012) = 1130 and N(PDADMAC 22) = 540
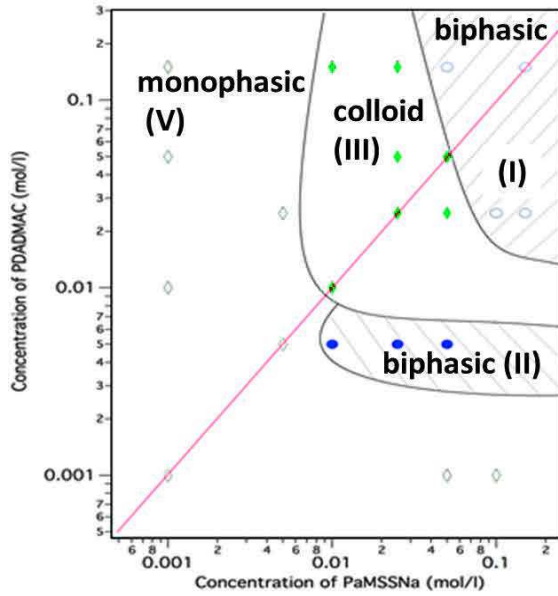
(a)
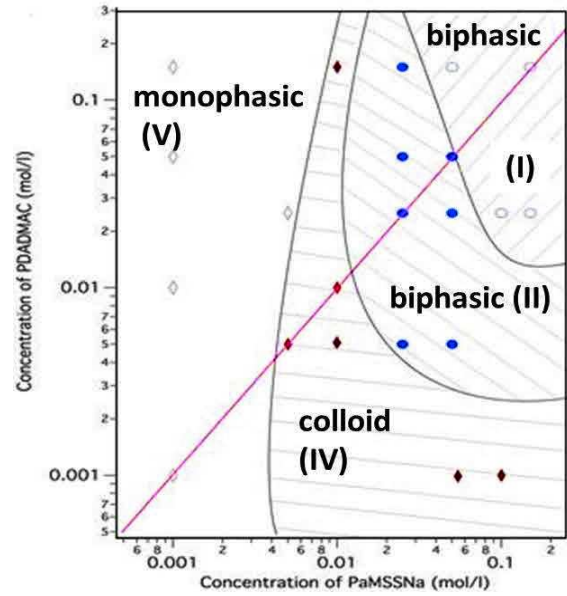
(b)
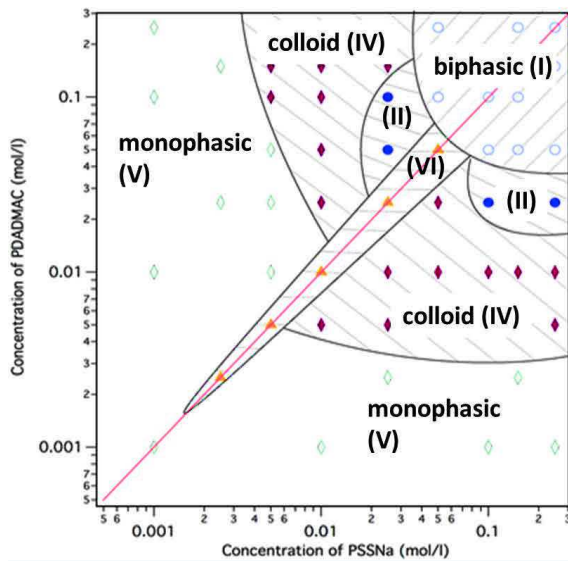
(c)

Figure 6.15. Time evolution of the state diagram for the PαMSSNa-PDADMAC PEC aqueous solutions
formed in the presence of 0.15 M NaCl: (a) immediately after mixing; (b) two weeks after preparation; (c)
PSSNa-PDADMAC in 0.15 M NaCl, two weeks after preparation (for comparison)

6.2.2. Complexation between oppositely charged polyelectrolytes: analogy with a gelation process

The complexation between polyelectrolytes of opposite charge can be described as a gelation process, provided we are concerned with semidilute or concentrated PE or PEC solutions. This analogy is reliable for distinct interpolyelectrolyte complexes and, specifically, for both PE couples investigated in this thesis: PSS-PDADMA and HA-PDADMA. It is rather universal. However, there are differences between the related complexation processes that are related to the difference in the intrinsic stiffness of both polyanions. We aim at showing and explaining these differences. Thus, before to present the X-ray and neutron scattering data obtained from PSS-PDADMA PEC aqueous solutions, we wish to describe this analogy with a gelation process that is useful for the analysis of PEC scattering functions. This analogy will be the basis for the understanding of our scattering results.

6.2.2.1. Description of PEC structure as an interpenetrating polyelectrolyte network with immersed heterogeneities

We can imagine the process of polyelectrolyte complex formation at high concentration as a gelation process. A two-dimensional representation of a semidilute or concentrated polymer solution is proposed in Figure 6.16. It corresponds to a close packing, or melt, of 'bobs' of size ξ (concentration blobs). Here it is just a representation of the binary system formed by the semidilute or concentrated aqueous solution of a polyelectrolyte. The related macroions are random walks on this lattice, but they are not shown. Such a network is also the reaction bath for the complexation with another polyelectrolyte of opposite charge. Then, the complexation process can be viewed as a gelation one, in which interchain bridges result from the complexes between parts of both polyanions and polycations. Moreover, the attractive electrostatic interaction is enough strong to ensure long junction lifetimes. In this way, the macroions of opposite charge play the role of gelling agents that allow forming interchain bridges, which contribute to the elasticity. Obviously, they could be represented as additional random walks that are linked to the previous ones via simple dots, or Tie points, on the lattice in Figure 6.16 (a). However, they could also be represented as parts of the previous random walks in Figure 6.16 (b), when the bridges involve large chemical sequences of both macroions. Since they are extended, they are slowly introduced and randomly dispersed after a certain time in the network associated with the semidilute or concentrated aqueous solution of the first polyelectrolyte. However, we note that the mesh sizes of the networks associated with the final PEC aqueous solutions are distinct, all initial PE concentrations being equal. Moreover, in the situation of the second sketch (Figure 6.16 (b)), the electrical charges are expected much more neutralized through the complexation

process than in the first one, even though the junctions are sufficiently numerous (of the order of the total number of chains, or macroions, from the percolation theory, i.e. c/N) to allow the transition towards a gel state in the situation of the first sketch (Figure 6.16.(a)). Finally, an increase in the intrinsic stiffness of one macroion should favor bridges involving large chemical sequences, and therefore the situation of the second sketch (Figure 6.16 (b)).

Like crosslinks in gels, the junctions resulting from the complexation with macroions of opposite charge tend to form large clusters, or heterogeneities, which are superimposed to the network describing the initial semidilute or concentrated polyelectrolyte solution[212–215]. These heterogeneities correspond to the large region of space where the crosslink density is higher than in others. They can be statistical (fractal or branched structure), or even with a specific geometry defined by an interface due to some further aggregation of crosslinks. They are however polydisperse in shape and size, and lead to some turbidity in most of the gels because of their large size distribution. Gels are thus heterogeneous materials. However, there are numerous possible gel states that are reached through different sol-gel transitions, related to distinct connection routes for the gelling units[215].

The monomers of both polyanions and polycations attached together through the attractive electrostatic interaction tend to set up clusters in the solvent. These clusters can be tenuous, even though they are expected to be widely branched and even partially interpenetrated. But, they can also be shrunk since water could become a bad solvent for the complexes. In this case, heterogeneities would tend to a further local shrinkage of the primary net, as shown in Figure 6.17.

When the clusters tend to precipitate, there is a competition between gelation and precipitation, which is well known[11]. It leads to some macroscopic phase demixing in between sol and gel phases. Such a process is similarly observed in semidilute aqueous solutions of complexes formed by polyelectrolyte of opposite charge.

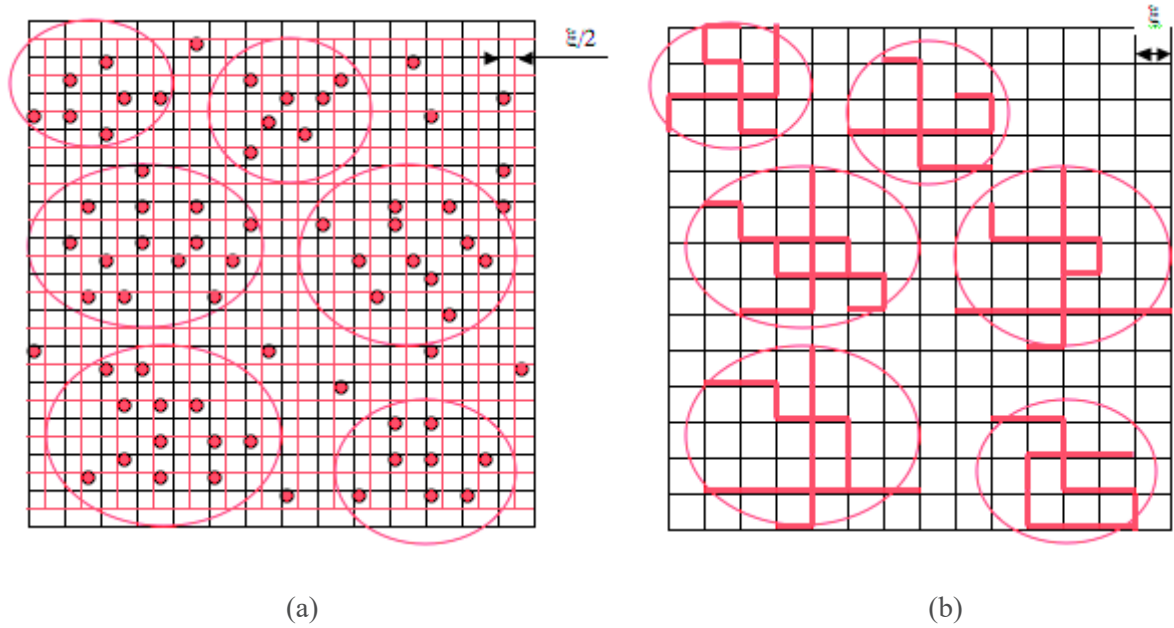(a)   (b)

Figure 6.16. Two-dimensional representations of a semidilute or concentrated polyelectrolyte solutions. The macroions correspond to random walks on these lattices of mesh size $\xi/2$ ορ ξ. The interchain crosslinks via the complexation between macroions of opposite charge are depicted by red dots (a) or red highlighted parts (b) of the lattices. Actually, they are randomly placed on the lattice and form clusters of higher crosslink density than the lattice

(a)   (b)
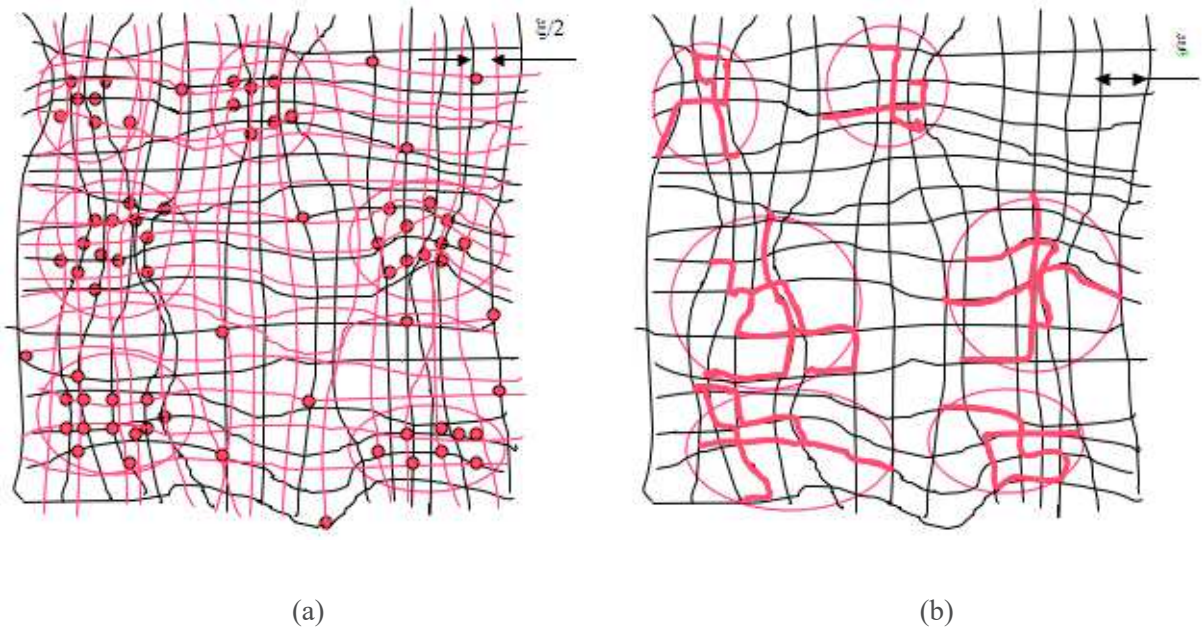
Figure 6.17. Same representation that those of Figures 6.16 (a) and 6.16 (b), but the clusters of electrostatic junctions shrink locally the primary networks

At this stage, we can emphasize that any randomly crosslinked network exhibits heterogeneities that are revealed through the swelling process, as shown in Figure 6.18. Figure 6.18 (a) refers to a preparation state in which the random distribution of crosslinks leads to the formation of zones rich in tie points, indicated in grey. Figure 6.18 (b) shows a sketch of large-scale statistical heterogeneities

114

then appear by overswelling the preparation state (excess of solvent). The grey zones tend to swell less than the average of the gel. For simplicity, any deformation of crosslink clusters is neglected in this figure.
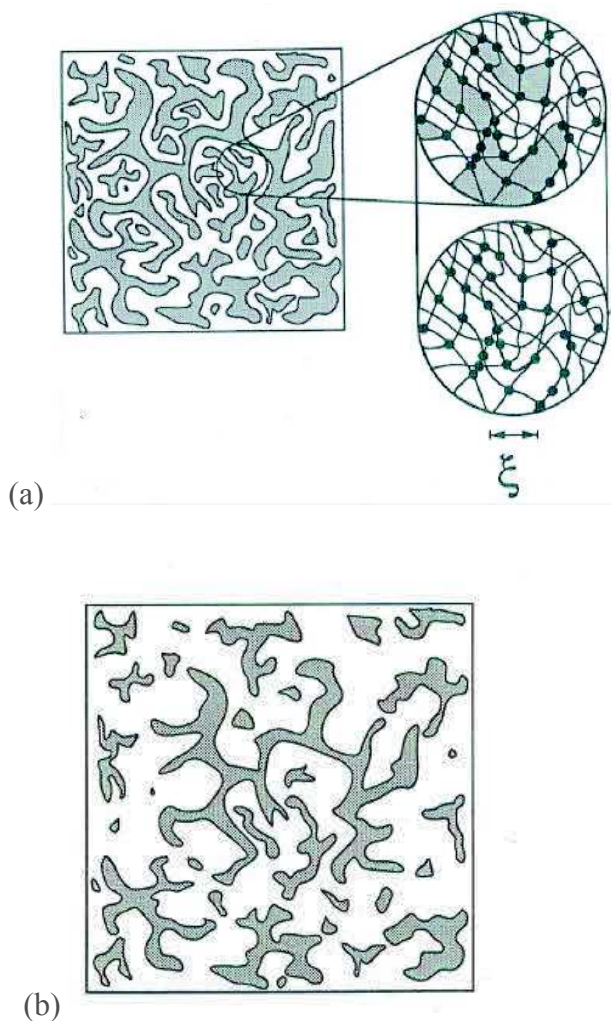

(a)

(b)

Figure 6.18. Schematic representation of a randomly crosslinked semidilute polymer solution, from reference[216]

6.2.2.2. Expected scattering patterns

The scattered intensity by such structures is very different from that of a semidilute or concentrated polymer, as well as polyelectrolyte, solution.

The scattering function $S(q)$ of a semidilute solution of neutral polymers exhibits two main regimes[11,215]:

1. For qξ < 1 $$S(q) \cong \frac{c^2\xi}{q^2+\xi^{-2}}$$ (107)

In this q-range, S(q) appears almost flat in log-log representation (close packing of blobs of size ξ). However, a forward scattering can also be observed as the concentration is increased. It has not yet received a satisfactory explanation and is presumably related to the way of preparing solutions.

2. For qξ > 1 $$S(q) = cg_1(q) \rightarrow \frac{1}{q^{1/\nu}}$$ (108)

S(q) is then reduced to the chain form factor, which is proportional to $q^{-1/\nu}$ beyond the Guinier range (qR_G <1), provided the local chain conformation is neglected; ν being the excluded volume exponent.

For free-salt semidilute solutions of polyelectrolytes, there are differences mainly associated with the long-range electrostatic repulsion in between monomers. Thus, the scattering function S(q) displays a broad maximum, the well-known polyelectrolyte peak, at q*=2π/ξ, resulting from a correlation hole of electrostatic character within the isotropic model[8,10,18]. Beyond this maximum, S(q) tends slowly to the form factor of macroions, which could be described either by a Gaussian statistics (mean field theory) or the wormlike chain model with some cross section term. At small q values, S(q) is related to the osmotic compressibility $\chi_T = \frac{1}{c} * \left(\frac{\partial c}{\partial \pi}\right)_T$:

$$S(q \rightarrow 0) = kTc\frac{\partial c}{\partial \pi}$$ (109)

It allows, in principle, to measure a number of free counterions, or the effective charge f_{eff} of macroions, since Π=kTf_{eff}c (ideal gas of free counterions), provided there is no contribution from the ubiquitous excess intensity at very q values.

In the gel of polyelectrolyte complexes, the presence of crosslink heterogeneities, characterized by concentration fluctuations of large amplitude, leads to an excess forward scattering. So, additional regimes at low q-values have to be considered:

-At very low q-values, i.e. in the Guinier range of the polydisperse clusters of crosslinks ($q < \frac{1}{R_G^2(H)>_Z}$), the scattering function is:

$$S(q) = <N_H>_W \left(1 - \frac{q^2 <R_G^2(H)>_Z}{3}\right)$$ (110)

$< N_H >_W$ and $< R_G^2(H) >_Z$ are the weight average degree of polymerization and the z-average square radius of gyration of the heterogeneities, respectively;

-For $\frac{1}{\langle R_Z^2(H) \rangle_z} < q < \frac{1}{\xi}$, S(q) will mainly describe the average internal structure of the crosslink heterogeneities. For fractal heterogeneities, it should scale as:

$$S(q) \sim q^{-D_f} \tag{111}$$

in analogy to the intermediate scattering vector range of the scattering from polydisperse randomly branched macromolecules[213,216]. D_f is then an effective fractal dimension accounting for the polydispersity of the heterogeneities (D_f = 8/5). For more dense clusters, or heterogeneities with a rather well defined geometry, the existence of interfaces could lead to the characteristic Porod's law:

$$S(q) \sim q^{-4} \tag{112}$$

However, such a characteristic scattering behaviour could also be observed in the intermediate scattering vector range of branched macromolecules (Gaussian stars for example[217]).

In principle, the scattering of the primary network, or semidilute solution, should also be considered. However, in this q-range, the variation of the scattered intensity from this interstitial medium is much slower than the one of the heterogeneities, except in the crossover region ($q \approx \frac{1}{\xi}$) where the Lorentzian law (Eq. (107)) can still be observed for neutral polymer solutions or polyelectrolyte solutions in the presence of added salt. For salt-free polyelectrolyte solutions, the characteristic "polyelectrolyte" peak of the scattering function could then be observed.

-Finally, in the q-range $q > \frac{1}{\xi}$, the chain conformation inside the concentration blobs of the primary semidilute solution is then explored. That is therefore the same scattering behaviour than the one previously described for the semidilute solutions.

To show the influence of heterogeneities on the scattering functions of semidilute or concentrated polyelectrolyte solutions, we have used a rather crude model in which the heterogeneities are described by monodisperse Gaussian star macromolecules of functionality f and arm degree of polymerization N_a. The polyelectrolyte solution is described by the mean field theory[24,27].

Neglecting intermolecular correlations, the scattering function of the clusters, $S_{cluster}(q)$, can be reduced to the form factor of Gaussian stars[217]:

$$\frac{S_{cluster}(q)}{c_{cluster}} = Ng_1(q) = N\frac{2}{x^2}\left[\frac{(f-3)}{2}+x-(f-2)\exp(-x)+\frac{f-1}{2}\exp(-2x)\right] \tag{113}$$

where
$$x = (qR_G(a))^2 = \frac{q^2 N_a b^2}{6}$$

$c_{cluster}$ is the concentration; f, the number of arms of the star; N, the number of statistical length of the star, so $N = fN_a$ with N_a denoting the one of each arm.

Neglecting the condensed counterions, the scattering function of the semidilute solution of polyelectrolytes, $S(q)$, can be written as:

$$\frac{c}{S(q)} = \frac{1}{g_0} + cv + w^2 c^2 + \frac{4l_B f}{k_D^2 + q^2} \tag{114}$$

with $g_0(q) = N[x - 1 + \exp(-x)]$ $\qquad x = (qR_G)^2 = \frac{q^2 Nb^2}{6}$ $\tag{115}$

and $\kappa^2 = 4\pi l_B(c + 2n)$ $\tag{116}$

Here, c is the polyelectrolyte concentration; n, that of an added monovalent salt as NaCl; l_B, the Bjerrum length equals to 7.14 Å in H₂O at a room temperature; $g_0(q)$, the form factor of an ideal chain of N statistical elements of length b equals, i.e. the well-known Debye function; κ^{-1}, the Debye screening length. Obviously, N does not play a role, as we are concerned with the semidilute or concentrated regime.

From these two scattering functions, we are able to propose some approximate shapes for the scattering patterns of the gels resulting from the complexation of two polyelectrolytes of opposite charge in the semidilute or concentrated regime. Indeed, we can use the simple relationship, neglecting any cross term:

$$\frac{S_{Gel(q)}}{c} = g(q,c) = \Phi\frac{S_{cluster(q)}}{c_{cluster}} + (1-\Phi)\frac{S(q,c)}{c}, \tag{117}$$

where Φ and (1-Φ) are the respective volume fractions of both media.

Some resulting scattering patterns are shown in Figure 6.19, for a rather small amount of heterogeneities (5% of the total structure of the gel). Two cases are considered according to the absence or the presence of added salt (low or high ionic strength). The latter tends to correspond to a random crosslinking of semidilute solutions of neutral polymers. In this Figure 6.19, the heterogeneities are large but also tenuous since rather weakly branched (N_a = 10000; f = 5). Then,

beyond q=0.001 Å^{-1}, two regimes are only observed: the intermediate q-range of the clusters corresponding to a rather slow decreasing of the scattered intensity; the asymptotic q-range that is associated with chain form factor. The Guinier range associated with the clusters is shifted towards low q values, i.e. in the q-range q < 0.001 Å^{-1}. We note that, in salt-free aqueous solutions, the "polyelectrolyte peak" associated with the scattering from the primary network remains observable.

In Figure 6.20, by considering denser or more branched clusters described as Gaussian star macromolecules with a higher functionality ($N_a = 10000; f = 100$), it is shown that the intermediate q-range associated with the internal structure of clusters can also display two distinct scattering behaviours. A q^{-4} power law is specifically observed, which only results from the Fourier transformation of the square average internal density of the Gaussian stars, and which cannot be ascribed to the existence of any interface (it is not the characteristic Porod's law)[169]. Finally, in Figure 6.20, the case of tenuous and rather small clusters is considered ($N_a = 100; f = 5$. The Guinier range of the clusters is then quite apparent in the q-range q < 0.01 Å^{-1}, leading to a rather small increase in the scattered intensity.

According to this analogy between a gelation process and the complexation of two polyelectrolytes of opposite charge, we expect two main q-ranges for the scattering patterns of polyelectrolyte complexes in semidilute or concentrated aqueous solutions. At small q-values, the scattered intensity is related to the heterogeneities resulting from the electrostatic junctions between polyelectrolytes. If these heterogeneities are small, their Guinier range (allowing a measurement of $<R_G^2(H)>_Z$, as well as their internal structure, could be investigated. If they are large, only their internal structure could be studied. Above we described the heterogeneities through a model of star-like branched polymers. However, other shapes and therefore other form factors could also be considered. According to the situation of the previous sketch 2 (Figure 6.16 (b), large sequences of polyanion and polycation are in contact through successive electrostatic links or junctions along the chemical sequences, forming neutral objects (as the ladder structure of PEC proposed in Chapter 2 in agreement with simulations). Obviously, such primary complexes could lead to large cylindrical particles via further aggregation. At high q-values (q > 1/ξ), the scattered intensity is related to the network formed by the macroions. The mesh size of this network could then be determined from the lowest q values of this regime, especially from the position q* of the polyelectrolyte peak that is still observable for the salt-free aqueous solutions. At larger q values, the form factor of the macroions (Small angle neutron scattering, SANS, as well as small angle X-ray scattering, SAXS, provided all

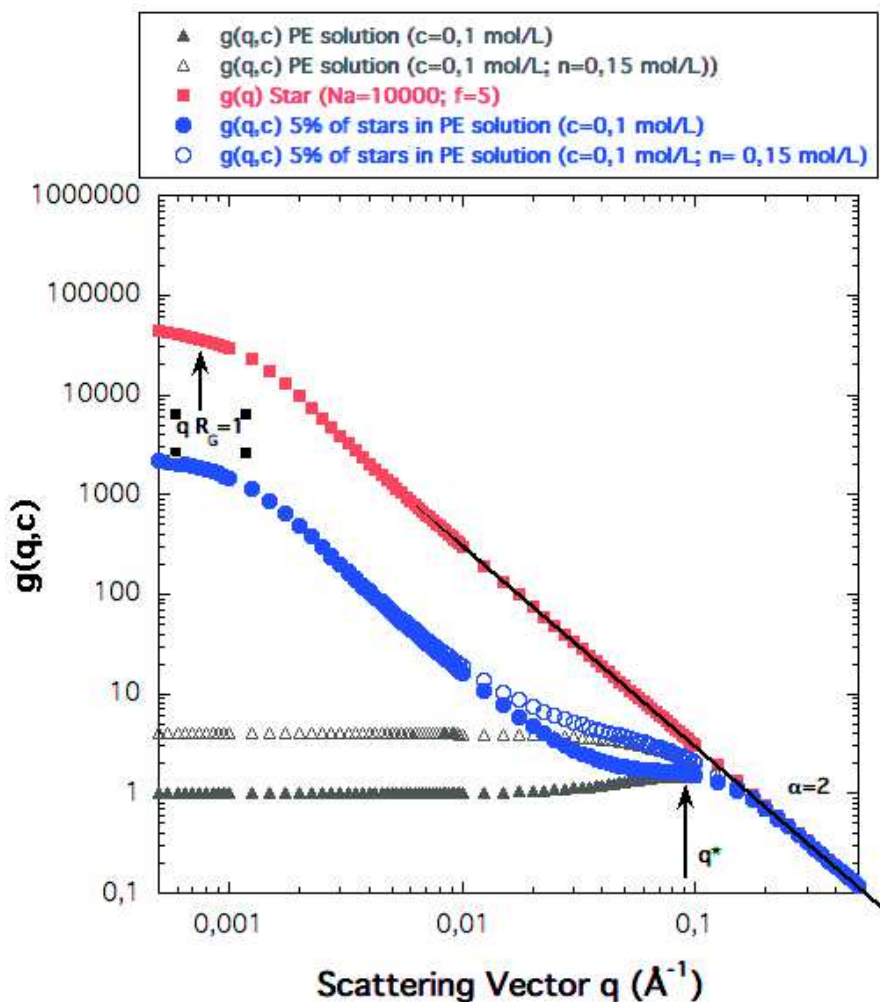counterions are free) and that of the condensed counterions (through SAXS) could also be investigated.

Figure 6.19. Scattering patterns of gels described as heterogeneities (Gaussian stars as clusters) immersed in a polyelectrolyte (PE) semidilute solution (a sea of blobs according to the Random Phase Approximation (RPA) and concentration c=0.1 mol/l). Two cases are considered for the polyelectrolyte network: absence (n=0) and presence (n=0.15 mol/l) of added monovalent salt
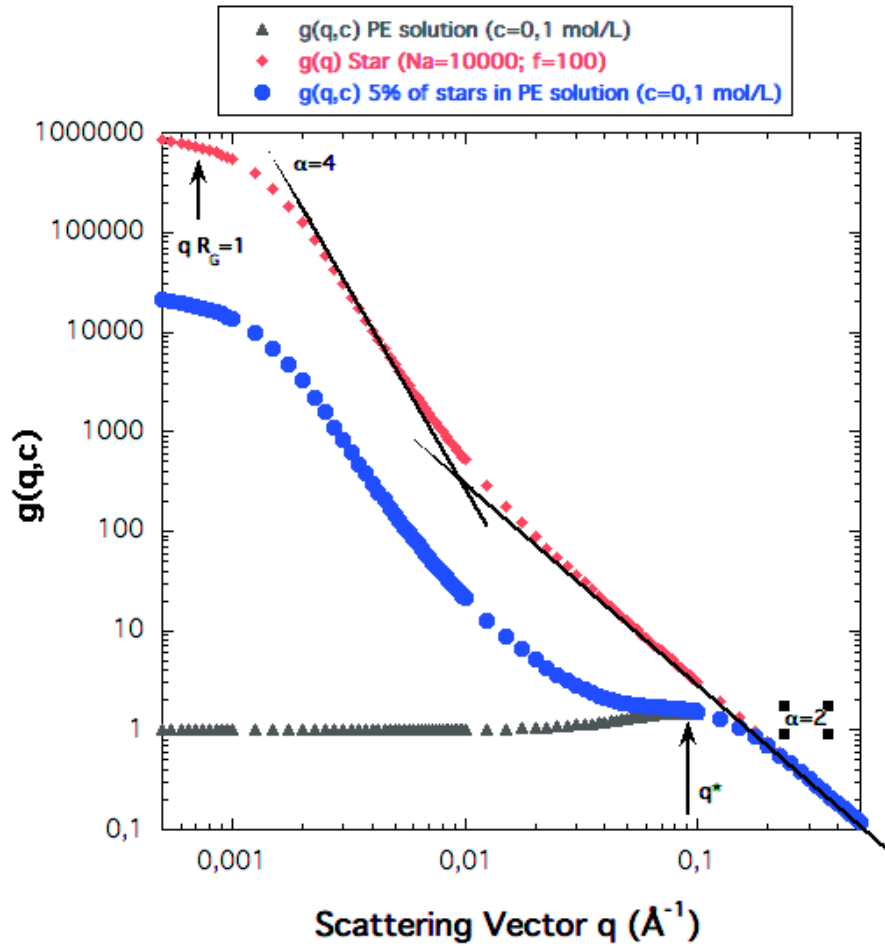
Figure 6.20. Scattering pattern of a gel described as heterogeneities immersed in a salt-free semidilute solution of polyelectrolytes (PE). This time, the heterogeneities are highly branched macromolecules described by Gaussian stars of high functionality; the salt-free PE aqueous solution corresponds to a concentration c=0.1 mol/l and is described through the RPA
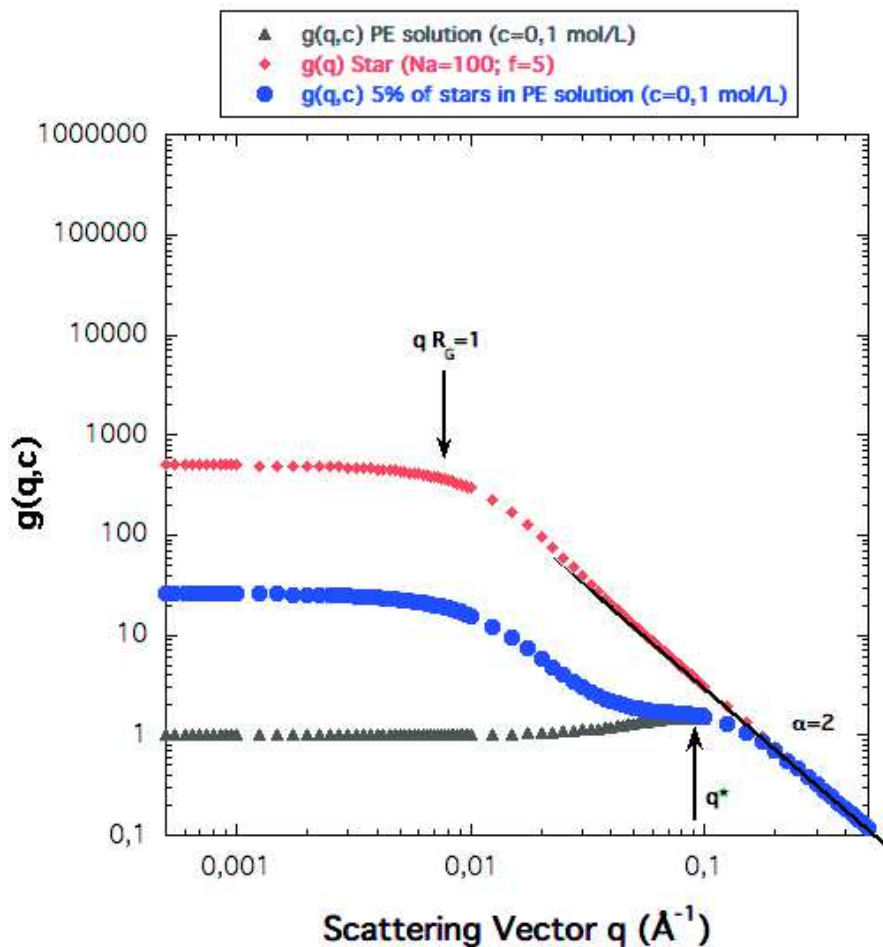
Figure 6.21. Scattering pattern of a gel described as heterogeneities immersed in a salt-free semidilute solution of polyelectrolytes (PE). The heterogeneities are small macromolecules described by Gaussian stars of small functionality; the salt-free PE aqueous solution corresponds to a concentration c=0.1 mol/l and is described through the RPA

6.2.3. Difficulty for determining the compositions of complex biphasic systems

We suggest that along the charge stoichiometric line all polyelectrolytes participate in the complex formation and there are not free PDADMA or PSS macroions in the aqueous solutions. This assumption is supported by DLS measurements. We did not find the appropriate way for determining the concentration of each polyelectrolyte in distinct phases. This question stays as an unsolved issue of our project. The compositions of each phase can be studied following some methods. The most frequently used for measuring component concentrations in ternary systems (two polymers and a

solvent) are the spectroscopic techniques: UV-visible[218–220], FTIR[220–223], fluorescence[224–226], circular dichroism[227–229]. They are based on the change in an analytical signal (position and shape of an adsorption maximum or angle of an optical rotation) according to the structural change resulting from the complex formation. The possibility to make direct measurements without previous sample alteration is an important advantage of these spectroscopic methods. However, they require that one or both components possess a chemical group with a characteristic signal. These techniques have been extensively applied in protein-polyelectrolyte and polysaccharide-polyelectrolyte complex investigations. For systems based on synthetic polyelectrolytes, they become less applicable, except via the use of fluorescence labelling. The determination of the bimodal compositions of complexes between modified poly(acrylic acid) of four different chain length by anhydrous methylpyrrolidone (MP) and triethylamine (TEA) and poly(N,N'-dimethylaminoethyl methacrylate) (PDMAEMA) of similar chain length was done by Spruijt and co-workers[230]. Potentiometry (pH-titration) is an alternative method for weak polyeletrolytes when fluorescence labelling is not possible. The pK of the weak dissociative group is sensitive to the local electrostatic environment and, hence, any conformation changes related to the binding with other polyelectrolytes[231]. The ratio between PSS and PDADMA in the complexes was measured by ^{1}H NMR spectroscopy after repeated dissolution completely dried complexes in 2.5 M KBr[207]. The spectra of the mixtures were compared with the spectra of PSS and PDADMAC in 2.5 M KBr under the same conditions. We tried to apply the same procedure for PSS/PDADMA complexes formed in our laboratory. The 2.5 M NaCl solution was added to the particular PECs formed in the absence and presence of salt to shift the reaction to go forwards. None of the tested PEC systems is returned to the previous state of a simple mixture of two polyelectrolyte solutions. Two reasons can be evoked. First, in our case the stronger bonding is formed at lower ionic strength comparing to the mentioned example. Second, sodium and chloride ions have lower desalting properties comparing to potassium and bromide. The difference in the thermodynamics of the diffusion process into complexes for different anions was shown by Ghostine[232]. The test of adding big excess of NaCl confirms the irreversibility of the obtained complexes.

The probable solution of the composition determination issue could be the investigation of the complexes with solid NMR, but it is the subject for a distinct study.

6.2.4. Total experimental scattering functions of the complexes: experimental results

We have established the state diagrams of the polyelectrolyte complexes formed by the addition of the aqueous solutions of poly(diallyldimethylammonium chloride) into poly(sodium styrene sulfonate) ones, in semidilute and concentrated regimes. The next and the most important step in this study is the experimental investigation of the average structure of the formed complexes. The description of the polyelectrolyte complex architecture is indeed a key to understand deeper already done experiments.

The average structure of the formed PSS-PDADMA complexes is complicated and depends on their location in the state diagrams. The colloid form of PECs has been studied in numerous works contrarily to the region associated with a high aggregation level. The lack of research in the high concentration range is explained by operative difficulties such as high viscosity, large heterogeneity, and low reproducibility. But the understanding of the polyelectrolyte complex structure in a dense phase plays a prominent role in many practical cases. Thus, we focused on the biphasic region with large gelled aggregates 'flocs' and viscous 'transparent liquid' as phases. The complexes formed in this region result from the interaction between the concentrated PDADMAC aqueous solutions and the semidilute PSSNa ones. This domain is located in the same concentration ranges for salt-free and brine systems (Figure 6.22).
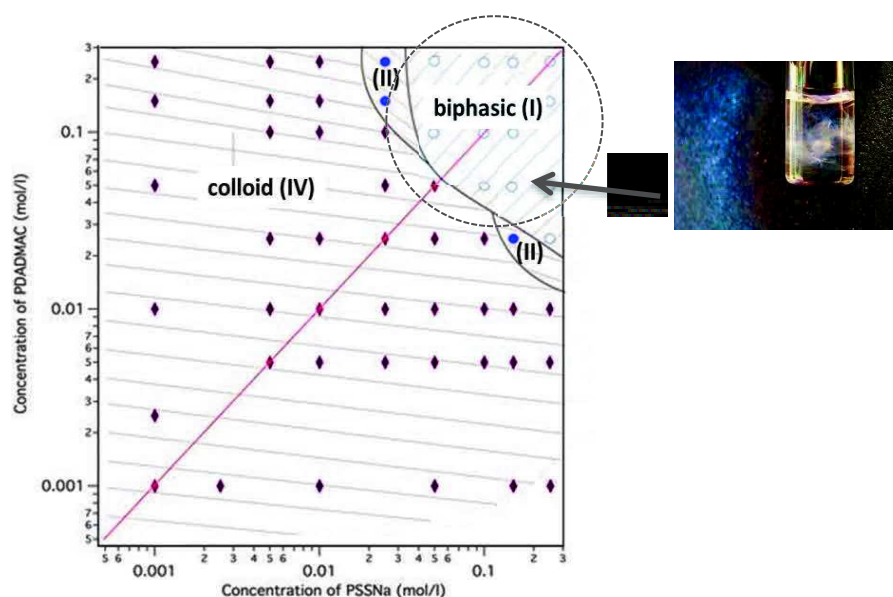

Figure 6.22. Location of the region with high level of heterogeneities (biphasic (I)) in the state diagram of free-salt PSS –PDADMA PEC aqueous solutions

6.2.4.1. Complexes formed at stoichiometric charge ratios

At high concentration, the two phases of the biphasic irreversible complexes PSSNa-PDADMAC (domain (I) in Figure 6.6 and 6.8) were investigated separately. The separation was done without preliminary centrifugation. The preparation of the samples for small-angle X-ray and neutron scattering investigations was challenging due to the high viscosity of these complexes. Especially, it was essential for the gelling 'flocs' phase where we sometimes used scissors to cut a part of PECs for analysis.

SAXS measurements

The SAXS patterns obtained from biphasic five salt-free and five brine systems following the charge stoichiometric line are presented in Figures 6.23 - 6.24. We remind that the 'flocs' phase is the turbid gel phase with a high level of heterogeneities. The 'transparent liquid' is a viscous solution.

The obtained SAXS results confirmed the proposed model of the complex structure as an interpenetrating polyelectrolyte network with immersed heterogeneities described in Chapter 6.2.2. As we expected for salt-free aqueous solutions, the SAXS patterns display a maximum that reminds us of the classical polyelectrolyte peak (Figure 6.23). This maximum is observed in "flocs" phases as well as the corresponding liquid ones. However, this maximum disappears, or at least strongly reduced depending on concentration, as we are concerned with aqueous complex solutions prepared in the presence of an added salt (0.15 M NaCl; Figure 6.24). When it disappears, we find again the scattering behaviour of semidilute solutions of neutral polymers (a sort of plateau associated with the classical Lorentzian behaviour). Beyond this maximum, the SAXS curves display a q^{-4} scattering behaviour that is related to the counterions condensed onto both macroions (specifically the condensed Na^+ counterions onto PSS macroions). This q^{-4} decreasing cannot be ascribed to the existence of any interface since it is no longer observed in SANS patterns (see later Figure 6.30). It is only related to the form factor of the condensed counterions which is that of an empty cylinder as previously shown in Philippe Lorchat's thesis[30]. It is the sharp decrease observed just before the classical oscillations of the form factor of the empty cylinder at high q values. Thus, the scattering patterns for $q > 0.03$ Å^{-1} are strongly related to the existence of a temporary network of polyelectrolytes or, more precisely, an interpenetrated network of polyelectrolytes. That is exactly what is expected from the analogy with a gelation process for the interpolyelectrolyte complexation. Moreover, at lower q values ($q < 0.03^{-1}$), classical upturns associated with large-scale heterogeneities are observed. They result from the existence of electrostatic junctions between macroions of opposite charge.

In summary, as expected by the analogy previously described (Chapter 6.2.2.), we observe the signal of an interpolyelectrolyte network at high q-values and that of heterogeneities related to electrostatic associations between macroions at low q-values.
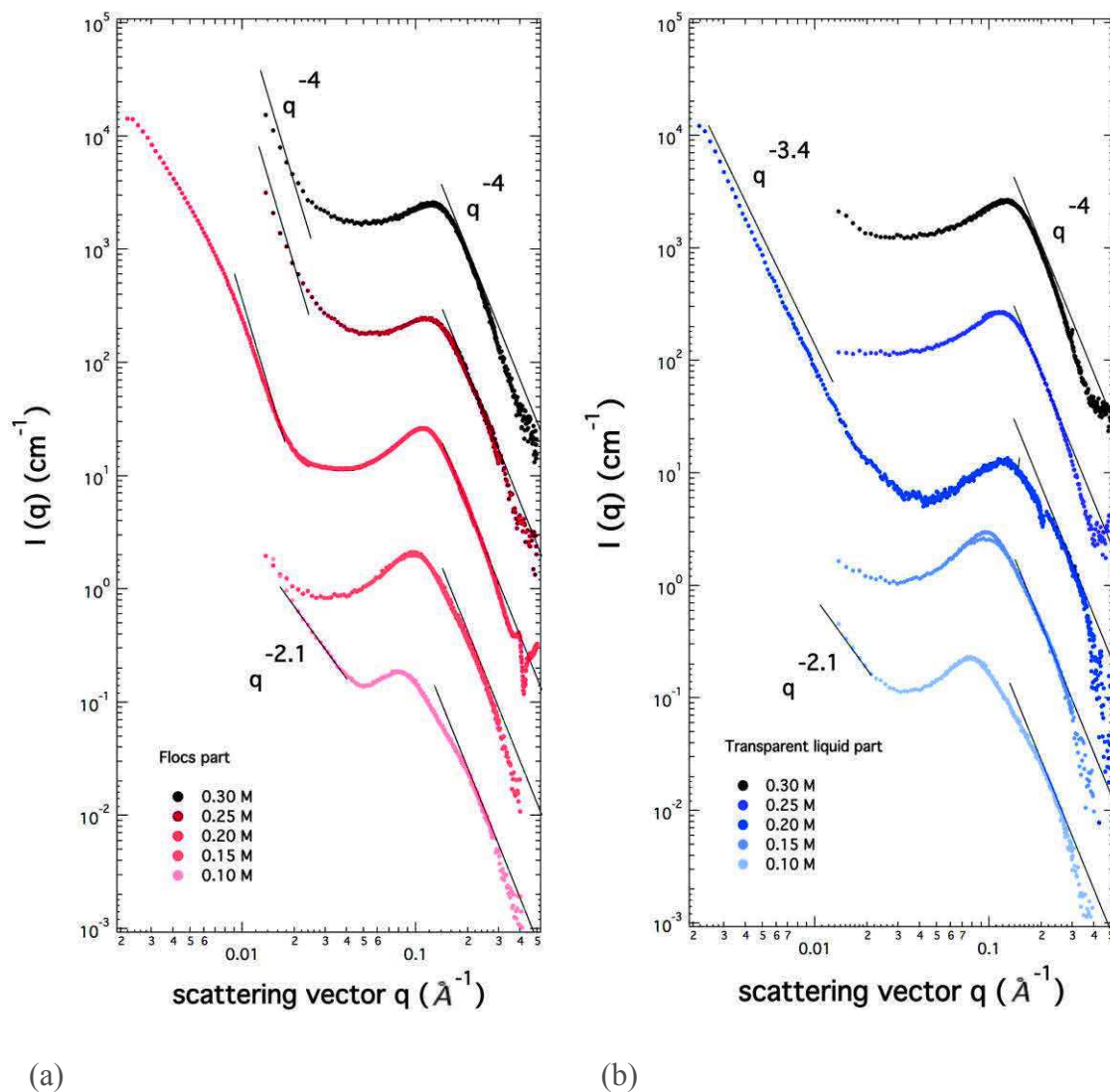

(a)   (b)

Figure 6.23. SAXS measurements of complexes formed through mixing salt-free solutions of PSSNa and PDADMAC in stoichiometric proportions: 'flocs' (a) and 'transparent liquid' (b) parts. The concentrations correspond to the expected concentrations that are calculated as the initial concentration of the polyelectrolyte solutions divided by two. The obtained SAXS curves are shifted from each other using a multiplication by a factor 10 to avoid any superimposition
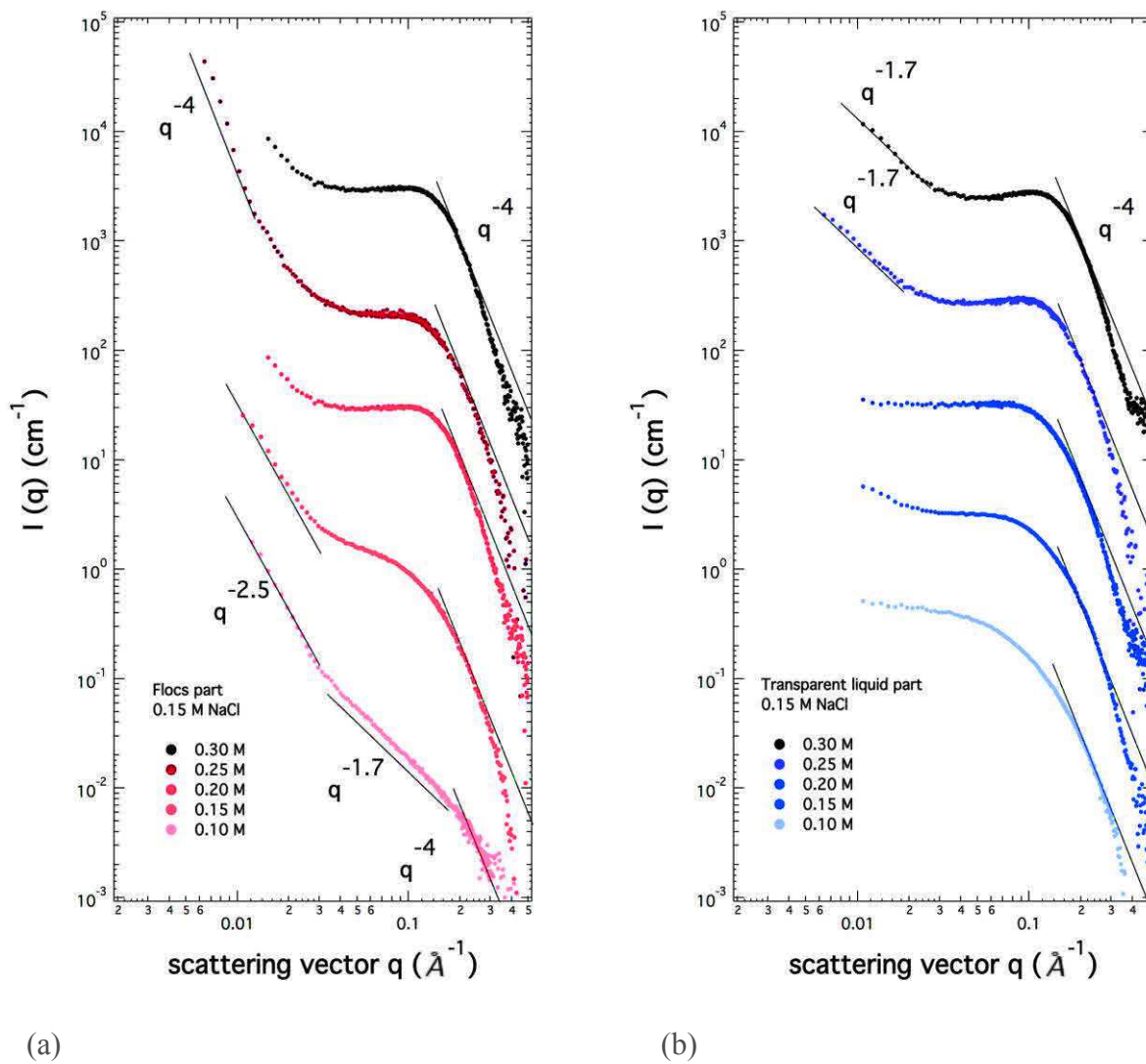
(a)

(b)

Figure 6.24. SAXS measurements of complexes formed by mixing 0.15 M NaCl aqueous solutions in stoichiometric proportions: 'flocs' (a) and 'transparent liquid' part (b). The concentrations correspond to the expected concentrations that are calculated as the initial concentration of the polyelectrolyte solutions divided by two. The obtained SAXS curves are shifted from each other using a multiplication by a factor 10 to avoid any superimposition

(a)   (b)
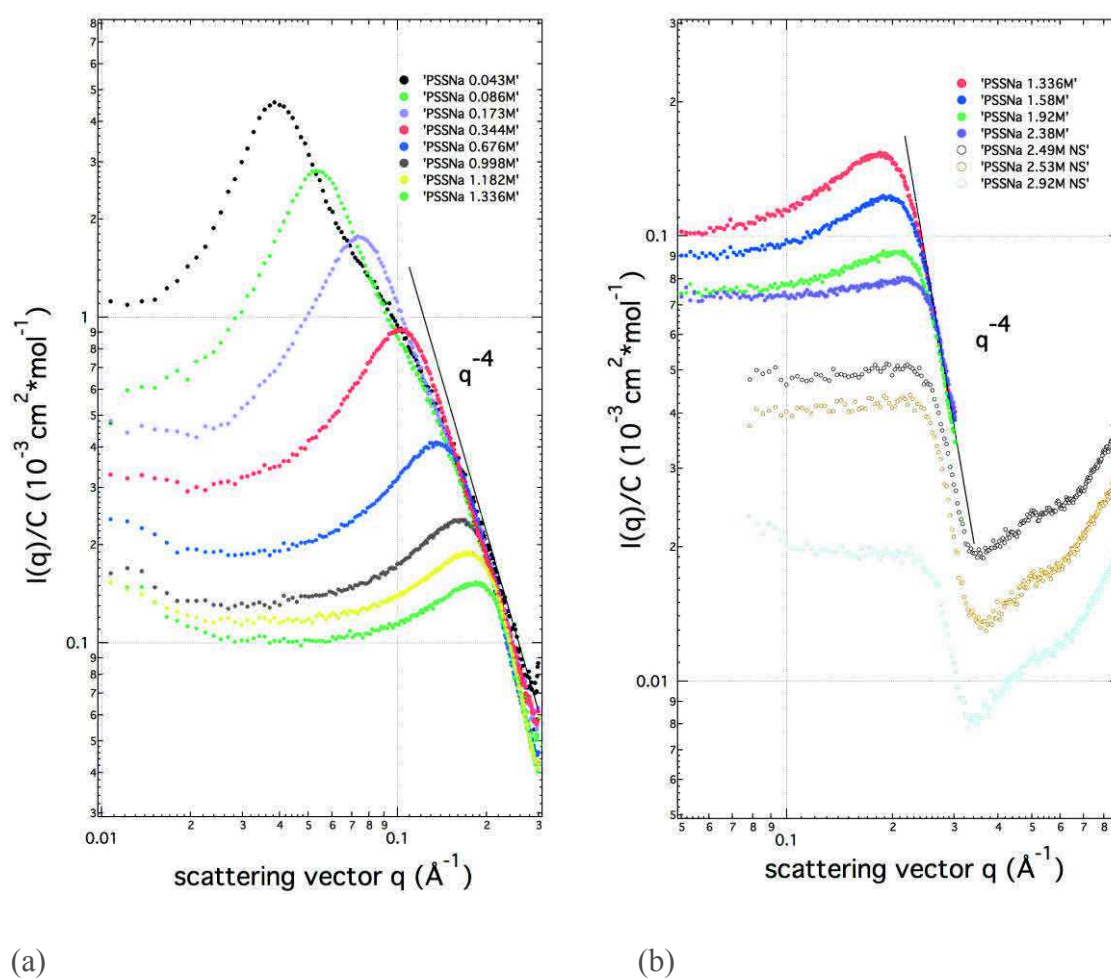
Figure 6.25. SAXS scattering curves from PSSNa semidilute (a) and concentrated (b) solutions. A q^{-4} scattering law is observed at high q-values, beyond the maximum. These scattering curves are kindly given by P. Lorchat[30]
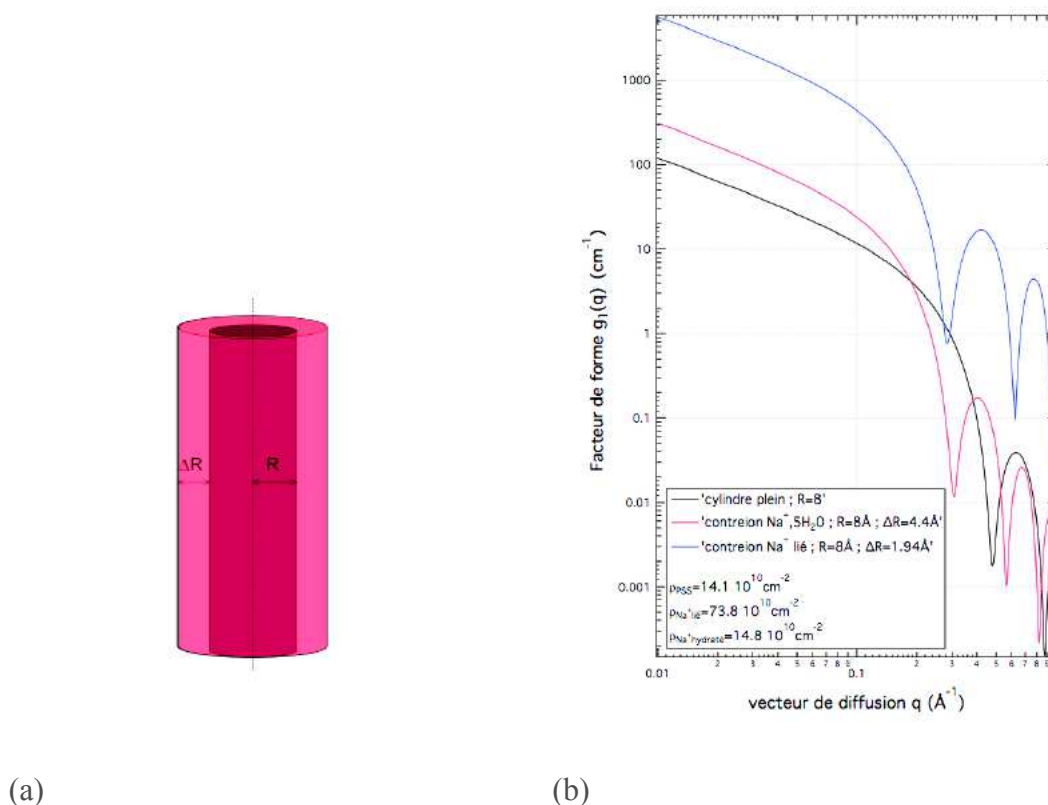
(a)   (b)

Figure 6.26. Scheme of coaxial cylinders allowing to describe the local structure of the poly(styrene sulfonate) macroion (R) and its sodium counterions sheath (ΔR) (a) and form factor of solid cylinder of radius R = 8 Å (black curve) and two coaxial cylinders of radius R = 8 Å and $\Delta R_{bounded}$ = 1.94 Å (blue curve) and $\Delta R_{hydrated}$ = 4.4 Å (red curve) (b)[30]

At high q-values (q > 0.20 Å^{-1}), the scattered intensities of the PSSNa aqueous solutions used for the PEC formation are closed to and reveal, those of the resulting PEC aqueous solutions for both in the absence or the presence of an added salt (Figure 6.27 and Figure 6.28). The scattered intensity of the complexes I(q)$_{comp}$ is in between those of the initial or parent polyelectrolytes. Thus, neglecting the cross term, it could be written:

$$I(q)_{comp} = I(q)_{PDADMA} + I(q)\rho_{PSS} \tag{118}$$

where I(q)$_{PDADMA}$ and I(q)$_{PSS}$ are the contributions of the macroions to the total scattering signal

All experimental SAXS curves shown in Figures 6.27 and 6.28 perfectly superimpose at high q >> 0.20 Å^{-1} after normalization to the concentration of the initial polyelectrolyte components (the normalized curves are not shown). This superimposition means that the average scattering objects, the single polyelectrolyte chains, are identical for all complexes systems whatever the concentration in the studied semidilute and concentrated regions of the state diagrams. Moreover, we could

conclude that the concentration of both polyelectrolytes in both phases are proportional to the initial polyelectrolyte concentration even though they are not the same in both phases.
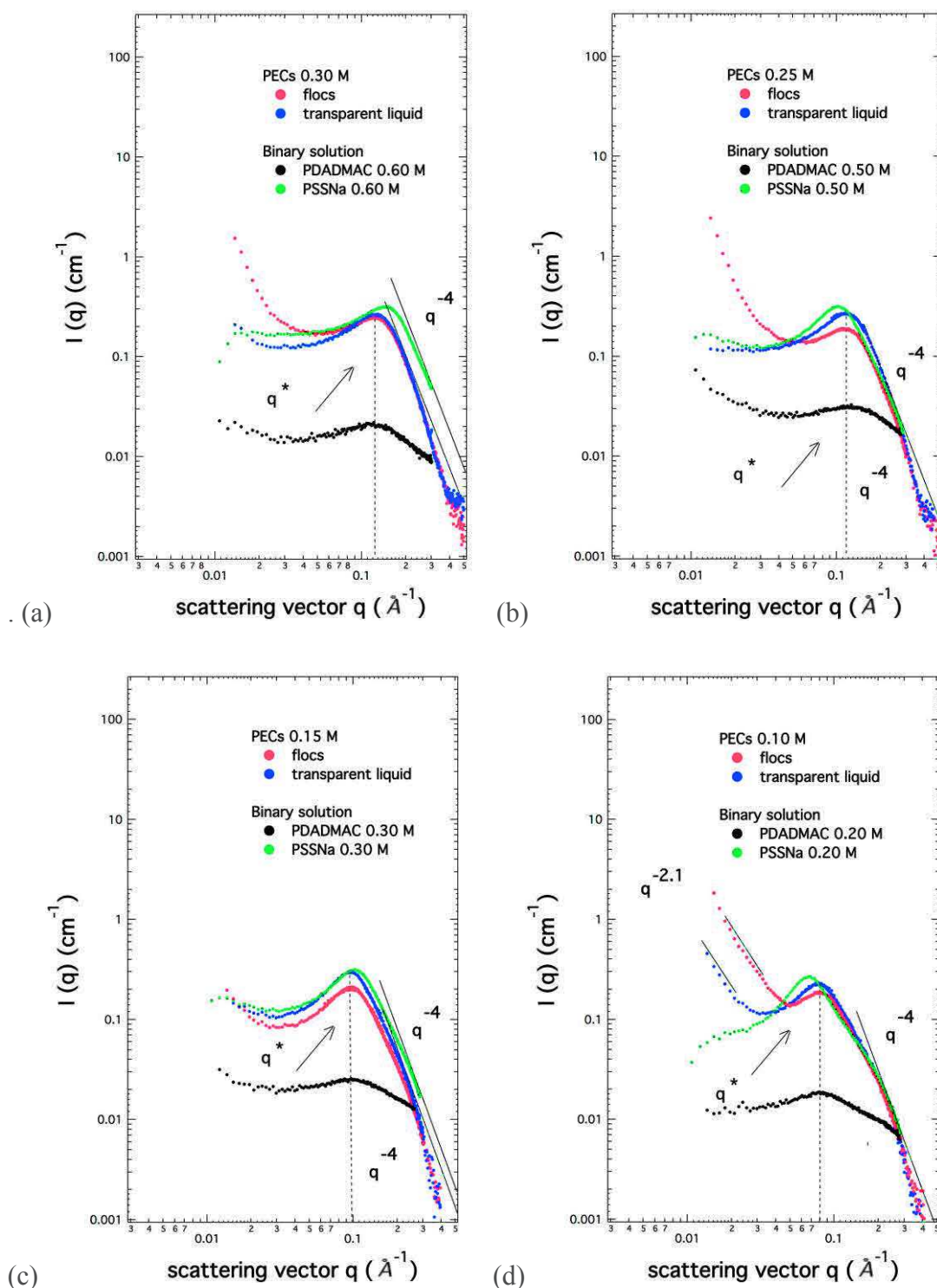

Figure 6.27. SAXS patterns measured from salt-free aqueous solutions of PSSNa- PDADMAC complexes of different concentrations in 1:1 charge or molar ratio: 0.60 M (a); 0.50 M (b); 0.30 M (c); 0.20 M (d). The red curve corresponds to the signal from 'flocs' part, or 'gel', phase and the blue one to that of the 'transparent liquid' part, or 'sol', phase. The black and green curves are the scattered intensities of the initial and related PDADMAC and PSSNa solutions (before mixing), respectively
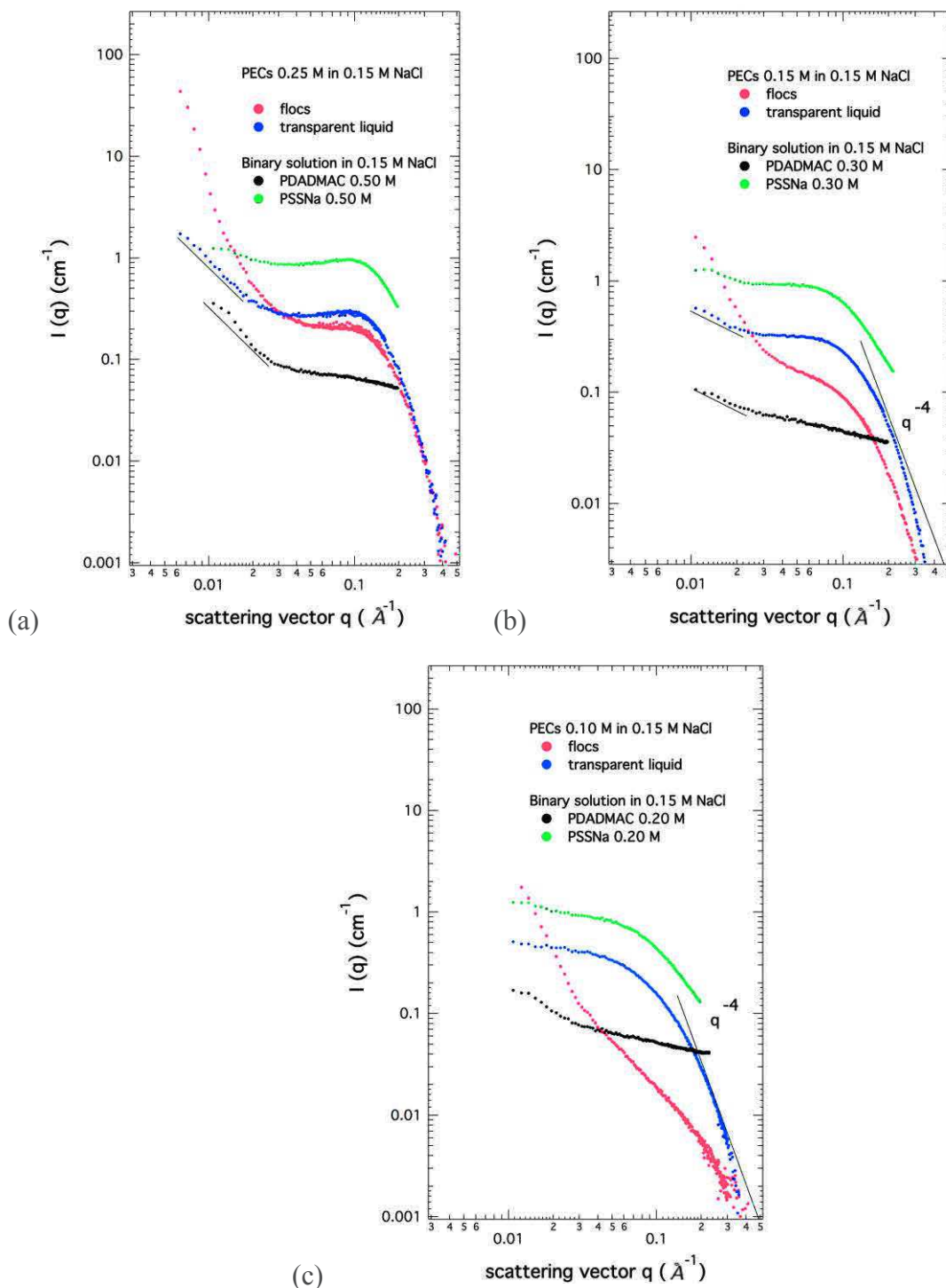
(a)

(b)

(c)

Figure 6.28. SAXS patterns measured from the 0.15 M NaCl aqueous solutions of PSSNa-PDADMAC complexes of different concentrations in 1:1 charge or molar ratio: 0.50 M (a); 0.30 M (b); 0.20 M (c). The red curve corresponds to the signal from 'flocs' part or gel phase and the blue one to that of the 'transparent liquid' part or 'sol' phase. The black and green curves are the scattered intensities of the initial PDADMAC and PSSNa solutions (before mixing), respectively

In the intermediate scattering vector q-range, the correlation peak q^*, which is attributed to the electrostatic interactions inside the mixed network of polyelectrolytes, is observed for the complexes formed in the absence as well as the presence of added salt. Obviously, it is reduced because of the electrostatic screening in 0.15 M NaCl aqueous solutions and even disappears at low PEC concentrations. The way the PEC scattering curves, change with the presence of low-molecular weight added salt reminds the semidilute solutions of polyelectrolytes alone (Figure 6.29).
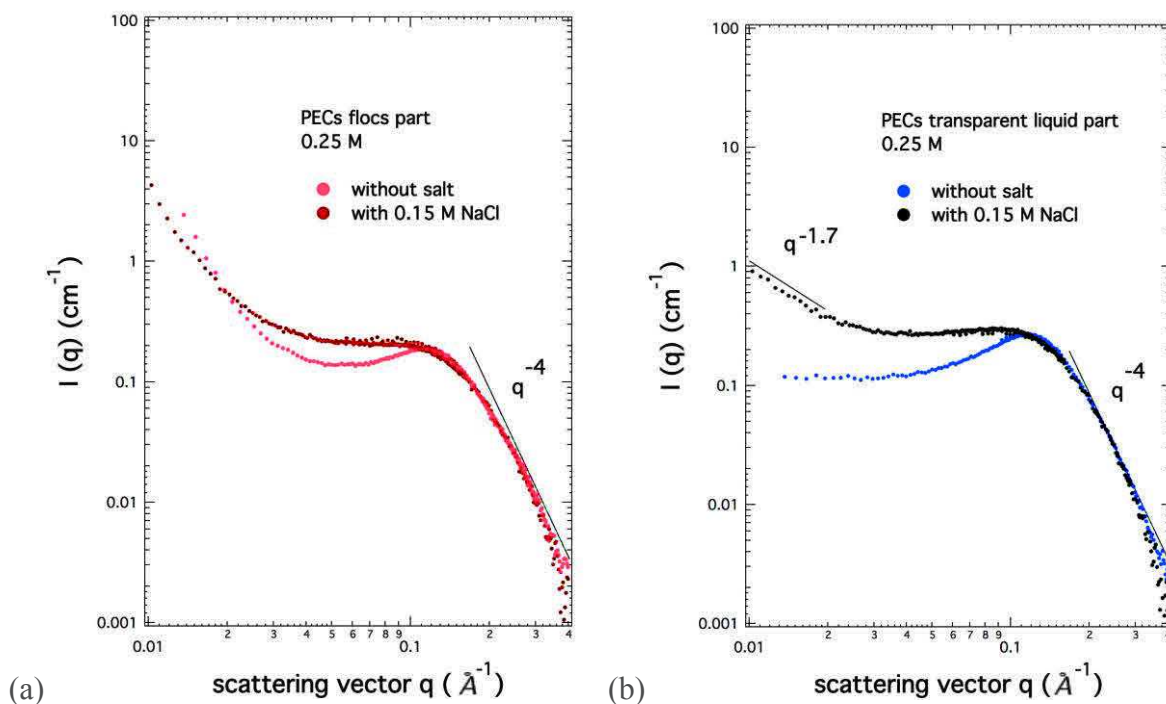

Figure 6.29. Comparison of the SAXS curves obtained from 'flocs' (a) and 'transparent liquid' (b) parts of the biphasic aqueous solutions of complexes formed by mixing salt-free and 0.15 M NaCl aqueous solutions of PDADMAC and PSSNa

The position of the correlation peak, q^*, is almost the same for both phases and corresponds to the position of the polyelectrolyte peak of the initial PDADMAC solution. The temporary network of concentrated poly(diallyldimethylammonium chloride) solution is basic for the polyelectrolyte complex network and dictates the PEC architecture. The position of the correlation peak is related to the mesh size of the network ξ and the average distance between the macroions:

$$\xi = d \sim \frac{2\pi}{q^*} \tag{119}$$

The maximum q^* shifts from 0.08 Å^{-1} to 0.13 Å^{-1} with the increase in the concentration of the initial polyelectrolyte solutions. Thus, the mesh size ξ of the network in 'flocs' and 'transparent liquid' parts or phases is correlatively reduced from 78.5 Å to 48 Å. When the presence of the added NaCl salt leads to complete disappearing of the correlation peak, the scattering signal in the range

between 0.025 Å^{-1} and 0.25 Å^{-1} is assumed to correspond to the one of a neutral polymer semidilute solution.

Strong upturns attributed to the large-scale clusters (> 300 nm) are observed at low q-values (q < 0.025 Å^{-1}; cf. Figures 6.23 - 6.24). These heterogeneities are introduced in the interpolyelectrolyte network by the complexation of oppositely charged monomer units belonging to both polyelectrolytes. Therefore, PDADMAC-PSSNa system could be discussed as that consisting of two spatial scales: the scale of the polyelectrolyte network (q > 0.02 Å^{-1}) and the scale of the crosslink clusters (q < 0.02 Å^{-1}). This two-level architecture could remind the two-step process proposed for analyzing the combined ITC, DLS and zeta-potential measurements in the dilute regime. In dilute solutions, the interaction between poly(diallyldimethylammonium chloride) and poly(sodium styrene sulfonate) leads to the primary complexes formation with their further aggregation. In semidilute and concentrated regimes, the cross-linking of the interpenetrated polyelectrolyte network formed by two oppositely charged PE could be considered as a primary step that is followed by the formation of crosslink clusters (secondary step).

Less viscous and macroscopically less dense, the salt-free 'transparent liquid' part posses a lower scattering exponent comparing to the 'flocs' part at low q-values (q < 0.02 Å^{-1}): q$^{-3.4}$ instead of q^{-4}. The presence of an added salt stronger reduces the exponent of the power law for the scattered intensity of the 'transparent liquid' part till q$^{-1.7}$. That can be ascribed to the fractal arrangement of clusters associated with the diffusion-limited colloid aggregation (DLCA) of uncharged objects[233,234]. The approach to the transition line with the colloid region in the state diagrams (at the component concentration 0.10 M) aligns the exponent of the q-dependence of the scattered intensity for both salt-free phases to q$^{-2.1}$ at q < 0.02 Å^{-1}. This power law can be attributed to the fractal arrangement of clusters according to the reaction limited colloid aggregation (RLCA)[234,235]. The limiting 'reaction' is suggested to be the electrostatic interactions between charged dense objects (crosslink clusters). Both, DLCA and RLCA, are non-equilibrium aggregation processes. The presence of salt during the complex formation at this concentration (0.10 M) changes the scattering law from q$^{-2.1}$ to q$^{-2.5}$.

The scattering behaviour of the fractal structure is described as:

$$S(q) \propto q^{-D_f} \quad \text{for } q < q_c \sim 1/\xi \tag{120}$$

and S(q) = 1 at q > q$_c$, (121)

where D$_f$ is the effective fractal dimension that can be close to 8/5 inside the analogy between heterogeneities and polydisperse randomly branched macromolecules[188,190]; q$_c$ is the critical value of

the scattering vector, beyond which the structure can no longer be considered as a fractal. 'Flocs' and 'liquid' parts of salt-free aqueous solutions of 0.10 M show fractal-like scattering behaviour with D_f = 2.1 at q < 0.05 Å^{-1}, which corresponds to a spatial scale larger than 125 Å in real space. In the presence of added salt, for the 'liquid' part q_c rather equals 0.03 Å^{-1} and that corresponds to a spatial scale larger than 210 Å.

The upturns with different scattering laws (since q$^{-2.1}$ up to q^{-4}) are observed down to the lowest explored q-value: no Guinier regime is observed or guessed for these clusters in the accessible q-range. The size of the secondary formed structure should, therefore, be larger than 500 Å (1/q$_{min}$).

SANS measurements

Similar to the SAXS curves, two main q regions associated with different scattering behaviours can be distinguished using SANS (Figure 6.30): q < 0.03 Å^{-1}, heterogeneities; q > 0.03 Å^{-1}, interpolyelectrolyte network.

At large q-values (q > 0.25 Å^{-1}), the scattered intensity decreases as $I(q) \sim q^{-\alpha}$ with an exponent $\alpha = -2$, which is equivalent for both phases, 'flocs' (gel) and 'transparent liquid' (sol), independently from the ionic strength and concentration (Figure 6.30). This scattering behaviour q^{-2} was expected inside our analogy of the complexation with a gelation process and can be attributed to the signal of the single macroions. The corresponding SAXS curves have a q^{-4} scattering behaviour that is mainly related to the signal of the condensed counterions. In SANS the counterion contribution to the total scattered intensity I(q) of the complexes can be neglected.

In the intermediate q range, SANS curves from salt-free aqueous solutions display a broad peak, that can be ascribed to the electrostatic interactions in the interpolyelectrolyte network since it disappears in the presence of added salt, which allows screening the Coulomb repulsion. We should note that at q > 0.02 Å^{-1} the 'transparent liquid' part of complexes formed at a highest polyelectrolyte concentration in the presence of added salt still shows a polyelectrolyte peak (Figure 6.30 (d)) due to not a complete screening of electrostatic repulsion.

At low q-values between 0.013 Å^{-1} and 0.025 Å^{-1}, the upturns of the scattered intensity scale as q^{-4} and suggest the existence of dense clusters. The exponent of the scattering behaviour changes and becomes equal to 2.5 at lower q-values, i.e. q < 0.013 Å^{-1}. Such q$^{-2.5}$ scaling law was already reported for the fractal arrangements of dense heterogeneities in gels[188,190]. No Guinier regime is visible for all observed SANS spectra. In the q-range between 0.003 Å^{-1} and 0.01 Å^{-1}, the scattered intensity also

(a)   (b)

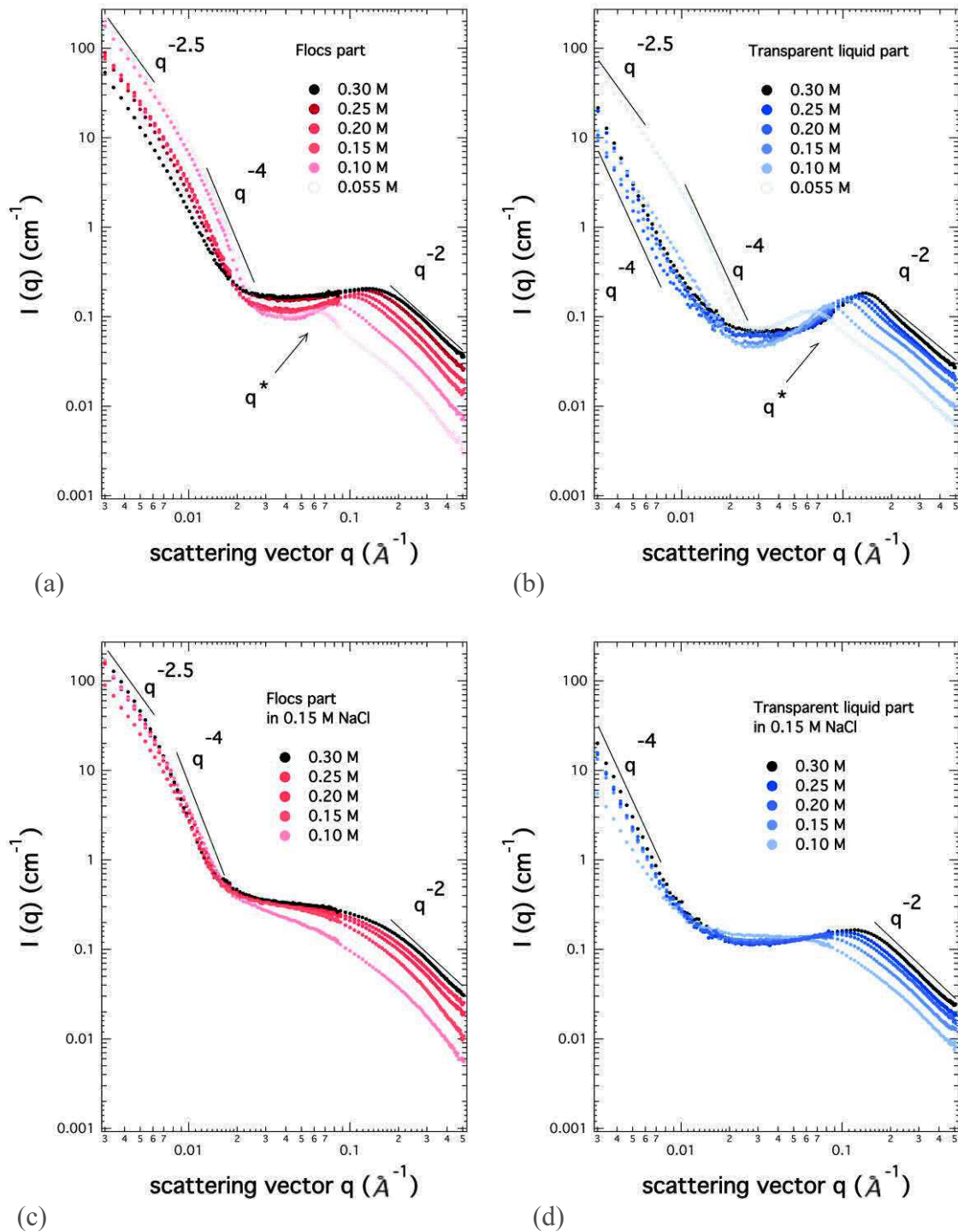(c)   (d)

Figure 6.30. SANS patterns measured from aqueous solutions of PSS-PDADMA complexes, prepared at different polyelectrolyte concentrations on the charge stoichiometry line and with of distinct ionic strengths: 'flocs' (a) and 'liquid' (b) parts for PECs formed in salt-free aqueous solutions; 'flocs' (c) and 'liquid' (d) parts, for PECs prepared in 0.15 M NaCl aqueous solutions

decreases as the polyelectrolyte concentration increases. The increase in PE concentrations makes indeed larger the ionic strength in the complex system and prevents the formation of heterogeneities. Such upturns dependence from the polyelectrolyte concentration is not observed in the case of the brine PEC solutions.

In the q-range between 0.01 Å^{-1} and 0.025 Å^{-1} the scattered intensity I(q) of the salt-free 'liquid' parts presents a single scattering law q^{-4} while the 'flocs' parts display in the same q-range two scattering laws (q^{-4} and q$^{-2.5}$). The difference between 'flocs' and 'liquid' parts is reduced with the approach of the transition towards the colloid region in the state diagrams. Both phases then display q$^{-2.5}$ and q^{-4} at low q.
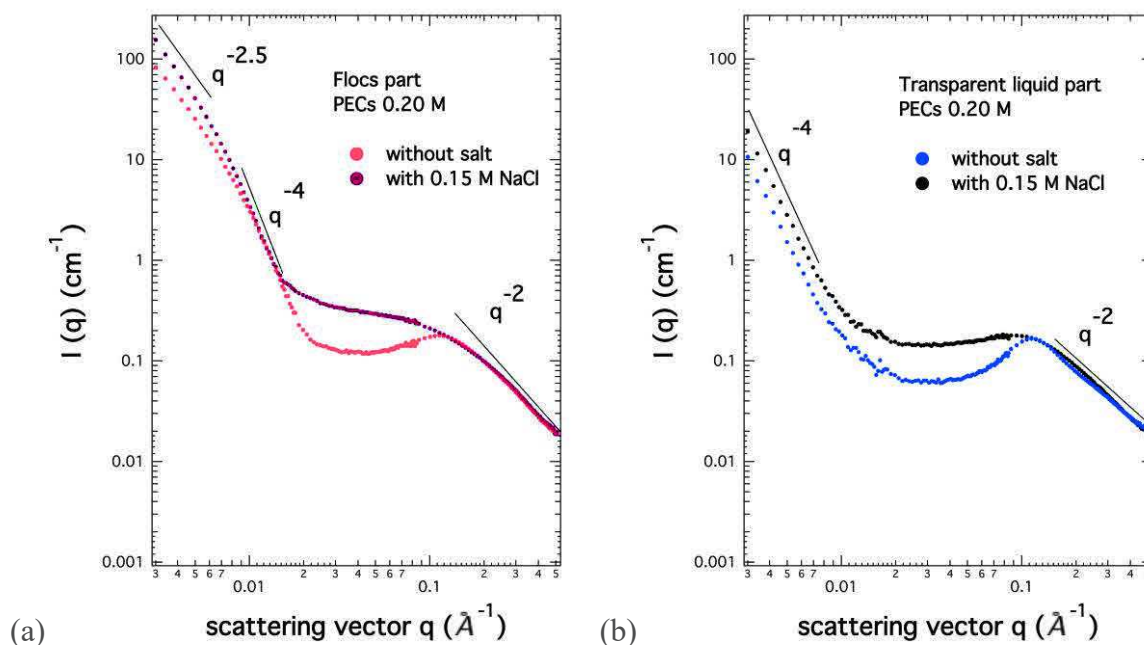

Figure 6.31. Comparison between the SANS scattered intensities of the complexes formed at different ionic strengths for (a) the 'flocs' and (b) the 'transparent liquid' parts

The presence of an added salt does not affect the scattered intensity in the q-region mainly controlled by the chain form factor, i.e. for q > 0.15 Å^{-1} (qξ >1). Moreover, the interpolyelectrolyte network formed by both macroions is almost the same, with a mesh size ξ of the same order of magnitude even though the characteristic polyelectrolyte peak is disappearing in the presence of an added salt, leading to a change in the scattered intensity in the intermediate q-range corresponding to 0.015 < q < 0.15 Å^{-1}. At low q-values (q < 0.15 Å^{-1}), there is no longer strong difference in the

scattering behaviour suggesting crosslink heterogeneities of the same kind and identical internal structure (Figure 6.31).

Comparison between SAXS and SANS measurements

A few differences have already been noticed in the q-dependences of SAXS and SANS scattered intensities. The comparison of the related scattering curves based on a single concentration (0.25 mol/l) is proposed in Figure 6.32. It represents the general case for all the studied samples. Because the contrasts of the polyelectrolytes are different in SAXS and SANS, we have shifted the scattering curves along the vertical axes so that SAXS and SANS curves overlap in the low q region. At high q-values (q > 0.25 Å^{-1}), SAXS and SANS have distinct power laws q^{-4} and q^{-2}, respectively. That is specifically an indirect proof that, in both 'flocs' and 'liquid' phases, all the counterions are not completely released. The polyelectrolyte complexes consist of intermacroion complexes and counterions. The scattered intensity by a PEC solution can then be described as:

$$I(q) = K_{comp}^2 S_{comp}(q) + K_c^2 S_{cc}(q) + 2K_{comp}K_c S_{comp-c}(q), \qquad (122)$$

In this approximation, the partial scattering functions are associated with the macroions, $S_{comp}(q)$, the counterions, $S_{cc}(q)$, and the cross term, $S_{comp-c}(q)$; K_{com} and K_c are the contrast lengths of the macroions and the counterions with respect to the solvent, respectively. K_{comp}^2 and K_c^2 the related contrast factors. The various contrast factors for the used polyelectrolytes in H$_2$0 and D$_2$O as solvents were calculated for SAXS and SANS and are listed in Table 6.2.

Table 6.2.: Macroion and counterion contrast factors for the aqueous solutions of polyelectrolyte complexes

	Polyelectrolyte and solvent	K_m^2 (10^{-24} cm^2)	K_c^2 (10^{-24} cm^2)	$2K_mK_c$ (10^{-24} cm^2)	$\mid 2K_mK_c \mid / \mid K_m^2 + K_c^2 + 2K_mK_c \mid$
SAXS	PSSNa – PDADMAC in H$_2$O (or D$_2$O)	40.99	18.44	55.66	0.48
	HANa – PDADMAC in H$_2$O (or D$_2$O)	156.08	4.41	52.47	0.25
SANS	PSS$_d$Na - PDADMAC in H$_2$O	51.14	0.27	7.43	0.13
	PSS$_d$Na – PDADMAC in D$_2$O	28.53	1.04	-10.89	0.58
	PSS$_h$Na – PDADMAC in H$_2$O	12.28	0.27	3.64	0.22
	PSS$_h$Na – PDADMAC in D$_2$O	80.78	1.04	-18.32	0.29

The Table 6.2 shows that for SAXS experiment, the counterions Na^+ and Cl^- have contrast factors of the order of the macroions and therefore a significant contribution to the total scattering function I(q) and cannot be neglected a priori. For SANS, the significance of the counterion contribution to the total scattered intensity depends on the contrast situation. However, in very rough approach for SANS we could, therefore, write that the total scattered intensity is mostly proportional to the signal of the macroion complexes:

$$I(q) \approx K_{comp}^2 S_{comp}(q) \tag{123}$$

As emphasized before, the partial condensation of the counterions onto the macroions is indicated by the q^{-4} scattering behaviot observed at high q-values in SAXS scattered intensity. The participation of Na^+ and Cl^- counterions to the total charge neutralization during the complexation between PSS and PDADMA is indeed possible as shown in simulations[236]. The probability of the external compensation mechanism (polyions with counterions) varies from 10% till 40%. The partial condensation of released counterions in PECs has been already experimentally reported for poly(sodium styrene sulfonate)-lysozyme systems[237].

For the PSSNa-PDADMAC aqueous solutions, we have applied another approach, which seems best suited because of the existence of a real interpenetrated network, which was suggested in Chapter 6.2. We also note that only considered a stoichiometric mixture of polyelectrolytes were considered. This is obviously questionable in the 'flocs' and 'liquid' phases. However, such stoichiometric mixtures remain reliable approximations. Here the macroion and counterion components are not gathered separately. Thus, the scattered intensity is written by distinguishing all the components: PSS^- (or HA^- in Chapter 7) (M1), $PDADMA^+$ (M2), Na^+ (C1) and Cl^- (C2). It becomes:

$$I(q) = K_{M1}^2\, S_{M1\text{-}M1}(q) + K_{M2}^2\, S_{M2\text{-}M2}(q) + 2K_{M1}K_{M2}S_{M1\text{-}M2}(q)$$

$$+ 2K_{M1}K_{C1}S_{M1\text{-}C1}(q) + 2K_{M2}K_{C2}S_{M2\text{-}C2}(q) + K_{C1}^2\, S_{C1\text{-}C1}(q) + K_{C2}^2\, S_{C2\text{-}C2}(q) \tag{124}$$

Obviously, the cross term between both counterions as well as the ones between macroion and counterion of identical charge can be neglected. The various contrast factors determined from the Table 4.1 and useful for the analysis of our SAXS and SANS experiments, are thus listed in Table 6.3. Here we included the contrast length for HA-PDADMAC as well, which will be used in the next Chapter 7. For the HANa-PDADMAC complex solutions, the Na^+ counterions can also be ignored, like for the HANa aqueous solutions.

This Table 6.3, or the second approach, shows that, for SAXS, the counterions can only be neglected for the HANa-PDADMAC complex solutions. On the other hand, for SANS, the counterions can be ignored in most contrast situations.

Table 6.3.: Macroion and counterion contrast factors for the aqueous solutions of PE complexes according to second approach, described by Eq. (124)

	Solution	K_{m1}^2 10^{-24} cm^2	K_{m2}^2 10^{-24} cm^2	$2K_{m1}K_{m2}$ 10^{-24} cm^2	$2K_{m1}K_{c1}$ 10^{-24} cm^2	$2K_{m2}K_{c2}$ 10^{-24} cm^2	K_{c1}^2 10^{-24} cm^2	K_{c2}^2 10^{-24} cm^2
SAXS	PSSNa-PDADMAC in H_2O	88.34	12.68	66.94	102.65	14.96	29.82	4.41
	HANa-PDADMAC in H_2O	459.05	12.68	35.73	_	14.96	_	4.41
SANS	PSSNa-PDADMAC in H_2O	33.30	1.53	14.30	2.39	-2.64	0.04	1.29
	PSSNa-PDADMAC in D_2O	52.92	114.50	155.83	-31.39	22.76	4.65	1.13
	PSS$_d$Na-PDADMAC in H_2O	170.68	1.53	32.37	5.41	2.82	0.04	1.29
	PSS$_d$Na-PDADMAC in D_2O	0.00	114.50	-0.40	0.08	22.76	4.65	1.13

The position of the PE peak, q*, shifts to higher q-values in SANS with respect to the one observed in SAXS. That is due to the absence of the condensed counterion contribution to the total scattered intensity in SANS[8]. This slight difference between both q*-values obtained by SAXS and SANS increases with concentration (Figure 6.33). It is another consequence of the counterion form factor which only play a role in SAXS[8]. We should note that at low q-values, at least for the 'flocs' phases, the SAXS and SANS curves are superimposed.
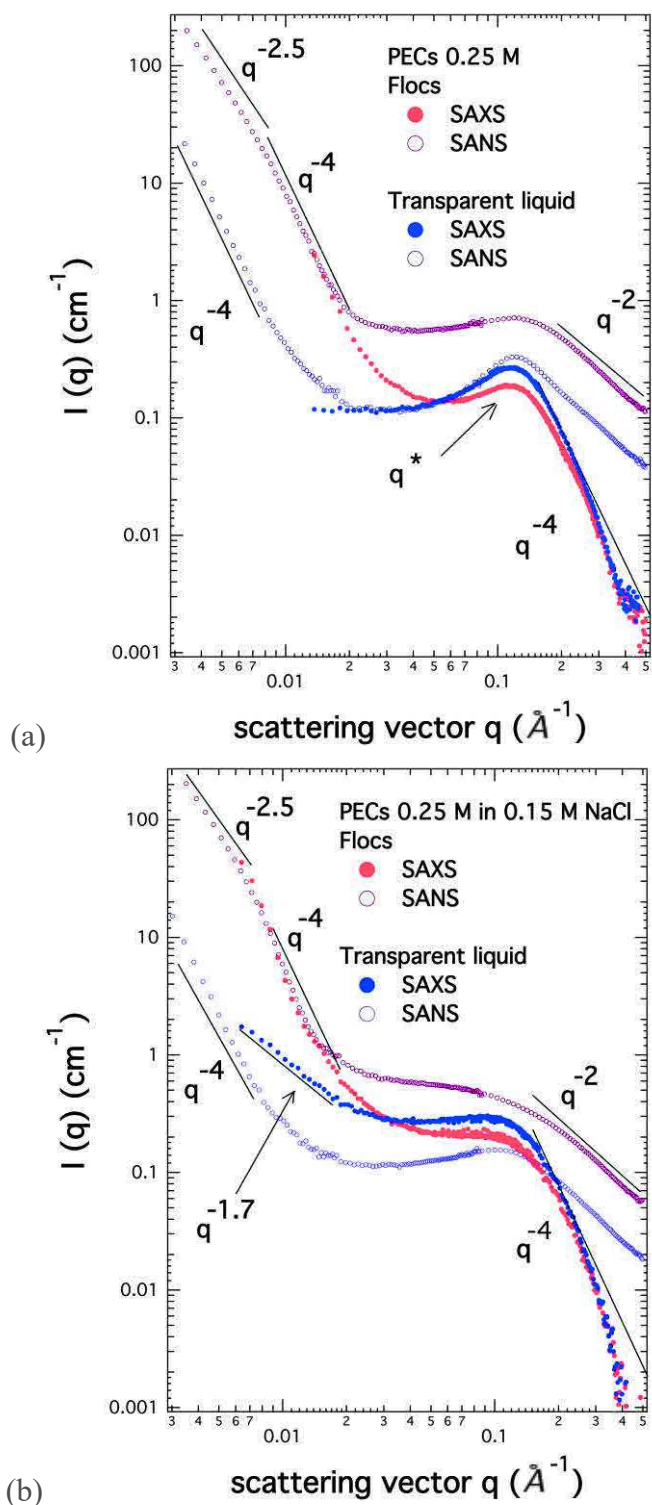
(a)

(b)

Figure 6.32. Combination of SANS and SAXS curves for the PSSNa-PDADMAC complexes formed at the same concentration (0.25 M) in the absence (a) and the presence of added salt (0.15 M NaCl) (b). The original concentration of both polyelectrolyte solutions before mixing was 0.5 M. The SANS curves were moved along the y-axis to superimpose the SAXS and SANS signals at low q

In Figure 6.32 the PE peak position, q*, for both 'flocs' and 'liquid' phases are the same and, consequently, the correlation length ξ is identical in both phases. In a first approximation, the concentration of the formed complex solutions is close to the concentration of the original, or parent, polyelectrolyte solutions, divided by two. Observed in SANS q^* have a concentration dependence with an exponent 0.47, which is close to that expected for semidilute polyelectrolyte solution ($q^* \sim C^{1/2}$) (Figure 6.33). The scaling law $q^* \sim C^{1/2}$ for the PECs has been already reported for PSSNa-gelatin systems by SANS[238]. The observed phase separation results in the coexistence of two phases, 'flocs' and 'liquid' phases, both with the structure of a semidilute solutions. This unusual type of phase separation between two semidilute phases has been already shown for polymer chains adsorbed onto micelles, or solutions of polymer-surfactant mixtures[239].
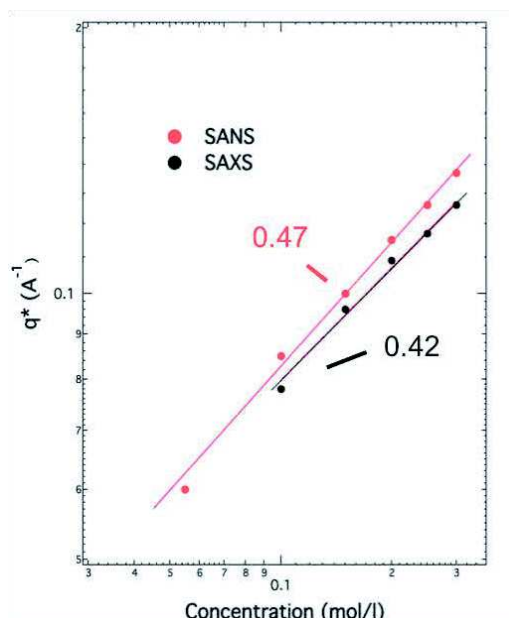

Figure 6.33. Variation the peak position, q*, with concentration. Red dots and line show, the experimental data and their curve fitting, respectively, obtained from SANS measurements; black ones, the same from SAXS

The mesh sizes ξ of the mixed polyelectrolyte networks are equal for both salt-free phases and can be calculated from the position of the peak q* ($\xi = 2\pi/q^*$). This approach for estimating ξ from q* can be used for the 0.15 M NaCl 'transparent liquid' phase as well. However, the scattering signal from the related 'flocs' phases does not longer present the characteristic correlation peak and rather follows a Lorentzian shape with a correlation length ξ such as, for $q\xi < 1$:

$$I(q) = \frac{I(0)}{1+q^2\xi^2} \qquad \text{or} \qquad I(q)^{-1} = I(0)^{-1}(1 + q^2\xi^2) \qquad (125)$$

The calculated mesh sizes are compiled in Table 6.4. We could notice that the ξ-values obtained from SANS experiments should be more realistic since they are deduced from q* values that are not

disturbed by the form factor of counterions. In the 'transparent liquid' phase in the presence of an added salt, a characteristic PE or correlation peak, while it does not appear in the related 'flocs' phases. The condensed or trapped counterions would be more numerous in 'the flocs' phase. Such disproportion of countreions during phase separation has been already described by Shklovskii and Zhang[59].

Table 6.4. Values of the mesh size ξ, estimated from the position in the reciprocal space of the correlation peak, from SAXS (q^*_{SAXS}) and SANS (q^*_{SANS}) and calculated from Eq.(125)

| Concentration of PECs | In the absence of NaCl | | | In the presence of NaCl | | |
| | Flocs and transparent liquid | | | Flocs | Transparent liquid | |
	q^*_{SAXS}, Å^{-1}	q^*_{SANS}, Å^{-1}	ξ_{SANS}, Å	ξ_{SANS}, Å	q^*_{SANS}, Å^{-1}	ξ_{SANS}, Å
0.055 M	-	0.058±0.001	108.3	-	-	-
0.10 M	0.078±0.003	0.085±0.003	73.9	12.5	0.064±0.002	98.1
0.15 M	0.096±0.003	0.010±0.004	62.8	10.8	0.085±0.002	73.9
0.20 M	0.109±0.004	0.115±0.003	54.6	8.1	0.100±0.002	62.8
0.25 M	0.117±0.003	0.126±0.003	49.8	7.2	0.113±0.003	55.6
0.30 M	0.126±0.005	0.137±0.005	45.8	6.5	0.125±0.005	50.2

According to this analogy between a gelation process and the complexation of two polyelectrolytes of opposite charge, we expect two main q-ranges for the scattering patterns of polyelectrolyte complexes in semidilute or concentrated aqueous solutions. At small q-values, the scattered intensity is related to the heterogeneities resulting from the electrostatic junctions between polyelectrolytes. If these heterogeneities are small, their Guinier range (allowing a measurement of $<R_G^2(H)>_Z$, as well as their internal structure, could be investigated. If they are large, only their internal structure could be studied. Above we described the heterogeneities through a model of star-like branched polymers. However, other shapes and therefore other form factors could also be considered. According to the situation of the previous sketch 2 (Figure 6.16 (b), large sequences of polyanion and polycation are in contact through successive electrostatic links or junctions along the chemical sequences, forming neutral objects (as the ladder structure of PEC proposed in Chapter 2 in agreement with simulations). Obviously, such primary complexes could lead to large cylindrical

particles via further aggregation. At high q-values ($q > 1/\xi$), the scattered intensity is related to the network formed by the macroions. The mesh size of this network could then be determined from the lowest q values of this regime, especially from the position q* of the polyelectrolyte peak that is still observable for the salt-free aqueous solutions. At larger q values, the form factor of the macroions (Small angle neutron scattering, SANS, as well as small angle X-ray scattering, SAXS, provided all counterions are free) and that of the condensed counterions (through SAXS) could also be investigated.

6.2.5. Partial scattering functions of the complexes: SANS contrast variation study

6.2.5.1. Structure of each macroion: use of the contrast matching method

We performed particular SANS experiments, where species belonging to a multicomponent system can be suppressed by an appropriate matching of its neutron scattering length density by varying the proton/deuteron ratio of the solvent. The scattering length density of 100 % D_2O solvent matches the one of the PSS_d polyions. The scattered intensity by PSS_dNa-PDADMAC complexes in this solvent is then a fingerprint of the PDADMA structure in the complexes. Indeed, the contribution of the condensed Na^+ and Cl^- counterions can always be neglected through the SANS technique. The scattering length density of the D_2O-H_2O mixture with a D_2O volume fraction $\Phi_v(D_2O) = 3\%$ does not match perfectly that of the PDADMA macroion. However, the scattered intensity by PSS_dNa-PDADMAC complexes in this solvent can be considered as mainly associated with the PSS_d macroions ($I(q)$ is proportional to $S_{PSS}(q)$) and, therefore, yields to the information about the PSS structure in the complexes. The SANS measurements from PSS_hNa-PDADMAC system in D_2O give the scattered intensities related to both macroions, i.e. the whole complexes.

The scattering patterns presented in Figure 6.34 and Figure 6.35 correspond to the three contrast situations, obtained in three solvents. The concentration of the original or parent polyelectrolyte aqueous solutions was kept constant at 0.30 M. Thus, the expected concentration of complexes in the final mixture is 0.15 M. We neglect the contribution of the condensed counterions to the scattered intensities as their contrast lengths are negligible.

The scattering curves of PDADMA and PSS have an identical scattering behaviours with q^{-2} at high q ($q > 0.15$ Å^{-1}). The identical power law was observed in the signal of the total complex and is

attributed to the signal of the single ideal polyelectrolyte chains. The similar conformation of poly(styrene sulfonate) and poly(diallyldimethylammonium chloride) at high q allows to suggest that both polyelectrolytes participate in the overlapping mixed network. The 'ladder' structure model for the complexes, in which the polyelectrolyte chains are parallel and in close interaction, is unlikely. Our SANS results rather suggest that the structure of the formed interpolyelectrolyte complexes corresponds to the 'scrambled eggs' model for polyelectrolyte complexation[42,240]. Correlatively, for the 'flocs' part in the salt-free system, both polyelectrolytes display a correlation peak in the intermediate q-range (Figure 6.34 (a)). This peak has been already ascribed to the repulsion between macroions and its position in the reciprocal space is related to the characteristic correlation length ξ, or mesh size of the polyelectrolyte network. It is almost the same in the partial scattering functions of polycations and polyanions. At low q-values (q < 0.02 Å^{-1}), the large upturns with q$^{-2.5}$ and q^{-4} decays, related to the heterogeneities and their fractal organization, is observed in the PDADMA signal. The PSS scattering at this scale has very low intensity. However, such an observation is specific to the concentration c=0.15 M. For other concentrations (See Figure 6.42.a) upturns, a q$^{-2.5}$ decay is still observed at low q-values. Surprisingly, in salt-free 'flocs' at c=0.15 M, the large-scale heterogeneities would mainly result from the PDADMA macroions. On the contrary, in the 'liquid' part of the salt-free PEC aqueous solutions (Figure 6.34 (b)), the PSS polyanion contributes to the strong increase of the intensity at low q, whatever the concentration (see Figure 6.42.b). Here, PSS causes the formation of cluster, as well as PDADMA, even at c=0.15 M. In the 'transparent liquid' part, the PSS scattered intensity always exhibits a correlation peak as in the 'flocs' part, while that is no longer the case for the PDADMA scattered intensity. For the polycation, the intermediate maximum is absent and replaced by a quasi-plateau (in the q-range 0.02 < q < 0.09 Å^{-1}). That could result from a strong influence of the heterogeneities. But, that is most likely due to the screening of the electrostatic interaction. The comparison of the scattered intensity amplitudes shows the material disproportion of PDADMA between the distinct phases. The larger part of the PDADMA polycation stays in the 'flocs' part. PSS chains practically distribute equally between the two co-existing phases, since the position of the maximum q* is specifically the same in both phases.

In the salt solutions, the intermediate peak is no longer present for all components (Figure 6.35(a)) mainly because of the screening effect of the salt. In the scattered intensity of PDADMA in the 'flocs' part, we observed a scattering law q$^{-2.5}$ at q < 0.007 Å^{-1} and q^{-4} in between q = 0.007 Å^{-1} and 0.015 Å^{-1}. In the contrary to salt-free aqueous solutions, here PSS shows upturns with a q^{-4} decay up to q = 0.012 Å^{-1} (Figure 6.35 (b)). In the 'liquid' part, the q$^{-2.5}$ and q^{-4} decays are observed for both

species at q < 0.008 Å^{-1} and between 0.008 Å^{-1} and 0.0125 Å^{-1}, respectively. PSS and PDADMA

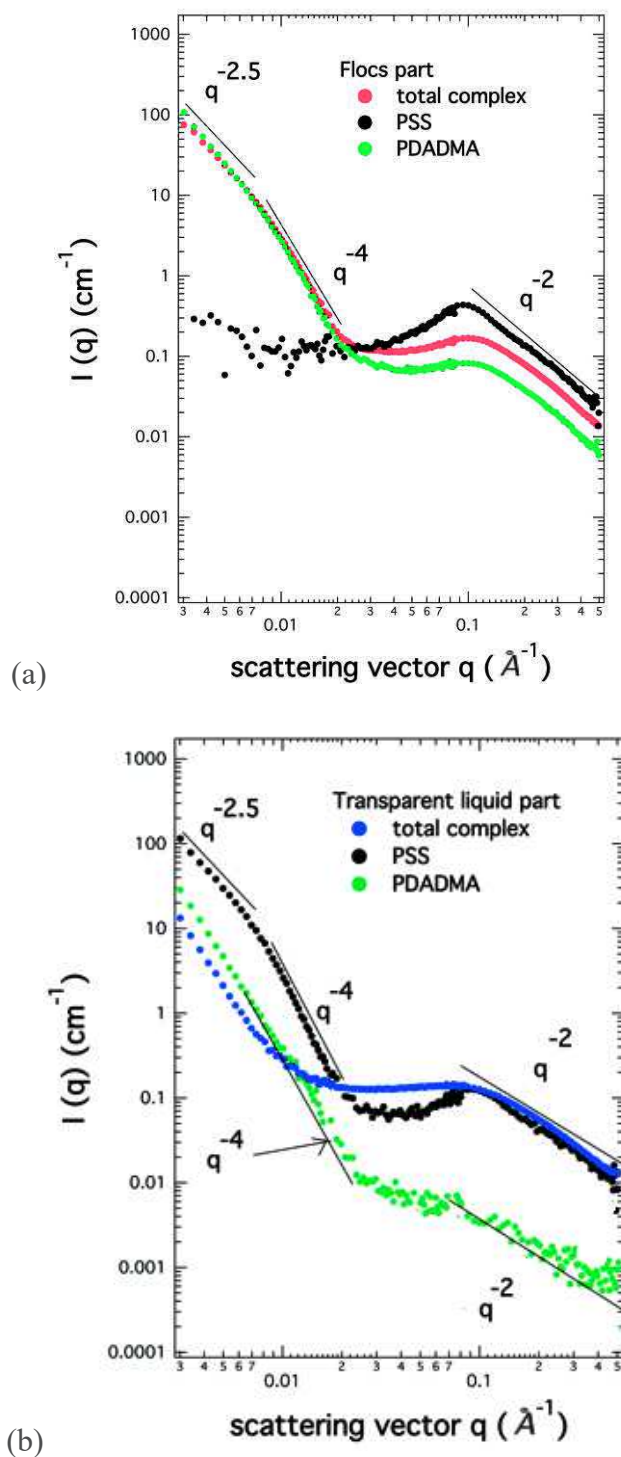display a quasi-plateau between q = 0.0125 Å^{-1} and 0.07 Å^{-1}.

(a)

(b)

Figure 6.34. Scattering patterns from 'flocs' (a) and 'transparent liquid' (b) parts of PDADMA-PSS, formed by mixing the salt-free 0.30 M solutions of the polyelectrolytes. Different contrast conditions are considered through SANS (see text). Partial PSS and PDADMA signals are shown in black and green; the total signal, i.e. that of the whole complex, is shown in red None of scattering curves has not been shifted along the y-axis
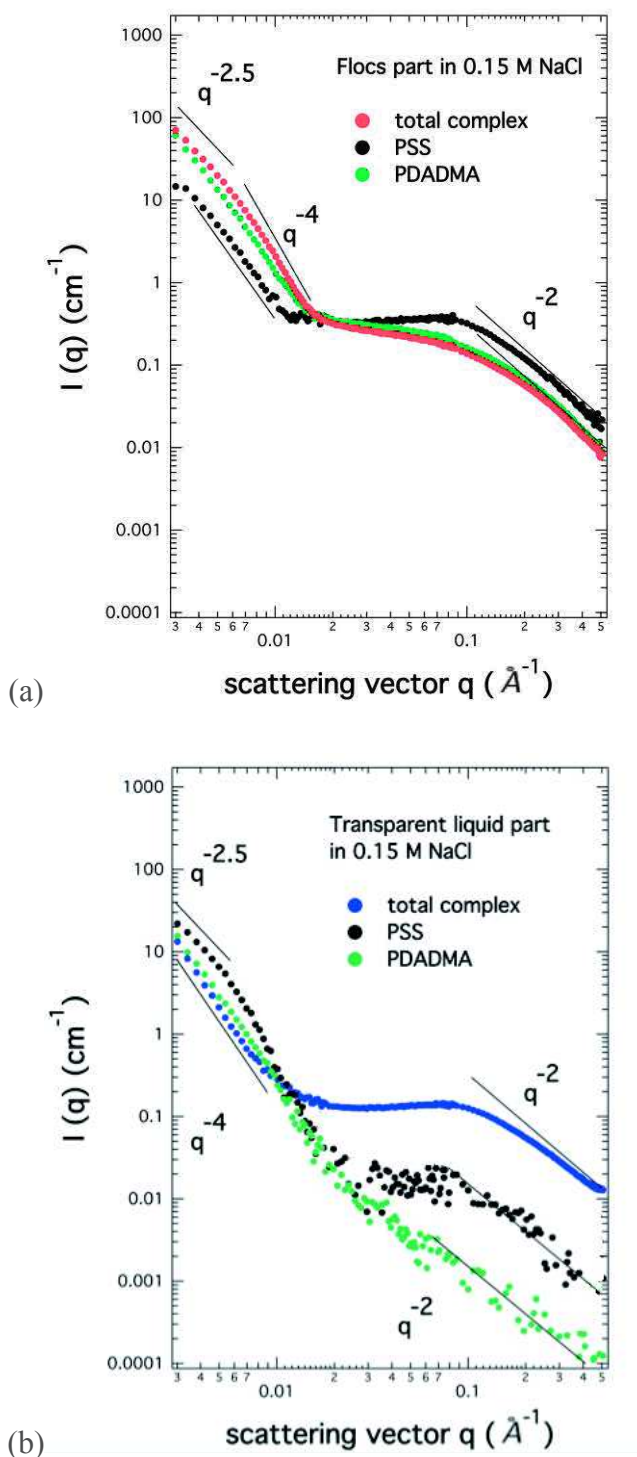
(a)

(b)

Figure 6.35. Scattering from 'flocs' (a) and 'transparent liquid' (b) parts of PDADMAC-PSSNa, formed by mixing 0.30 M solutions of the polyelectrolytes in 0.15 M NaCl. Different contrast conditions are considered through SANS (see text). Partial PSS and PDADMA signals are shown in black and green; the total signal, i.e. that of the whole complex, is shown in red None of scattering curves has not been shifted along the y-axis

With the addition of salt, in each phase the conformations of the PSS and PDADMAC polyions become more similar between PSS and PDADMAC than in the PECs formed in the absence of salt. The screening of the electrostatic interactions improves the symmetry of the mixed polyelectrolyte system.

6.2.5.2. Correlations within each component and crossed correlations: use of the contrast variation method

The scattered intensity measured by SANS from a PSS$_d$Na-PDADMAC solution in D$_2$O yields the PDADMA partial scattering function, S$_{11}$(q, C) (see Table 6.2 and Table 6.3 of contrast lengths and contrast factors). Indeed, as the contribution of condensed counterions is negligible in SANS experiments, we have:

$$I_1(\vec{q},C) = K^2_{PDADMA/D_2O}S_{11}(\vec{q},C). \tag{126}$$

Where C is the concentration of the PEC solution.

The scattered intensity measured by SANS from a PSS$_d$Na-PDADMAC solution in the D$_2$O-H$_2$O mixture with a D$_2$O volume fraction Φ_v(D$_2$O) = 3% yields approximately the PSS partial scattering function, S22(q) (see Table 6.2 and Table 6.3 of contrast lengths and contrast factors). For the same PEC concentration, we can write:

$$I_2(\vec{q},C) \approx K^2_{PSS/3\%D_2O}S_{22}(\vec{q},C). \tag{127}$$

For PSS$_2$Na-PDADMAC solutions in a D$_2$O-H$_2$O mixture with Φ_v(D$_2$O) = 54% the macroions have almost equal absolute values of contrast length:

$$K_{PDADMA} \approx -K_{PSS} \approx K \tag{128}$$

and the scattered intensity can be written as:

$$I_3(\vec{q},C) = K^2_{PDADMA/D_2O}S_{11}(\vec{q},C) + K^2_{PSS/3\%D_2O}S_{22}(\vec{q},C) + 2K_{PDADMA/D_2O}K_{PSS/3\%D_2O}S_{12}(\vec{q},C)$$

$$\approx K^2S_{11}(\vec{q},C) + K^2S_{22}(\vec{q},C) - 2K^2S_{12}(\vec{q},C) = K^2[S_{11}(\vec{q},C) + S_{22}(\vec{q},C) - 2S_{12}(\vec{q},C)] \tag{129}$$

S$_{11}$(q,C) and S$_{22}$(q,C) are the partial scattering functions of the PDADMA and PSS macroions, respectively, describing their distinct structures in the PEC solution at concentration C. S$_{12}$(q,C) is the cross term, which is a fingerprint of the interactions between the oppositely charged macroions. Performing scattering experiments in three different solvents, as D$_2$O, 3% D$_2$O - 97% H$_2$O and 54% D$_2$O - 46% H$_2$O, the partial scattering functions S$_{11}$, S$_{22}$ and S$_{12}$ can be extracted.

The calculated $S_{11}(q,C)$, $S_{22}(q,C)$ and $S_{12}(q,C)$ partial scattering functions for the PSSNa-PDADMAC complexes, formed in the absence and the presence of added salt at c= 0.10 mol/l of polyelectrolyte complexes are presented in Figure 6.36 and in Figure 6.37, respectively.
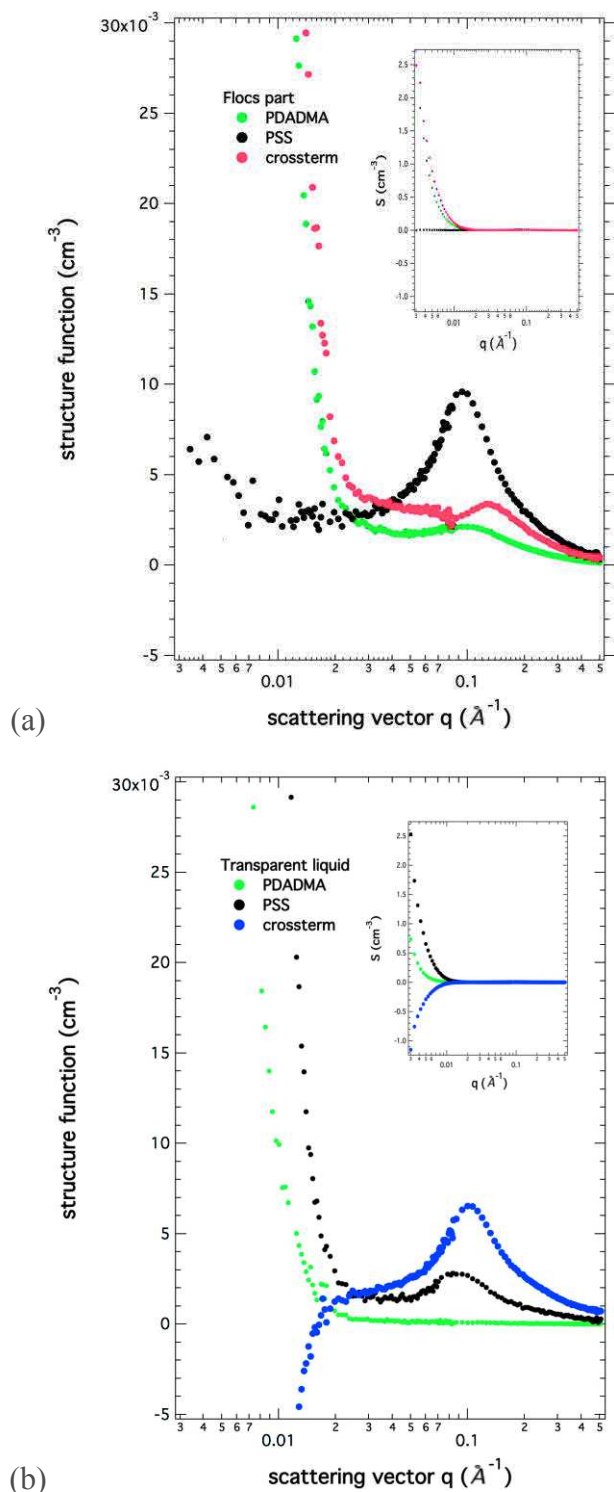

(a)

(b)

Figure 6.36. Partial scattering functions of both polyions and cross term in 'flocs' (a) and 'transparent liquid' parts (b) of the PSSNa-PDADMAC complexes, formed in salt-free solution at concentration of polyelectrolyte complexes C = 0.10 mol/l. Green and black symbols represent the PDADMA and PSS scattering functions, respectively. The cross terms in 'flocs' and 'liquid' parts of these PECs are shown in red and blue, respectively
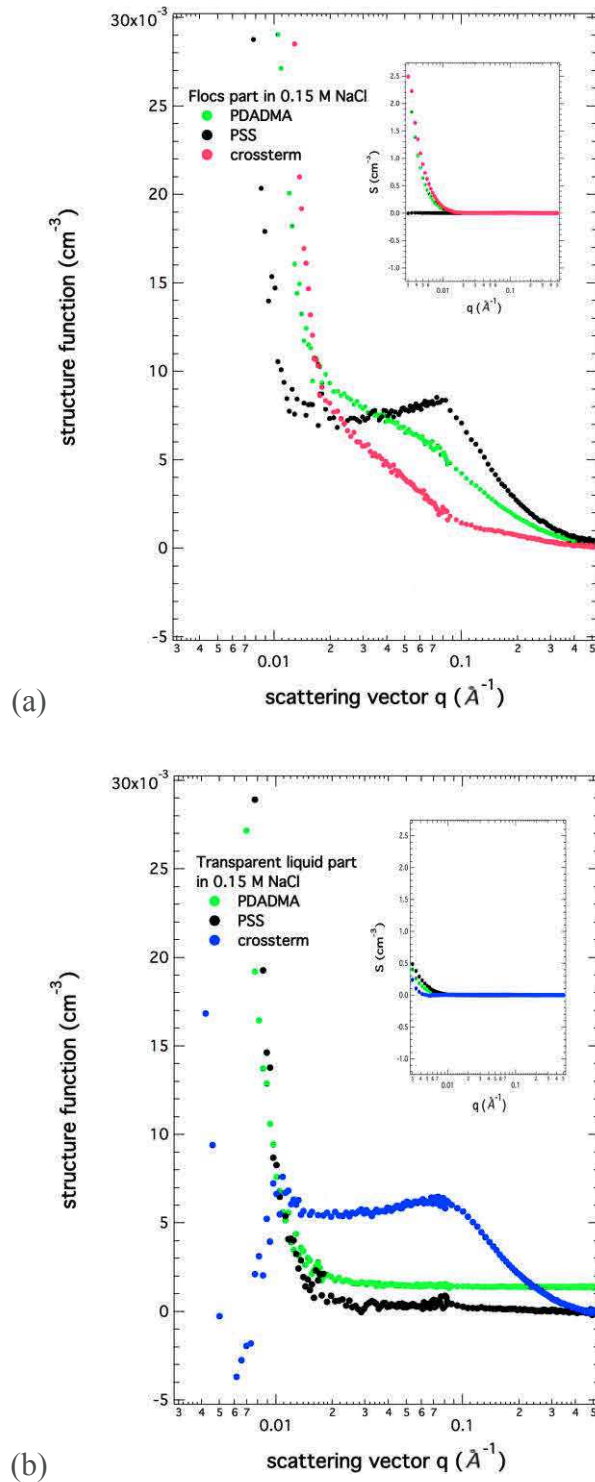
(a)

(b)

Figure 6.37. Partial scattering functions of both polyions and cross terms in 'flocs' (a) and 'transparent liquid' parts (b) of the PSSNa-PDADMAC complexes, formed at a concentration of polyelectrolyte complexes C = 0.10 mol/l in the presence of 0.15 M NaCl. Green and black symbols represent the PDADMA and PSS scattering functions, respectively. The cross terms in 'flocs' and 'liquid' parts of these PECs are shown in red and blue, respectively

149

The analyses of the partial scattering functions S_{11} and S_{22}, respectively associated with the PDADMA and PSS macroions, can be skipped as we have already described in details their q-dependence. The cross terms S_{12} are distinct from zero, independently of the ionic strength and the considered phase. Such non-null intermolecular functions suggest that the two components are not homogeneously located in space. In salt-free solutions, the functions S_{12} of both phases display a correlation peak at q^* that can be attributed to the electrostatic interactions between opposite charges. In 'flocs', q^* is observed at 0.132 Å^{-1} (d or ξ ~ 47.6 Å in real space) and, in 'transparent liquid', at 0.10 Å^{-1} (d or ξ ~ 62.8 Å). Remarkably, the position of the peak observed in the cross term is shifted to higher q values, comparing to that of the peaks observed in the partial scattering functions S_{11} and S_{22}, in both phases. However, the shift is higher for the 'flocs' phase than in the 'transparent liquid' one. For PEC solutions in the presence of 0.15 M NaCl, the cross terms of 'flocs' and 'liquid' phases also display a maximum at the same position q* close to 0.075 Å^{-1} (d or ξ ~ 83.8 Å). We note that the average distance ξ is larger for the solutions in the presence of an added salt than for the free-salt solutions.

6.2.5.3. Concentration dependence of the PDADMA scattering function

The small-angle neutron scattered intensities obtained from the PSS$_d$Na-PDADMA complex solutions in 100 % D$_2$O, yield the PDADMA scattering functions, $I_1(q) = K_{PDADMA/D2O}^2 S_{PDADMA}(q)$, and therefore give information about the PDADMA structure in the complexes. They are presented in Figure 6.38 and Figure 6.39 for different concentrations of the PEC solutions. The curves are shifted by a factor 10 to avoid superimposition of the distinct signals. The complexes were prepared by varying the concentration and the ionic strength.

In both 'flocs' and 'liquid' parts for q > 0.15 Å-1 the PDADMA scattering curves have the characteristic q^{-2} decreasing of the single PDADMA chains, whatever the concentration and the ionic strength (Figure 6.38 and Figure 6.39). The PDADMA macroions keep their original conformation during the complexation. That is in an agreement with the "scrambled eggs' model for the PEC structure.

In the salt-free 'flocs' phase, the intermediate PE peak appears in the q range between 0.09 Å^{-1} and 0.12 Å^{-1} and shifts to higher q-value with the increase in concentration. The position q* of this PE peak characterizes the mesh size ξ of the PDADMA network (q*≈2π/ξ). It is determined by the initial concentration of the PDADMAC solution. The values of the mesh sizes are given in Table 6.4 and are much smaller than the ones of the PDADMA network in D$_2$0 and H$_2$0 (Table 6.5), obtained with SANS and SAXS, respectively. That relates to the shrinking of the macroion network during

complexation with oppositely charged PSS in an analogy with a gelation process, that was suggested in Chapter 6.2.2.

Table 6.4. The position of the polyelectrolyte peak, observed by SANS (q^*_{SANS}), for the PDADMA signal and the mesh size ξ of the corresponding network in the salt-free 'flocs' part or phase ($\xi = 2\pi/ q^*$)

Initial concentration of PDADMAC solutions, divided by two	q^*_{SANS}, Å^{-1}	ξ, Å
0.10 M	0.092 ± 0.005	68.3±3.7
0.15 M	0.102 ± 0.005	61.6±3.0
0.25 M	0.118 ± 0.003	53.3±1.4

Table 6. 5. The position of the polyelectrolyte peak, observed by SANS (q^*_{SANS}) in D_2O and by SAXS (q^*_{SAXS}) in H_2O, for the PDADMA signal in binary systems (one polyelectrolyte/solvent) and the mesh size ξ of the corresponding network ($\xi = 2\pi/ q^*$). Data are kindly given by P. Lorchat[30]

PDADMAC concentration	q^*_{SANS}, Å^{-1} in D_2O	ξ_{SANS}, Å in D_2O	q^*_{SAXS}, Å^{-1} in H_2O	ξ, Å in H_2O
0.10 M	0.069±0.004	91.0±5.3	0.065±0.002	96.6±3.0
0.15 M	0.080±0.002	78.5±2.0	0.083±0.002	75.7±1.8
0.25 M	0.115±0.005	54.6±2.4	0.115±0.005	54.6±2.4

In the presence of added salt, at least for the largest concentrations, the scattered intensity appears almost flat in this q-range and corresponds to the concentration blobs associated with a temporary network of a semidilute or concentrated solution of neutral PDADMA chains.

The upturns at $q < 0.025$ Å^{-1} correspond to the existence of large heterogeneities in the networks and gels resulting from the complexation process. For $0.01 < q < 0.025$ Å^{-1}, a q^{-4} scattering behaviour is observed that can be attributed to dense clusters, presumably related to some aggregation between links or junctions formed through the complexation between monomer units of oppositely charged polyelectrolytes. For $q < 0.01$ Å^{-1}, a $q^{-2.5}$ scattering behaviour is observed that can be ascribed to the fractal arrangement of the clusters. It tends up to the lowest q values (0.003 Å^{-1}). These two scattering laws do not change with the presence of an added salt.
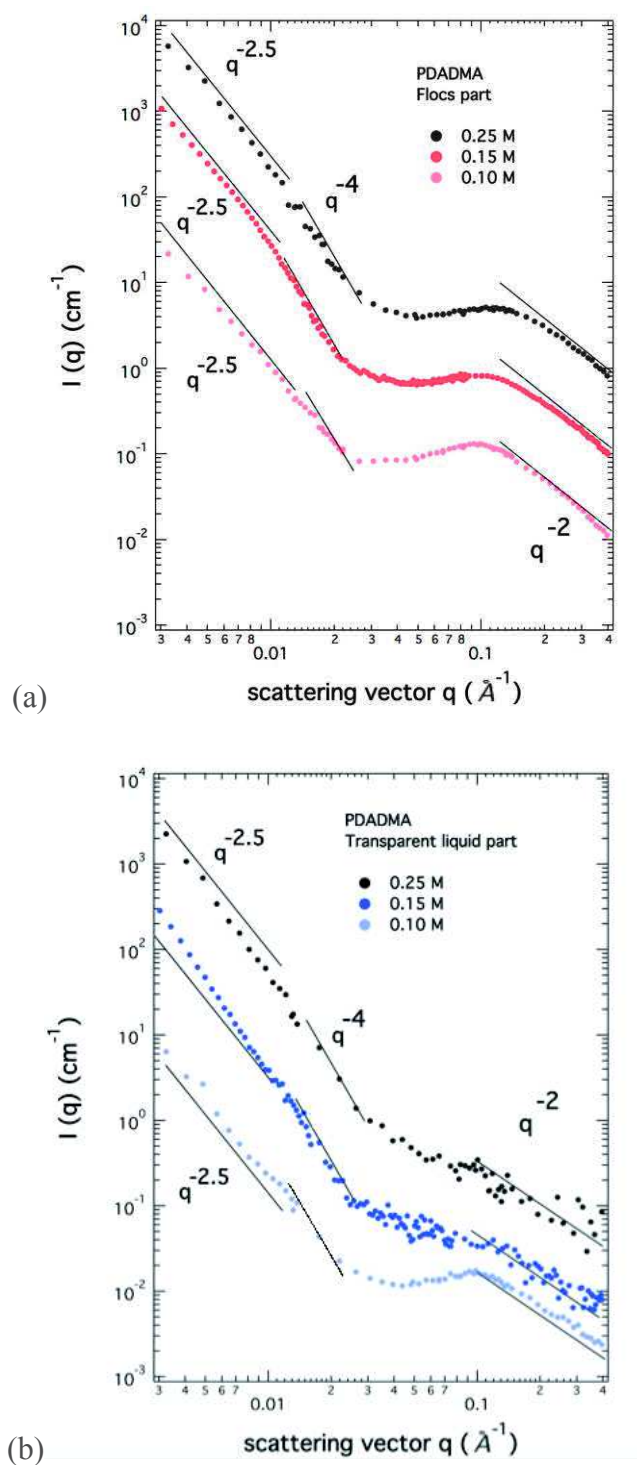
(a)

(b)

Figure 6.38. SANS signal of the PDADMA macroions as a function of PEC concentration, in 'flocs' (a) and 'transparent liquid' (b) parts of salt-free solutions of PSSNa-PDADMAC complexes. The SANS curves are shifted by a factor 10 to avoid their superimposition of the curves

It is interesting to note that, in the 'transparent liquid' part, the SANS curve of the lowest concentration (c=0.10 mol/l) displays a PE peak. Probably, for such low polyelectrolyte component concentration counterions have released completely. Moreover, the PE peak position in the reciprocal space corresponds to the PE peak of the curve associated with the 'flocs' part at the same concentration ($q^*=0.092$ Å^{-1}). This concentration, c=0.10 mol/l, is close to the transition line of 'flocs'/'transparent liquid' domain with 'colloid' region in the phase diagrams. In 'colloid' region, polyelectrolyte complex mixture has a 'segregative' phase separation type, when all polymer material concentrates in one 'colloid' phase with another internal structure than in 'flocs' or 'transparent liquid'. We suggest that at c=0.10 mol/l, the polyelectrolyte complex organization start already changing to the denser one observed in PEC colloids.

In the 'liquid' part the scattering behaviour of PDADMA remains identical to that in the 'flocs' part at low q values till 0.03 Å^{-1}. In salt-free systems and in the intermediate q-range 0.03 Å^{-1} < q < 0.1 Å^{-1}, the polyelectrolyte peak is only visible at the lowest concentration (0.10 M). For higher concentrations, the polyelectrolyte peak is no longer observed and replaced by a flat signal or a power law with an exponent lower than 1, which could be attributed to the superimposition with the scattering signal of dense clusters (upturns).

The disproportion of PDADMA between both phases (gel and transparent liquid phases) is concluded after the analysis the scattering amplitudes (Figure 6.38 (a) with respect to Figure 6.38 (b)). The larger amount of polycation stays in 'flocs', or gel, part.

In 0.15 M NaCl aqueous solutions, the scattered intensity from the 'liquid' part in the q-range $0.012 < q < 0.025$ Å^{-1} corresponds to a power law with an exponent α less that 4. The heterogeneities formed here are therefore less dense than the ones observed in the salt-free case. We can conclude that the conformation of PDADMA macroions in the liquid part, or phase, is more sensitive to the change in the original concentration or ionic strength.

Whatever the ionic strength as well as the initial concentration of both components of the PEC system, the larger part of PDADMA stays in the 'flocs' part or gel phase.
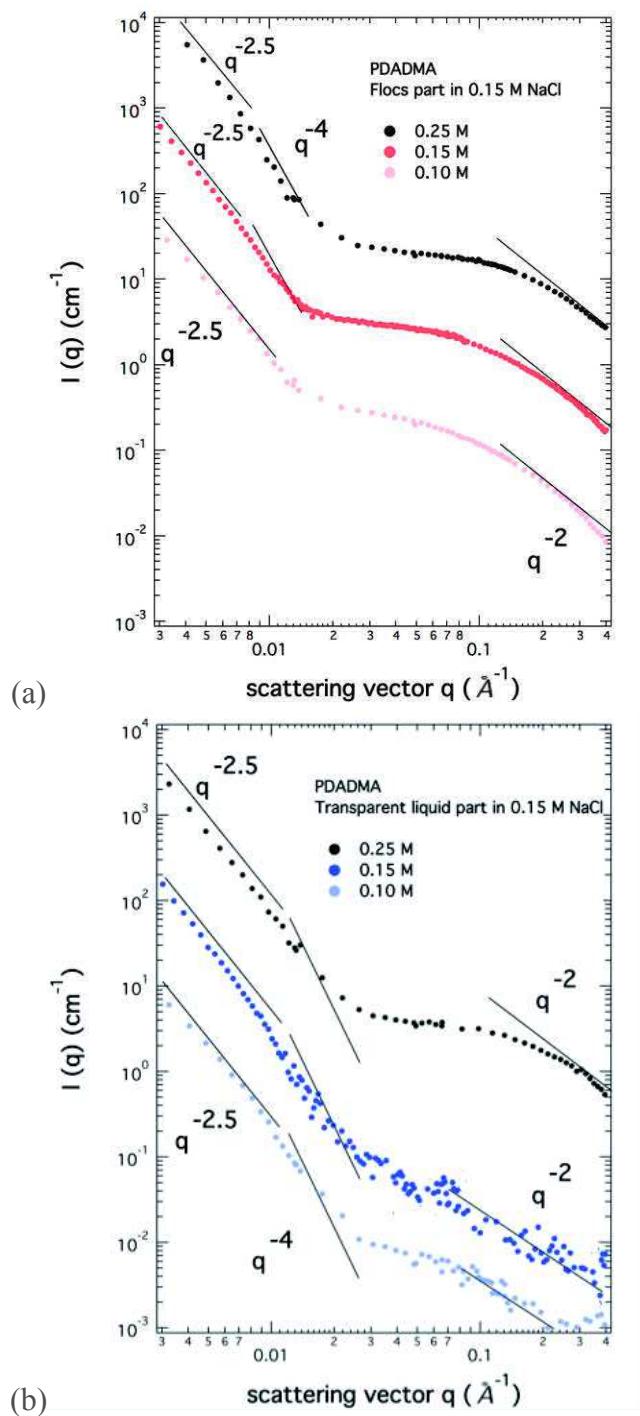
Figure 6.41. SANS signal of the PDADMA macroions as a function of PEC concentration in 'flocs' (a) and 'transparent liquid' (b) parts of PSSNa-PDADMAC complexes formed in the presence of 0.15 M NaCl. The SANS curves are shifted by a factor 10 to avoid their superimposition

6.2.6. Role of the complex preparation procedure

6.2.6.1. PEC preparation through direct mixing of two PE solutions: influence of the mixing order

The complexation between oppositely charged PSS and PDADMA macroions in semidilute or concentrated aqueous solutions was proposed to be analysed as a gelation process. We have shown that the polyelectrolyte complex structure can be gel-like. Most of gels have inhomogeneous morphology that strongly depends on the way in which they have been formed. Thus, it is reasonable to study first the effect of the mixing order. Three preparation procedures were used: by pouring the PDADMAC solution out into the PSSNa one (protocol 1), the reverse by pouring the PSSNa solution out into the PDADMAC one (protocol 2) and finally by a simultaneous mixing of both polyelectrolyte solutions (protocol 3).

The macroscopic observations show the difference in the location of the 'flocs' phase in the vial after the phase separation. Thus, the 'flocs' phase is at the top of the vial after demixing when the PDADMAC solution is poured out into the PSSNa one. For the other mixing orders, the 'flocs' phase is at the bottom of the vial.

SAXS characterization

The previously discussed five concentrations (0.10 M, 0.15 M, 0.20 M, 0.25 M, 0.30 M) along the charge stoichiometric line in the state diagrams were investigated for both cases in the absence and in the presence of an added salt (0.15 M NaCl), i.e. both distinct ionic strengths. All samples display the similar scattering behaviour. The SAXS patterns measured from 0.3 M PEC aqueous solutions are presented as examples in Figures 6.42 and 6.43. For these largest concentrated solutions, the differences are indeed more significant.

The way of the PEC preparation does not affect the q^{-4} scattering law associated with the scattering signal of the single polyelectrolyte chains at $q > 0.15$ Å^{-1}. Specifically, it is the footprint of the condensed counterions onto the free macroions. A weak correlation peak, or a maximum, is observed at $q \sim 0.37$ Å^{-1}. The same correlation peak has already been reported for PSS-PDADMA complexes by Schlenoff using SANS[241]. A similar peak was also noticed for highly concentrated aqueous solutions of PSSNa, close to the bulk by Lorchat[30]. It was explained by the existence of clusters corresponding to the associations of dipoles formed by the monomer units and the condensed counterions due to the drastic change in the dielectric constant of the medium occurring at high polyelectrolyte concentration (ionomer regime). Then, the correlation peak results from the

impenetrability of the clusters that behave like hard spheres. Its position q* allows measuring the size of the clusters ($\xi = 2\pi/q^*$). Here, the same explanation could be used. The dipoles are however formed this time by the complexes of oppositely charged monomers, i.e. they are the junctions and the clusters are the primary associations in between junctions leading to heterogeneities. Surprisingly, the size of the primary associations is the same than the one of the clusters observed in the binary system PSSNa in H_2O. The maximum at high q-value (q ~ 0.37 Å^{-1}) could also correspond to a simple intramolecular characteristic, as the first maximum of the form factor of a hollow-cylinder associated with the condensed counterions onto the free macroions. However, such a maximum could only be observed at a slightly high q-value (q ~ 0.5 or 0.6 Å^{-1}). So, this last explanation is not realistic.

In the intermediate q range, 0.02 Å^{-1} < q < 0.2 Å^{-1}, the position of the classical polyelectrolyte peak is independent of the way of preparing the PEC solutions and is defined by the concentration of the initial stock solutions. In this q range the scattered amplitude changes according to the way of preparing the samples presumably due to the influence of the scattering signal associated with the heterogeneities, $I(q)_{cluster}$. At small q-values, we have:

$$I(q) = I(q)_{PE} + I(q)_{cluster}. \tag{130}$$

where $I(q)$ is the total scattered intensity; $I(q)_{PE}$, that of the semidilute or concentrated interpolyelectrolyte solution.

At small q values (q < 0.02 Å^{-1}) the scattering curves from 'flocs' phase, or gel samples, successively display the scaling laws $q^{-2.5}$ and q^{-4}, but the amplitudes of the scattered intensities are distinct. Consequently, this difference affects the scattering amplitude in the intermediate q-range, where the PE peak is observed q*. In Figure 6.42 the formation of the clusters with a well-defined shape is visible in the q-range 0.016 < q < 0.022 Å^{-1}.

(a)

(b)
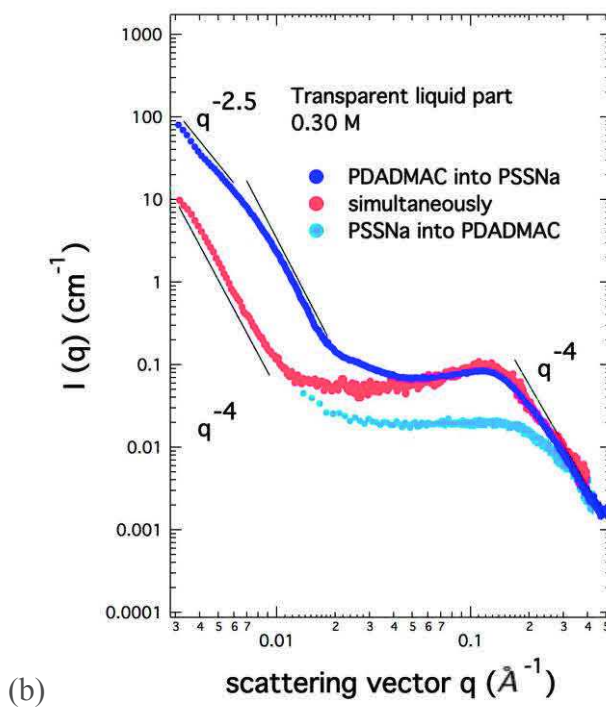
Figure 6.42. Effect of the preparation procedure on SAXS scattered intensities from 'flocs' (a) part and 'transparent liquid' part (b) for the complexes formed by mixing salt-free aqueous solutions of 0.6 M PDADMAC and 0.6 M PSSNa
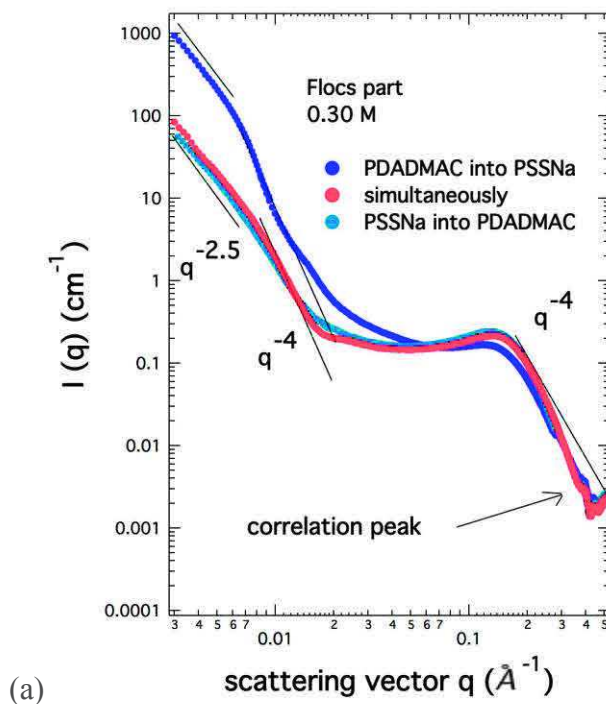
157

(a)

(b)
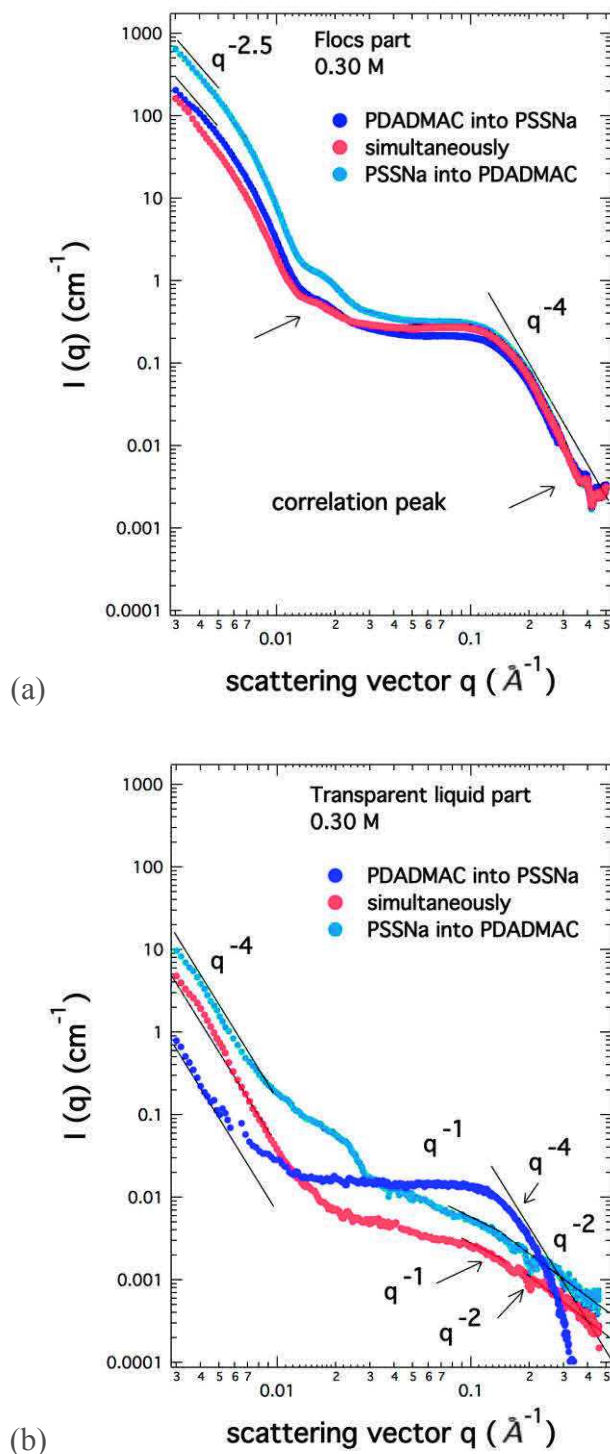
Figure 6.43. Effect of the preparation procedure on SAXS scattered intensities from 'flocs' (a) part and 'transparent liquid' (b) part for the complexes formed by mixing 0.15 M NaCl aqueous solutions of 0.6 M PDADMAC and 0.6 M PSSNa

In 'liquid' phase, or sol phase, of salt-free complex solutions (Figure 6.42 (a)), the way of preparing samples mainly influences the formation of the heterogeneities. And, consequently, the scattered intensity in the q-range 0.015 Å^{-1} < q < 0.18 Å^{-1} is affected by the scattering signal of the

clusters. Remarkably, in the 'liquid' phase of the PEC solutions in the presence of an added salt and at high q-values ($q > 0.2$ Å^{-1}), the scattered intensities from samples prepared following the protocol 2 (PSSNa solution into PDADMAC one) and protocol 3 (simultaneous mixing) display the scattering law q^{-2} instead of q^{-4}. We can explain this change by a complete counterion release during the complex formation through both these two ways.

There is a correlation between the 'flocs' phase, or gel phase, and the 'liquid' phase, or sol phase, by considering the amplitude of the scattered intensity. It is higher in the gel phase when it is lower in the sol phase.

SANS characterization

We prepared the samples following the same three protocols for studying by small-angle neutron scattering using the contrast variation method the effect of the mixing order on the structure of each polyelectrolyte in the formed complexes. We investigated just the lowest concentration on the charge stoichiometric line, 0.10 M, in two D$_2$O-H$_2$O mixtures (the related curves are not shown). The measurement of the PSS partial scattering function was carried out from PSSdNa-PDADMAC in a D$_2$O-H$_2$O mixture with a D$_2$O volume fraction φ(D$_2$O) = 3%. The study of the PDADMA partial scattering function was performed from PSS$_d$Na-PDADMAC in D$_2$O. The conclusions based on SANS are in good agreement with those based on SAXS. The mixing order of the polyelectrolyte solutions mainly affects the large-scale heterogeneities and does not strongly affect the structure of the interpolyelectrolyte network. The PSS polyanion separates roughly equally between both phases. The large fraction of PDADMA polycation stays in the 'flocs' phase. This disproportion of PDADMA leads to a difference in the amplitude of the scattered intensities in 'flocs' and 'liquid' parts.

6.2.6.2. PEC preparation through dialysis of a brine solution of PE mixture

We have already described the structure of the complexes prepared through three protocols of mixing. We also tested the structure of the complexes formed between poly(diallyldimethylammonium chloride) and poly(sodium styrene sulfonate) according to a 'dialysis' or 'desalting' way of preparing them (protocol 4) as well as the mixing of 0.30 M NaCl stock aqueous solutions (protocol 5). These two additional preparation methods were implemented just for a complex concentration 0.10 M (so formed by mixing 0.20 M PE solutions). Such a PSSNa-PDADMAC system is close to the transition line between the biphasic and the colloid zones in the state diagrams. At this concentration, the ionic strength of the system $I = \sum C_i Z_i^2$ is mainly controlled by the low-molecular weight added salt as compared with the other concentrations in the biphasic

region. Thus, the slight increase in salt concentration could easily force to move this 0.1 M PEC system from the biphasic region to the colloid domain. It is demonstrated in Figure 6.44.
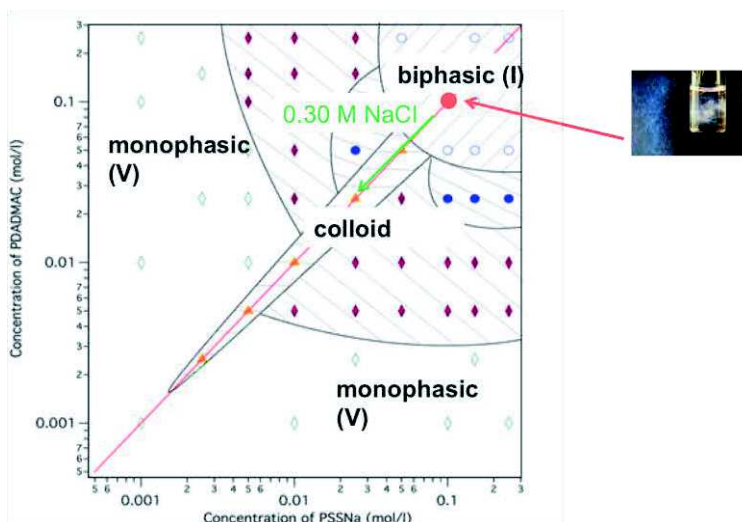

Figure 6.44. The state diagram of PDADMAC-PSSNa aqueous solutions, prepared in the presence of 0.15 M NaCl, with the marked location of 0.10 M complexes (red point)

Dialysis. The stock solutions of PDADMAC and PSSNa were prepared in 2.5 M NaCl aqueous solutions. The salt concentration was chosen based on the work of Schlenoff, where it was shown the possibility to dissolve the already formed PDADMA-PSS complexes using 2.5 M solution of low-weight molecular salt[207,232]. After mixing, the system was dialyzed against deionized water with a 10 kD cutoff membrane. The volume of the dialysis bath was 100 times larger than that of the sample. The kinetics of desalting was controlled by conductivity measurements ($\leq$ 1 μS). The whole process reached a stationary and final state in 24 hours. The formed complexes are large grey aggregates.

(a)

(b)
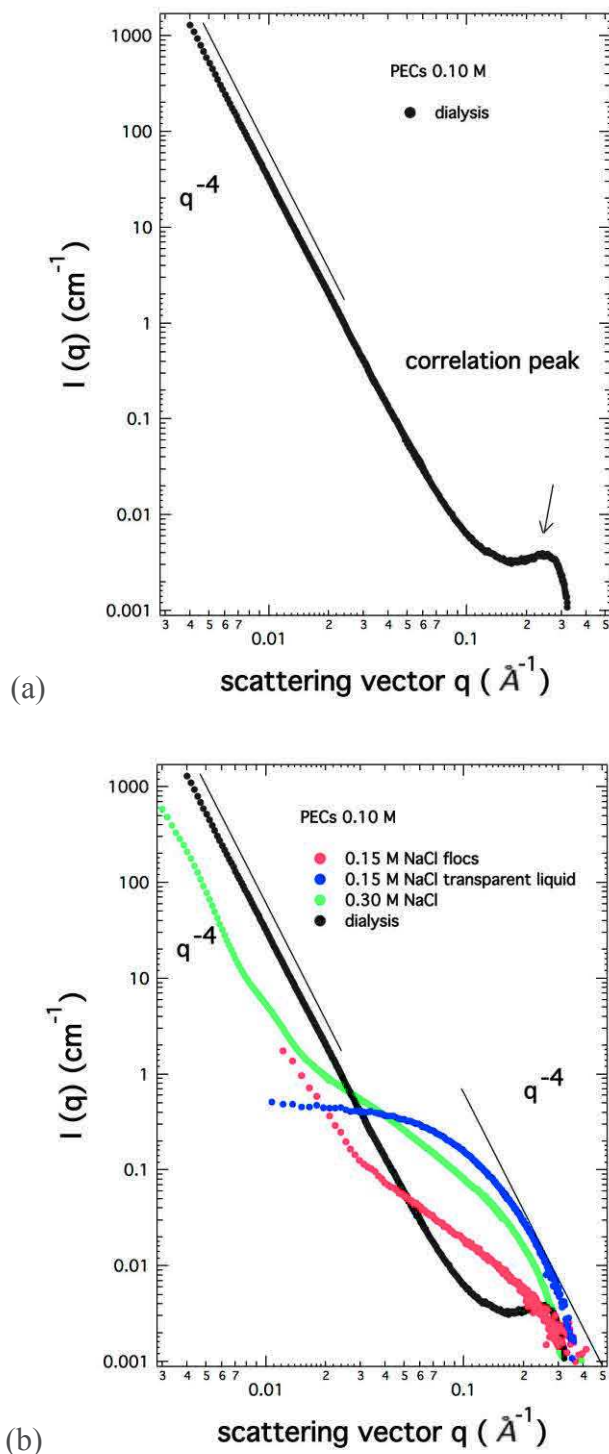
Figure 6.45. SAXS patterns measured from the PSSNa-PDADMAC complexes formed through mixing 0.20 M stock solutions of both polyelectrolytes. The black dots correspond to PECs prepared through the dialysis way (a, b). The green dots show the scattering signal from PECs in 0.30 M NaCl aqueous solution (b). The biphasic case of 0.15 M NaCl system are presented in red ('flocs' phase) and blue ('transparent liquid' phase) (b)

The SAXS pattern obtained from the PSSNa-PDADMAC system, formed following the dialysis protocol, is shown in Figure 6.45 (a). The presence of the large and dense aggregates is indicated by the characteristic decay q^{-4} of the scattered intensity for $q < 0.1$ Å^{-1}. No Guinier regime

161

(qRg < 1) is observed for these aggregates. We can just estimate that their size is larger than 250 Å (or 25 nm). However, the scattered intensity has a correlation peak at q ~ 0.25 Å^{-1}. We suggest that these large particles are dense mixed system of overlapping polyelectrolytes. The position q* of the correlation peak corresponds to a mesh size ξ ~ 25 Å (ξ ~ 2π/q*) for the interpenetrated polymer chains. This q* value could be compared with the q* measured from the concentrated aqueous solutions of PSSNa and PDADMAC. This value of q* for the correlation peak, 0.25 Å^{-1}, belongs to the bulk regime of these polyelectrolytes[30], i.e. beyond the semidilute and concentrated regime in the framework of the isotropic model of de Gennes). The dialysis way of preparing the complexes leads to a drastic increase in the complex density in comparison with the structure of the stock solutions.

0.3M NaCl. Higher salinity of the stock solutions prevents the separation into two phases. Instead of gel and sol phases as in the case of 0.15 M NaCl, large soluble aggregates are formed. The SAXS signal from these complexes is shown in Figure 6.45 (b). We add the SAXS measurements from the complexes formed in a 0.15 M NaCl aqueous solution and according to the dialysis way for comparison. At q > 0.02 Å^{-1}, the scattered intensity corresponds to the structure of the mixed polyelectrolyte or interpolyelectrolyte network. At q < 0.02 Å^{-1}, the upturns with a q^{-4} scattering behaviour comes from the large-scale dense aggregates.

6.2.7. Complexes formed outside the charge stoichiometry: titration pathways

Since the complexation between oppositely charged polyelectrolytes was proposed to be viewed as a gelation process, we studied the change in the scattered intensity as the concentration of one macroion was varied. This scenario allows concerning one polyelectrolyte as the reaction bath for gelation and the other one as the gelling agent. The ways for the change in concentration of the latter are shown in Figure 6.46. Red line (series 1) presents the series of samples formed by adding the solution of PDADMAC of fixed concentration (0.5 M) into the PSSNa solutions of identical volume, increasing C(PSSNa) from 0.01 M towards 0.5 M. Blue line (series 2) corresponds to the variation in the PDADMAC concentration while that of PSSNa, C(PSSNa), is maintained equal to 0.5 M.
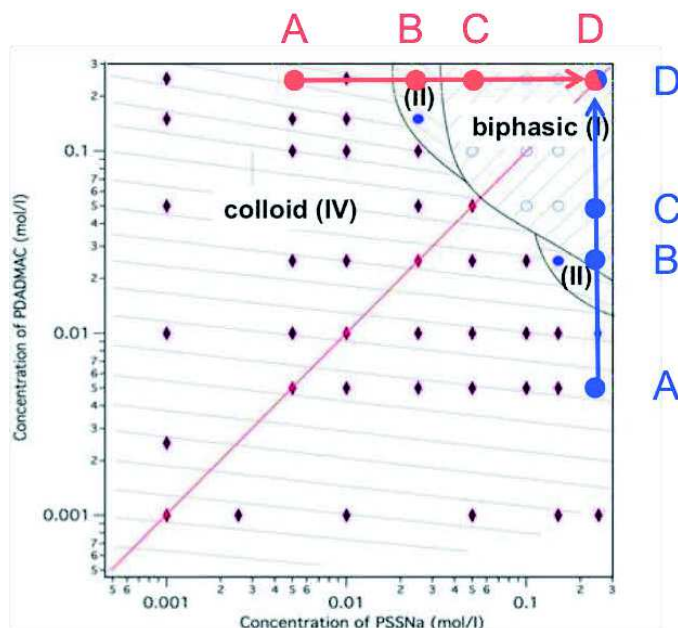
Figure 6.46. The state diagram for the salt-free aqueous solutions of PSSNa-PDADMAC complexes with marked concentration lines. Red line (series 1) corresponds to the variation in concentration of PSSNa; blue line
(series 2), to the variation in concentration of PDADMAC

We remind the equivalent phase diagram proposed by de Gennes for gelating system of the semidilute polymer solution in a good solvent (Figure 6.47)[11]. There is a one-phase region that corresponds to homogeneous systems. This region is divided with a coexistence line into two parts: one-sol phase and one gel phase. At some critical values of the concentration of the gelling agent, J is actually an attractive interaction energy, the sol phase or the gel phase divides into two phases: a sol and a gel. The compositions of the formed sol and gel phases depend on the concentration of the monomer units and the concentration of the gelling agent. A gelation process in the presence of solvent always brings in a trend towards segregation of the gelating species. The demixing proceeds in the system due to the precipitation of the dense clusters. Gelation prevents precipitation because of the crosslinking. This phase diagram is the representation of the competition between gelation and precipitation.
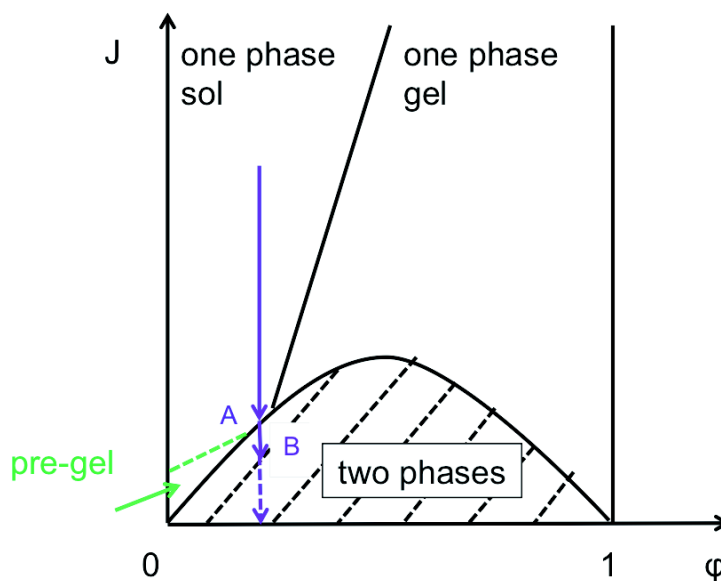
Figure 6.47. Equivalent phase diagram proposed by de Gennes for a gelating system in semidilute solutions with a good solvent. φ is the monomer concentration; J, the inverse of the concentration of gelling agent or the temperature of the corresponding lattice gas. The green line shows the limitation region of the analogy between a gelation process of polymers and a complexation process of oppositely charged polyelectrolytes in semidilute and concentrated regimes

The measured scattering patterns from studied samples are shown in Figure 6.48 (series 1) and Figure 6.49 (series 2). Colloidal associations (A) (violet curves in scattering patterns) are proposed to be the precipitation of large clusters with internal gel-like structure, but without integration into the polyelectrolyte network. In the theoretical phase diagram these samples A remain a sol, at which some gel begins to precipitate. The increase in the concentration of the gelling agent brings PEC systems to the biphasic region (B, C, D): 'flocs' aggregates reveal a gel and a transparent liquid that possesses a pre-gel structure. The separation occurring between two gel phases has not been described by de Gennes. The marked with the green dash line region could be a limitation in the analogy between the complexation and the gelation processes. The most probable reason is that the gelling agents are longer and more extended than in the de Gennes's model.

The change in the scattered intensity with the variation of the gelling agent concentration is more visible, or significant, in the series 1 (Figure 6.48), when the gelling agent is PSSNa (Figure 6.49). We can recall that for X-ray radiation the contrast of PDADMAC in H_2O is low. It makes the analysis of the series 2 more difficult, as the scattered intensity does not strongly change with the increase in the PDADMAC concentration.

(a)

(b)

Figure 6.48. Change in the scattered intensity from the PSSNa-PDADMAC complexes with the variation of
the PSSNa concentration (series 1): measurements from 'flocs' (a) and 'transparent liquid' (b) parts
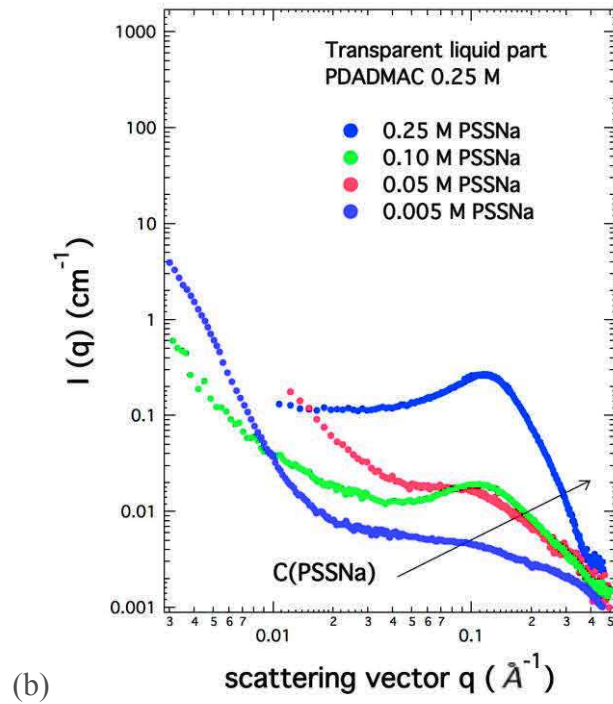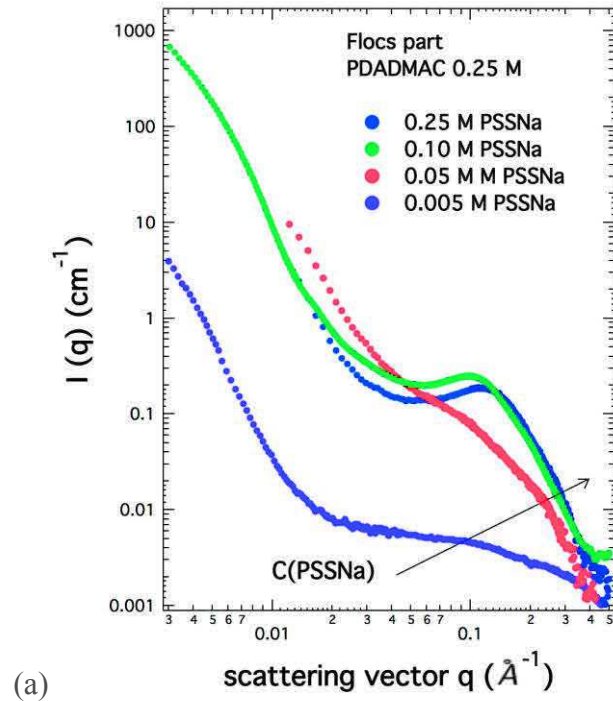
(a)

(b)
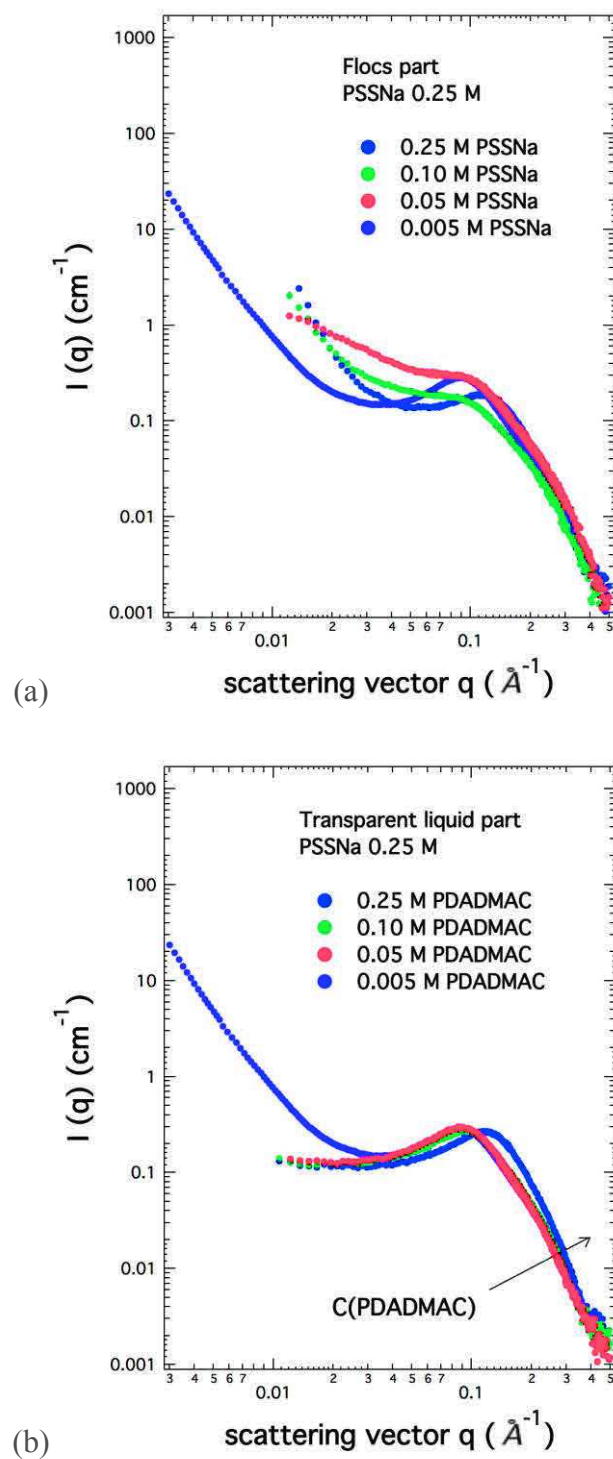
Figure 6.49. Change in the scattered intensity from PSSNa-PDADMAC complexes with the variation of the PDADMAC concentration (series 2): measurements from 'flocs' (a) and 'transparent liquid' (b) parts

6.2.8. Cryo-transmission electron microscopy
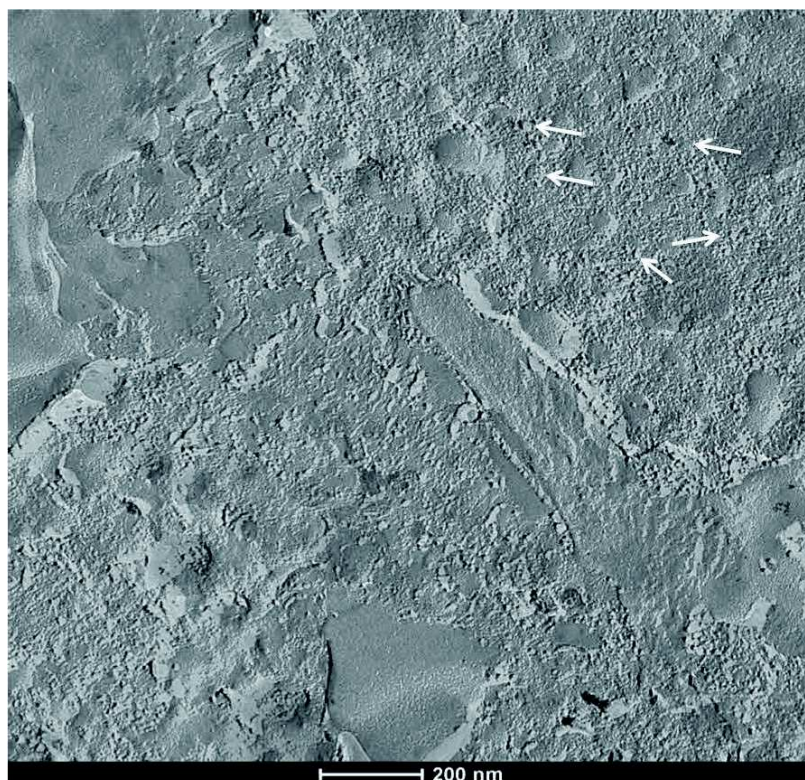
Figure 6.50. TEM-image after cryo-fracture cut of the flocs part of PSSNa-PDADMAC prepared through mixing salt-free 0.3 M solutions of the polyelectrolytes

TEM-image of the gel or flocs part of 0.30 M salt-free aqueous solution of PSSNa-PDADMAC complexes after cryo-fracture (Figure 6.50) displays objects of finite size. These objects are displayed with black and white spots, while grey regions of the image correspond to sample part without any structural elements.

The randomly located dense clusters (black and white spots) are polydisperse in shape and have the approximate size of 30-60 nm. These visible objects in the structure of the PDADMAC-PSSNa complexes correspond to the heterogeneities or clusters of junctions, formed between oppositely charged polyelectrolyte units. This result is coherent with the ones obtained from SAXS and SANS measurements. Such heterogeneities have q^{-4} scattering behaviour at low q values ($q < 0.01$ Å^{-1}).

6.3. Conclusions

We have carried out a comparative study of the complexation between oppositely charged flexible PSS and semiflexible PDADMA in dilute and semidilute or concentrated aqueous solutions. Both thermodynamics or macroscopic, and structural or microscopic, points of views were considered. The complexation between these two model polyelectrolytes proceeds at the charge ratio equal to 1, independently from the component concentration regime, the ionic strength, and the preparation procedure. The exothermic and entropy-driven interactions between PSS and PDADMA are suggested to consist of two steps based on the ITC investigations. In dilute solution, the primary process is the formation of highly charged polyelectrolyte complexes of size 73-105 nm. The secondary process is an aggregation one that makes the particles of size 220 nm that strongly scatter light. In semidilute and concentrated solutions the complexation can be viewed as a gelation process, in which the network of one polyelectrolyte can be presented as the gelation bath and the second one plays a role of the gelling agent. The attractive electrostatic interaction allows forming interchain bridges equivalent to chemical crosslinks that can be considered as resulting from the primary process. Obviously, these junctions tend to form clusters, or heterogeneities, that are superimposed on the network structure. That is like a secondary process leading to a more complex structure quite analogous to that of the usual chemical gels. The clusters are polydisperse in shape and size (>20 nm) and can lead to some macroscopic turbidity.

These two distinct routes for the complexation process and the resulting complex structure depend on the initial polyelectrolyte concentration or regime. They could be yet recognized visually due to the different phase separation phenomena. The state diagrams with variation in the ionic strength were established summarizing the macroscopic investigations. They involve monophasic colloidal and biphasic regions. The aspects of the state diagrams are in agreement with the calculated ones from the Overbeek-Voorn theory and show limitations in the analogy with the theoretical phase diagram for the gelation in the polymer semidilute solution proposed by de Gennes.

These results are completed with detail investigations of the complex structure through the use of such useful tools as small-angle X-ray and neutron scattering with hydrogen/deuterium labelling and Cryo-TEM microscopy. We suggest the formed mixed polyelectrolyte network corresponds to the 'scrambled eggs' model for polyelectrolyte complexation and is defined by the initial PDADMAC solution structure of the 'concentration blobs'. The different preparation procedures (mixing or desalting kinetics), the different mixing orders, the initial or stock polyelectrolyte solutions and the

ionic strength mainly affect the structure of heterogeneities. The material disproportion of PDADMA and the different charge distributions between the distinct phases were proposed based on the analysis of the partial scattering functions as well as the charge and density structure functions. On the contrary, PSS separates roughly equally between both phases. Such an asymmetry in the polyelectrolyte complexes decreases with the addition of a monovalent salt, or an increase in the ionic strength. This asymmetry still insures the electroneutrality condition, as monovalent ions of the additional salt are able to have a different concentration in both phases. This type of phase separation during complexation between oppositely charged polyelectrolytes and the charge distribution has been described in details by Zhang and Shklovskii.

The colloids are suggested to be large aggregates with an internal structure of densely compacted overlapping polyelectrolytes. An effort has to be made for studying the structure of dilute complexes and this part of the study stays for the future research on the subject.

Chapter 7

Sodium Hyaluronate - Poly(diallyldimethylammonium Chloride) Complexes

7.1. Complexes formed in the dilute regime

7.1.1. Combined ITC, DLS and zeta potential measurements

The complexation between oppositely charged sodium hyaluronate (HANa) and poly(diallyldimethyl ammonium chloride) (PDADMAC) in the dilute regime was investigated from the thermodynamic point of view with isothermal titration calorimetry (ITC). To study the correlation between the thermodynamics of the complexation process and the size and charge changes during this process, the same experimental protocol was used for dynamic light scattering and zeta potential measurements. The procedure and the experimental conditions were kept similar to the ones used for investigating the PSSNa-PDADMAC polyelectrolyte complexes. They have been explained in details in Chapter 6.1.1. Now, we mainly focus on the effects of the ionic strength and the mixing order of the polyelectrolyte solutions on the thermodynamics of the PEC formation. We remind that the hyaluronate (HA) is a negatively charged macroion while the poly(diallyldimethyl ammonium) (PDADMA), a positively charged one with therefore a positive zeta potential.

The thermograms and the binding isotherms obtained from the HANa-PDADMAC systems are presented in Figures 7.1-7.4. All titration curves, except the one corresponding to the addition of HANa into PDADMAC solutions in 0.15 M NaCl (Figure 7.4.), show a sigmoidal shape or close to it. In the case of the addition of HANa into PDADMAC solutions in 0.15 M NaCl, the binding isotherm decreases exponentially. The reaction heat associated with the complexation in the absence of added salt goes from negative (endothermic) to positive (exothermic) as the mole ratio, Z = PDADMA/HA or HA/PDADMA, is increased. The enthalpy of the complexation, or binding enthalpy, of the rest PEC formation always remains negative, or endothermic.

(a)

(b)

(c)

Figure 7.1. HANa-PDADMAC complex formation (titration by addition of the PDADMAC salt-free aqueous solution into the HANa one): (a) thermogram (top) and binding isotherm (bottom) as a function of time and the Z=PDADMA/HA mole ratio, respectively. Hydrodynamic diameter D_H (b) and zeta potential ζ (c) as a function of the Z=PDADMA/HA mole ratio. The normalized heat is corrected by subtraction of the dilution component

(a)

(b)

(c)
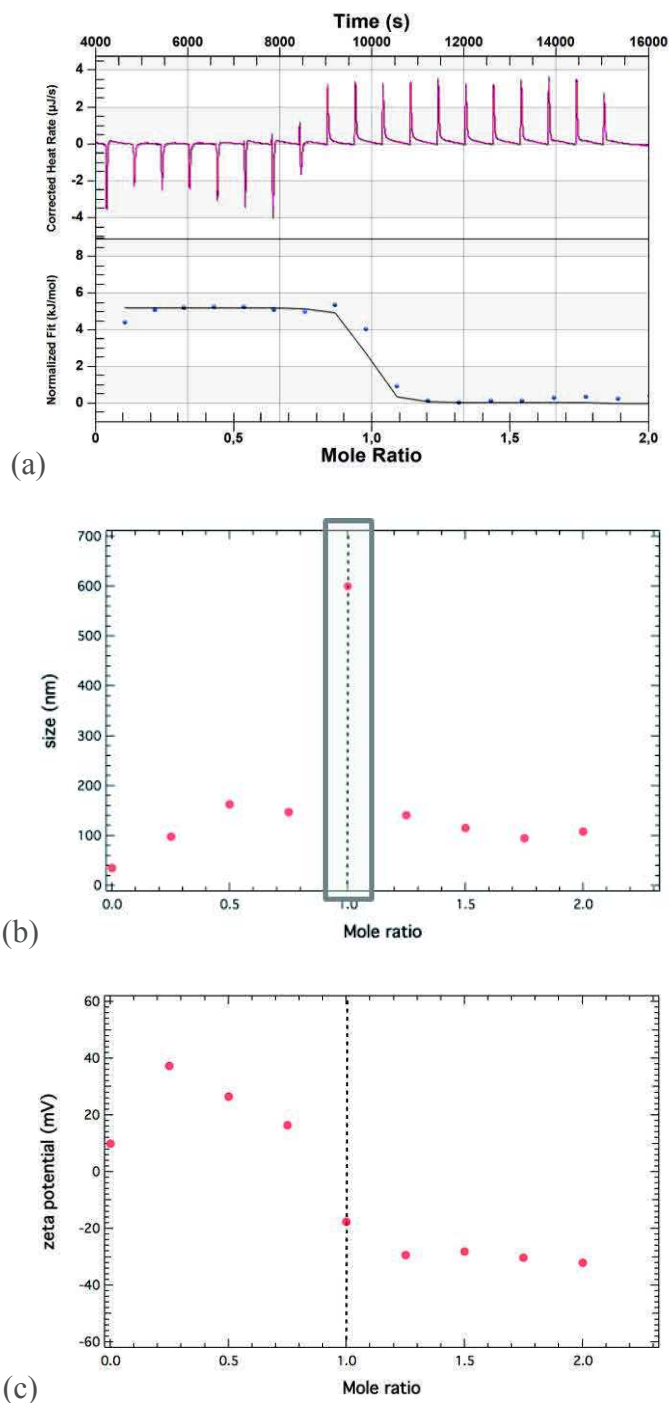
Figure 7.2. HANa-PDADMAC complex formation (titration by addition of the HANa salt-free aqueous solution into the PDADMAC one): (a) thermogram (top) and binding isotherm (bottom) as a function of time and the Z=HA/PDADMA mole ratio, respectively. Hydrodynamic diameter D_H (b) and zeta potential ζ (c) as a function of the Z=HA/PDADMA mole ratio. The value of D_H was set at 600 nm only to display the abrupt in size and corresponds to the case, where the measured size of complexes was out of the equipment limitation. The normalized heat is corrected by subtraction of the dilution component

Figure 7.1 shows the relationship between the binding enthalpy ΔH, the hydrodynamic diameter D_H and the zeta potential ζ by mixing the salt-free PDADMAC aqueous solution into the HANa one. The addition of the polycation PDADMA initiates the complexation with formation of negatively charged (-34 mV) particles of average size 120 nm. Next injection of PDADMA slightly increases the complex size. The variation of D_H with the mole ratio Z=PDADMA/HA displays a 'W'-shape with a local minimum at Z=0.75. The values of the hydrodynamic diameter are between 102 and 158 nm. The addition of PDADMAC decreases the absolute value of the negative charge up to Z equals 1. At Z=1 the zeta potential increases rapidly until a high positive value (+20.3 mV) and continues to grow slightly with further additions of PDADMAC. Thus, two critical points are observed at: Z=0.75 and Z=1. In parallel, the binding isotherm shows two inflection points, which can be typically originated from the presence of two types of independent binding sites on the polysaccharide. However, the dissociated carboxyl group is the only interacting group on the hyaluronate. Therefore, the two inflexion points are more indicating that two different steps are involved in the complexation process. In the first step or first plateau, the interaction between PDADMAC and HANa takes place until the saturation of HA by PDADMA, corresponding to the first plateau. This part of the complexation is endothermic. The positive binding enthalpy can be interpreted as an outcome of the breaking of the intra- and intermolecular H-bonding in the hyaluronan structure. Then, the second step begins with the plateau and takes place till the mole ratio Z=1. The saturation of the second step of the process indicates the moment when all possible oppositely charged groups in the titration mixture have reacted. The difference in the behaviour of the reactive groups could be explained due to the interaction with nonspecific nature (solvation and hydrophobic interactions, H-bonds etc)[151,242] and hydration as well as conformational changes.

In the reverse mode always using the salt-free aqueous solutions (the salt-free HANa aqueous solution is poured into the salt-free PDADMAC aqueous solution), just after the first injection of the polyanion, the formed complexes have an average hydrodynamic diameter 97.5 nm and an effective charge corresponding to +37 mV (Figure 7.2). The particle charge decreases continuously with the mole ratio Z=HA/PDAMA. It becomes negative for Z≥1. The ζ-potentials of PECs at low and high Z values in direct and reverse mixing orders are in perfect symmetry. The value of ζ is -20 mV at Z=1 for both ways of complex preparation. The hydrodynamic diameters of PECs D_H, obtained using the reverse protocol, are varied between 97 and 160 nm. At the charge stoichiometry (Z=1), D_H drastically increases up to values, which are out of the equipment limitation. The binding enthalpy is endothermic below Z=1 and exothermic above it.
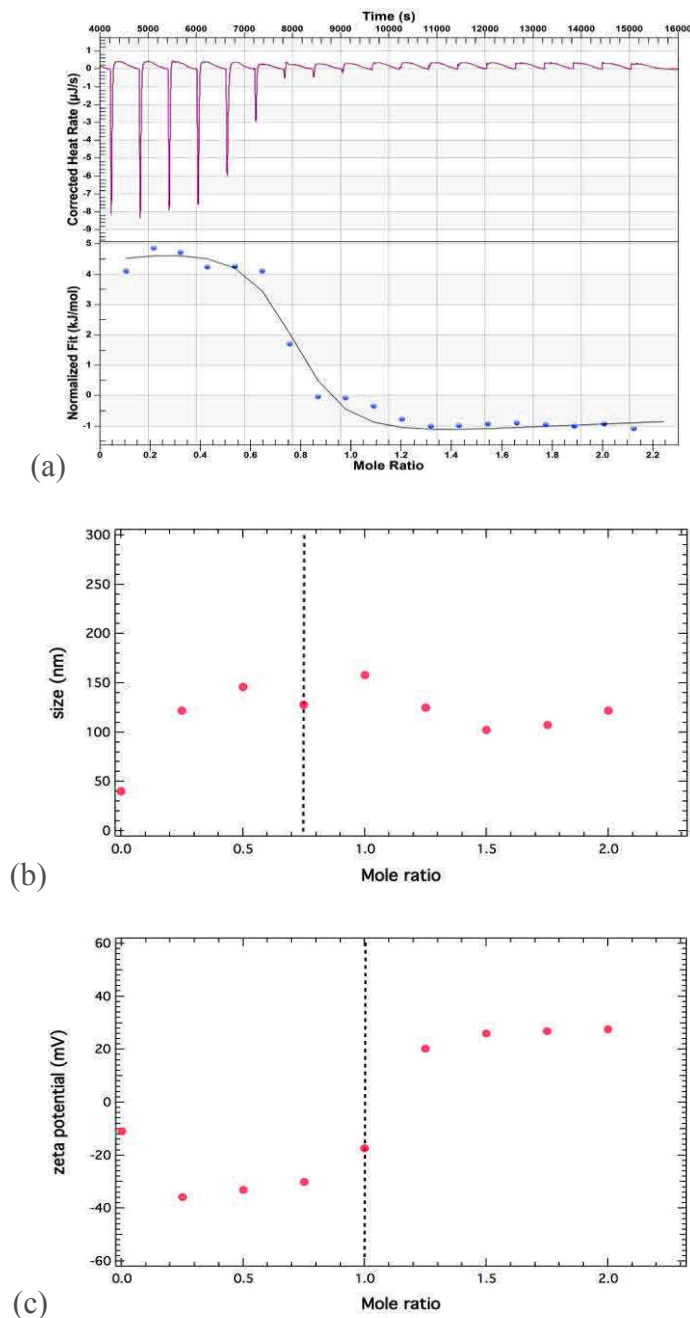
Figure 7.3. HANa-PDADMAC complex formation (titration by addition of the PDADMAC aqueous solution into the HANa one, both in the presence of 0.15 M NaCl): (a) thermogram (top) and binding isotherm (bottom) as a function of time and the Z=PDADMA/HA mole ratio, respectively. Hydrodynamic diameter D_H (b) and zeta potential ζ (c) as a function of the Z=PDADMA/HA mole ratio. The normalized heat is corrected by subtraction of the dilution component. Grey rectangle shows cases, where the measured size of complexes was out of the equipment limitation (hydrodynamic domain $qR_h<1$)
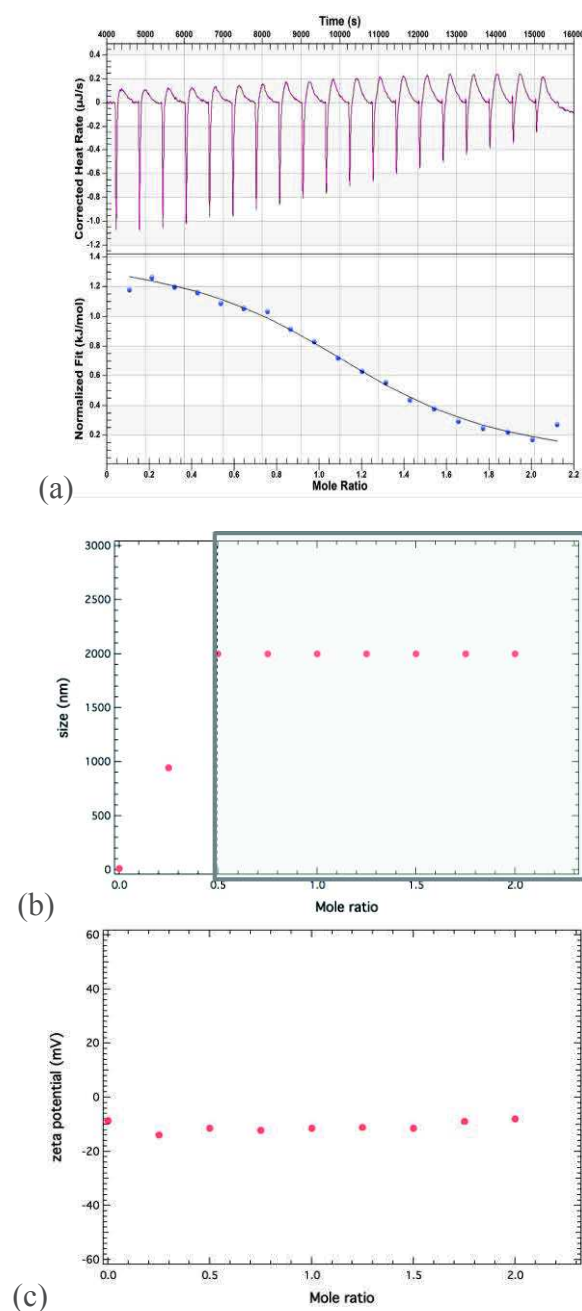
(a)

(b)
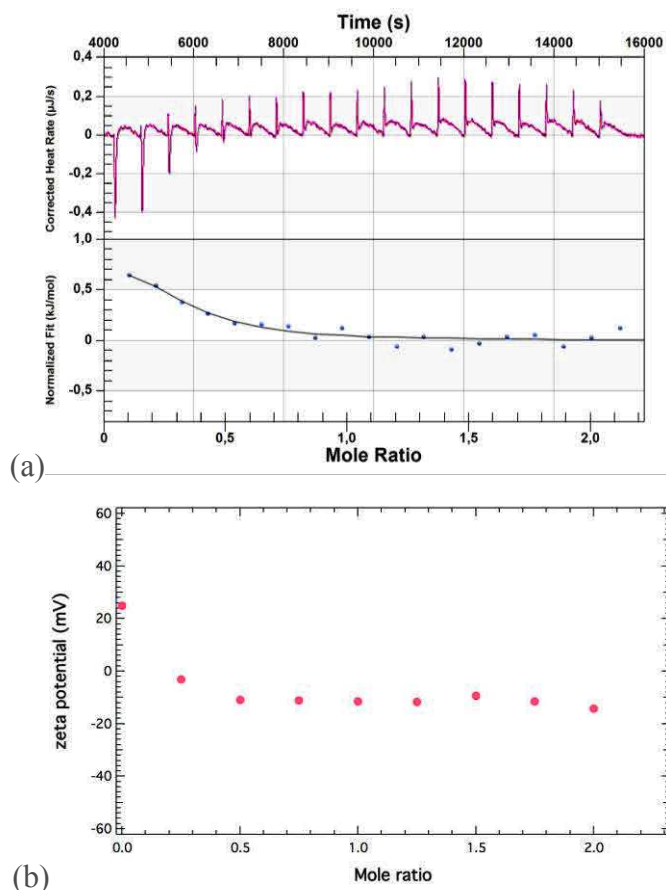
Figure 7.4. HANa-PDADMAC complex formation (titration by addition of the HANa aqueous solution into the PDADMAC one, both in the presence of 0.15 M NaCl): (a) thermogram (top) and binding isotherm (bottom) as a function of time and the Z=HA/PDADMA mole ratio, respectively. Hydrodynamic diameter D_H (b) and zeta potential ζ (c) as a function of the Z=HA/PDADMA mole ratio. The normalized heat is corrected by subtraction of the dilution component

The thermodynamics of the complex formation is quite different with the presence of an added salt. According to the direct mixing protocol, large complexes of size 900 nm are formed with the first injection (Figure 7.3 (b)). Their size drastically increases with the next injections. Then, the light scattering is no longer appropriate for evaluating their hydrodynamic diameters. D_H was set up at 2000 nm only to show the large size increase, but the real size is out of the equipment limitation. The zeta potential of the complexes shows a slight raise from -14.0 mV to -8.00 mV as the mole ratio Z=PDADMA/HA is increased. The binding enthalpy decreases gradually with the addition of PDADMA.

The change in the mixing order results in similar formation of huge complexes with a size too large to be measured with light scattering (Figure 7.4). Thus, the evolution of D_H with the mole ration

Z=HA/PDADMA is not shown. The zeta potential ξ changes from -3.00 mV to -14.00 mV according to the titration procedure. The binding enthalpy decreases, correlatively with the zeta potential, until no more energy is released. For both mixing orders none transition point can be really defined.

The observation of the structural and size changes is summarized in Table 7.1.

Table 7.1. Characteristics of HANa/PDADMAC complexes formed according to different ionic strengths and titration ways.

System	D_H (nm)	ζ (mV) at low Z	ζ (mV) at high Z	Z of transition
PDADMAC into HANa	120	-34	+28	0.75; 1
HANa into PDADMAC	97.5	+37	-32	1
PDADMAC into HANa in 0.15 M NaCl	$>10^4$	-14	-8	-
HANa into PDADMAC in 0.15 M NaCl	$>10^4$	-8	-3	-

Based on the observations described above, we suggest that the complexation between HANa and PDADMAC is likely a one-step process, in contrary to the PSSNa-PDADMAC complex formation. We remind that the interaction between PSSNa-PDADMAC occurred in two steps: the primary complex formation and then their further aggregation. Two steps were proposed for the addition of the PDADMAC salt-free aqueous solution to the into HANa one, as well. But these two steps come from the different reaction abilities of two kinds of interacting sites and not from the mechanism of the complex formation. In the presence of an added salt, none effective charge transition was observed and PECs remained negatively charged. That means PDADMAC does not compensate all the charges of HA.

7.1.2. Analysis of the ITC data using the independent site model

The thermodynamic parameters of the complexation were calculated by fitting the ITC data with the model of one independent site. The model of two independent sites was used exceptionally for the addition of the PDADMAC salt-free aqueous solution to the HANa one. The main equations have been already given in the Chapter 6.1 for the PSSNa-PDADMAC complexes. The fitting curves are presented in Figure 7.5. The obtained thermodynamic parameters are compiled in Table 7.2.
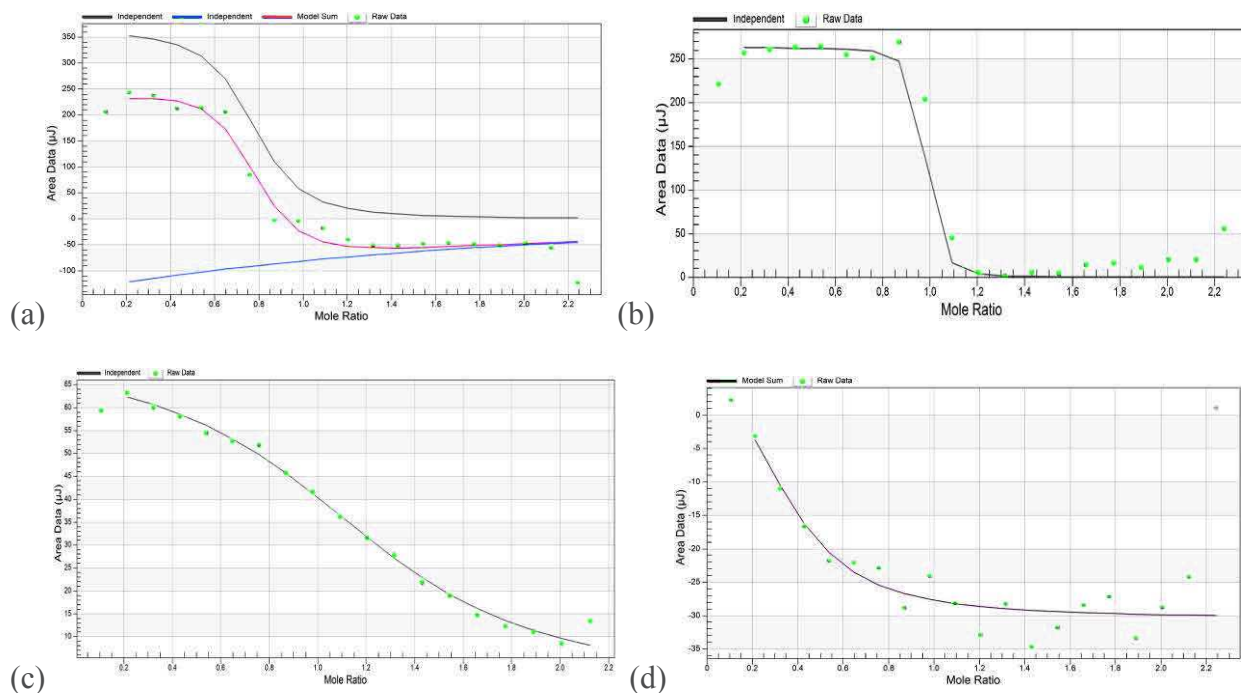
Figure 7.5. Binding isotherms for the HANa-PDADMAC complexes, obtained through different preparation procedures and ionic strengths: PDADMAC into HANa in the absence of added salt (a); HANa into PDADMAC in the absence of added salt (b); PDADMAC into HANa in the presence of 0.15 M NaCl (c); HANa into PDADMAC in the presence of 0.15 M NaCl (d). Black thin lines correspond to the fits of the ITC data by the model of one independent site. In Figure (a) the red line is the summation for a two-step reaction considered for describing the specific case of PDADMAC into HANa in the absence of salt. Black and blue lines then show, respectively, the primary and secondary processes for this case. The green points correspond to the ITC data. Here, we depicted each individual injection without normalization by the amount of titrant in the contrary to the presenting way in Figure 7.1 - 7.4

Table 7.2. Thermodynamic parameters obtained from the fits to the model of independent site. The complexation is characterized by a binding constant K, a stoichiometry n, a bending enthalpy ΔH, a free energy change ΔG and an entropy change ΔS.

Preparation procedure	K, (M^{-1})	n	ΔH, (kJ*mol^{-1})	ΔG, (kJ*mol^{-1})	ΔS, (kJ*mol^{-1}*K^{-1})
PDADMAC into HANa	$9.4*10^5$	0.70	+5.16	-34.1	+131.6
	$1.0*10^3$	1.00	-4.03	-17.1	+43.9
HANa into PDADMAC	$8.8*10^6$	0.93	+5.06	-39.6	+149.9
PDADMAC into HANa in 0.15 M NaCl	$1.4*10^4$	1.20	+1.40	-23.7	+84.4
HANa into PDADMAC in 0.15 M NaCl	$2.3*10^5$	0.36	+0.86	-30.5	+105.3

The interaction between HANa and PDADMAC is associated with a positive binding enthalpy and corresponds to an entropy-driven process whatever the mixing order and the ionic strength for the complex formation. This type of interaction belongs to the entropy-enthalpy compensation phenomena[151]. The gain of enthalpy of the reaction is of the order of $+k_BT$ and the entropy cost of the reaction corresponds to $+10k_BT$. The endothermic characteristic of the reaction could be logically caused by the destroying H-bonding in the hyaluronan structure, but we have not observed any H-bonding in Chapter 5. Thus, the understanding of the real reason of this phenomenon is still under an open question. The Coulomb energy change also depends on the ratio of the Bjerrum length, l_B, and the charge separation distance along the macroion chemical sequence, l_0. In theoretical simulation studies the Coulomb energy change was shown to be the most negative in the range $1.0 < l_B/l_0 < 2.5$ as for PDADMAC and PSSNa polyelectrolytes[44]. For HANa, $l_B/l_0 < 1.0$ and the attractive energy between two oppositely charges of HA and PDADMA is smaller.

The presence of an added salt decreases the binding enthalpy, ΔH, as well as the entropy change, ΔS. This behavior is consistent with the results obtained by theoretical simulations[44,52].

The stoichiometric coefficient n is close to Z=1 in salt-free aqueous solutions and is in a good agreement with the transition observed by DLS and zeta potential measurements. The presence of an added salt strongly shifts the stoichiometry coefficient, n, to the complex formation with high [+]/[-] mole ratio or low [-]/[+] mole ratio. This behavior suggests that, in low salinity solution, PDADMA can interact with few carboxyl groups on the hyaluronan macroion due to its closer conformation and, more generally, polyelectrolytes is a brine solution. That causes lower access to the binding groups. The ITC measurements cannot define which groups exactly participate in the reaction. That issue is out of scope of this study and could be solved with employing another technic (for instance, fluorescence quenching).

The reverse mixing order of polyelectrolyte solutions slightly shifts the stoichiometry coefficient, n, to lower Z values, but does not strongly affect the heat of the reaction. Such a deviation from the stoichiometry has already been observed for DNA-poly(ethylenimine) complexes[92]. It can be ascribed to the involvement of hydrodynamic effects. In heterogeneous polyelectrolyte systems the point of vanishing mobility may not match the point of vanishing charges. These differences in n are related to a conformational change of the polyelectrolyte in complexes, which leads to different electrophoretic behavior, and is more important for macroions with high intrinsic stiffness.

7.1.3. Summary

The interaction between sodium hyaluronate and poly(diallyldimethylammonium chloride) in the dilute solution is proposed to be a one-step process. The complexes formed in salt-free aqueous solutions are charged and have sizes of the order of 100-120 nm. The charges are defined by the polyelectrolyte that is in the measuring cell. In the presence of added salt and for low salt concentration, the PECs are huge aggregates negatively charged. The polyelectrolyte complexation leads to a positive binding enthalpy independently from the ionic strength and preparation procedure. The endothermic character of the reaction, or complexation, could result from the destruction of H-bonds in the hyaluronan structure, but it is not yet completely defined.

The increase in the intrinsic stiffness of the macroanion (HA instead of PSS) relatively to the macrocation (PDADMAC) is accompanied by a decrease in the charge separation distance along the chemical sequence of macroion. That implies two main changes in the thermodynamics of the polyelectrolyte complex formation. There are the decrease in the Coulomb interaction energy, which leads to the positive binding enthalpy, and the shift in the stoichiometry of the complexation.

7.2. Complexes formed in the semidilute and concentrated regimes

7.2.1. Macroscopic state diagrams

The visual observations of the complexes formed by addition a salt-free PDADMAC stock aqueous solution to a HANa one is summarized in Figure 7.6. We remind that this diagram does not correspond to a phase diagram mainly because the various phases are rather far from equilibrium. The red line (the first bisector of the diagram) corresponds to the systems with equal concentration between polycation and polyanion, i.e. the stoichiometric component ratio as well as the stoichiometric electrical charge ratio ([+]/[-]=1). Several regions can be distinguished depending on the concentration range.

In the mixtures of sodium hyaluronate between 0.025 and 0.15 mol/l and ratio [PDADMAC]/[HANa] > 1, an associative phase separation is observed between a supernatant solution (clear liquid, pure solvent or extremely dilute solution of complexes) and a lower, thus dense, phase with yellow tint at the bottom of the vial ('biphasic' (I) region, Figure 7.6). The appearance of

the dense coacervate part is similar to the one given in the literature for other systems[65,69,243] and is considered as a 'single drop'[59]. The coacervation is preferable than precipitation if the one of the interacting component is an anionic polysacharide[209]. The behavior of such type of complexes is close to that of hydrophobic polymers because of the charge neutralization during the complex formation. As suggested by Veis and Aranyi[61,244], the electrostatic interaction first leads to the formation of neutral aggregates and then to the coalescence into a coacervate phase due to hydrophobic interaction.
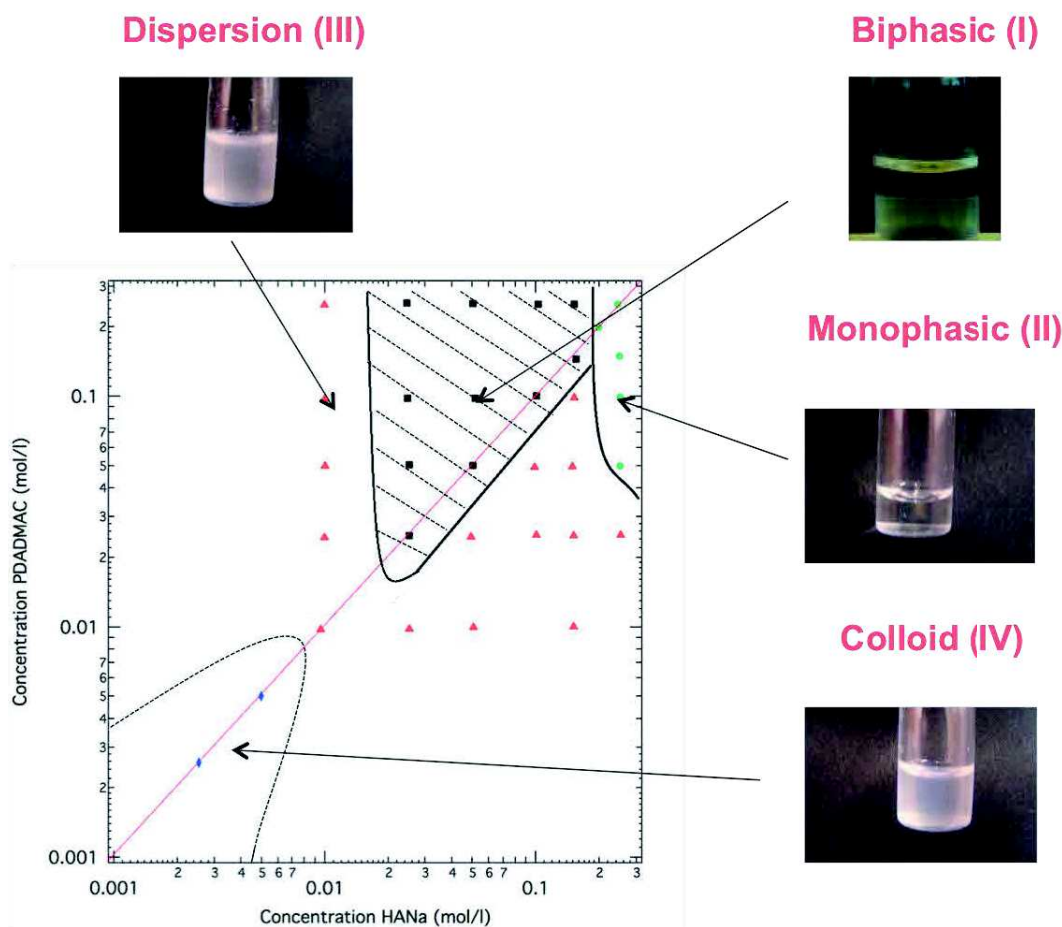
Figure 7.6. State diagram of salt-free HANa-PDADMAC aqueous solutions immediately after mixing the HANa and PDAMAC stock solutions:

■ Biphasic region (I), dense coacervate / supernatant; ● Monophasic region (I); ▲ Dispersion (III); ♦ Colloid (IV). The red line corresponds to the stoichiometric component ratio as well as the stoichiometric electrical charge ratio [+]/[-]=1. The degrees of polymerization of the used polyelectrolytes are: N(HA 3) = 110 and N(PDADMAC J240412) = 190

At C (HANa) = 0.20 - 0.25 mol/l for the mole ratios [PDADMAC]/[HANa] < 1, monophasic gel or highly viscous solution ('monophasic (II)' region) is stable during all visual examination time

(at least 1 month). The monophasic region is formed when the initial HA solution is jammed (above the concentrated regime C > 0.4 mol/L).

The turbid mixtures of dense polymer rich droplets with light yellow tint, shown as red triangle in the state diagram ('dispersion (III)' region), have appearance close to dispersions. The formation of the thick foam on the top of the mixture after shaking confirms the presence the existence of a hydrophobic character of the samples.

At stoichiometric component ratio and low concentration (0.0025 < c < 0.005 mol/l), white colloids that strongly scatter light stay stable for weeks ('colloid (IV)' region). We separated the 'dispersions (III)' region from the 'colloid (IV)' one by a dotted line, which position is rather uncertain and has exceptionally symbolic function. Both of these regions, 'dispersions (III)' and 'colloid (IV)', correspond to the turbid system, but '(IV)' has much smaller particles.

The state diagram of the sodium hyaluronate - poly(diallyldimethylammonium chloride) complexes changes on a time scale between one and two days (Figure 7.7). The 'colloid (IV)' region, formed at low concentrations; as well as the 'biphasic (I)' and 'monophasic (II)' regions are stable during whole the observation time scale. On the other hand, the 'dispersion (III)' region transforms into neighboring domains: the 'biphasic (I)' one, when the ratio between polyanion and polycation is not far from 1, and the 'monophasic (II)' one as the non-stoichiometry of complexes is increased. The symmetry of the state diagram with respect to the stoichiometry line [polyanion]/[polycation]=1 is lost. The complexation in non-equal proportions leads to an asymmetry in the counterion release process and an asymmetry in the electrical charge that improves the solubility of the polyelectrolyte complexes[211]. Thus, the monophasic domain is wider for HANa-PDADMAC then for PSSNa-PDADMAC.

The full state diagram for HANa-PDADMAC complexes achieved in the presence of 0.15 M NaCl was not established due to the limitation of the thesis duration. Just the complexes associated with the stoichiometric line were prepared. The summary of the visual investigations of these HANa-PDADMAC PECs, formed in 0.15 M NaCl, as well as their time evolution is presented in Table 7.3. We consider that these systems reached their background state two days after the mixing of the stock polyelectrolyte solutions. We can remark that the addition of a low-molecular weight electrolyte prevents any phase separation. That is coherent with our previous observations from aqueous solutions of other polyelectrolyte complexes.

(a)   (b)
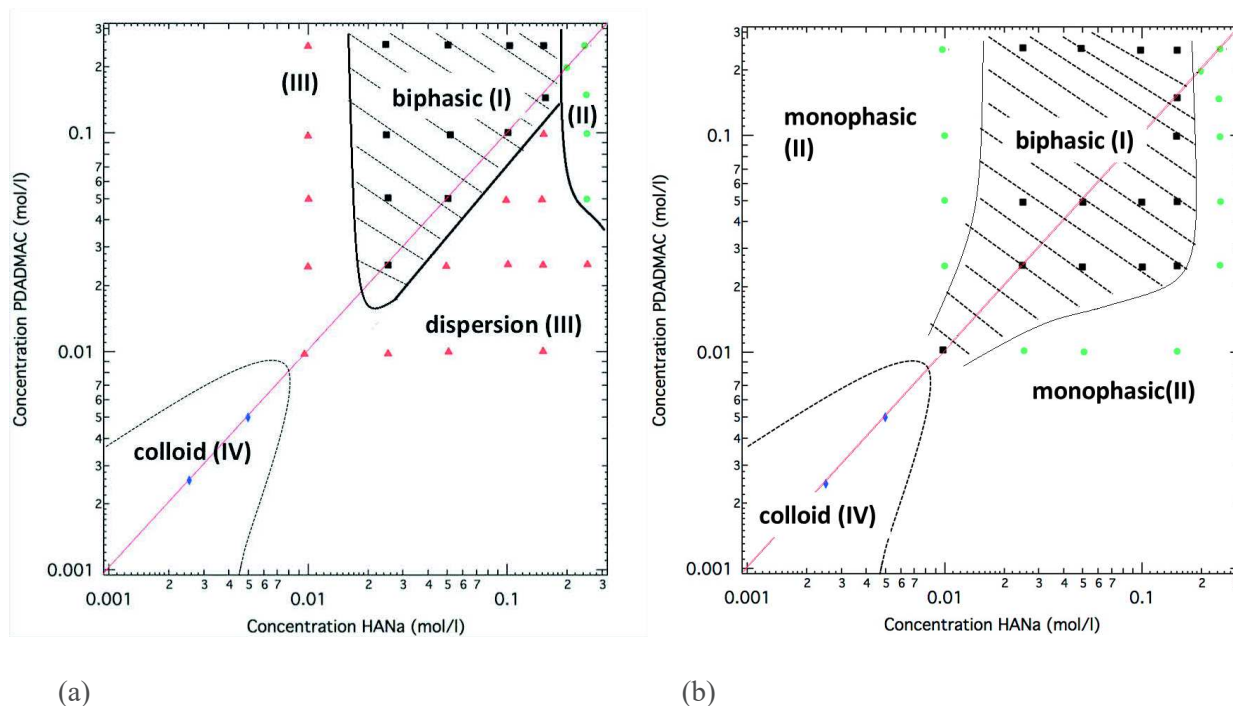
Figure 7.7. Time evolution of the state diagram of the salt-free HANa-PDADMAC aqueous solutions: immediately after their preparation, i.e. after mixing the stock polyelectrolyte solutions (a) and two days after their preparation (b). No further evolution of state diagram was noticed. The degrees of polymerization of the used polyelectrolytes are: N(HA 3) = 110 and N(PDADMAC J240412) = 190

Table 7.3. Visual investigations from aqueous solutions stoichiometric sodium hyaluronate - poly(diallyldimethylammonium chloride) complexes, formed in 0.15 M NaCl. The table shows the states of the mixtures the day of mixing and two days after their preparation

Concentration, mol/l	Day of mixing	Two day after mixing
0.25	Clear transparent monophasic gel	Clear transparent monophasic gel
0.20		
0.15		
0.10		
0.05	Turbid dispersion-like mixture with yellow tint	Biphasic: bottom phase - dense top phase - supernatant
0.025		
0.005		Turbid dispersion-like mixture with yellow tint
0.0025	White colloid	White colloid

7.2.2. Structure of the complexes from SAXS measurements

7.2.2.1. Salt-free aqueous solutions of the HANa-PDADMAC complexes

During the structural investigation with SAXS, we focused only on the complexes all along the charge stoichiometric line (see red line in Figure 7.6 and 7.7). We remind that the complexes were formed between sodium hyaluronan HA3 with polymerization degree 110 and poly(diallydimethylammonium) chloride PDADMAC J240412 with polymerization degree 190.

For any measured HANa-PDADMAC complex, the total scattered intensity measured by SAXS suggests that a new structure, different from a simple mixing of both components leading to an interpolyelectrolyte network, is arising (Figures 7.8, 7.10 and 7.11). Visible in the low-q region in all SAXS data, the characteristic q^{-4} decay of the scattering intensity indicates the existence of sharp interfaces (Porod's law) and, therefore, the presence of rather macroscopic observable particles, or droplets, of large finite size (> 210 nm). The Porod's law is, neglecting the corrective terms associated with the local curvatures of the interfaces:

$$I(q) = \Delta\rho^2 2\pi \frac{S}{V} * \frac{1}{q^4} \approx \frac{\Delta\rho^2}{R} , \qquad (131)$$

where S and V are the whole area of the interfaces and the whole volume of the solution, respectively; R is the average size of the particles, or droplets, in the spherical approximation; $\Delta\rho$ is the scattering length density of these particles, or droplets, relatively to the solvent (cm^{-2}). As both complexes and solvent form the particles or droplets, we have:

$$\Delta\rho = \bar{\rho} - \rho_{solv} = (\phi_v^{int}\rho_c + (1 - \phi_v^{int})\rho_{solv})) - \rho_{solv} , \qquad (132)$$

where ϕ_v^{int} is the complex, or polymer, volume fraction inside the particles, or droplets; ρ_c and ρ_{solv} are the scattering length density of the complexes, or polymers, and the solvent, respectively.

The analogy between the complexation and a gelation process is still reliable for the couple HANa-PDADMAC and the large-scale particles remind the droplets of microgels with an internal structure described by the scattering signal beyond q = 0.01 Å^{-1}, i.e. beyond the Porod's law characterizing the existence of interfaces. For the upper or liquid phase of the demixed salt-free polyelectrolyte of the colloid (IV) and biphasic (I) regions, the scattered intensity at low q does not change with the initial polyelectrolyte concentrations (Figure 7.8, green empty circle→blue

183

triangle→black full circle). That suggests through Eq. (131) and Eq. (132) the increase in C only affects the internal structure of the droplets (ϕ_v^{int}) without changes in their size R.

For the microgels formed at the lowest concentration (C=0.025 M; green empty circles in Figure 7.8), the scattered intensity above q=0.1 Å^{-1} can be assigned to the cylindrical structure of the primary complexes between HANa and PDADMAC. Actually, next characteristic q-ranges can be distinguished:

- At low q-values (q < 0.01 Å^{-1}), we observe the characteristic Porod's law indicating the existence of sharp interfaces. These interfaces are the ones that define the microgels or droplets. Obviously, these droplets are polydisperse (in size and/or shape) since none oscillation is displayed, or superimposed to the Porod's law (q^{-4}). The size of these droplets is larger then R =1/0.003 Å^{-1} > 330 Å, since even at q = 0.003 Å^{-1} no Guinier regime is not observable in the scattering behaviour.

- Consequently, at q > 0.01 Å^{-1} the scattered intensity gives us an information about the internal structure of the droplets.

- In the intermediate q-range between 0.08 Å^{-1} and 0.3 Å^{-1}, the rod-like structure is observed with the characteristic q^{-1} decay of the scattered intensity. The fit of the data in this q-range using the following equation:

$$I(q) \sim \frac{\pi V}{qH} \exp\left(-\frac{q^2 R_g^2}{2}\right) \simeq \frac{\pi^2 R^2}{q} \exp\left(-\frac{q^2 R^2}{4}\right) \qquad (133)$$

yields an estimation for the cross-section radius R of the primary complex R_1 = 8.3 Å. That indicates that we are dealing with a primary complex with a cylindrical geometry. That is quite original with respect to the complexes PSSNa-PDADMAC and is due to the increase of the intrinsic stiffness of polyanions through the replacement of PSS by HA.

- In the asymptotic region (qR$_1$ >> 1; R$_1$ being the radius of the cylinder cross-section), i.e. at q > 0.3 Å^{-1}, we observe the interface of these primary complexes that have a cylindrical geometry. The scattering curve displays a q^{-4} decreasing followed by a rather sharp increase. Such a scattering behaviour could be the first characteristic oscillation of the form factor associated with the cross section of the cylinder. So, in a quite small q-range 0.3 Å^{-1} <q < 0.4 Å^{-1} the q^{-4} scattering law is the decrease of the form factor just before the first minimum of the oscillations of the form factor associated with the cylinder cross section. For monodisperse cylinders of radius R and in the approximation qR → ∞, the minima of

the form factor are defined by the equation: $\cos(qR-3\pi/4) = 0$. It leads to $(qR-3\pi/4) = k\pi$ (k being a real number). The first minimum corresponds to the relation $qR = 3\pi/4$. In Figure 7.8 the minima is observed at q close to 0.4 Å^{-1} and thus R = 6 Å, which is roughly in agreement with the value obtained in the intermediate q-range ($0.08 < q < 0.3$ Å^{-1}). Here, polydispersity is not taken into account.
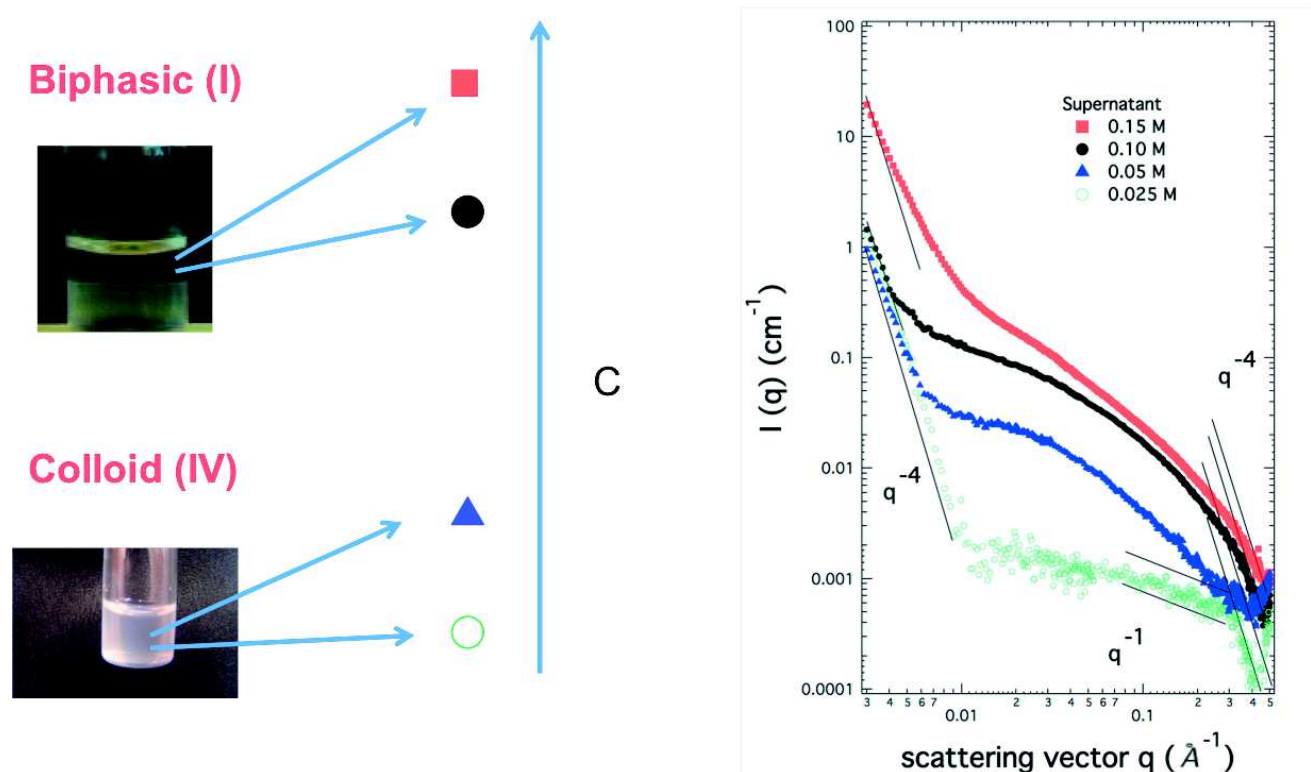
Figure 7.8. Comparison of the SAXS curves measured from the supernatant according to the variation of the complex concentration: green circles – 0.025 M; blue triangles – 0.05 M; black disks – 0.10 M; red squares– 0.15 M

- At low q-values ($0.01 < q < 0.08$ Å-1), the observed scattered intensity can be ascribed to the overlapping of the cylinders describing the conformation of the primary complexes. That is like the structure of a semidilute polymer solution, on the spatial scale corresponding to $q > 1/\xi$, where ξ is the mesh size of the network. The chains in this network are replaced by the cylinders and are therefore stiffer. That is described by a Lorentzian curve and x is of the order of $1/0.08$ Å^{-1} = 12.5 Å. This plateau cannot correspond to the Guinier range of a primary complex or a single cylinder. Indeed, we could not imagine that there would be only one primary complex in a droplet.

- It should be stressed that no local maximum, or polyelectrolyte peak, usually assigned to the repulsive interactions is observed. We suggest that the primary complexation between HA and PDADMA proceeds through successive electrostatic links along large chemical

sequences of the polycation and the polyanion in contact, forming large partially or completely neutral and rigid objects. These partially or completely neutral objects are immersed in the basic HA network, which scattered intensity does no longer display any peak due to a neutralization of the HA and the counterion release that is sufficiently significant to screen the rest of the electrostatic interactions. The formation of rod-like complexes and the absence of the electrostatic peak have been already reported for the complexes of hyaluronan with lysine[90].

As the polyelectrolyte concentration is increased (Figure 7.8, blue triangles→black disks→ red squares), the primary complexes tend to form secondary clusters due to hydrophobic interactions (Figure 7.9) that are accompanied by a change in the scattering behaviour in the q-range corresponding to the internal structure of the droplets, i.e. 0.01 Å^{-1} < q < 0.3 Å^{-1}. Obviously, the electrostatic interactions do not play a role in the formation of these secondary clusters, which also could be considered as heterogeneities.
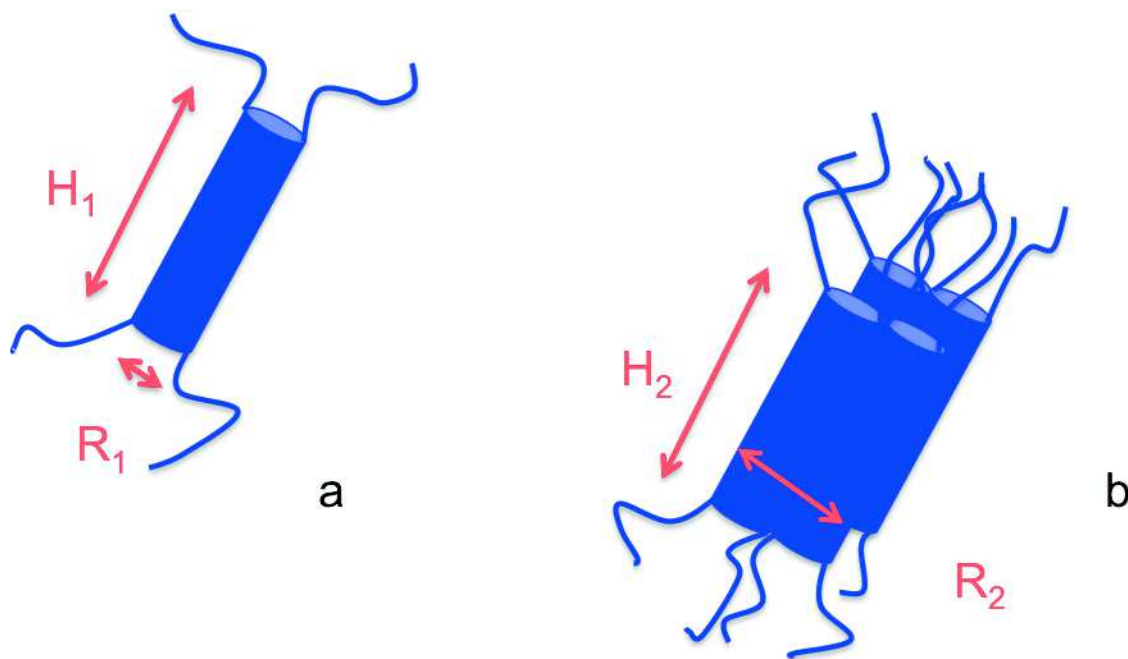

Figure 7.9. Schematic representation of a primary rod (a) and a secondary cluster (b), formed in salt-free aqueous solutions of HANa-PDADMAC stoichiometric complexes

Then the SAXS scattered intensity from the microgel internal structure becomes:

$$I(q) = xI(q)_{primary\ cylinders} + (1-x)I(q)_{secondary\ clustres} \qquad (134)$$

Here x is the volume fraction of the primary complexes or primary cylinders. The secondary complexes are other cylinders having a higher cross-section comparing to the primary ones that can evolve towards 3-dimensional or quasi-2-dimensional objects like disks. For a disk shape of radius R and thickness H, the following three characteristic regimes are observable for the scattered intensity $I(q)_{secondary\ compexes}$:

- In the Guinier range (qR$_g$ < 1), we have:

$$I(q) \sim I(q)_0 \left(1 - \frac{q^2 R_g^2}{3}\right), \text{ where } R_g^2 = \frac{R^2}{2} \text{ provided H} \ll \text{R} \tag{135}$$

- In the strict intermediate q-range (1/R<< q << 1/H):

$$I(q) \sim \frac{4\pi H}{q^2} \exp\left(-\frac{q^2 H^2}{12}\right); \tag{136}$$

- In the asymptotic q-range qH>>1, neglecting the oscillations of the thickness form factor:

$$I(q) \sim q^{-4} \tag{137}$$

We managed to estimate from Eq. 134-137 the geometric sizes, the height H$_2$ = 5.6 nm and the cross-section R$_2$ = 36.1 nm, of the disks involved in the mixture 0.05 M. The secondary structure is progressing with the increase in the concentration and leads to the phase separation. The volume fraction of polymer material ϕ_v^{int} in Eq.134 is distinct for different concentration, C.

We can propose a simple relationship, by neglecting any cross term as well as the condensed counterions, that describes the scattering behaviour of the microgel droplets in the monophasic liquid (Figure 7.6) and the distinct parts of the biphasic region (Figure 7.8):

$$I(q) = \alpha \left[\Delta\rho^2 2\pi \frac{S}{V} * \frac{1}{q^4}\right] + \beta[K^2 C_{int} g(q, C)] \tag{138}$$

with $K = \frac{\upsilon}{N}(\rho_{polymer} - \rho_{solvent})$ $\tag{139}$

and $g(q, C) = \phi^{clusters} g_{clusters}(q, C) + (1 - \phi^{clusters}) g_{primary\ complexes}(q, C)$ $\tag{140}$

Here, α and β are the adjustable coefficients; ρ, the scattering length density of the polymers, i.e. complexes; ρsolvent, that of the solvent; N, Avogadro's number; υ, the polymer molar volume; Cint, the polymer concentration inside the microgel droplets; $g_{primary\ complexes}(q, C)$, the form factor of the primary polyelectrolyte complexes or the scattering function associated with the related

network of rods; $g_{clusters}(q, C)$, that of the secondary polyelectrolyte clusters, or heterogeneities; $\phi^{clusters}$ is the fraction of clusters inside the droplets and ($1-\phi^{clusters}$), that of primary complexes.

Obviously, the first term in Eq. 140 corresponds to Eq. 133 that describes the droplet interfaces.
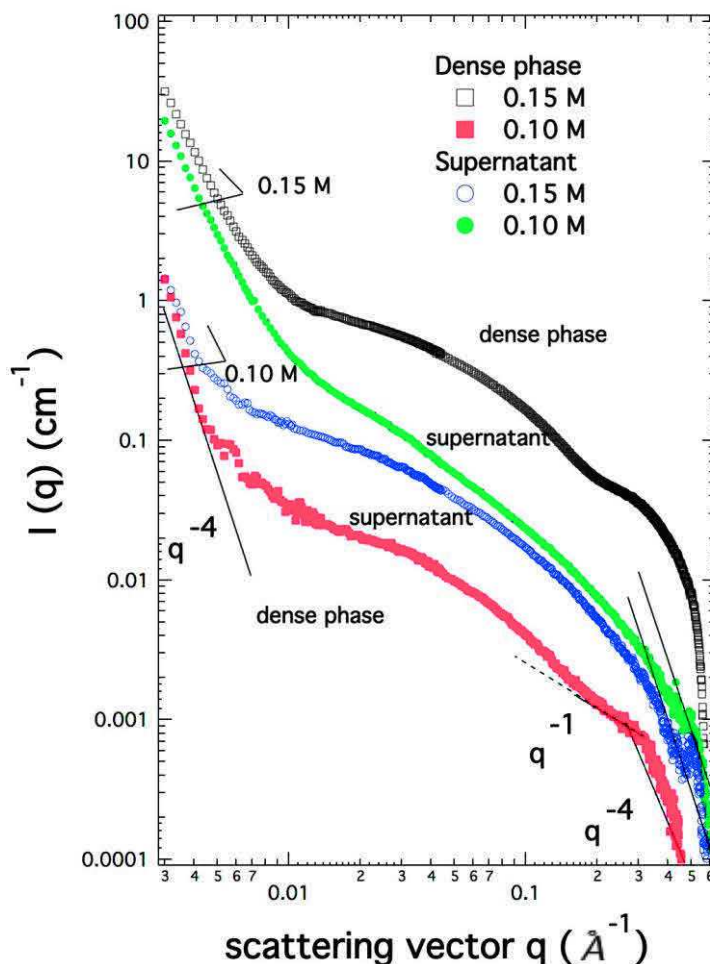
Figure 7.10. Comparision of the scattered intensities measured from the supernatant and dense phases: green circles and black squares refer to supernatant and dense phases of the 0.15 M HANa-PDADMAC mixture, respectively; blue full circles and red full squares refer to supernatant and dense phases of 0.10 M HANa-PDADMAC mixture, respectively

The analysis of the scattering curves obtained from 0.15 M, 0.20 M and 0.25 M mixtures (Figure 7.10 and Figure 7.11) allows suggesting the existence of the third kind of cylinders with a length H3 = 12.6 nm and a cross-section R3 = 6 nm. The oscillations associated with the form factor of their cross-sections are observable at q > 0.1 Å^{-1}. That affects the shape of the total complex signal (see Figure 7.10, black empty squares).

We must emphasize that the objects of well-defined geometry, which are present in these mixtures, extend to larger length scales than the intrinsic persistence lengths of HA and PDADMA macroions in binary solution. An additional stiffening of the particles could, therefore, result from the binding of the PDADMA and HA macroions or even from further aggregation.
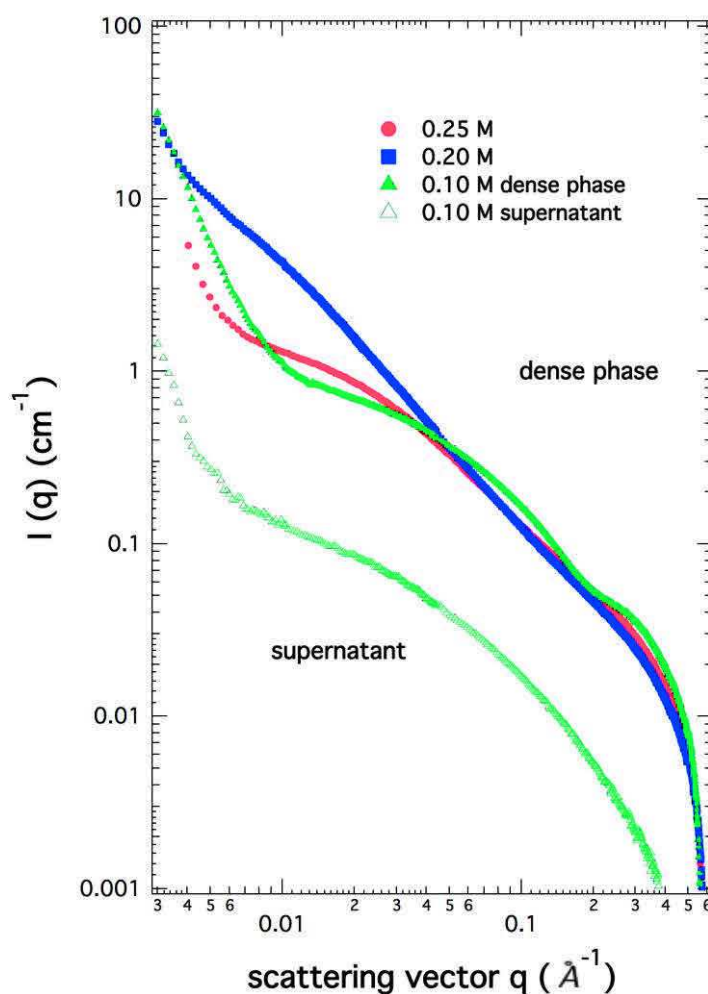
Figure 7.11. SAXS scattered intensity from HANa-PDADMAC complexes: monophasic 0.25 M (blue full squares) and 0.20 M (red full circles) mixtures; dense (green full triangles) and supernatant (green empty triangles) of biphasic 0.15 M mixtures

7.2.2.2. Aqueous solutions of the HANa-PDADMAC complexes formed in the presence of 0.15 M added NaCl salt
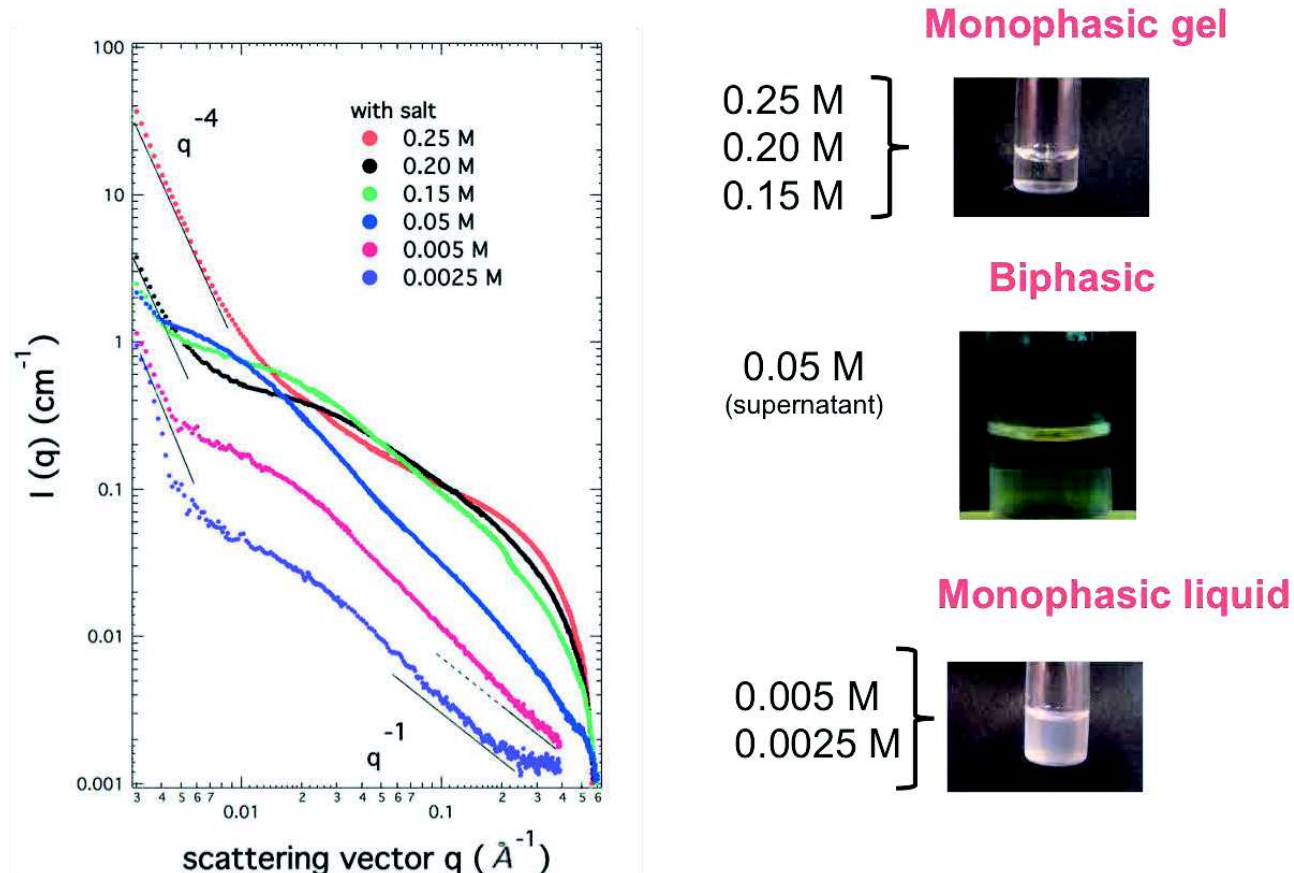
Figure 7.12. Scattering from HANa-PDADMAC aqueous solutions in the presence of 0.15 M NaCl as a function of the PE complex concentration: red – 0.25 M; black - 0.20 M; green – 0.15 M; blue – 0.05 M; purple -0.005; violet – 0.0025 M

Similar to the case of the salt-free aqueous solutions, the scattering from the brine aqueous solutions of HANa-PDADMAC can be interpreted as a linear combination of two signals, or functions: one for the simple network of rods, or primary complexes; another one for the clusters, or heterogeneities, with distinct well-defined geometry according to the concentration range (Figure 7.12).

Thus, the added salt does not influence strongly the extended structures, or heterogeneities, that are present in the HANa-PDADMAC aqueous solutions. That proves the interactions, leading to the formation of the secondary extended structures, are not purely electrostatic.

7.2.3. Cryo-transmission electron microscopy
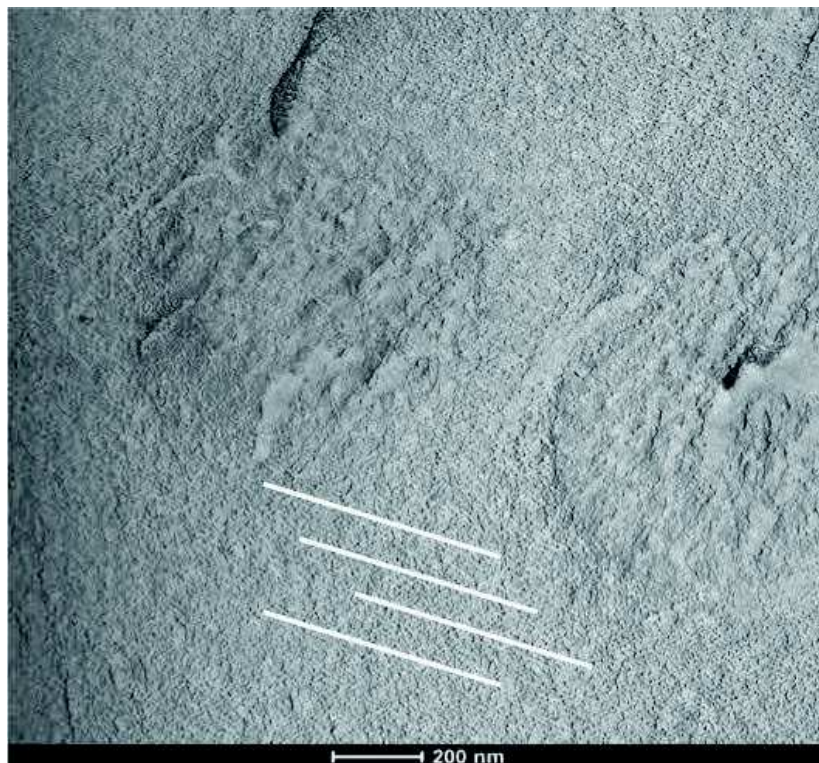
Figure 7.13. TEM-image after cryo-fracture cut of 0.005 M HANa-PDADMAC mixture

Dense clusters, orientated along the straight lines, of average size 30-40 nm are visible in the TEM image presented in Figure 7.13. This size corresponds to the length scale of the disk-shape complexes estimated by SAXS. The organisation in the extended domains is also coherent with the SAXS results.

7.3. Conclusions

The one-step endothermic interaction between HANa and PDADMAC observed in dilute solutions leads to different polyelectrolyte complex structures that essentially depend on the concentration in the semidilute and concentrated solutions. The interaction between HA and PDADMA is not longer stoichiometrical as in the case of flexible polyelectrolytes PSSNa and PDADMAC. The variety of PEC morphologies is yet visible macroscopically following the changes in the phase, or state, behaviour. A few kinds of formed particles could coexist together: the network of primary rod-like complexes decorated by heterogeneities or secondary clusters, cylinders, and disks. For these interconnected primary rod-like complexes and clusters, the high stiffness of the HA backbone is a strong prerequisite. The additional stiffening of the primary complexes, or rods, could, therefore, results from the binding of the PDADMA macroions on the HA backbones and even leads to further aggregation.

The primary complexation between HA and PDADMA proceeds through successive electrostatic links along large chemical sequences of polycation and polyanion, forming partially or completely neutral objects. The role of the electrostatic interactions as a driven force in the secondary structure formation is still questionable, but the hydrophobic interactions must play an important role. The complexation between HA and PDADMA can always be considered as a gelation process and HA, as a gelling agent.

General conclusion

In this thesis, the thermodynamics, macroscopic behaviour and structure of the aqueous solutions the polyelectrolyte complexes formed from the same polycation poly(diallyldimethylammonium) and three polyanions with different intrinsic stiffness, poly(styrene sulfonate), poly(α-methyl styrene sulfonate) and hyaluronan have been investigated.

We have synthesized or modified three polyelectrolytes. Their salt forms are: PDADMAC, PSSNa (hydrogenated as well as deuterated) and PαMSSNa. The aim was to get model polyelectrolytes with close contour length or polymerization degree. The industrial HANa kindly provided by Soliance was also considered. We have characterized all these PEs using ^{1}H-NMR, SEC, TGA, and SAXS.

The polyelectrolyte complex (PEC) aqueous solutions were prepared in a wide concentration range, with two ionic strengths: in the absence and in the presence of 0.15 M NaCl. PECs were characterized with different techniques according to the concentration regime. The PEC formation process in dilute regime was investigated with the combination of the isothermal titration calorimetry, dynamic light scattering, and zeta-potentiometry. The PEC structure, as well as those of each polyelectrolyte, were studied in the semidilute or concentrated regime by SAXS, SANS and cryo-electron microscopy.

The analysis of the obtained results leads to the following conclusions.

For the complexes PSS-PDADMA:

- The stoichiometry of the complexation between these two model polyelectrolytes is equal to 1 and the interaction is exothermic and entropy-driven independently from the component concentration regime, the ionic strength, and the preparation procedure

- The complexation between PSS and PDADMA is proposed to be distinct according to the concentration regime. In dilute solution, it is suggested to consist of a two-step process: a primary complexation and then a further aggregation. In semidilute or concentrated solutions the complexation can be viewed as a gelation process, in which the network of one polyelectrolyte represents the gelation bath and the polyelectrolyte of opposite charge plays the role of a gelling

agent. The resulting structure of the complexes is a mixed polyelectrolyte network in which heterogeneities or clusters formed by the polyelectrolyte associations are immersed. These two distinct processes and PEC structure can be recognized visually due to the different phase separation phenomena.

-In the semidilute and concentrated regimes, the structure of PECs also depends on the preparation procedures (mixing or desalting kinetics). Thus, the order of the initial polyelectrolyte solution mixing and their ionic strength play a role. These factors mainly affect the heterogeneities, but don't really influence the mesh size of the mixed polyelectrolyte network.

- The increase in the ionic strength prevents the macroscopic phase separationand leads to the extension of the monophasic domain in the state diagram and equalizes the distribution of PDADMAC between the distinct macroscopically separated phases.

-The transition line between the macroscopically different colloidal and biphasic regions is correlated with the crossover concentration between semidilute and concentrated regimes of the initial PDADMAC.

For the complexes PαMSS-PDADMA:

The ionic strength and the concentration of the initial PE aqueous solutions affect the complexation between PαMSS and PDADMA in the same way as PSS-PDADMA. The increase in the intrinsic stiffness of the polyanion leads to some change in the stoichiometry of the complexation and extension of the monophasic region in the state diagram.

For the complexes HA-PDADMA:

The further increase in the non-electrostatic persistence length of the polyanion leads to:

- A change in the complexation process, which becomes a two-step exothermic to one-step endothermic process with a stoichiometry of the interaction that is distinct from 1. That was coherently observed in dilute, semidilute and concentrated regimes.

- The complexation between HA and PDADMAC can always be considered as a gelation process and the hyaluronate as a gelling agent.

- The structure of HA-PDADMA PECs changes from the 'scramble egg model' as in case of PSS-PDADMA to rod-like, or "ladder" model. Specifically, the organisation of the polyelectrolyte complexes can have a higher orientation order provided the PEC solutions were sheared.

- The primary complexation between HA and PDADMAC comes down to a neutralization of the HA and suppresses the role of the electrostatic interactions as a driven force in the secondary structure formation, where the hydrophobic interactions must play an important role.

-The transition between distinct domains in state diagram is correlated with the crossovers between the semidilute and concentrated regimes and between concentrated and jammed ones of HA aqueous solutions.

References

1. Wang, S., Granick, S. & Zhao, J. Charge on a weak polyelectrolyte. *J. Chem. Phys.* **129,** 1–4 (2008).

2. Dobrynin, A. V. & Rubinstein, M. Theory of polyelectrolytes in solutions and at surfaces. *Prog. Polym. Sci.* **30,** 1049–1118 (2005).

3. Fuoss, R. M. Viscosity function for polyelectrolytes. *J. Polym. Sci.* **3,** 603–604 (1948).

4. Manning, G. S. Limiting Laws and counterion condensation in polyelectrolyte solutions I. Colligative properties. *J. Chem. Phys.* **51,** 924 (1969).

5. Oosawa, F. A simple theory of thermodynamic properties of polyelectrolyte solutions. *J. Polym. Sci.* **XXIII,** 421–430 (1957).

6. Manning, G. S. & Ray, J. Counterion condensation revisited. *J. Biomol. Struct. Dyn.* **16,** 461–476 (1998).

7. Manning, G. S. Counrerion condensation theory constructed from different models. *Physica A* **231,** 236–253 (1996).

8. Combet, J., Isel, F., Rawiso, M. & Boué, F. Scattering functions of flexible polyelectrolytes in the presence of mixed valence counterions: Condensation and scaling. *Macromolecules* **38,** 7456–7469 (2005).

9. Kuhn, W., Kunzle, O. & Katchalsky, A. Verhalten polyvalentre fadenmolekelionen in losung. *Helv Chim Acta* 1994–2037 (1948).

10. De Gennes, P. G., Pincus, P., Velasco, R. M. & Brochard, F. Remarks on polyelectrolyte conformation. *J. Phys.* **37,** 1461–1473 (1976).

11. De Gennes, P. G. *Scaling concept in Polymer Physics*. (Cornell University Press, 1979).

12. Dobrynin, A. V, Colby, R. H., Rubinstein, M. & York, N. Scaling Theory of Polyelectrolyte Solutions. *Macromolecules* **28,** 1859–1871 (1995).

13. Khokhlov, A. & Khachaturian, K. On the theory of weakly charged polyelectrolytes. *Polymer* **23,** 1742–1750 (1982).

14. Khokhlov, A. R. On the collapse of weakly charged polyelectrolytes. *J. Phys. A. Math. Gen.* **13,** 979–987 (1980).

15. Pfeuty P. Conformation des polyelectrolytes ordre dans les solutions de polyelectrolytes. *J Phys* **39,** 2–149 (1978).

16. Dobrynin, A. V., Rubinstein, M. & Obukhov, S. P. Cascade of transitions of polyelectrolytes in poor solvents. *Macromolecules* **29,** 2974–2979 (1996).

17. Nishida, K., Kaji, K. & Kanaya, T. High concentration crossovers of polyelectrolyte solutions. *J. Chem. Phys.* **114,** 8671–8677 (2001).

18. Nierlich, M. *et al.* Small-angle neutron-scattering by semi-dilute solutions of polyelectrolyte. *J. Phys.* **40,** 701–704 (1979).

19. Ise, N. *et al.* '"Ordered"' structure in dilute solutions of sodium polystyrenesulfonates as studied by small-angle x-ray scattering. *J. Chem. Phys.* **81,** 3294–3306 (1984).

20. Nierlich, M., Boué, F., Lapp, A. & Oberthür, R. Radius of gyration of a polyion in salt free polyelectrolyte solutions measured by SANS. *J. Phys.* **46,** 649–655 (1985).

21. Nierlich, M., Boué, F., Lapp, A. & Oberthür, R. Characteristic lengths and the structure of salt free polyelectrolyte solutions. A small angle neutron scattering study. *Colloid Polym. Sci.* **263,** 955–964 (1985).

22. Combet, J., Rawiso, M., Rochas, C., Hoffmann, S. & Boué, F. Structure of polyelectrolytes with mixed monovalent and divalent counterions: SAXS measurements and Poisson-Boltzmann analysis. *Macromolecules* **44,** 3039–3052 (2011).

23. Barrat, J.-L. & Joanny, J.-F. Theory of polyelectrolyte solutions. *Adv. Chem. Phys.* **94,** 1–66 (1996).

24. Joanny, J. F. & Leibler, L. Weakly charged polyelectrolytes in a poor solvent. *J. Phys.* **51,** 545–557 (1990).

25. Muthukumar, M. Double screening in polyelectrolyte solutions: Limiting laws and crossover formulas. *J. Chem. Phys.* **105,** 5183–5199 (1996).

26. Doi, M. & Edwards, S. F. *The theory of polymer dynamics*. (Vol. 222. Oxford: Clarendon Press, 1986).

27. Borue, V. Y. & Erukhimovich, I. Y. A statistical theory of weakly charged polyelectrolytes: fluctuations, equation of state and microphase separation. *Macromolecules* **21,** 3240–3249 (1988).

28. Lorchat, P. *et al.* New regime in polyelectrolyte solutions. *EPL(Europhys. Lett.)* **106,** 28003–8 (2014).

29. von Klitzing, R., Kolaric, B., Jaeger, W. & Brandt, A. Structuring of poly(DADMAC) chains in aqueous media: a comparison between bulk and free-standing film measurements. *Phys. Chem.* **4,** 1907–1914 (2002).

30. Lorchat, P. Structure des solution aqueuses de polyélectrolytes fortement chargés. PhD thesis, Université de Strasbourg (2012).

31. Nyrkova, I., Shusharina, N. & Khokhlov, A. Liquid-crystalline ordering in solutions of polyelectrolytes. *Macromol. Theory Simulations* **6,** 965–1006 (1997).

32. Carri, G. & Muthukumar, M. Attractive interactions and phase transitions in solutions of similarly charged rod-like polyelectrolytes. *J. Chem. Phys.* **111,** 1765–1777 (1999).

33. Gobeaux, F. *et al.* Cooperative ordering of collagen triple helices in the dense state. *Langmuir* **16,** 6411–6417 (2007).

34. Durand, D., Doucet, J. & Livolant, F. A study of the structure of highly concentrated phases of DNA by X-ray diffraction. *J. Phys. II* **2,** 1769–1783 (1992).

35. Dogic, Z. & Fraden, S. Cholesteric phase in virus suspensions. *Langmuir* **16,** 7820–7824 (2000).

36. Grelet, E. Hexagonal order in crystalline and columnar phases of hard rods. *Phys. Rev. Lett.* **100,** 168301–4 (2008).

37. Odijk, T. & Houwaart, A. On the theory of the excluded-volume effect of a polyelectrolyte in a 1-1 electrolyte solution. *J. Polym. Sci. Polym. Phys. Ed.* **16,** 627–639 (1978).

38. Skolnick, J. & Fixman, M. Electrostatic persistence length of a wormlike polyelectrolyte.

Macromolecules **10,** 944–948 (1977).

39. Le Bret, M. Electrostatic contribution to the persistence length of a polyelectrolyte. *J. Chem. Phys.* **76,** 6243–6255 (1982).

40. Fixman, M. The flexibility of polyelectrolyte molecules. *J. Chem. Phys.* **76,** 6346–6353 (1982).

41. Barrat, J.-L. & Joanny, J.-F. Persistence length of polyelectrolyte chains. *Europhys. Lett.* **24,** 333–338 (1993).

42. Thünemann, A. F., Müller, M., Dautzenberg, H. & Löwen, J. J. H. Polyelectrolyte complexes. *Adv. Polym. Sci.* **166,** 113–171 (2004).

43. Laugel, N. *et al.* Relationship between the growth regime of polyelectrolyte multilayers and the polyanion/polycation complexation enthalpy. *J. Phys. Chem. B* **110,** 19443–19449 (2006).

44. Ou, Z. & Muthukumar, M. Entropy and enthalpy of polyelectrolyte complexation: Langevin dynamics simulations. *J. Chem. Phys.* **124,** 154902–11 (2006).

45. Abe, K., Koide, M. & Tsuchida, E. Selective complexation of macromolecules. *Macromolecules* **10,** 1259–1264 (1977).

46. Krayukhina, M. A., Samoilova, N. A. & Yamskov, I. A. Polyelectrolyte complexes of chitosan: formation, properties and applications. *Russ. Chem. Rev.* **77,** 799–813 (2008).

47. Kudlay, A. & Olvera de la Cruz, M. Precipitation of oppositely charged polyelectrolytes in salt solutions. *J. Chem. Phys.* **120,** 404–12 (2004).

48. Silva, R. A., Urzúa, M. D., Petri, D. F. S. & Dubin, P. L. Protein adsorption onto polyelectrolyte layers: effects of protein hydrophobicity and charge anisotropy. *Langmuir* **26,** 14032–8 (2010).

49. Kosmella, S., Beitz, T. & Ko, J. Self-assembled polyelectrolyte systems. *Prog. Polym. Sci.* **26,** 1199–1232 (2001).

50. Krotova, M. K., Vasilevskaya, V. V & Khokhlov, A. R. The effect of a low-molecular-mass salt on stoichiometric polyelectrolyte complexes composed of oppositely charged macromolecules with different solvent affinities. *Polym. Sci. Ser. A* **51,** 1075–1082 (2009).

51. de Vries, R. & Cohen Stuart, M. Theory and simulations of macroion complexation. *Curr. Opin. Colloid Interface Sci.* **11,** 295–301 (2006).

52. van der Gucht, J., Spruijt, E., Lemmers, M. & Cohen Stuart, M. A. Polyelectrolyte complexes: bulk phases and colloidal systems. *J. Colloid Interface Sci.* **361,** 407–422 (2011).

53. Castelnovo, M. & Joanny, J.-F. Formation of polyelectrolyte multilayers. *Langmuir* **16,** 7524–7532 (2000).

54. Castelnovo, M. & Joanny, J.-F. Complexation between oppositely charged polyelectrolytes: beyond the random phase approximation. *Eur. Phys. J. E* **6,** 377–386 (2001).

55. Biesheuvel, P. M. & Stuart Cohen, M. A. Electrostatic Free Energy of Weakly Charged Macromolecules in Solution and Intermacromolecular Complexes Consisting of Oppositely Charged Polymers. *Langmuir* **20,** 2785–2791 (2004).

56. Maarten Biesheuvel, P. & Cohen Stuart, M. A. Cylindrical cell model for the electrostatic free energy of olyelectrolyte complexes. *Langmuir* **20,** 4764–4770 (2004).

57. Hayashi, Y., Ullner, M. & Linse, P. Oppositely charged polyelectrolytes. Complex formation and effects of chain asymmetry. *J. Phys. Chem. B* **108,** 15266–15277 (2004).

58.   Lee, J., Popov, Y. O. & Fredrickson, G. H. Complex coacervation: a field theoretic simulation study of polyelectrolyte complexation. *J. Chem. Phys.* **128,** 224908–20 (2008).

59.   Zhang, R. & Shklovskii, B. I. Phase diagram of solutions of oppositely charged polyelectrolytes. *Physics (College. Park. Md).* **55455,** 1–26 (2004).

60.   Zhang, R. & Shklovskii, B. I. Phase diagram of solution of oppositely charged polyelectrolytes. *Phys. A Stat. Mech. its Appl.* **352,** 216–238 (2005).

61.   Veis, A. A review of the early development of the thermodynamics of the complex coacervation phase separation. *Adv. Colloid Interface Sci.* **167,** 2–11 (2011).

62.   Hugerth, A., Caram-Lelham, N. & Sundelöf, L.-O. The effect of charge density and conformation on the polyelectrolyte complex formation between carrageenan and chitosan. *Carbohydr. Polym.* **34,** 149–156 (1997).

63.   Klitzing, R. V. *et al.* Forces in foam films containing polyelectrolyte and surfactant. *Colloids Surfaces A Physicochem. Eng. Asp.* **149,** 131–140 (1999).

64.   Shovsky, A., Varga, I., Makuska, R. & Claesson, P. M. Formation and stability of water-soluble, molecular polyelectrolyte complexes: effects of charge density, mixing ratio, and polyelectrolyte concentration. *Langmuir* **25,** 6113–21 (2009).

65.   Chollakup, R., Beck, J. B., Dirnberger, K., Tirrell, M. & Eisenbach, C. D. Polyelectrolyte molecular weight and salt effects on the phase behavior and coacervation of aqueous solutions of poly(acrylic acid) sodium salt and poly(allylamine) hydrochloride. *Macromolecules* **46,** 2376–2390 (2013).

66.   Jeon, B. J. & Muthukumar, M. Polymer capture by α-hemolysin pore upon salt concentration gradient. *J. Chem. Phys.* **140,** 15101–7 (2014).

67.   Sæther, H. V., Holme, H. K., Maurstad, G., Smidsrød, O. & Stokke, B. T. Polyelectrolyte complex formation using alginate and chitosan. *Carbohydr. Polym.* **74,** 813–821 (2008).

68.   Schmitt, C. *et al.* Effect of protein aggregates on the complex coacervation between β-lactoglobulin and acacia gum at pH 4.2. *Food Hydrocoll.* **14,** 403–413 (2000).

69.   Jha, P. K., Desai, P. S., Li, J. & Larson, R. G. pH and salt effects on the associative phase separation of oppositely charged polyelectrolytes. *Polymers (Basel).* **6,** 1414–1436 (2014).

70.   Naderi, A., Claesson, P. M., Bergström, M. & Dedinaite, A. Trapped non-equilibrium states in aqueous solutions of oppositely charged polyelectrolytes and surfactants: Effects of mixing protocol and salt concentration. *Colloids Surfaces A Physicochem. Eng. Asp.* **253,** 83–93 (2005).

71.   Wang, J. & Muthukumar, M. Encapsulation of a polyelectrolyte chain by an oppositely charged spherical surface. *J. Chem. Phys.* **135,** 194901–194909 (2011).

72.   Kudlay, A., Ermoshkin, A. V. & de la Cruz, M. O. Complexation of oppositely charged polyelectrolytes: effect of ion pair formation. *Macromolecules* **37,** 9231–9241 (2004).

73.   Laugel, N. *et al.* Relationship between the growth regime of polyelectrolyte multilayers and the polyanion/polycation complexation enthalpy. *J. Phys. Chem. B* **110,** 19443–9 (2006).

74.   Izumrudov, V. A., Ortiz, H. O., Zezin, A. B. & Kabanov, V. A. Temperatre controllable interpolyelectrolte substitution reactions. *Macromol. Chem. Phys.* **199,** 1057–1062 (1998).

75.   Ankerfors, C., Ondaral, S., Wågberg, L. & Ödberg, L. Using jet mixing to prepare polyelectrolyte complexes: Complex properties and their interaction with silicon oxide

surfaces. *J. Colloid Interface Sci.* **351,** 88–95 (2010).

76. Chen, J., Heitmann, J. A. & Hubbe, M. A. Dependency of polyelectrolyte complex stoichiometry on the order of addition. 1. Effect of salt concentration during streaming current titrations with strong poly-acid and poly-base. *Colloids Surfaces A Physicochem. Eng. Asp.* **223,** 215–230 (2003).

77. Vitorazi, L. *et al.* Evidence of a two-step process and pathway dependency in the thermodynamics of poly(diallyldimethylammonium chloride)/poly(sodium acrylate) complexation. *Soft Matter* **10,** 9496–9505 (2014).

78. Dautzenberg, H. Polyelectrolyte complex formation in highly aggregating systems. 1. Effect of salt: polyelectrolyte complex formation in the presence of NaCl. *Macromolecules* **30,** 7810–7815 (1997).

79. Kabanov, V. A. & Zezin, A. B. Soluble interpolymeric complexes as a new class of synthetic polyelectrolytes. *Pure Appl. Chem.* **56,** 343–354 (1984).

80. Kabanov, V. A. Polyelectrolyte complexes in solution and in bulk. *Russ. Chem. Rev.* **74,** 3–20 (2007).

81. Bronich, T., Kabanov, A. V. & Marky, L. A. A Thermodynamic Characterization of the Interaction of a Cationic Copolymer with DNA. *J. Phys. Chem. B* **105,** 6042–6050 (2001).

82. Pergushov, D. V. *et al.* Novel Water-Soluble Micellar Interpolyelectrolyte Complexes †. *J. Phys. Chem. B* **107,** 8093–8096 (2003).

83. Tsuchida, E., Osada, Y. & Ohno, H. Formation of interpolymer complexes. *J. Macromol. Sci. Part B Phys.* **17,** (1980).

84. Tsuchida, E., Osada, Y. & Sanada, K. Interaction of poly(styrene sulfonate) with polycations carrying charges in the chain backbone. *J. Polym. Sci. Part A-1 Polym. Chem.* **10,** 3397–3404 (1972).

85. Zezin, A. B. & Kabanov, V. a. A New Class of Complex Water-soluble Polyelectrolytes. *Russ. Chem. Rev.* **51,** 833–855 (2007).

86. Philipp, B., Dautzenberg, H., Linow, K.-J. & Kotz, J. Polyelectrolyte complexes - Recent Developments and Open Problems. *Prog. Polym. Sci.* **14,** 91–172 (1989).

87. Brand, F. & Dautzenberg, H. Structural analysis in interpolyelectrolyte complex formation of sodium poly(styrenesulfonate) and diallyldimethylammonium chloride-acrylamide copolymers by viscometry. *Langmuir* **13,** 2905–2910 (1997).

88. Chollakup, R., Smitthipong, W., Eisenbach, C. D. & Tirrell, M. Phase Behavior and Coacervation of Aqueous Poly(acrylic acid)−Poly(allylamine) Solutions. *Macromolecules* **43,** 2518–2528 (2010).

89. Netz, R. R. & Joanny, J.-F. Complexation between a semiflexible polyelectrolyte and an oppositely charged sphere. *Macromolecules* **32,** 9026–9040 (1999).

90. Morfin, I., Buhler, E., Cousin, F., Grillo, I. & Boué, F. Rodlike complexes of a polyelectrolyte (hyaluronan) and a protein (lysozyme) observed by SANS. *Biomacromolecules* **12,** 859–870 (2011).

91. Shi, L., Carn, F., Boué, F., Mosser, G. & Buhler, E. Control over the electrostatic self-assembly of nanoparticle semiflexible biopolyelectrolyte complexes. *Soft Matter* **9,** 5004–5015 (2013).

92. Mengarelli, V., Auvray, L., Pastré, D. & Zeghal, M. Charge inversion, condensation and

decondensation of DNA and polystyrene sulfonate by polyethylenimine. *Eur. Phys. J. E* **34,** 127–136 (2011).

93. Mengarelli, V., Auvray, L. & Zeghal, M. Phase behaviour and structure of stable complexes of oppositely charged polyelectrolytes. *EPL (Europhysics Lett.* **85,** 58001–6 (2009).

94. Annaka, M. Salt effect on microscopic structure and stability of colloidal complex obtained from neutral/polyelectrolyte block copolymer and oppositely charged surfactant. *Colloids Surf. B. Biointerfaces* **99,** 127–35 (2012).

95. Knaapila, M. *et al.* Polyelectrolyte complexes of a cationic all conjugated fluorene − thiophene diblock copolymer with aqueous DNA. *J. Phys. Chem. B* **119,** 3231–3241 (2015).

96. Hone, J. H. E., Howe, A. M. & Cosgrove, T. A rheological and small-angle neutron scattering study of the structure of gelatin / polyelectrolyte complexes under shear. *Macromolecules* **33,** 1206–1212 (2000).

97. Spruijt, E. *et al.* Structure and dynamics of polyelectrolyte complex coacervates studied by scattering of neutrons, X-rays, and light. *Macromolecules* **46,** 4596–4605 (2013).

98. Turbak, A. F. Polymer sulfonation without cross linking. The sulfur trioxide-phosphate system. *I&EC Prod. Res. Dev.* **1,** 275–278 (1962).

99. Turbak, A. F., Allen, N. & Gabriel, K. Sulfonation of an olefin polymer. (1965). at <http://www.google.com/patents/US3205285>

100. Carroll, W. R. & Eisenberg, H. Narrow molecular weight distribution poly(styrenesulfonic Acid). Part I . Preparation, solution properties, and phase separation. *J. Polym. Sci. Part A-2* **4,** 599–610 (1966).

101. Vink, H. A new convenient method for the synthesis of poly(styrene sulfonic acid). *Macromol. Chem.* **281,** 279–281 (1981).

102. Heinrich, M. Structures de solutions aqueuses de polyélectrolytes en étoile. PhD thesis, Université Louis Pasteur de Strasbourg. (Université Louis Pasreur de Strasbourg, 1998).

103. Makowski, H. S., Lundberg, R. D. & Singhal, G. S. US Patent 3870841 to Exxon Research and Engineering Company. (1975).

104. Osa, M., Yoshizaki, T. & Yamakawa, H. Mean-Square Radius of Gyration of Oligo- and Poly(R -methylstyrene)s in Dilute Solution. *Macromolecules* **33,** 4828–4835 (2000).

105. Balland-Longeau, A. Calonne, M., Jouss, F. & Catala, J.-M. Procédé de préparation du Poly(alpha-methylstyrene) FR2852960. (2004).

106. Balland-Longeau, A. Calonne, M., Jouss, F. & Catala, J.-M. Method for the preparation of Poly(alpha-methylstyrene) CN 200480004810. (2006).

107. Zhao, Q., An, Q. F., Ji, Y., Qian, J. & Gao, C. Polyelectrolyte complex membranes for pervaporation, nanofiltration and fuel cell applications. *J. Memb. Sci.* **379,** 19–45 (2011).

108. Chen, J. *et al.* Preparation and biocompatibility of nanohybrid scaffolds by in situ homogeneous formation of nano hydroxyapatite from biopolymer polyelectrolyte complex for bone repair applications. *Colloids Surf. B. Biointerfaces* **93,** 100–7 (2012).

109. John, W., Buckley, C. A., Jacobs, E. P. & Sanderson, R. D. Synthesis and use of polydadmac for water purification. in *Biennial Conference of the Water Institute of Southern Africa (WISA)* (2001).

110. Wandrey, C., Hermindez-Barajas, J. & D. Hunkeler. Diallyldimethylammonium chloride and its polymers. *Adv. Polym. Sci.* **145,** 123–183 (1999).

111. Tüzün, N. S., Aviyente, V. & Houk, K. N. Theoretical study of factors controlling rates of cyclization of radical intermediates from diallylamine and diallylammonium monomers in radical polymerizations. *J. Org. Chem.* **67,** 5068–75 (2002).

112. Seetharaman, V., Kalyanasundaram, S. & Gopalan, a. Ultrasonic studies of aqueous solutions of poly diallyl dimethyl ammonium chloride. *Indian J. Pure Appl. Phys.* **42,** 735–740 (2004).

113. Brand, F., Dautzenberg, H., Jaeger, W. & Hahn, M. Polyelectrolytes with various charge densities : Synthesis and characterization of diallyldimethylammonium chloride-acrylamide copolymers. *Die Angew. Makromol. Chemie* **248,** 41–71 (1997).

114. Jaeger W., Hahn M., Wandrey C., Seehaus F., R. G. Cyclopolymerization kinetics of dimethyldiallylammoniumchloride. *J. Macromol. Sci.* **21,** 593–614 (1984).

115. López, R. G. *et al.* A kinetic description of the free radical polymerization of vinyl acetate in cationic microemulsions. *Macromolecules* **33,** 2848–2854 (2000).

116. Destarac, M. *et al.* Aqueous MADIX/RAFT polymerization of diallyldimethylammonium chloride :extension to the synthesis of poly(DADMAC) - based double hydrophilic block copolymers. *J. Polym. Sci. Part A Polym. Chem.* **48,** 5163–5171 (2010).

117. Hahn, M. & Jaeger, W. Kinetics of the free radical polymerization of dimethyl diallyl ammonium chloride. 5. Kinetic model with persulfate as initiator. *Angew. Makromol. Chem.* **198,** 165–178 (1992).

118. Jaeger, W., Hahn, M., Kieskc, A. & Zimmermann, A. Polymerization of water soluble cationic vinyl monomers. *Macromol. Symp.* **111,** 95–106 (1996).

119. Dautzenberg, H., Gornitz, E. & Jaeger, W. Synthesis and characterization of poly(diallyldimethylammonium chloride) in a broad range of molecular weight. *Macromol. Chem. Phys.* **199,** 1561–1571 (1998).

120. Meyer, K. & Palmer, J. W. The polysaccharide of the vitreous humor. *J. Biol. Chem.* 629–634 (1934).

121. Necas, J., Bartosikova, L., Brauner, P. & Kolar, J. Hyaluronic acid (hyaluronan): a review. *Vet. Med. (Praha).* **2008,** 397–411 (2008).

122. Price, R. D., Berry, M. G. & Navsaria, H. a. Hyaluronic acid: the scientific and clinical evidence. *J. Plast. Reconstr. Aesthet. Surg.* **60,** 1110–9 (2007).

123. Rothenhöfer, M., Grundmann, M., Bernhardt, G., Matysik, F.-M. & Buschauer, A. High performance anion exchange chromatography with pulsed amperometric detection (HPAEC-PAD) for the sensitive determination of hyaluronan oligosaccharides. *J. Chromatogr. B* **988,** 106–115 (2015).

124. Kogan, G., Soltés, L., Stern, R. & Gemeiner, P. Hyaluronic acid: a natural biopolymer with a broad range of biomedical and industrial applications. *Biotechnol. Lett.* **29,** 17–25 (2007).

125. Robert, L. Hyaluronan, a truly 'youthful' polysaccharide. Its medical applications. *Pathol. Biol. (Paris).* **63,** 32–34 (2015).

126. Kadajji, V. G. & Betageri, G. V. Water soluble polymers for pharmaceutical applications. *Polymers (Basel).* **3,** 1972–2009 (2011).

127. Jin, Y., Ubonvan, T. & Kim, D. Hyaluronic Acid in Drug Delivery Systems. *J. Pharm. Investig.*

40, 33–43 (2010).

128. Ghasemi, Z. *et al.* Aptamer decorated hyaluronan/chitosan nanoparticles for targeted delivery of 5-fluorouracil to MUC1 overexpressing adenocarcinomas. *Carbohydr. Polym.* **121,** 190–8 (2015).

129. Cleland, R. L. & Wang, J. L. Ionic polysaccharides. III. Dilute solution properties of hyaluronic acid fractions. *Biopolymers* **9,** 799–810 (1970).

130. Ghosh, S., Hoselton, S. A., Dorsam, G. P. & Schuh, J. M. Hyaluronan fragments as mediators of inflammation in allergic pulmonary disease. *Immunobiology* **220,** 575–588 (2015).

131. Evanko, S. P., Potter-Perigo, S., Petty, L. J., Workman, G. a & Wight, T. N. Hyaluronan controls the deposition of fibronectin and collagen and modulates TGF-β1 induction of lung myofibroblasts. *Matrix Biol.* **42,** 74–92 (2014).

132. Gřundělová, L. *et al.* Viscoelastic and mechanical properties of hyaluronan films and hydrogels modified by carbodiimide. *Carbohydr. Polym.* **119,** 142–8 (2015).

133. Reichelt, S. *et al.* Studies on the formation and characterization of macroporous electron-beam generated hyaluronan cryogels. *Radiat. Phys. Chem.* **105,** 69–77 (2014).

134. Gatej, I., Popa, M. & Rinaudo, M. Role of the pH on hyaluronan behavior in aqueous solution. *Biomacromolecules* **6,** 61–7 (2005).

135. Esquenet, C. & Buhler, E. Aggregation behavior in semidilute rigid and semirigid polysaccharide solutions. *Macromolecules* **35,** 3708–3716 (2002).

136. Anik, N. *et al.* Determination of polymer effective charge by indirect UV detection in capillary electrolphoresis: toward the characterization of macromolecular architecture. *Macromolecules* **42,** 2767–2774 (2009).

137. Rawiso, M., Duplessix, R. & Picot, C. Scattering function of polystyrene. *Macromolecules* **20,** 630–648 (1987).

138. Buhler, E. & Boué, F. Persistence length for a model semirigid polyelectrolyte as seen by small angle neutron scattering: a relevant variation of the lower bound with ionic strength. *Eur. Phys. J. E* **10,** 89–92 (2003).

139. Boris, D. C. & Colby, R. H. Reology of sulfonate polystyrene solutions. *Macromolecules* **31,** 5746–5755 (1998).

140. Cowman, M. K. & Matsuoka, S. Experimental approaches to hyaluronan structure. *Carbohydr. Res.* **340,** 791–809 (2005).

141. Higgins, J. S. & Benoît, H. C. *Polymers and neutrons scattering*. (Oxford University Press, New York, 1996).

142. Linder, P. & Zemb, T. *Neutrons, X-rays and lights: scattering methods applied to soft condensed matter*. (Elsevier Science, North-Holland, 2002).

143. Fan, L., Degen, M., Bendle, S., Grupido, N. & Ilavsky, J. The absolute calibration of a small-angle scattering instrument with a laboratory X-ray source. *J. Phys. Conf. Ser.* **247,** 12005 (2010).

144. Cotton, J. P. Variations on contrast in SANS: determination of self and distinct correlation functions. *Adv. Colloid Interface Sci.* **69,** 1–29 (1996).

145. Sears, V. F. Neutron scattering lengths and cross sections. *Neutron News* **3,** 26–37 (1992).

146. Stoyanov, E. S., Stoyanova, I. V & Reed, C. A. The structure of the hydrogen ion in water. *J. Am. Chem. Soc.* **132,** 1484–1485 (2010).

147. Marcus, Y. Ionic radii in aqueous solutions. *Chem. Rev.* **88,** 1475–1498 (1988).

148. Ohtaki, H. & Radnai, T. Structure and dynamics of hydrated ions. *Chem. Rev.* **93,** 1157–1204 (1993).

149. Ohtomo, N. & Arakawa, K. Neutron diffraction study of aqueous ionic solutions. II. Aqueous solutions of sodium chloride and potassium chloride. *Bull. Chem. Soc. Jpn.* **53,** 1789–1794 (1980).

150. Boué, F., Cotton, J. P., Lapp, A. & Jannink, G. A direct measurement of the polyion conformation in aqueous solutions at different temperatures. Small angle neutron scattering of PSSNa using zero average and full contrast. *J. Chem. Phys.* **101,** 2562–2568 (1994).

151. Ball, V. & Maechling, C. Isothermal microcalorimetry to investigate non specific interactions in biophysical chemistry. *Int. J. Mol. Sci.* **10,** 3283–315 (2009).

152. Romanini, D., Braia, M. J. & Porfiri, M. C. *Applications of calorimetric techniques in the formation of protein-polyelectrolytes complexes*. *http://dx.doi.org/10.5772/54260* (2013).

153. Freyer, M. W. & Lewis, E. A. Isothermal titration calorimetry: experimental design, data analysis, and probing macromolecule/ligand binding and kinetic interactions. *Methods Cell Biol.* **84,** 79–113 (2008).

154. Lapčík, L., De Smedt, S., Demeester, J. & Chabreček, P. Hyaluronan: preparation, structure, properties, and applications. *Chem. Rev.* **98,** 2663–2684 (1998).

155. Hargittai, I. & Hargittai, M. Molecular structure of hyaluronan: An introduction. *Struct. Chem.* **19,** 697–717 (2008).

156. Atkins, E. & Sheehan, J. K. Hyaluronantes: relation between molecular conformation. *Science* **179,** 562–564 (1973).

157. Turner, R. E., Lin, P. Y. & Cowman, M. K. Self-association of hyaluronate segments in aqueous NaCl solution. *Arch. Biochem. Biophys.* **265,** 484–95 (1988).

158. Scott, J., Cummings, C., Brass, A. & Chen, Y. Secondary and tertiary structures of hyaluronan in aqueous solution, investigated by rotary shadowing-electron microscopy and computer simulation. *Biochem. J* **274,** 699–705 (1991).

159. Morris, E. R., Rees, D. A., Robinson, G. & Young, G. A. Competitive inhibition of interchain interactions in polysaccharide systems. *J. Mol. Biol.* **138,** 363–374 (1980).

160. Tsutsumi, K. & Norisuye, T. Excuded-Volume Effects in Sodium Hyaronate Solutions Revisited. *Polym. J.* **30,** 345–349 (1998).

161. Almond, A., Deangelis, P. L. & Blundell, C. D. Hyaluronan: the local solution conformation determined by NMR and computer modeling is close to a contracted left-handed 4-fold helix. *J. Mol. Biol.* **358,** 1256–69 (2006).

162. Porod, G. Zusammenhang zwischen mittlerem Endpunktsabstand und Kettenlange bei Fadenmolekulen. *Monatshefte f??r Chemie* **80,** 251–255 (1949).

163. Kratky, O. & Porod, G. Rontgenuntersuchung geloster fadenmolekule. *Recl. des Trav. Chim. des Pays-Bas* **68,** 1106–1122 (1949).

164. Cowman, M. K. *et al.* Extended, relaxed, and condensed conformations of hyaluronan

observed by atomic force microscopy. *Biophys. J.* **88,** 590–602 (2005).

165.   Ghosh, S., Li, X., Reed, C. E. & Reed, W. F. Apparent persistence lengths and diffusion behavior of high molecular weight hyaluronate. *Biopolymers* **30,** 1101–1112 (1990).

166.   Milas, M., Roure, I. & Berry, G. C. Crossover behavior in the viscosity of semiflexible polymers: Solutions of sodium hyaluronate as a function of concentration, molecular weight, and temperature. *J. Rheol. (N. Y. N. Y).* **40,** 1155–1166 (1996).

167.   Gřundělová, L., Mráček, A., Kašpárková, V., Minařík, A. & Smolka, P. The influence of quarternary salt on hyaluronan conformation and particle size in solution. *Carbohydr. Polym.* **98,** 1039–44 (2013).

168.   Almond, A., Brass, A. & Sheehan, J. K. Deducing polymeric structure from aqueous molecular dynamics simulations of oligosaccharides: predictions from simulations of hyaluronan tetrasaccharides compared with hydrodynamic and X-ray fibre diffraction data. *J. Mol. Biol.* **284,** 1425–37 (1998).

169.   Rawiso, M. De l'intensité à la structure en physico-chimie des polymères. *J. Phys. IV Fr.* **9,** 147–195 (1999).

170.   Debye, P. The intrinsic viscosity of polymer solutions. *J. Chem. Phys.* **14,** 636–639 (1946).

171.   Benoit, H. & Doty, P. Light scattering from non gaussian chains. *J. Phys. Chem.* **57,** 958–963 (1953).

172.   Oberthür, R. C. Radius of gyration versus molar mass relations from light scattering for polydisperse non-gaussian chain molecules. Polystyrene in toluene and short DNA-fragments in aqueous NaCl-solution. *Die Makromol. Chemie* **179,** 2693–2706 (1978).

173.   des Cloizeaux, J. Form Factor of an Infinite Kratky-Porod Chain. *Macromolecules* **6,** 403–407 (1973).

174.   Yamakawa, H. & Fuji, M. Intrinsic Viscosity of Wormlike Chains. Determination of the Shift Factor. *Macromolecules* **7,** 128–135 (1974).

175.   Yamakawa, H., Yoshizaki, T. & Fujii, M. Transport Coefficients of Helical Wormlike Chains. 1. Characteristic Helices. *Macromolecules* **10,** 934–943 (1977).

176.   Yamakawa, H. & Yoshizaki, T. Transport Coefficients of Helical Wormlike Chains. 2. Translational Friction Coefficient. *Macromolecules* **12,** 32–38 (1979).

177.   Fouissac, E., Milas, M., Rinaudo, M. & Borsali, R. Influence of the ionic strength on the dimensions of sodium hyaluronate. *Macromolecules* **25,** 5613–5617 (1992).

178.   Cleland, R. L. Viscometry and sedimentation equilibrium of partially hydrolyzed hyaluronate: Comparison with theoretical models of wormlike chains. *Biopolymers* **23,** 647–666 (1984).

179.   Yanaki, T. & Yamaguchi, M. Share-rate dependence of the intrinsic viscosity of sodium hyaluronate in 0.2M sodium chloride solution. *Chem. Pharm. Bull.* **42,** 1651–1654 (1994).

180.   Tinland, B., Mazet, J. & Rinaudo, M. Characterization of water-soluble polymers by multidetection size-exclusion chromatography. *Macromol. Rapid Commun.* **9,** 69–73 (1988).

181.   Bonnet, F., Schweins, R., Boué, F. & Buhler, E. Suppression of aggregation in natural-semiflexible/flexible polyanion mixtures, and direct check of the OSF model using SANS. *EPL (Europhysics Lett.* **83,** 48002 (2008).

182.   Edwards, S. F. The theory of polymer solutions at intermediate concentration. *Proc. Phys. Soc.*

88, 265–280 (2002).

183. Daoud, M. *et al.* Solutions of Flexible Polymers. Neutron Experiments and Interpretation. *Macromolecules* **8,** 804–818 (1975).

184. Koberstein, J. T., Picot, C. & Benoit, H. Light and neutron scattering studies of excess low-angle scattering in moderately concentrated polystyrene solutions. *Polymer (Guildf).* **26,** 673–681 (1966).

185. Benoit, H. & C. Picot. Étude par diffusion de la lumière des solutions macromoleculaires moyennement concentrees. *Pure Appl. Chem.* **12,** 54–561 (1966).

186. Buhler, E. & Rinaudo, M. Structural and dynamical properties of semirigid polyelectrolyte solutions: a light-scattering study. *Macromolecules* **33,** 2098–2106 (2000).

187. Ermi, B. D. & Amis, E. J. Domain structures in low ionic strength polyelectrolyte solutions. *Macromolecules* **31,** 7378–7384 (1998).

188. Sedlak, M. Domain structure of polyelectrolyte solutions: is it real? *Macromolecules* **26,** 1158–1162 (1993).

189. Reed, W. F., Ghosh, S., Medjahdi, G. & Francois, J. Dependence of polyelectrolyte apparent persistence lengths, viscosity, and diffusion on ionic strength and linear charge density. *Macromolecules* **24,** 6189–6198 (1991).

190. Reed, W. F. Comments on' Domain Structure of Polyelectrolyte Solutions: Is it Real?' *Macromolecules* **27,** 873–874 (1994).

191. Li, X. & Reed, W. F. Polyelectrolyte properties of proteoglycan monomers. *J. Chem. Phys.* **94,** 4568–4580 (1991).

192. Villetti, M., Borsali, R., Diat, O., Soldi, V. & Fukada, K. SAXS from polyelectrolyte solutions under shear: xanthan and Na-hyaluronate examples. *Macromolecules* **33,** 9418–9422 (2000).

193. Brulet, A., Boué, F. & Cotton, J. P. About the Experimental Determination of the Persistence Length of Wormlike Chains of Polystyrene. *Journal de Physique II* **6,** 885–891 (1996).

194. Alber, C., Englom, J., Falkmann, P. & Kocherbitov, V. Effect of Hydration on Structural and Thermodynamic Properties of Mucin. *J. Phys. Chem. B* **119,** 4211–4219 (2015).

195. Nishida, K., Urakawa, H., Kaji, K., Gabrys, B. & Higgins, J. S. Electrostatic persistence length of NaPSS polyelectrolytes determined by a zero average contrast SANS technique. *Polymer* **38,** 6083–6085 (1997).

196. Nishida, K., Kaji, K., Kanaya, T. & Shibano, T. Added salt effect on the intermolecular correlation in flexible polyelectrolyte solutions: Small-angle scattering study. *Macromolecules* **35,** 4084–4089 (2002).

197. Matteini, P. *et al.* Structural behavior of highly concentrated hyaluronan. *Biomacromolecules* **10,** 1516–1522 (2009).

198. Haxaire, K., Maréchal, Y., Milas, M. & Rinaudo, M. Hydration of polysaccharide hyaluronan observed by IR spectrometry. I. Preliminary experiments and band assignments. *Biopolym. - Biospectroscopy Sect.* **72,** 10–20 (2003).

199. Haxaire, K., Maréchal, Y., Milas, M. & Rinaudo, M. Hydration of hyaluronan polysaccharide observed by IR spectrometry. II. Definition and quantitative analysis of elementary hydration spectra and water uptake. *Biopolym. - Biospectroscopy Sect.* **72,** 149–161 (2003).

200. Maréchal, Y., Milas, M. & Rinaudo, M. Hydration of hyaluronan polysaccharide observed by IR spectrometry. III. Structure and Mechanism of Hydration. *Biopolym. - Biospectroscopy Sect.* **72,** 162–173 (2003).

201. Scott, J. E. & Heatley, F. Hyaluronan forms specific stable tertiary structures in aqueous solution: a 13C NMR study. *Proc. Natl. Acad. Sci. U. S. A.* **96,** 4850–4855 (1999).

202. Arnott, S., Mitra, A. K. & Raghunathan, S. Hyaluronic acid double helix. *J. Mol. Biol.* **169,** 861–72 (1983).

203. Mitra, A. K., Raghunathan, S., Sheehan, J. K. & Arnott, S. Hyaluronic acid: molecular conformations and interactions in the orthorhombic and tetragonal forms containing sinuous chains. *J. Mol. Biol.* **169,** 829–859 (1983).

204. Sheehan, J. K. & Atkins, E. D. T. X-ray fibre diffraction study of conformational changes in hyaluronate induced in the presence of sodium, potassium and calcium cations. *Int. J. Biol. Macromol.* **5,** 215–221 (1983).

205. Sukhishvili, S. A., Kharlampieva, E. & Izumrudov, V. Where polyelectrolyte multilayers and polyelectrolyte complexes meet. *Macromolecules* **39,** 8873–8881 (2006).

206. Plantenberg, T. & Kotz, J. Liquid crystalline polyanion / polycation / water systems. *Polymers (Basel).* **42,** 3523–3532 (2001).

207. Wang, Q. & Schlenoff, J. B. The polyelectrolyte complex/coacervate continuum. *Macromolecules* **47,** 3108–3116 (2014).

208. Dautzenberg, H. & Karibyants, N. Polyelectrolyte complex formation in highly aggregating systems. Effect of salt: response to subsequent addition of NaCl. *Macromol. Chem. Phys.* **200,** 118–125 (1999).

209. De Kruif, C. G., Weinbreck, F. & De Vries, R. Complex coacervation of proteins and anionic polysaccharides. *Curr. Opin. Colloid Interface Sci.* **9,** 340–349 (2004).

210. Kovacevic, D., van der Burgh, S., de Keizer, A. & Cohen Stuart, M. A. Kinetics of formation and dissolution of weak polyelectrolyte multilayers: role of salt and free polyions. *Langmuir* **18,** 5607–5612 (2002).

211. Tainaka, K.-I. Effect of counterions on complex coacervation. *Biopolymers* **19,** 1289–1298 (1980).

212. Hecht, A.-M., Duplessix, R. & Geissler, E. Structural inhomogeneities in the range 2.5-2500 Å in polyacrylamide gels. *Macromolecules* **18,** 2167–2173 (1985).

213. Bastide, J., Leibler, L. & Prost, J. Scattering by deformed swollen gels : butterfly isointensity patterns. *Macromolecules* **23,** 1821–1825 (1990).

214. Hecht, A.-M., Guillermo, A., Simon, H., Legrand, J. F. & J, E. G. Structure and dynamics of a poly(dimethylsiloxane) network : a comparative investigation of gel and solution. *Macromolecules* **25,** 3677–3684 (1992).

215. Cabane, B. & Hénon, S. *Liquides (solutions, dispersions, emulsions, gels)*. (Berlin Ed, 2003).

216. Bastide, J. & Leibler, L. Large-scale heterogenities in randomly cross-linked networks. *Macromolecules* **21,** 2647–2649 (1988).

217. Benoit, H. On the effect of branching and polydispersity on the angular distribution of the light scattered by gaussian coils. *J. Polym. Sci.* **22,** 223–230 (1953).

218. Lvov, Y., Ariga, K., Ichinose, I. & Kunitake, T. Assembly of multicomponent protein films by means of electrostatic layer-by-layer adsorption. *J. Am. Chem. Soc.* **117,** 6117–6123 (1995).

219. Bromberg, L. E. Interactions among proteins and hydrophobically modified polyelectrolyte. *J. Pharm. Pharmacol.* **53,** 541–547 (2001).

220. Jiang, H. L. & Zhu, K. J. Polyanion / Gelatin Complexes as pH-Sensitive Gels. 1416–1425 (2001).

221. van de Weert, M., Andersen, M. & S., F. Complex coacervation of lysozyme and heparin: complex characterization and protein stability. *Pharm. Res.* **21,** 2354–2359 (2004).

222. Wittemann, A. & Ballauff, M. Secondary structure analysis of proteins embedded in spherical polyelectrolyte brushes (SPB) by FT-IR spectroscopy. *Anal. Chem.* **76,** 2813–2819 (2004).

223. Müller, M., Rieser, T., Dubin, P. L. & Lunkwitz, K. Selective interaction between proteins and the outermost surface of polyelectrolyte multilayers: Influence of the polyanion type, pH and salt. *Macromol. Rapid Commun.* **22,** 390–395 (2001).

224. Caruso, F. & Möhwald, H. Protein multilayer formation on colloids through a stepwise self-assembly technique. *J. Am. Chem. Soc* **121,** 6039–6046 (1999).

225. Anikin, K. *et al.* Polyelectrolyte-mediated protein adsorption: fluorescent protein binding to individual polyelectrolyte nanospheres. *J Phys Chem B* **109,** (2005).

226. Teramoto, A., Takagi, Y., Hachimori, A. & Abe, K. Interaction of albumin with polysaccharides containing ionic groups. *Polym. Adv. Technol.* **10,** 681–686 (1999).

227. Xia, J. L., Dubin, P. L., Kokufuta, E., Havel, H. & Muhoberac, B. B. Light scattering, CD, and ligand binding studies of ferrihemoglobin-polyelectrolyte complexes. *Biopolymers* **50,** 153–161 (1999).

228. Mekhloufi, G., Sanchez, C., Renard, D., Guillemin, S. & Hardy, J. pH-induced structural transitions during complexation and coacervation of beta-lactoglubulin and acacia gum. *Langmuir* **21,** 386–394 (2005).

229. Gong, J. *et al.* Structural transformation of cytochromec and apo cytochrome c induced by sulfonated polystyrene. *Biomacromolecules* **4,** 1293–1300 (2003).

230. Spruijt, E., Westphal, A. H., Borst, J. W., Cohen Stuart, M. A. & van der Gucht, J. Binodal compositions of polyelectrolyte complexes. *Macromolecules* **43,** 6476–6484 (2010).

231. Cooper, C. L., Dubin, P. L., Kayitmazer, a. B. & Turksen, S. Polyelectrolyte–protein complexes. *Curr. Opin. Colloid Interface Sci.* **10,** 52–78 (2005).

232. Ghostine, R. A., Shamoun, R. F. & Schlenoff, J. B. Doping and diffusion in an extruded saloplastic polyelectrolyte complex. *Macromolecules* **46,** 4089–4094 (2013).

233. Lin, M. Y. *et al.* Universal diffusion-limited colloid aggregation. *Journal of Physics: Condensed Matter* **2,** 5283–5283 (2002).

234. Fenistein, D. *et al.* Viscosimetric and neutron scattering study of asphaltene aggregates in mixed toluene / heptane solvents. *Langmuir* **14,** 1013–1020 (1998).

235. Lin, M. Y. *et al.* Universal reaction-limited colloid aggregation. *Phys. Rev. A* **41,** 2005–2020 (1990).

236. Qiao, B., Cerdà, J. J. & Holm, C. Poly(styrenesulfonate)−Poly(diallyldimethylammonium) Mixtures: Toward the Understanding of Polyelectrolyte Complexes and Multilayers via

Atomistic Simulations. *Macromolecules* **43,** 7828–7838 (2010).

237. Gummel, J., Cousin, F. & Boué, F. Counterions release from electrostatic complexes of polyelectrolytes and proteins of opposite charge: a direct measurement. *J. Am. Chem. Soc.* **129,** 5806–7 (2007).

238. Hone, J. H. E., Howe, A. M. & Cosgrove, T. A rheological and small-angle neutron scattering study of the structure of gelatin/polyelectrolyte complexes under shear. *Macromolecules* **33,** 1199–1205 (2000).

239. Currie, E. P. K., Cohen Stuart, M. A. & Borisov, O. V. New mechanisms for phase separation in polymer-surfactant mixtures. *EPL(Europhysics Lett.* **438,** 438–444 (2000).

240. Lazutin, A. A., Semenov, A. N. & Vasilevskaya, V. V. Polyelectrolyte complexes consisting of macromolecules with varied stiffness: computer simulation. *Macromol. Theory. Simul.* **21,** 328–339 (2012).

241. Markarian, M. Z., Hariri, H. H., Reisch, A., Urban, V. S. & Schlenoff, J. B. A small-angle neutron scattering study of the equilibrium conformation of polyelectrolytes in stoichiometric saloplastic polyelectrolyte complexes. *Macromolecules* **45,** 1016–1024 (2012).

242. Maude, G., Turgeon, S. & Gauthier, S. Thermodynamic parameters of lactoglobulin-pectin omplexes assessed by isothermal titration calorimetry. *J. Agric Food Chem.* **51,** 4450–4455 (2003).

243. Perry, S. L., Li, Y., Priftis, D., Leon, L. & Tirrell, M. The effect of salt on the complex coacervation of vinyl polyelectrolytes. *Polymers (Basel).* **6,** 1756–1772 (2014).

244. Burgess, D. J. Practical analysis of complex coacervate systems. *J. Colloid Interface Sci.* **140,** 227–238 (1990).

Iuliia KONKO

Solutions aqueuses de complexes formés par des polyélectrolytes modèles de charge opposée

Résumé en français

Cette thèse présente une étude des solutions aqueuses de trois complexes de polyélectrolytes (PECs) modèles. Les PECs résultent de la complexation de deux polyélectrolytes linéaires de charge opposée: un polycation (le PDADMA) et trois polyanions de longueur de persistance non électrostatique distinctes: le polystyrene sulfoné (PSS), le poly(α-méthyl styrène sulfoné) (PαMSS) et l'acide hyaluronique (HA). En plus de l'influence de la rigidité intrinsèque des polyanions sur la formation et la structure des PECs, les effets de la force ionique et de la méthode de préparation des solutions aqueuses de PECs ainsi que l'influence de la concentration des solutions binaires de polyélectrolytes initiales ont également été abordés. Nous suggérons que le processus de complexation entre polycations et polyanions en régimes semidilué et concentré est analogue à une gélification. Il y a toutefois une différence entre les deux complexes qui est reliée à la différence de rigidité intrinsèque.

Mots clés : complexes des polyélectrolytes ; solutions des polyélectrolytes ; rigidité intrinsèque ; diffusion de rayons X aux petites angles ; diffusion de neutrons aux petites angles ; poly(chlorure de diallyldimethylammonium) ; polystyrène sulfoné ; acide hyaluronique

Résumé en anglais

This PhD thesis presents a study of the aqueous solutions of three model polyelectrolyte complexes (PECs). PECs were formed between hydrophilic and highly charged linear macrocations of poly(diallyldimethyl ammonium) (PDADMA) and linear macroanions of distinct intrinsic persistence lengths: sulfonated polystyrene (PSS), sulfonated poly(α-methyl styrene) (PαMSS) and hyaluronate (HA). In addition to the effect of the macroion stiffness on the PEC formation and structure, those of the ionic strength and the way of preparing the PEC aqueous solutions as well as that of the concentration regimes of the initial PE aqueous solutions were also tackled. We suggest the complexation between macrocations and macroanions in the semidilute and concentrated regimes can be described as a universal gelation process. A difference between PDADMA-PSS and PDADMA-HA complexes is related to the primary self-assembling process and is associated with the distinct structural models for PECs.

Keywords : polyelectrolyte complexes ; polyelectrolyte solutions ; intrinsic stiffness ; small angle X-ray scattering; small angle neutron scattering; poly(diallyldimethylammonium chloride); polystyrene sulfonate; hyaluronate